1988

Scapolite phase equilibria and carbon isotope variations in high grade rocks: Tests of the carbon-dioxide-flooding hypothesis of granulite genesis.

Moecher, David Paul

Order Number 8907106

Scapolite phase equilibria and carbon isotope variations in high grade rocks: Tests of the CO_2-flooding hypothesis of granulite genesis

Moecher, David Paul, Ph.D.

The University of Michigan, 1988

U·M·I
300 N. Zeeb Rd.
Ann Arbor, MI 48106

SCAPOLITE PHASE EQUILIBRIA AND CARBON ISOTOPE VARIATIONS IN HIGH GRADE ROCKS: TESTS OF THE CO_2-FLOODING HYPOTHESIS OF GRANULITE GENESIS

by

David Paul Moecher

A dissertation submitted in partial fulfillment
of the requirements for the degree of
Doctor of Philosophy
(Geology)
in The University of Michigan
1988

Doctoral Committee:

Professor Eric J. Essene, Chairman
Associate Professor Richard J. Arculus
Professor Donald R. Peacor
Associate Professor John W. Valley, University of Wisconsin
Professor Edgar F. Westrum, Jr.

To Amy Elizabeth Luchsinger

ACKNOWLEDGMENTS

In a break with the conventional order of acknowledgments, and to keep everything in perspective, I am going to publicly thank my partner, unacknowledged co-author, advisor, patron, and wife, Amy Elizabeth Luchsinger for **everything**!

During my tenure as a Ph.D. student at the University of Michigan, scores of people made important contributions to my research and my growth as a scientist. Others simply, but just as importantly, made my stay more enjoyable and worthwhile. Professor Eric Essene had the perception to conceive of a fundamental and simple test of a widely accepted but poorly tested hypothesis on the petrogenesis of high grade rocks. He sets an excellent example of simply not accepting a reasonable sounding explanation, and instead asking the right questions and developing the definitive tests. I have learned much from Eric, and will always have the thought of his examples in the back of my head. Eric also set an excellent example of how to treat graduate students. He was generous with financial aid, and usually went out of his way to make sure there was some form of assistance. He was considerate enough to allow me use of one of his computers so I could work at home after our son arrived. For that my family and I are grateful. Most importantly he treats students with professional respect, considering them an asset and not a liability, and being generous with credit for a job well done.

A number of other faculty went out of their way to help me either professionally or financially. Professsors Richard Arculus, Donald Peacor, and John Valley provided valuable discussion and advice on various aspects of this thesis. Richard wrote an endless number of letters of recommendation for grants or jobs, usually on very short notice. John did likewise and allowed me free reign in his stable isotope geochemistry lab at Wisconsin. Professor Peacor provided support for analytical work and appointments when they were badly needed. Professor Edgar Westrum Jr. made arrangements to do extensive low temperature calorimetry in his lab. Professor James O'Neil provided a careful review of Chapter V, many useful ideas on the isotopic analysis of scapolite, and held a sumptuous dinner party in celebration of my defense. The critical comments of

Professors Arculus, O'Neil, Peacor, Valley, and Westrum on various aspects of this dissertation are greatly appreciated. Professor Bruce Wilkinson provided summer support, allowing me to spend one of the nicest summers I can remember, at Camp Davis teaching Geological Sciences 116. Professor K.C. Lohman saved me from many computer blunders and on short notice provided isotope measurements.

Anne Bloomfield, Mike Cosca, Annie Kersting, and Zach Sharp are thanked for their patient instruction in various aspects of computing and analytical work, and for being good friends. Zach went to great lengths to set up the FINALWORD format for his dissertation, and allowed me to use it for my dissertation. Carl Henderson provided patient instruction on the electron microprobe, and was willing to be on call till late in the evening. Scott Carpenter provided instruction on the luminoscope. At the University of Wisconsin Kevin Baker, Steve Dunn, Jean Morrison, and Bill Reinthall provided instruction in various aspects of stable isotope analytical methods, provided valuable feedback on ideas and problems, and made my many stays in Madison enjoyable. In a pinch Kevin ran some oxygen isotope analyses.

The following people provided samples for this work, many of them going to personal expense to send samples of scapolite gneisses: L.M. Anovitz, H. Austreim (Mineralogisk-Geologisk Museum, Oslo), W.L. Brown (University of Paris), A. Davidson (Geological Survey of Canada), T.C. Devaraju (Karnataka University, Dharwad, India), C.A. Francis (Harvard Museum), D.L. Hogarth (Ottawa University), C. Marmont (Ontario Ministry of Mines and Northern Development), D. Mogk (Montana State University), C. Srikantappa (University of Mysore, Mysore, India), and A.J. Stolz (University of Tasmania).

I want to thank the office staff in the Department of Geological Sciences, particularly Marlene Allen and Nancy Ballis, for helping out with administrative procedures. Jim Hinchcliff did an excellent job of providing high quality thin sections and fast turn around time. Scott Baird helped with a number of computing problems. Susie Fast helped out considerably by drafting some of the figures.

This work was supported by NSF grant EAR-84-08169 to Eric Essene, academic support from the Department of Geological Sciences, a discretionary grant from the Graduate School of the University of Michigan, and by grants-in-aid of research from GSA, Sigma Xi, and the Turner Fund of the University of Michigan. Occasional operating grants from Carol Moecher and from Sam and Margaret Luchsinger are greatly appreciated.

One other person arrived just in time to help out with finishing touches and keep me at home: Patrick John Moecher. He'll never know it but he was a constant source of inspiration.

TABLE OF CONTENTS

LIST OF TABLES

CHAPTER II

CHAPTER III

CHAPTER IV

CHAPTER V

LIST OF FIGURES

CHAPTER II

CHAPTER III

CHAPTER IV

CHAPTER V

LIST OF APPENDICES

Appendix

CHAPTER I

INTRODUCTION

The granulite facies is distinguished from other metamorphic facies by its relatively anhydrous nature (low water activities) compared to lower grade equivalents. Although Eskola (1939) originally defined the granulite facies based on the absence of hydrous minerals, it was later redefined to include rocks that contained primarily anhydrous minerals but that may contain amphibolte or mica, depending on bulk composition. How granulites attain this relatively anhydrous state has developed into a point of contention among many workers in this field. This dissertation was designed to evaluate one of the hypotheses that attempts to account for the development of low water activities (a_{H_2O}) in granulites, that of CO_2 flooding or carbonic metamorphism. Originally, Touret (1971) noted that fluid inclusions in granulites were generally high density, CO_2-rich inclusions while those in amphibolite facies equivalents were H_2O-rich inclusions. The CO_2 inclusions were interpreted to have been entrapped at or near the thermal peak of metamorphism and reflect the composition of the fluid with which the minerals equilibrated. Subsequent studies have corroborated Touret's observations (see refs. Chap 4), although the interpretation that these inclusions represent peak fluid compositions has been questioned (Lamb et al. 1987). Thus, CO_2 was implicated as the diluent of the granulite facies fluid phase, and CO_2 flooding or carbonic metamorphism was proposed as a mechanism to account for the regional metamorphic scale of this phenomenon (Janardhan et al. 1979, Newton et al. 1980, Newton 1987). Initially, it was proposed that CO_2 derived from the mantle, mantle-derived basalt ponded at the base of the crust, or CO_2 dissolved in tonalitic

melts emplaced during crustal accretion, copiously pervaded the crust driving out the H_2O. The resulting anhydrous fluid would stabilize orthopyroxene relative to amphibole or biotite. The dehydration of the system via this mechanism was also used to account for the variable LIL element depletion of some granulites. Later modifications of the model proposed that CO_2 could be derived from subducted or underthrusted carbonates in orogenic zones (Newton 1987), from decarbonation of high grade carbonate units in the lower crust during high grade metamorphism (Glassley 1983) or decarbonation in response to melting of lithologies enclosing marble or calc-silicate units at high temperatures brought on by basaltic underplating (Wickham 1988).

Where carbonic fluid inclusions have been recorded, CO_2-flooding has often been the accepted mechanism to account for their formation (e.g., Santosh, 1985), and a CO_2-rich or pure CO_2 fluid phase has been proposed to be the peak metamorphic fluid (e.g., Rudnick et al. 1984). However, there are few quantitative constraints or direct tests of the model (c.f., Lamb and Valley 1984, Vry et al. 1988, Baker 1988). The available fluid inclusion, LIL element, and textural evidence (Janardhan et al. 1979) for CO_2 streaming is mostly consistent with such a process and do not prove or directly test its implications. If rocks have been infiltrated on a grain boundary scale by a free, CO_2-rich fluid, one would expect this process to be recorded mineralogically. The mineral assemblages and compositions should reflect a CO_2-rich fluid composition. One would also expect to see homogenization of fluid compositions. Carbonate or graphite mineral equilibria could be used to constrain high grade fluid compositions (Lamb et al. 1987). Unfortunatley, most granulite facies orthogneisses do not contain a primary carbonate phase. Scapolite, a carbonate-bearing silicate, is reported in some high-grade rocks from a variety of metamorphic terranes, and by virtue of the CO_3, Cl, and SO_4 groups is potentially a sensor of fluid composition and fluid source. In addition, if the mantle, subducted carbonate and organic matter, or high grade calc-silicate gneisses were the dominant source of the CO_2 leading to dehydration, it should have a distinct carbon isotopic signature or a limited range of $\delta^{13}C$ that

would be recorded in carbon bearing species in the rocks. One would also predict homogenization of regional carbon isotopic compositions and swamping of isotopic gradients. The present work will use scapolite in this role to determine whether the granulite facies fluid is rich in CO_2, whether there is a free fluid phase in high grade rocks, and to use the carbon isotopic compositions to constrain potential fluid sources.

In order to perform calculations of fluid composition in high grade rocks, a number of data are required. Ther are no accurate geobarometers for many scapolite-bearing assemblages, and regional metamorphic pressures are not known in some terranes that contain scapolite-bearing gneisses. The assemblage clinopyroxene-garnet-plagioclase-quartz was found to occur in many of the scapolite gneisses investigated for this study. In Chapter II of this thesis I describe the thermodynamic calculation and evaluation of geobarometers based on the reactions 3Hd + 3An = 2Gr + Alm + 3 Qz and 3Di + 3An = 2Gr + Py + 3Qz. In the absence of regional thermometry, the assemblage also allows metamorphic temperatures to be calculated using the garnet-clinopyroxene thermometer. Many of the samples for this study were collected in the Central Gneiss Belt of the southwestern Grenville Province where regional thermobarometric work has been performed (Anovitz 1987). However many of the Grenville samples were collected in ductile shears or settings that may postdate the peak of granulite facies metamorphism, or are samples from other terranes and crustal xenoliths for which P-T data have not bee estimated. These barometers and the garnet-clinopyroxene thermometer allow calculation of P and T in most of the samples analyzed for this study.

In Chapter III, a discussion is presented of the derivation of thermodynamic data needed to calculate fluid composition in scapolite-bearing assemblages. Thermodynamic data for meionite scapolite are derived from a number of sources and constrained by experiments on scapolite stability. An internally consistent thermodynamic data set is derived for phases in the $CaO-Al_2O_3-SiO_2-CO_2-H_2O$

(CASCH) system, constrained by available experimental equilibria in CASCH. Quantitative phase equilibria for this system, including meionite-bearing reactions, are calculated at 5 and 10 kbar. Finally, activity-composition relations for carbonate scapolite solid solutions are calculated from data on natural scapolite-plagioclase-calcite assemblages. These data allow calculation of CO_2 activities in scapolite- bearing granulites, amphibolites, mafic gneisses, meta-anorthosite, and calc-silicates from the Grenville Province and other granulite terranes, the subject of Chapter III. Scapolite-plagioclase-garnet-quartz assemblages are common in scapolite gneisses and buffer the activity of CO_2 (a_{CO_2}) by the reaction 2Me + Qz = 5An + Gr + $2CO_2$. This reaction was used to calculate a_{CO_2} in the above lithologies.

In Chapter IV the carbon isotope systematics of scapolite are presented. Carefully characterized scapolite mineral separates are used to evaluate quantitative extraction of the CO_3 group of scapolite by standard phosphoric acid techniques at 25 and 75°C, and by combustion at high temperature. The fractionation of ^{13}C between scapolite and calcite was measured on natural scapolite-calcite pairs, in order to constrain the carbon isotope composition of the fluid phase inferred to have formed scapolite. These techniques are tested where scapolite is developed in a meta-anorthosite adjacent to marble to determine if scapolite accurately records the carbon isotope composition of the source marble. They were applied to high grade gneisses from the Grenville Province in order to determine carbon sources and extent of homogeneity on a regional scale.

If CO_2-flooding is a pervasive and significant process, it should be recorded in scapolite gneisses as uniformly high values of a_{CO_2}, and as uniform values of $\delta^{13}C$ for the Central Gneiss Belt of Ontario (assuming no retrograde exchange of carbon). These constraints on fluid composition in high grade rocks are preferred over indirect evidence such as fluid inclusions, whose entrapment history may not record conditions at or near the peak of metamorphism.

References

Anovitz LM (1987) Pressure and Temperature Constraints on Metamorphism in the Grenville Province, Ontario. PhD thesis, University of Michigan

Baker A (1988) Stable isotope evidence for limited fluid infiltration of deep crustal rocks from the Ivrea Zone, Italy. Geology **16**:492–495

Eskola P (1939) Die metamorphen Gesteine, "Die Entstehung der Gesteine" (Barth TFW, Correns TW, Eskola P) 263–407, Springer, Berlin

Glassley WE (1983) Deep crustal carbonates as CO_2 fluid sources: evidence from metasomatic reaction zones. Contrib Mineral Petrol **84**:15–24

Janardhan AS, Newton RC, Smith JV (1979) Ancient crustal metamorphism at low p_{H_2O}: charnockite formation at Kabbaldurga, South India. Nature **278**:511–514

Lamb WM, Valley JW (1984) Metamorphism of reduced granulites in low-CO_2 vapour-free environment. Nature **312**:56–58

Lamb WM, Valley JW, Brown PE (1987) Post-metamorphic CO_2-rich fluid inclusions in granulites. Contrib Mineral Petrol **96**:485–495

Newton RC (1987) Late Archean/early Proterozoic CO_2 streaming through the lower crust and geochemical segregation. Geophys Res Lett **14**:287–290

Newton RC, Smith JV, Windley BF (1980) Carbonic metamorphism, granulites and crustal growth. Nature **288**:45–50

Rudnick RL, Ashwal LD, Henry DJ (1984) Fluid inclusions in high-grade gneisses of the Kapuskasing structural zone, Ontario: metamorphic fluids and uplift/erosion path. Contrib Mineral Petrol **87**: 399–406

Santosh M (1986) Carbonic metamorphism of charnockites in the southwestern Indian Shield: a fluid inclusion study. Lithos **19**:1–10

Touret J (1971) Le facies granulite en Norvege meridionale. II. Les inclusions fluides. Lithos **4**:423–436

Vry J, Brown PE, Valley JW, Morrison J (1988) Constraints on granulite genesis from carbon isotope compositions of cordierite and graphite. Nature **332**:66–68

Wickham SM (1988) Evolution of the lower crust. Nature **333**:119–120

CHAPTER II

CALCULATION OF CLINOPYROXENE-GARNET-PLAGIOCLASE-QUARTZ GEOBAROMETERS: EVALUATION AND APPLICATION TO HIGH GRADE METAMORPHIC ROCKS

Introduction

Major advances in the accuracy and precision of geobarometers have been made in the last decade, in part a result of careful experimental reversal of pressure dependent equilibria (Bohlen et al. 1980; Bohlen and Boettcher 1982; Bohlen et al. 1983a 1983b; Gasparik 1984a, 1984b; Gasparik and Newton 1984; Bohlen and Liotta 1986; Koziol and Newton 1986), more precise thermodynamic data (e.g. Haselton and Newton 1980; Metz et al. 1983; Bohlen et al. 1983; Robie and Hemingway 1984; Haselton et al. 1987; Robie et al. 1987), and more accurate modeling of activity-composition relations for mineral phases involved in geobarometric equilibria (e.g., Newton et al. 1980; Newton and Haselton 1981; Ganguly and Saxena 1984; Davidson and Lindsley 1985; Anovitz and Essene 1987a). Reasonably accurate and precise geobarometers now exist for most granulite facies metabasites, charnockites and high grade metapelites, and for some upper amphibolite facies metabasites and metapelites. The above experiments also serve as important constraints on thermodynamic data for mineral phases involved in the particular reaction. In concert with precise thermodynamic data for other phases, the experimentally constrained thermodynamic data may be used to calculate geobarometers that are not easily reversed experimentally. Using this approach we have calculated the location of the pressure dependent reactions

Hedenbergite + Anorthite = Grossular + Almandine + Quartz (1)

$3\ CaFeSi_2O_6 + 3\ CaAl_2Si_2O_8 = 2\ Ca_3Al_2Si_3O_{12} + Fe_3Al_2Si_3O_{12} + 3\ SiO_2$

the "Hedenbergite (HD) barometer") and,

Diopside + Anorthite = Grossular + Pyrope + Quartz (2)

$3\ CaMgSi_2O_6 + 3\ CaAl_2Si_2O_8 = 2\ Ca_3Al_2Si_3O_{12} + Mg_3Al_2Si_3O_{12} + 3\ SiO_2$

(the "Diopside (DI) barometer"), in order to expand the range of assemblages for which there exist reasonably precise geobarometers. Because garnet, plagioclase and quartz are phases common to both barometers we have chosen to distinguish them on the basis of the particular pyroxene present. Reaction 2 was previously calculated by Newton and Perkins (1982) based on the best available thermochemical data. Their version of Reaction 2 typically underestimated pressure by an average of 2.2 kbar relative to their orthopyroxene geobarometer (Newton and Perkins 1982), which was ascribed to imprecise thermodynamic data (Newton and Perkins 1982).

This paper presents calculations of new calibrations for clinopyroxene - garnet - plagioclase - quartz geobarometers in the system $CaO - Al_2O_3 - FeO - MgO - SiO_2$, based on thermodynamic data derived from a number of sources and constrained by a variety of experimental equilibria. The precision and accuracy of these calibrations are tested by comparing pressures obtained for Reactions 1 and 2 against the equilibrium

Ferrosilite + Anorthite = Almandine + Grossular + Quartz (3)

$6\ FeSiO_3 + 3\ CaAl_2Si_2O_8 = 2\ Fe_3Al_2Si_3O_{12} + Ca_3Al_2Si_3O_{12} + 3\ SiO_2$

(the "Ferrosilite (FS) barometer"), and the location of the polymorphic transition

Sillimanite = Kyanite (4)

(Richardson et al. 1968, Holdaway 1971, Robie and Hemingway 1984). Reaction 3 is derived by addition of the experimentally reversed reactions

Fayalite + Quartz = 2 Ferrosilite (5)

$Fe_2SiO_4 + SiO_2 = FeSiO_3$

(Bohlen et al. 1980) and

Fayalite + Anorthite = Almandine + Grossular (6)

$3\ Fe_2SiO_4 + 3\ CaAl_2Si_2O_8 = (2\ Fe_3Al_2Si_3O_{12} + Ca_3Al_2Si_3O_{12})_{SS}$

(where SS is a 2/3 almandine + 1/3 grossular solid solution produced in the experiments, Bohlen et al. 1983a), and has proven to be an extremely useful geobarometer for granulites. Calculations of Reaction 3 as a geobarometer have been presented by Bohlen et al. (1983a), Perkins and Chipera (1985), and Anovitz and Essene (1987a) that differ in the choice of thermodynamic data and garnet mixing model used to calculate the position of the end member reaction (Reaction 3). For these purposes we have used the garnet mixing model of Ganguly and Saxena (1984) with Ca–Fe mixing parameters derived by Anovitz and Essene (1987a). Sources of thermodynamic data are discussed in detail in the following sections.

Thermodynamic data

A variety of sources and experimental studies were used in the compilation of thermodynamic data for the present study. Carefully reversed experiments on Reactions 5, 6 and the reactions

Almandine + Rutile = Ilmenite + Sillimanite + Quartz (7)

$Fe_3Al_2Si_3O_{12} + 3TiO_2 = 3FeTiO_3 + Al_2SiO_5 + 2SiO_2$

Almandine + Grossular + Rutile = Ilmenite + Anorthite + Quartz (8)

$2\ Fe_3Al_2Si_3O_{12} + Ca_3Al_2Si_3O_{12} + 6\ TiO_2 = 6\ FeTiO_3 + 3\ CaAl_2Si_2O_8 + 3\ SiO_2$

(Bohlen et al. 1983b, 1983c, Bohlen and Liotta 1986)

Anorthite = Grossular + Kyanite + Quartz (9)

$3\ CaAl_2Si_2O_8 = Ca_3Al_2Si_3O_{12} + 2\ Al_2SiO_5 + SiO_2$

(Koziol and Newton 1988) and

$$\text{Wollastonite} + \text{Anorthite} = \text{Grossular} + \text{Quartz} \qquad (10)$$
$$2\ CaSiO_3 + CaAl_2Si_2O_8 = Ca_3Al_2Si_3O_{12} + SiO_2$$

(Newton 1966, Hays 1967, Boettcher 1970, Huckenholz et al. 1975) combined with heat capacity functions and volume data serve to constrain the 1 bar Gibbs free energy (ΔG°_{298}) of fayalite, ferrosilite, kyanite, grossular, almandine and anorthite. The latter data were compiled by Anovitz and Essene (1987a; Table 1) from a number of sources and comprise part of an internally consistent thermodynamic data set for selected phases in the system $CaO–FeO–Al_2O_3–SiO_2–TiO_2$ (Table 1 and 2). Thermodynamic data for diopside (Tables 1 and 2) have been compiled and evaluated by Sharp et al. (1986) from various sources and experiments in the system $CaO–MgO–SiO_2–CO_2$. The reader is referred to these sources for a detailed discussion of the methods used in deriving the respective data. Thermodynamic data for enstatite are taken from Robinson et al. (1982), and derivation of thermodynamic data for pyrope and hedenbergite is described below.

There has been considerable discussion concerning the presence of Al–Si disorder in synthetic anorthite produced in phase equilibrium experiments such as Reaction 9, and the necessity of adding a configurational entropy term to S°_{298} of anorthite in order to fit the experimental reversals (e.g., Gasparik 1984a, Wood & Holloway 1984, Koziol & Newton 1986). Anovitz & Essene (1987a) also address this problem, concluding that use of different values for S°_{298} of grossular, and lack of application of thermal expansion and compressibility in phase equilibrium calculations may require an S°_0 term for anorthite in order to fit the reversals. However, the thermodynamic data set derived by Anovitz & Essene (1987a: Tables 1 and 2 of this study) uses an alternative S°_{298} for grossular and includes the effects of expansivity and compressibility of solids, providing an adequate fit to the reversals for Reaction 9 and other equilibria. Following their conclusion we do not believe a configurational entropy term is warranted for anorthite.

TABLE 1. Molar volume, entropy, entropy coefficients, and Gibbs free energies (relative to oxides) of phases involved in thermodynamic calculations.

PHASE	V°_{298} cc/mol	ref	S°_{298} J/mol K	A	B	C	D	ref	ΔG°_{298} kJ/mol	ref
Ni	6.59	1	29.87	29.397	4.410	1.473	-187.3	1	0	-
NiO	10.97	1	37.99	41.660	11.707	5.964	-234.2	1	-211.6	17
α-Quartz	22.69	1	41.46	73.488	0.782	15.376	-436.1	11	-856.3	2
β-Quartz	22.30	2	41.46	70.601	4.255	32.715	-421.1	11	-853.2	18
Corundum	25.57	1	50.92	116.336	11.983	19.514	-688.3	1	-1582.2	1
Hematite	30.28	2	87.49	84.429	92.839	1.987	-511.0	2	-745.3	2
Magnetite	44.52	2	160.33	376.660	-139.983	122.478	-2242.1	2	-1017.5	2
Kyanite	44.21	3	82.42	177.000	24.849	29.564	-1049.1	3	-2445.8	4
Sillimanite	50.02	3	96.77	169.439	28.903	25.623	-1002.8	3	-2440.7	4
Wollastonite	39.79	2	81.67	102.236	28.447	13.443	-605.9	2	-1549.2	2
Enstatite	31.35	2	66.32	118.248	11.159	20.280	-699.6	1	-1457.4	2
Ferrosilite	32.99	4	96.82	116.496	15.201	16.159	-686.3	12	-1116.2	18
Fayalite	46.15	5	152.13	156.620	35.066	15.619	-920.4	2	-1377.1	18
Diopside	66.11	6	142.72	230.948	22.916	34.840	-1361.3	13	-3025.0	19
Hedenbergite	67.85	7	173.59	214.116	48.359	24.698	-1262.0	14,15	-2678.8	20
Anorthite	100.79	2	199.28	263.706	62.848	31.468	-1556.7	2	-4010.9	18
Grossular	125.30	2	255.98	494.298	7.895	83.893	-2912.6	4	-6282.3	18
Andradite	131.67	8	316.82	470.395	46.903	63.743	-2765.6	16	-5413.2	20
Almandine	115.11	9	342.63	429.345	90.458	53.133	-2532.8	9	-4940.8	18
Pyrope	113.27	10	266.27	452.332	44.807	65.538	-2664.2	10	-5936.4	20

$$S^{\circ}_{T} = S^{\circ}_{298} + A\ \mathrm{Ln}(T) + B\ 10^{-3}T + C\ 10^{5}T^{-2} + D$$

1: Robie et al. 1979; 2: Robinson et al. 1982; 3: Robie and Hemingway 1984; 4: Anovitz and Essene 1987b; 5: Essene unpbl; 6: Levien and Prewitt 1981; 7: Cameron et al. 1973; 8: Huckenholz et al. 1974; 9: Metz et al. 1983; 10: Haselton and Newton 1980; 11: Hemingway 1987; 12: Bohlen et al. 1983c; 14: Krupka et al. 1985a, 1985b; 14: Bennington et al. 1984; 16: Haselton et al. 1987; 16: Robie et al. 1987; 17: Holmes et al. 1986; 18: Anovitz and Essene 1987; 19: Sharp et al. 1986; 20: this study

TABLE 2. Compressibility and thermal expansion data used in thermodynamic calculations

PHASE	a	b	ref.	c	d	e	f	ref.
Ni	0.535	0.900	21	1.092E-01	4.207E-03	1.663E-06	-5.856E-10	30
NiO	0.600	1.000	22	-3.570E-02	1.347E-03	-2.295E-08	-1.066E-10	31
α-Quartz	4.300	24.000	17	1.944E-03	3.274E-03	2.876E-06	6.922E-10	2
β-Quartz	0	0	17	3.861E-01	1.983E-02	2.562E-05	1.044E-08	2
Corundum	0.380	0	21	-7.526E-02	2.034E-03	0.876E-06	-3.160E-10	30
Hematite	0.509	0.454	2	9.682E-02	3.870E-03	1.066E-09	-1.402E-12	2
Magnetite	0.560	0	2	-6.156E-02	2.320E-03	3.481E-06	-1.486E-09	2
Kyanite	0.790	5.000	23	5.427E-02	2.144E-03	8.101E-10	-3.296E-10	32
Sillimanite	0.788	4.810	23	1.964E-02	7.618E-04	1.476E-06	-7.665E-10	32
Wollastonite	1.465	9.819	2	1.118E-01	5.009E-03	-4.166E-06	1.554E-09	2
Enstatite	1.010	0	2	4.569E-03	-3.2922E-04	5.928E-06	-2.534E-09	2
Ferrosilite	0.990	0	24	9.590E-02	3.822E-03	5.737E-11	2.778E-13	4
Fayalite	0.767	0.978	2	-2.810E-01	1.017E-03	3.881kE-06	-1.672E-09	2
Diopside	1.108	11.020	6,21,26	9.536E-02	4.005E-03	-1.420E-06	7.625E-10	7
Hedenbergite	2.117	31.313	26	-5.224E-02	4.148E-03	-4.245E-06	2.999E-09	7
Anorthite	1.087	0	27	1.566E-01	1.311E-03	-8.876E-08	2.075E-10	2
Grossular	0.721	3.200	2	-4.468E-02	1.761E-03	9.401E-07	2.674E-10	2
Andradite	0.725	0	28	-4.731E-02	2.107E-03	5.732E-07	7.252E-01	30
Almandine	0.571	0	4	4.541E-02	1.654E-03	1.231E-06	-3.023E-10	4
Pyrope	0.137	2.650	29	4.876E-02	2.084E-03	8.206E-07	-2.678E-10	30

$V^{P}_{298} = V^{o}_{298} (1 - aP10^{3} + bP^{2}10^{6})$, P kbar

$V^{T}_{i} = V^{o}_{298} + V^{o}_{298}/100\ [c + dT + eT^{2} + fT^{3}]$, T°C .

2, 4, 6, 7: Table 1; 21: Birch 1966; 22: Hazen and Prewitt 1977; 23: Brace et al. 1969; 24: Bass and Weidner 1984; 25: Hazen and Finger 1981; 26: Vaidya et al. 1978; 27: Liebermann and Ringwood 1976; 28: Babuska et al. 1978; 29: Hazen and Finger 1978; 30: Skinner 1966; 31: Nielson and Leipold 1965; 32: Winter and Ghose 1979

The loci of relevant equilibria were calculated with a computer program (EQUILI, Wall and Essene unpubl) that solves the relation

$$\Delta G^{P_2}_{T_2} - \Delta G^{P_1}_{T_1} = \int_{P_1}^{P_2} \Delta V dP - \int_{T_1}^{T_2} \Delta S dT$$

with an experimental reversal or a known Gibbs free energy of reaction as the starting point for the calculation. Using EQUILI, reactions are then calculated at 1 bar, 298 K in order to obtain the Gibbs free energy (ΔG°_{298}) of each reaction. Algebraic combinations of the reactions allows calculation of the ΔG°_{298} of each phase assuming that the ΔG°_{298} of quartz and other simple phases (e.g., hematite, magnetite, wollastonite) are known (Robie et al. 1979, Robinson et al. 1982). Equilibria for which there are no experimental reversals can then be calculated at high P and T using the 1 bar, 298 K data as a starting point.

Thermodynamic data for hedenbergite (Tables 1, 2) are constrained by the following experiments in the system Ca–Fe–Si–O:

Andradite = Wollastonite + Hematite (11)

$Ca_3Fe_2Si_3O_{12} = 3\ CaSiO_3 + Fe_2O_3$

(Huckenholz et al. 1974, Suwa et al. 1976),

Andradite = Wollastonite + Magnetite + O_2 (12)

$6\ Ca_3Fe_2Si_3O_{12} = 18\ CaSiO_3 + 4\ Fe_3O_4 + O_2$

(Gustafson 1974),

Andradite + Magnetite + Quartz = Hedenbergite + O_2 (13)

$3\ Ca_3Fe_2Si_3O_{12} + Fe_3O_4 + 9\ SiO_2 = 9\ CaFeSi_2O_6 + 2\ O_2$

(Burton et al. 1982), and,

Andradite + Quartz = Hedenbergite + Wollastonite + O_2 (14)

$2\ Ca_3Fe_2Si_3O_{12} + 4\ SiO_2 = 4\ CaFeSi_2O_6 + 2\ CaSiO_3 + O_2$

(Liou 1974).

The calculated position of these reactions in fO_2–T space at 2 kbar (relative to MH) are shown in Fig. 1, along with the calculated position of the NNO and QFM buffers. The HM and QFM buffers are calculated from data in Robinson et al. (1982, Table 1), and the NNO buffer is calculated from the solid state electrochemical measurements of Holmes et al. (1986, Table 1). All buffers were corrected for pressure and temperature using the expansivity and compressibility data in Table 2.

Thermodynamic data for hematite, magnetite, and wollastonite are taken from Robinson et al. (1982), and data for andradite and hedenbergite are compiled from sources listed in Table 2. The $\Delta G^\circ_{.298}$ for andradite was calculated from Reaction 11 using the experimental reversal of Huckenholz et al. (1974) (1 bar, 1137±5°C) as a starting point, yielding $\Delta G^\circ_{.298}$ (And) = −5413.2 kJ/mol. If the reversal of Suwa et al. (1976: 1bar, 1165°C) is used as a starting point, the free energy of andradite changes by −0.3 kJ. Use of the latter value for $\Delta G^\circ_{.298}$ (And) shifts Reaction 12 to higher temperature, increasing the discrepancy between the experimental reversal for Reaction 12 and its calculated position (Fig 1). Therefore, we have used the reversal of Huckenholz et al. (1975) as the reference point for $\Delta G^\circ_{.298}$ (And).

The experimental reversal at 800°C of Burton et al. (1982) for Reaction 13 was selected as the starting point for the calculation of $\Delta G^\circ_{.298}$ (Hd), and the calculated position of Reaction 13 is in good agreement with the reversals at 600 and 700°C (Fig 1). The position of Reaction 14 was calculated using the $\Delta G^\circ_{.298}$ (Hd) (−2677.7 kJ/mol) determined from these latter experimental constraints. Assuming that the reversals of Burton et al. (1982) are reliable, there is a discrepancy of 1.5 log units between the calculated position of Reaction 14 and the experimental reversals of Liou (1974) (Fig. 1) that is not ascribable to errors in the thermodynamic data. The direction of the shift suggests that the synthetic andradite used in the experiments of Liou (1974) may not be stoichiometric andradite with

Figure 1. fO_2–T equilibria at 2 kbar in the system Fe–Si–Ca–O (relative to MH buffer) that constrain ΔG°_{298} of hedenbergite and andradite. Vertical bars: reversals of Gustafson (1974) for And = Wo + Mt + O_2; diamonds: reversals of Liou (1974) for Hd + Wo = And + Qz + $2O_2$; triangles: reversals of Burton et al. (1982) for Mt + And + Qz = Hd + O_2. Note disparity between calculated and experimental positions of the latter reactions as denoted by arrows between reversals and reactions to which they correspond.

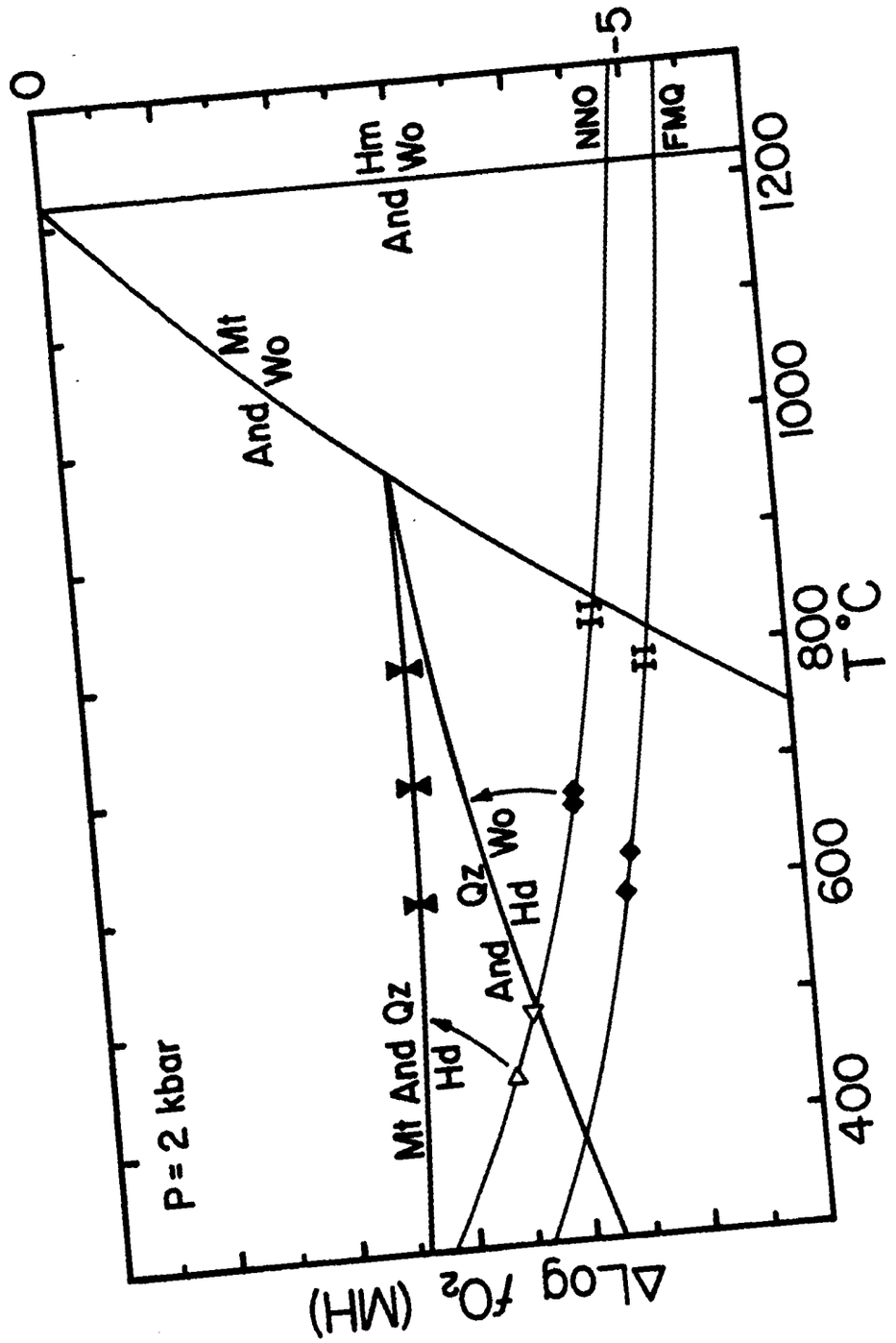
0
-5
Hm
Wo
And
NNO
FMQ
1200
Mt
Wo
And
1000
800
T°C
Qz
Wo
And
Hd
600
Mt And Qz
Hd
P = 2 kbar
400
ΔLog fO2 (MH)

possible substitutions of the nature $Fe^{+2}Fe^{+3}$–$CaFe^{+2}$ or $(OH)_4^{-4}$–(SiO_4^{-4}). The reactants used in the experiments of Burton et al. (1982) were stoichiometric, but analyses of run products for Reaction 13 are not given. More thorough characterization of the run products for all experiments or new experiments in the Ca–Fe–Si–O system are required in order to resolve the discrepancy. Further calculation of reactions involving hedenbergite rest on the assumption of the choice of experimental constraints used here.

Using a slightly different experimental and thermodynamic data base, Robie et al. (1987) obtained values for $\Delta G^\circ_{.298}$ (And) = −5414.8 ± 5.5 and $\Delta G^\circ_{.298}$ (Hd) of −2674.3 ± 5.8 kJ/mole. The values differ somewhat from ours because we have included the effects of thermal expansion and compressibility in our calculation, and have started with a different thermodynamic data base. Helgeson et al. (1978) report values of $\Delta G^\circ_{.298}$ (And) = −5428.7 kJ/mol and $\Delta G^\circ_{.298}$ (Hd) = −2674.5 kJ/mol.

Volume and entropy data for pyrope are taken from Haselton and Westrum (1980) and Haselton and Newton (1980). The Gibbs free energy of pyrope was calculated from experimental data on the reaction

Enstatite + Corundum = Pyrope (15)

$$3\ MgSiO_3 + Al_2O_3 = Mg_3Al_2Si_3O_{12}$$

(Gasparik and Newton 1984), using thermodynamic data for enstatite from Robinson et al. (1982) and data for corundum from Robie et al. (1979).. In the system MgO–Al_2O_3–SiO_2 (MAS), enstatite contains significant solid solution of Mg–Tschermak's component ($Mg_{0.5}AlSi_{0.5}O_3$) (Boyd and England 1964, Hensen and Essene 1971, Anastasiou and Seifert 1972, MacGregor 1974, Danckwerth and Newton 1978, Lane and Ganguly 1980, Perkins and Newton 1980, Perkins et al. 1981, Perkins 1983). In order to calculate the location of the end member Reaction (15) one must correct for the reduction in enstatite activity. Aranovich and Kosyakova (1987) have recently published activity–composition relations for orthopyroxene that are based on experimental equilibria in the MAS and FMAS systems. For the range of aluminum

contents encountered in the above experimental studies the model of Aranovich and Kosyakova (1987) yields activity coefficients for the $MgSiO_3$ component in enstatite–Mg–Tschermak's solid solutions ($\gamma^{Opx}_{MgSiO_3}$) that are slightly less than one, suggesting only slight departures from ideality. However, the difference between the ideal model and the model of Aranovich and Kosyakova (1987) may yield significant differences in the Gibbs energy of pyrope because reactions involving pyrope and enstatite are extremely sensitive to changes in pressure. We have employed the latter model in the calculations to follow.

Using the midpoint of the reversal for Reaction 15 (Gasparik and Newton 1984, 850°C and 16.25±0.25 kbar, X^{En}_{MgTs} = 0.06) as a starting point for the calculation, the shift in position of Reaction 15 due to orthopyroxene solid solution was calculated from the relation

$$RT\ln(K_2/K_1) = \int_{P_1}^{P_2} \Delta V dP$$

where K_2 = 1 for the position of the corrected reversal,

$$K_1 = (1/a^{Opx}_{MgSiO_3})^3,$$

and pyrope, sillimanite and quartz are assumed to be pure phases. For these calculations we have followed the convention of Hensen and Essene (1971) and Aranovich and Kosyakova (1987) by writing the formula of enstatite and Mg–Tschermak based on 2 cations (see Appendix I). The location of Reaction 15, adjusted to pure enstatite, is at 12.7 kbar, 850°C, and serves as the starting point for calculation of the Gibbs free energy of pyrope. The calculated value of ΔG°_{298} (Reaction 15) is 18.1 kJ/mol, yielding ΔG°_{298} (Py) = −5936.4 kJ/mol. As in deriving the Gibbs energy of hedenbergite, the Gibbs energy for pyrope is dependent on our choice of experiments and Gibbs free energies for enstatite and corundum.

Wood and Holloway (1984) present an analysis of equilibria in the CMAS system, deriving an ΔH°_{1000} for pyrope (relative to oxides) of −84.9 kJ/mol ($S_{1000\ K}$ =

777.8 J/mol, Haselton and Newton 1980). Using enthalpy and entropy data for the oxides (Robie et al. 1979), this yields ΔG°_{1000} (Py) for the study of Wood and Holloway of −87.8 kJ/mol, in fair agreement with the value derived in this study (ΔG°_{1000} = −83.4 kJ/mol, ΔH°_{1000} = −79.3 kJ/mol).

Newton (1987) has re-evaluated experiments in the system $MgO-Al_2O_3-SiO_2$ that constrain ΔH°_{298} and ΔG°_{298} of pyrope and enstatite. Based on analysis of the available experimental and thermochemical data base Newton (1987) obtains values for ΔH°_{298} (Py) and ΔH°_{298} (En) (relative to oxides) of −74.2 and −32.7 kJ/mol, respectively. Combined with entropy data for these phases the calculated values of ΔG°_{298} (oxides) are −77.2 and −32.1, respectively. Our values of ΔG°_{298} are in very good agreement with those of Newton (1987): −77.7 and −31.9 for pyrope and enstatite, respectively. The same experimental data base was used in both studies, but different values of S°_{298} for enstatite were used and the mechanics of calculating the location of the equilibria using EQUIL1 differ slightly from the method used by Newton (1987).

Other thermodynamic compilations yield Gibbs free energies for enstatite that are in good agreement with the values used in this study. Berman et al. (1986) give a value for ΔG°_{298} (En) = −1458.5 kJ/mol, and Helgeson et al. (1978) report a value of −1459.9 kJ/mol.

The free energies of pyrope and enstatite have also been evaluated using the experimentally reversed equilibrium

$$\text{Enstatite} + \text{Sillimanite} = \text{Pyrope} + \text{Quartz} \qquad (16)$$
$$3\ MgSiO_3 + Al_2SiO_5 = Mg_3Al_2Si_3O_{12} + SiO_2$$

(Hensen and Essene 1971; Perkins 1983), with various estimates of the high temperature heat capacity of pyrope. There are some significant disparities between the experiments of Hensen and Essene (1971) and Perkins (1983) on Reaction 16, and among the possible high temperature extrapolations for the entropy of pyrope in the temperature range of the available experiments (Haselton and Newton 1980;

Figure 2. Experimental constraints on S°_{298} and ΔG°_{298} for pyrope. Filled squares: adjusted reversals of Hensen and Essene (1971: HE); open circles: adjusted reversals of Perkins (1983) using quoted Al_2O_3; filled circles: adjusted reversals of Perkins (1983) using Al_2O_3 contents of Hensen and Essene (1971) for that temperature. Lines represent position of Reaction 16 using different extrapolations of high temperature heat capacity for pyrope. BB: Berman and Brown (1985); RH: Robinson and Hass (1983); HN: Haselton and Newton. Lowest line is 0.3% increase in HN extrapolation.

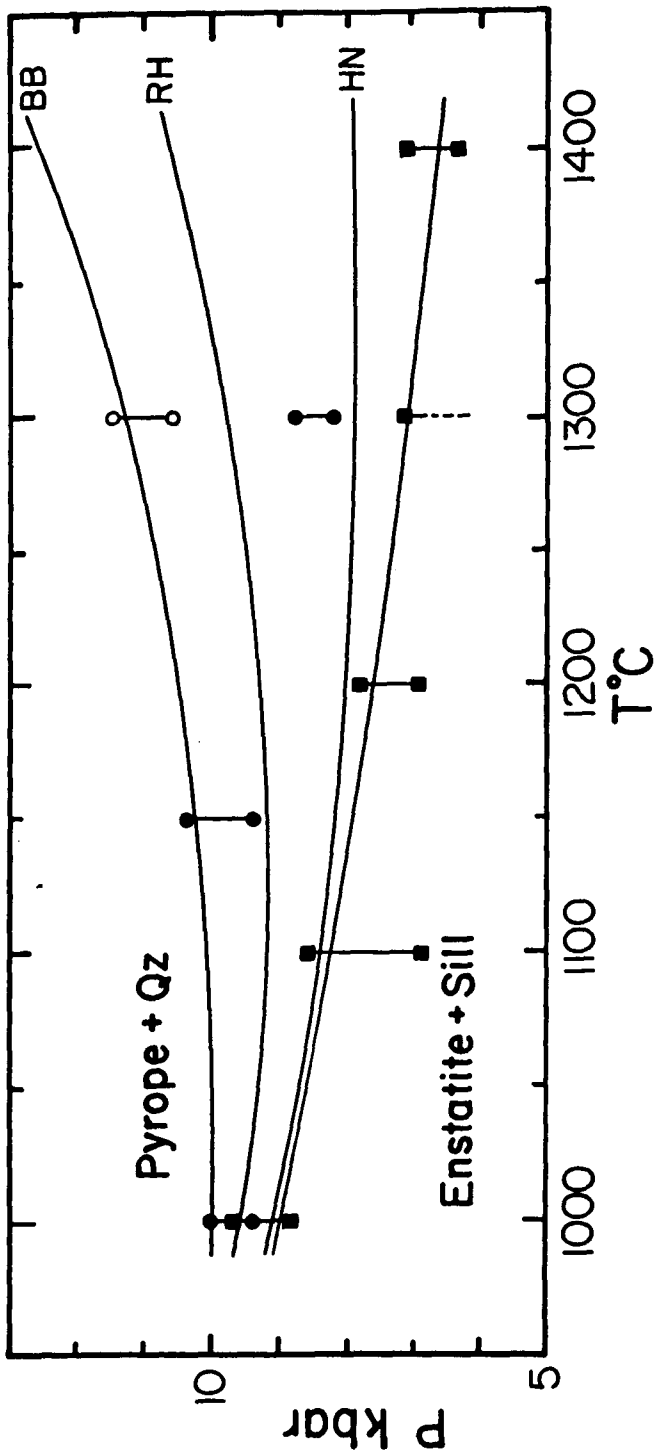
BB
RH
HN
Pyrope + Qz
Enstatite + Sill
1000
1100
1200
1300
1400
T°C
10
5
P kbar

Robinson and Haas 1983; Berman and Brown 1985). However, both experimental data sets (adjusted for the Al content of the orthopyroxene using the methods discussed above) and the various heat capacity expressions converge at 1000°C. The thermodynamic data used in the present study for pyrope (with the heat capacity of pyrope from Haselton and Newton 1980) and enstatite are in very good agreement with both sets of experiments at 1000°C.

The experimental reversals for Reaction 16 lie outside of the temperature range for heat capacity data on pyrope (greater than 1200 K: Haselton and Newton 1980). The high temperature end of the heat capacity expression of Haselton and Newton (1980) is based on an arbitrary extrapolation (Haselton, pers comm 1987), but a thermodynamically based extrapolation is preferred. Robinson and Haas (1983) present an empirical estimation scheme for calculating heat capacities and entropies based on the relative contribution of various oxides in different crystal chemical coordinations within a lattice. However, constraints on the lattice contribution to heat capacity from Mg in 8-coordination as in garnet are derived solely from Haselton's (1979) data and should not be extrapolated above 1200 K. Berman and Brown (1985) present an alternative method of extrapolating C_p data. We have tested the effect of each of these extrapolation methods against the original heat capacity expression of Haselton and Newton (1980) on the shift in the location of Reaction 16 (Fig. 2).

Experimental reversals for Reaction 16 were adjusted for MgTs component in a manner similar to Reaction 15. We have used the analyzed MgTs contents for the aluminous enstatite produced in the experiments of Hensen and Essene (1971) to correct the positions of Perkins' (1983) reversals at 1000° and 1150°C, as these latter pyroxenes produced in the experiments were not analyzed. The location of the adjusted experimental reversals are presented in Fig. 2, along with the calculated position of Reaction 16 based on the heat capacity expressions of Haselton and Newton (1980; HN), and extrapolations based on Robinson and Haas (1983; RH) and Berman and Brown (1985; BB). The differences in calculated entropy at 1600 K

between the RH, and RH and BB extrapolations is only +0.6 and 0.9% of the HN value, respectively. Above approximately 1000°C these apparently small differences produce a significant change in sign and magnitude of the slope of Reaction 16. The heat capacity expression of HN approaches the adjusted position of the reversals of Hensen and Essene (1971) and the BB extrapolation gives a reasonably good fit to the adjusted reversals of Perkins (1983). Increasing the entropy at 1800 K obtained from the HN expression by 0.3%, and smoothing the entropy data by eye to 1400 K yields a reasonable fit to the adjusted experiments of Hensen and Essene (1971: Fig. 2).

The apparent discrepancy in the experimental data base for Reaction 16 makes the choice of high temperature values for the entropy of pyrope rather subjective. Both the experiments and entropy data converge near the lower temperature range of the experiments where the original data for pyrope were obtained and where the data will be applied to granulites. Therefore, we retain the heat capacity expression of Haselton and Newton (1980). Because the calculations tend to converge in the temperature range of the reversal for Reaction 15, the various heat capacity expressions change the Gibbs free energy of pyrope by less than 1.5 kJ.. Clearly, more complete characterization of synthetic reactants and experimental products for Reaction 15, or high temperature (> 1200 K) calorimetry on pyrope are needed in order to resolve the discrepancy.

Geobarometry

Clinopyroxene Barometers

The positions of Reactions 1, 2, and 3 were calculated using 1 bar, 298 K as a starting point (Figs. 3a – 3c). The clinopyroxene reactions have average slopes ($\Delta P/\Delta T$) of 23 (HD) and 20 bar/°C (DI). These slopes are not as low as Reaction 3 (14.5 bar/°C), but are still useful for geobarometry, with the HD barometer having the greatest temperature dependency of the three barometers. The calculated slopes become less steep at lower pressure and more negative values of $\log_{10}K$

Figure 3a-c. Calculated position and values of $\log_{10}K$ for Reactions 1 through 3. a: HD barometer; b: DI barometer; c: FS barometer.

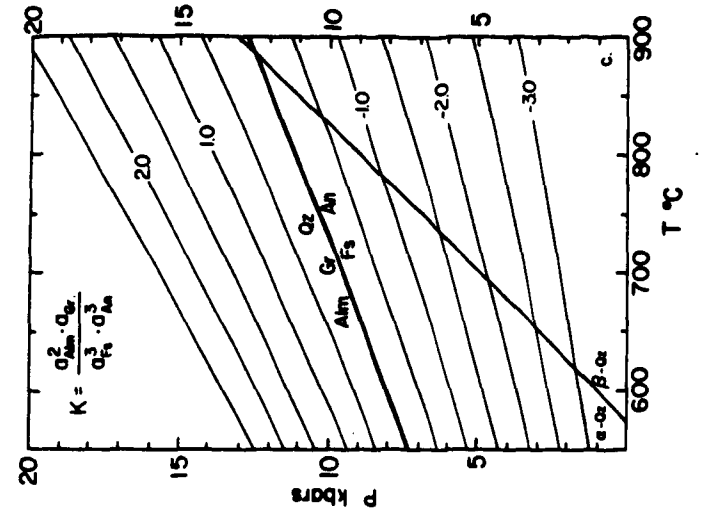
P kbars
T °C
c.
Qz
An
Gr
Fs
Alm
α-Qz
β-Qz
-1.0
-2.0
-3.0
1.0
2.0

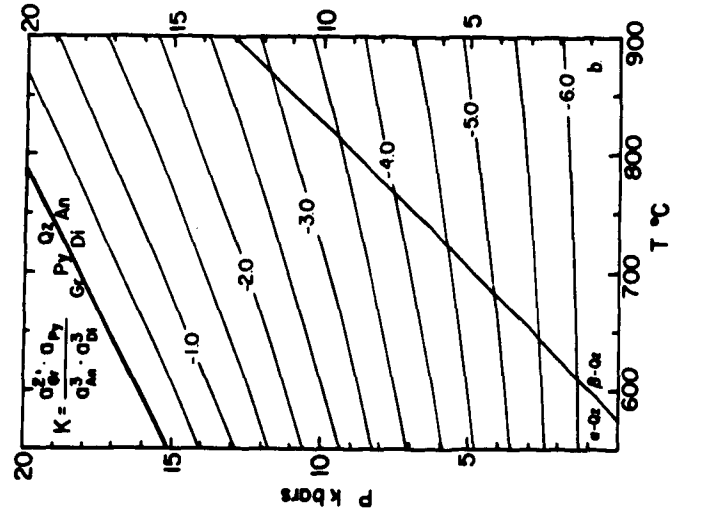
P kbars
T °C
b
Qz
An
Gr
Py
Di
α-Qz
β-Qz
-1.0
-2.0
-3.0
-4.0
-5.0
-6.0

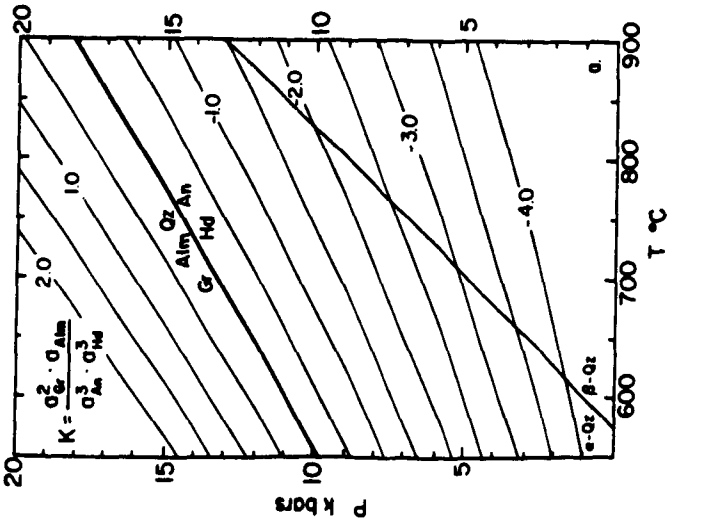
P kbars
T °C
a.
Qz
An
Gr
Alm
Hd
α-Qz
β-Qz
1.0
2.0
-1.0
-2.0
-3.0
-4.0

(Fig. 3), particularly for the FS and DI barometers. An uncertainty of 5 kJ in the value of ΔG°_{298} (rxn) results in an uncertainty of approximately 0.7 kbar for both Reactions 1 and 2. Uncertainties of 5 kJ in the ΔG°_{298} for any phase involved in the reaction will yield an uncertainty of 0.7 kbar per mole of that phase in Reactions 1 and 2.

Activity Models

Application of these equilibria to natural systems requires consideration of the reduction in activity of end member components due to solid solutions in plagioclase, garnet, orthopyroxene, and clinopyroxene. Included in Figs. 3a, 3b, and 3c are the calculated positions for values of $\log_{10}$ of the equilibrium constant K for each reaction. For example K is defined for Reaction 1 by the relation:

$$K = \{([a^{Gt}_{Ca_3Al_2Si_3O_{12}}]^2[a^{Gt}_{Fe_3Al_2Si_3O_{12}}])/([a^{Pg}_{CaAl_2Si_2O_8}][a^{Cpx}_{CaFeSi_2O_6}])\}^3$$

Variations in $\log_{10}K$ with pressure were calculated from the relation:

$$RT\ln(K_2/K_1) = \Delta G^{P_2}_{T_2} - \Delta G^{P_1}_{T_2} = \int_{P_1}^{P_2} \Delta V dP$$

Given appropriate activity models for plagioclase, garnet, and pyroxene, the equilibrium constant can be calculated from analyses of the coexisting phases, and with an estimate of temperature the pressure can be read from Figure 3.

The activity models for plagioclase, garnet, or pyroxene will ultimately limit the accuracy and precision of a geobarometer. The models of Newton et al. (1980) or Orville (1972) for plagioclase, Perkins (1979), Newton and Haselton (1981), or Ganguly and Saxena (1984) for garnet, and an ideal two site approximation (e.g., Wood and Banno, 1973) for pyroxenes are typically selected by most workers. For this study the plagioclase activity model of Newton et al. (1980) (Appendix 4) was used in evaluation of the geobarometers. At 700°C and constant garnet and pyroxene activities, this latter plagioclase activity model yields slightly lower pressures (on the order of 0.1 kbar) than that of Orville (1972).

The quaternary garnet mixing model of Ganguly and Saxena (1984) with modified values for Ca–Fe mixing parameters (Anovitz and Essene, 1987a) was used to calculate the activity of $Ca_3Al_2Si_3O_{12}$, $Fe_3Al_2Si_3O_{12}$, and $Mg_3Al_2Si_3O_{12}$ in garnet, and to calculate the position of the FS reaction (Reaction 3). The derivation of these parameters are discussed by Anovitz and Essene (1987a), and analytical expressions for calculating activities are outlined in Appendix 4. The model used here typically yields $Ca_3Al_2Si_3O_{12}$ and $Fe_3Al_2Si_3O_{12}$ activities 1 to 5% greater than values obtained from the original formulation of Ganguly and Saxena (1984).

Activity coefficients for $Mg_3Al_2Si_3O_{12}$ in garnet (γ^{Gt}_{Mg}) obtained from the model of Ganguly and Saxena (1984: GS) are significantly greater than those obtained from the model of Haselton and Newton (1980: HN). For a garnet of composition $Alm_{50}Py_{25}Gr_{25}$ at 700°C, γ^{Gt}_{Mg} (GS) = 1.7 and γ^{Gt}_{Mg} (HN) = 1.3. This difference is due to the sign for the ternary constants as discussed by Ganguly and Saxena (1984, p 94, eq 16). If the sign of the ternary constant in the expression for γ^{Gt}_{Mg} is changed from that given in Ganguly and Saxena (1984), one obtains similar values for γ^{Gt}_{Mg} for the two models. This discrepancy needs further evaluation. In general, use of the GS model as it now stands yields significantly greater pressures than the HN model for the DI barometer, all other factors being equal.

Chatillon–Colinet et al. (1983) proposed that an ideal mixing approximation for Mg–Fe orthopyroxenes is consistent with solution calorimetric data on orthopyroxene solid solutions. Therefore the activity of $FeSiO_3$ in orthopyroxene was calculated using the ideal model of Wood and Banno (1973) (Appendix II). Davidson and Lindsley (1985) have modeled the phase equilibria of quadrilateral pyroxenes in order to derive a pyroxene activity model. Although Davidson and Lindsley do not present an explicit analytical formulation for activity coefficients similar to garnet and plagioclase, we obtained a computer program (PM Davidson pers comm 1987) that calculates activities of $Fe_2Si_2O_6$, $Mg_2Si_2O_6$, $CaFeSi_2O_6$, and $CaMgSi_2O_6$ for quadrilateral pyroxene. The pyroxene projection scheme of Lindsley (1983) was used to calculate mole fractions of Wo, En, and Fs, the components

upon which the activity model of Davidson and Lindsley (1985) is calculated. The pyroxene activity model of Davidson and Lindsley (1985) yields activities of $a^{Opx}_{Fe_2Si_2O_6}$ that are similar to or only slightly less than ideal two site activities calculated with the Wood and Banno (1973) model (Fig. 4a).

Activities of $CaFeSi_2O_6$ and $CaMgSi_2O_6$ were also calculated using a modified ideal model, in comparison with the model of Davidson and Lindsley (1985). Ideal $CaFeSi_2O_6$ activities were approximated by the relationship

$$a^{Cpx}_{CaFeSi_2O_6} = [X^{M2}_{Ca}][X^{M1}_{Fe^{2+}}] \quad (17)$$

where $X^{M1}_{Fe^{2+}}$ = Fe^{2+} − (1− Ca − Na − Mn), X^{M2}_{Ca} = Ca, and Ca, Na, Mn, and Fe^{2+} are the number of atoms of the respective cations. Pyroxene analyses taken from the literature are re-normalized to four cations, and values of ferric and ferrous iron were calculated from charge balance and stoichiometry. Analyses taken from the literature were of varying quality, and not all of these pyroxenes were analyzed for Na, which usually occurs in significant quantities in high grade clinopyroxenes. Failure to analyze for Na will affect the calculation of Fe^{2+} and Fe^{3+}, and ultimately the value of $X^{M2}_{Fe^{2+}}$. Ideal $CaMgSi_2O_6$ activities were calculated as

$$a^{Cpx}_{CaMgSi_2O_6} = [X^{M2}_{Ca}][X^{M1}_{Mg}]. \quad (18)$$

where X^{M2}_{Ca} = Ca and X^{M1}_{Mg} = Mg, based on a 4-cation pyroxene formula. The clinopyroxene model is based on crystal chemical observations on igneous pyroxenes that iron and magnesium do not mix ideally on the M1 and M2 sites, with iron showing a greater tendency relative to magnesium to partition into the M2 site (Cameron and Papike 1980, Dal Negro et al. 1982). Although there are no cation partitioning data on granulite facies augites, one might predict that the ordering would be even more pronounced in granulite facies augites compared to igneous augites, as temperatures are lower and cooling histories are likely to be slower for the former. Single crystal refinements and Mossbauer studies of homogeneous natural pyroxenes from the granulite facies are needed to evaluate this assumption.

Figure 4a-c. Ideal activities of ferrosilite, hedenbergite, and diopside (e.g., a_{Hd} ideal) versus activities calculated using model of Davidson and Lindsley (1985).

Figure 4d, 4e Ideal activities of hedenbergite and diopside versus Davidson and Lindsley activities adjusted for non-quadrilateral components (DL').

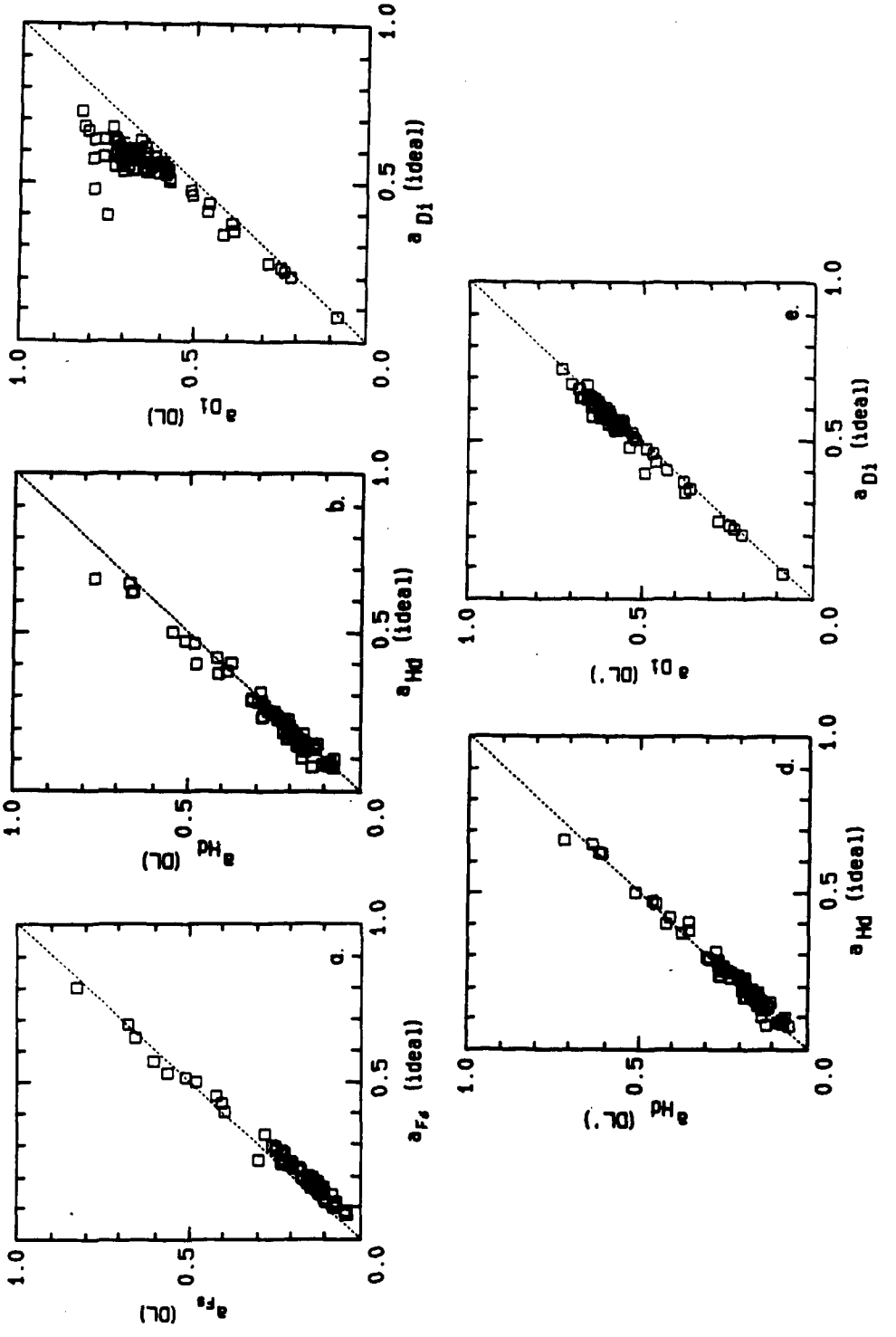
a.
b.
c.
d.
e.
a_{Fe} (ideal)
a_{Hd} (ideal)
a_{Di} (ideal)
a_{Fe} (DL)
a_{Hd} (DL)
a_{Di} (DL)
0.0
0.5
1.0

Activities of $CaFeSi_2O_6$ in Cpx ($a^{Cpx}_{CaFeSi_2O_6}$) calculated with the model of Davidson and Lindsley (1985) yield $a^{Cpx}_{CaFeSi_2O_6}$ that are usually similar to or slightly greater than values obtained using the ideal approximation (Fig. 4b). The values for $a^{Cpx}_{CaMgSi_2O_6}$ calculated from the model of Davidson and Lindsley (1985) are generally greater than ideal activities (Fig. 4c). The scatter in $a^{Cpx}_{CaMgSi_2O_6}$ is an artifact of the projection scheme used to correct natural compositions to those appropriate for the activity model. The effect of subtracting non-quadrilateral components (mainly Al, Na, and Fe^{3+} in granulite facies pyroxenes) in the projection scheme is to overestimate the amount of quadrilateral pyroxene components, and this projection scheme is not strictly valid for clinopyroxenes with a large fraction of non-quadrilateral components (Lindsley 1983). The greatest departure from quadrilateral space is for aluminous and sodic pyroxenes in granulites from Doubtful Sound, N.Z., in granulite xenoliths from Lesotho, and from the Westchester Prong, PA, granulites. When the Davidson and Lindsley (1985) activities are reduced by an amount equal to the mole fraction of non-quadrilateral components ($1 - Al^{vi} - 2Ti - Fe^{3+} - Mn$), the degree of scatter is significantly reduced (Figs. 4d, 4e).

Evaluation of Barometers

Pressures were calculated using the Gt-Cpx-Pg-Qz (HD, DI) barometers (Reactions 1 and 2) and the Gt-Opx-Pg-Qz (FS) geobarometer (Reaction 3) for 68 samples with Gt-Cpx-Opx-Pg-Qz assemblages (Tables 3 and 4). Widespread application of the FS barometer in the Central Gneiss Belt of the Grenville Province of Ontario has yielded pressures that are in good agreement with aluminosilicate occurrences and other geobarometers (Anovitz and Essene, 1987b). The FS barometer also yields pressures that are consistent with reported aluminosilicate occurrences for the terranes studied here (Table 3) and previous estimates of pressure for other terranes (Table 4).

Figure 5a. Pressure obtained for FS barometer with ideal fs activities (P_{Fs}ideal) versus pressure obtained with model of Davidson and Lindsley (P_{Fs}DL).

Figure 5b. Pressure obtained for HD barometer vs. those for FS barometer, both with ideal approximation for pyroxene activities.

Figure 5c. Pressure obtained for DI barometer vs. those for FS barometer, both with ideal approximation for pyroxene activities.

Figure 5d. Pressure obtained for HD barometer vs. those for FS barometer, with HD activities adjusted for non-quad components (DL') and ideal ferrosilite activities

Figure 5e. Pressure obtained for DI barometer vs. those for FS barometer, with DI activities adjusted for non-quad components (HD') and ideal diopside activities.

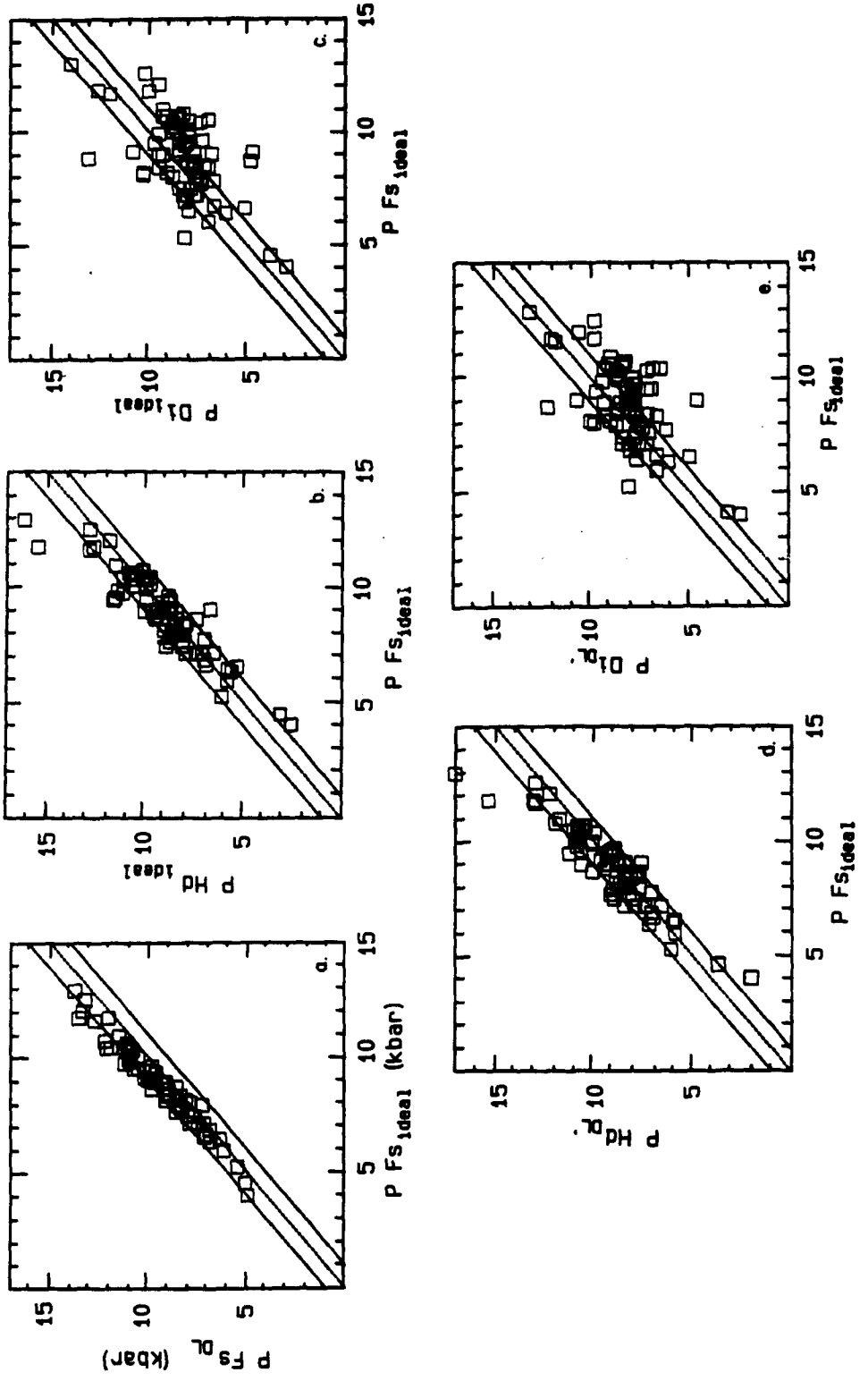
a.
b.
c.
d.
e.
P Fs$_{DL}$ (kbar)
P Hd$_{ideal}$
P Di$_{ideal}$
P Hd$_{P.}$
P Di$_{P.}$
P Fs$_{ideal}$ (kbar)
5
10
15

TABLE 3. Sources of analytical data on Gt-Cpx-Opx-Pg-Qz assemblages and quoted aluminosilicate occurrences used to evaluate geobarometers of this study.

TERRANE	SAMPLES	REF	ALS[1]	T°C/P kbar[2]
Grenville Province				
Parry Sound ONT	S3B O15B S10B M65 S32 S86E33	1	Sil	800/<9.8
Otter Lake QUE	A12 DL2	2	Sil	700/<7.8
Adirondack Mts NY				
Highlands	BM2 BM13 ET15 ET24 LL6 MM4 MM18 PH4 SL5 SL26 SR31 WO	3	Sil	800/<9.8
Lowlands	74C248B	4	Sil	700/<7.8
Pikwitonei Belt MAN	A41 C104 D50 D110 E18	5	Sil	800/<9.8
India				
Sargur Belt	S33	6	-	
	S3 S4	7	Ky/Sil	700/<7.8
Karnataka	113E GN4A	8	-	
	DT MB GV2	9	-	
Nilgiri Hills	332 352 680	10	Sil	750/<8.8
Mysore	K21	11	-	
Bengal	SM4B SM44B	12	Sil	700/<7.8
Furua Complex TANZ	MF283.3 MF268.1 WE322.3 ZC.8 DMa40 C247.1 C311.1 C352.2	13	Ky/Sil	800/9.8
Westchester PA	74-67 -71 -207A -322C	14	Ky	650/>6.8
Wind R. Range WY	A22	15	Sil	700/<7.8
SW Minnesota	DM4C2	16	Sil	700/<7.8
Lesotho	LT2	17	-	
Oaxacan Complex	16076 25277 169076	18	Sil	730/<8.3
West Greenland				
Buksefjorden	174087	19	Sil	800/<9.8
	174102		Ky/Sil	600/6.3
Isortoq	88589 91141	20	-	
Finnish Lapland	47III 66II	21	Sil	750/<8.8
Doubtful Sound NZ	36461 36468	22	-	
Broken Hill	911 10770	23	Sil	800/<9.8

1: ALS = aluminosilicate: Ky = kyanite, Sil = fillimanite. 2: Quoted T with P constraint.
1: Moecher (1988); 2: Perkins (1979); 3: Bohlen (1979); 4: Stoddard (1976);
5: Paktunc and Baer (1986); 6: Janardhan and Gopalkrishna (1983); 7: Srikantappa et al. (1985);
8: Janardhan et al. (1982); 9: Hansen et al. (1984); 10: Harris et al. (1982);
11: Devaraju and Coolen (1983); 12: Bhattacharya and Mukherjee (1987); 13: Coolen (1980);
14: Wagner and Srogi (1987); 15: Sharp (1988); 16: Moecher (1984); 17: Griffen et al. (1979);
18: Mora and Valley (1986); 19: Wells (1977); 20: Glassley and Sorensen (1980);
21: Hormann et al. (1980); 22: Oliver (1977); 23: Phillips (1980).

TABLE 4. Comparison of quoted pressures from other Opx-Pg-Gt-Qz barometers with orthopyroxene and clinopyroxene barometers of this study (using ideal pyroxene activities). References as in Table 3. nd = pressure not determined.

LOCALITY	REF	BWB-FS	PC-FS	MAE-FS	NP-EN	PC-EN	MAE-HD	MAE-DI
Parry Sound	1	nd	nd	7.5 - 11.7	nd	nd	8.1 - 12.8	8.2 - 12.0
Otter Lake	2	8.1, <8.4	8.0, <7.5	8.4, <8.5	6.6, <8.1	9.7,<9.1	8.5, <7.9	7.8, <7.2
Adir. High.	3	7.1 - 8.2	7.1 - 8.6	6.5 - 8.8	8.5 - 9.9	10.4 - 11.5	5.8 - 9.5	7.4 - 13.1
Adir. Low.	4	6.6	nd	6.4	6.1	nd	5.6	6.1
Pikwitonei*	5	6.6 - 9.2	7.9 - 11.7	6.6 - 9.1	7.1 - 9.5	11.1 - 12.8	5.3 - 9.4	4.7 - 8.3
Sargur*	6	nd	nd	9.0	9.0	nd	10.1	8.3
	7	nd	nd	10.5, 10.5	9.1, 9.1	nd	9.7, 10.1	7.0, 7.1
Karnataka*	8	9.0, 9.2	10.0, 9.5	9.5, 10.4	8.3, 9.5	9.4, 9.8	8.7, 10.7	8.1, 8.8
	9	nd	nd	8.4 - 9.1	9.1, 9.1	nd	8.0 - 8.7	7.0 - 7.7
Nilgiri*	10	nd	nd	9.0 - 10.2	6.9 - 8.8	nd	9.1 - 10.0	8.5 - 9.5
Mysore*	11	nd	nd	12.1	9.9	nd	11.8	9.5
Bengal*	12	nd	nd	7.5, 7.2	6.2, 6.3	nd	8.9, 7.9	7.9, 7.6
Furua Complex	13	9.6 - 11.4	9.9 - 12.1	10.1-12.6	9.4 - 12.7	9.8 - 11.6	9.9 - 12.8	7.4 -10.2
Westchester*	14	8.9 - 9.6	9.8 - 10.8	9.6 - 10.0	5.6 - 9.4	9.1 - 12.3	9.9 - 11.5	7.3 - 8.8
Wind R Range*	15	5.0	nd	5.3	nd	nd	6.1	8.2
Minn R Valley*	16	nd	nd	6.0	nd	nd	5.8	7.0
Lesotho	17	nd	nd	11.8	10.1	nd	12.6	10.0
Oaxaca Complex*	18	6.3 - 7.3	nd	7.3 - 8.0	7.5 - 7.8	nd	7.0 - 8.0	6.7 - 8.0
Buksefjorden	19	8.3, 7.4	9.3, 8.5	9.5, 8.7	7.6, 7.5	9.2, 8.6	11.6, 7.4	9.1, 4.8
Isortoq	20	nd	nd	7.7, 7.7	7.6, 8.3	nd	8.1, 8.7	7.4, 7.6
Finnish Lapland	21	7.6, nd	7.9, 8.0	9.0, 9.0	7.3, nd	9.1, 9.1	8.8, 9.6	8.5, 9.2
Doubtful Sound	22	11.2, 9.6	11.2, 12.7	13.0, 11.8	12.1	12.5, 12.7	16.1, 15.4	14.0, 12.6
Broken Hill	23	nd	nd	4.5, 4.0	nd	nd	3.0, 2.5	3.8, 3.0

*:pressure quoted by reference for a particular locality otherwise pressure quoted by authors of calibration.
NP: Newton & Perkins (1982) Mg-opx + Pg = Gt + Qz barometer
BWB: Bohlen, Wall and Boettcher (1983a) Fe-opx + Pg = Gt + Qz barometer
PC: Perkins and Chipera (1985) Fe-opx and Mg-opx + Pg = Gt + Qz barometer
MAE: Moecher, Anovitz and Essene, this study, FS, HD, and DI barometers

Shown in Fig. 5a are pressures obtained from the FS barometer as calculated for the different models for $a^{Opx}_{Fe_2Si_2O_6}$. Using the Davidson and Lindsley (1985: DL) model one obtains slightly greater pressures than with the ideal model, with the greatest departures being at high pressures (low $a^{Opx}_{Fe_2Si_2O_6}$). The pressure difference between the two models is well within a liberal estimate of precision for the FS barometer of $\pm$1 kbar. If the DL ferrosilite activities are adjusted for non-quadrilateral components in a manner similar to clinopyroxene activities, the pressure difference does not change or increases on the order of only 0.1 kbar, because of the lower amount of non-quadrilateral components in Opx relative to Cpx. For convenience we will compare the HD and DI barometers using ideal ferrosilite activities for the FS barometer.

Pressures obtained for the HD and DI barometers are plotted against pressures obtained for the FS barometer in Figs. 5c and 5d, using ideal activities for clinopyroxene and orthopyroxene. There is a significant difference between the two clinopyroxene barometers relative to the orthopyroxene barometer in terms of apparent relative pressure differences and apparent precision. Some 53 of the 68 pressures obtained for the HD barometer fall within 1 kbar of equal pressure, with an average pressure difference ($P_{FS} - P_{HD}$) of -0.2 ± 1.0 kbar. For the DI barometer 28 of the 68 samples fall within 1 kbar of the values obtained from the orthopyroxene barometer, and the average pressure difference ($P_{FS} - P_{DI}$) is 0.6 ± 1.6 kbar. The same general distribution of pressures with slightly less scatter is observed if clinopyroxene component activities are calculated using the model of Davidson and Lindsley (1985), corrected for non-quadrilateral components (Figs. 5d and 5e).

We have also evaluated the HD and DI barometers by comparison with pressure constraints from reported aluminosilicate occurrences in high grade terranes (Table 4). For this purpose pyroxene activities were calculated using the ideal model. In general the HD barometer is consistent with aluminosilicate constraints when a reasonable temperature uncertainty is included, although presssures are

overestimated for some samples from Parry Sound, Ontario, Canada, the Sargur Belt, India and the Furua Complex, Tanzania. The DI barometer yields pressures consistent with aluminosilicates, but pressures are lower than both the FS and HD barometers.

To a first approximation, the HD and DI barometers yield reasonable estimates of pressure for most garnet two-pyroxene granulites, assuming the FS barometer is recording accurate pressures. Considering the possible sources of error in deriving the thermodynamic data, the agreement with FS pressures is satisfying. The HD barometer shows a slight tendency to overestimate pressure relative to the FS barometer for some samples, and the DI barometer shows an opposite trend. In testing the barometers it was generally observed that the greatest pressure discrepancies using the HD barometer were for pyroxenes with a high Mg number (100 Mg/[Mg+Fe^{2+}]), e.g., Doubtful Sound, NZ, sample 36461. In general pyroxenes in the assemblage Gt-Cpx-Opx-Pg-Qz become more magnesian and aluminous with increasing pressure. Therefore, higher pressures are accompanied by greater extrapolations from the end member Fe system and the pressures will be less reliable. Aside from the general tendency for the DI barometer to underestimate pressure, the DI barometer overestimates pressure in Fe-rich systems such as high grade banded iron formation from the Wind River Range and samples of Fe-rich metabasites from the Adirondack Highlands and Minnesota River Valley. This accounts for the samples that fall 3 to 4 kbar above the line of equal pressure in Figs. 5c and 5e. Conversely, Mg-rich samples with Fe-poor Opx yield high FS pressures causing the largest excursions below the line of equal pressure (Fig 5c, 5e). The apparent disagreement between the DI and FS barometers is in part an artifact of the comparison scheme and is not seen when comparing the HD and FS barometers (Fig 5b, 5d), because in Mg-rich rocks both $X^{Cpx}_{CaFeSi_2O_6}$ and $X^{Opx}_{FeSiO_3}$ will be low, yielding high pressures for both HD and FS. Therefore the highest pressures in Figs. 5b and 5d are likely to be overestimates of pressure. The data are consistent with a pressure dependence for some compositions, and in application of these barometers one should be aware of the possible errors involved

in extrapolation of the HD barometer to Mg-rich systems, and the DI barometer to Fe-rich systems.

The observed pressure difference for the DI barometer relative to the FS barometer cannot be a result of the clinopyroxene barometers equilibrating at lower pressure relative to the FS barometer. If the agreement in pressure between the HD and FS barometers is real, it suggests that the DI barometer is yielding lower pressures as a result of errors in thermodynamic data and/or activity models. The difference ($P_{FS} - P_{DI}$) is well within a reasonable error in $\Delta G^{\circ}_{f,298}$ for any of the phases involved in the reaction, and we cannot identify any one phase as having an erroneous $\Delta G^{\circ}_{f,298}$. We believe the pressure discrepancy can be tied to ideal diopside activities. By assigning all the Mg to the M1 site, the ideal model for diopside (Eq. 18) may overestimate the activity of diopside, as some of the Mg is likely to partition into the M2 site (Cameron and Papike 1980, Dal Negro et al. 1983). This will tend to lower the X^{M1}_{Mg}, decreasing the $a^{Cpx}_{CaMgSi_2O_6}$ and raising the pressure calculated from Reaction 2. For example, diopside activities calculated using the Wood and Banno (1973) approximation (in which Mg and Fe^{2+} are equipartitioned between the M1 and M2 sites) raises pressures by 0.1 to 0.6 kbars, with the greatest pressure increase being for the most Mg-rich clinopyroxenes.

The temperature dependence of the HD and DI barometers has been evaluated by carrying through a $\pm$50°C temperature uncertainty in the calculation of $\log_{10}K$ and pressure. For this temperature range the value of $\log_{10}K$ changes by only 1 to 2%, but pressure varies by $\pm$1.0 and $\pm$ 0.3 kbar for the HD and DI barometers respectively. The former is a relatively high temperature dependence for a barometer and illustrates the need for reasonably precise temperatures ($\pm$30°C) when applying the HD barometer. Compositional variations on the order of 1 mol% anorthite in plagioclase, hedenbergite and diopside in clinopyroxene, and almandine and pyrope in garnet correspond to pressure variations on the order of 0.1 kbar. A compositional variation of 1 mol% grossular has approximately twice the effect as

other components, as grossular activities are raised to a higher exponent in the expression for $\log_{10}K$.

Application of Barometers

Orthopyroxene barometry is the preferred technique for calculating pressure in Gt–Opx–Cpx–Pg–Qz granulites. The available FS geobarometers have a sound experimental and thermodynamic basis, and modeling of a–X relations for orthopyroxene is relatively straightforward. However, clinopyroxene barometry is required for rocks containing Gt–Cpx–Pg–Qz assemblages without orthopyroxene. To evaluate the utility of the clinopyroxene barometers we have applied them to Gt–Cpx–Pg–Qz assemblages in rocks from several high grade metamorphic terranes.

The Whitestone Anorthosite (WSA) is a 170 km^2 gabbroic anorthosite metamorphosed to granulite facies in the western Grenville Province of Ontario (Thompson 1983). Gt–Cpx–Pg–Qz assemblages occur within the main body of the anorthosite and within segments of the WSA intersected by the Parry Sound Shear Zone (PSSZ), a high grade ductile shear zone separating a predominantly amphibolite facies tectonic domain from one at granulite facies (Davidson 1984, 1986). Calculation of pressure (using ideal activities) for samples within the main body of the WSA average 9.8 (HD) and 9.5 (DI) kbar (at 750°C, Gt–Cpx thermometry), identical to regional metamorphic pressures deduced from a variety of geobarometers (10 $\pm$ 1.0 kbar, Anovitz 1987). In comparison, pressures from assemblages within the PSSZ average 10.8 (HD) and 11.4 kbar (DI) at 700°C (Gt–Cpx thermometry), or essentially the same as the regional data considering a 1 kbar pressure uncertainty. The pressures are consistent with the occurrence of kyanite in pelitic gneisses within the PSSZ ($P > 7.8 \pm 1.0$ kbar at 700 $\pm$ 50°C), and indicate that ductile shearing occurred in a deep crustal setting.

Gt–Cpx–Pg–Qz–($\pm$Wo$\pm$Cc$\pm$Scap) assemblages are also common in calc–silicate rocks from the western Grenville Province. The primary compositional difference between calc–silicate and mafic granulite assemblages is that garnet in the calc–silicates has higher X_{Ca}^{Gt}, and lower $X_{Fe^{2+}}^{Gt}$ and X_{Mg}^{Gt} than in mafic rocks.

Clinopyroxene is typically a diopside–hedenbergite solid solution with minor Al, Fe^{3+} and Na, and plagioclase shows the same range of composition as in samples of mafic granulite. Calc–silicate assemblages from the Parry Sound–Muskoka area of Ontario (Moecher, unpbl data) with high X_{Ca}^{Gt} (> 0.90) yield unrealistic pressures (13 to 15 kbar) using the HD barometer and low pressures using the DI barometer (5 – 6 kbar), with pressure varying widely with slight variations in $X_{Fe^{2+}}^{Gt}$ and X_{Mg}^{Gt}. It is likely that the garnet activity model used here is not accurate at such extreme garnet compositions, and in garnet with large amounts of andradite component. However some calc–silicate samples with intermediate garnet compositions (e.g., X_{Ca}^{Gt} = 0.35 to 0.40, $X_{Fe^{2+}}^{Gt}$ = 0.45 to 0.55) yield pressures (8.9 (DI) to 11.9 kbar (HD)) that are consistent with regional pressure estimates (Anovitz and Essene 1987b). To avoid the subjective choice of which samples yield accurate pressure, calculations based on Reaction 10 would be more appropriate for high grade calc–silicate rocks.

Percival (1983) describes Gt–Cpx–Pg–Qz–(±Hbl±Ilm±Ti) assemblages in mafic gneisses from the Chapleau–Foleyet area of the Wawa Belt of western Ontario, which are regarded as a cross section of deep crust upthrust along the Kapuskasing Structural Zone (Percival and McGrath 1986). Sillimanite is the only aluminosilicate found and is reported in one sample from this terrane. Application of the DI barometer of Newton and Perkins (1982) yields pressures in the range 3.9 to 8.3 kbar, with an average of 6.3 kbar for peak temperatures of 800°C (Percival 1983). These values do not include the +1.6 kbar correction suggested by Newton and Perkins (1982), which would raise the average pressure to approximately 7.9 kbar. Gt–Opx–Pg–Qz barometry by Percival and McGrath (1986) yield pressures that average 9.4 kbar (at 800°C) using the FS barometers of Bohlen et al. (1983a) and Perkins and Chipera (1985). The FS barometry indicates that the DI barometer of Newton and Perkins (1982) underestimates pressure by 3.1 kbar for these samples. We have applied the present clinopyroxene barometers to 27 samples of Gt–Cpx–Pg–Qz metabasites from this terrane, obtaining pressures from the HD and DI barometers that average 9.6 ± 1.3 kbars (HD, 1σ) and 8.9 ± 1.4 kbar (DI). Some of the pressure variation may be real variations in regional pressure. The pressures are

consistent with a maximum pressure of approximately 10 kbar imposed by the occurrence of sillimanite at 800°C, and are in excellent agreement with the orthopyroxene barometery.

Tella and Eade (1986) report Gt–Cpx–Pg–Qz assemblages in fragments of mafic gneisses entrained within the Tulemalu fault zone, a high grade ductile shear zone in the Northwest Territories, Canada. The samples are interpreted as deep crustal relics brought to the surface in granitic melts along the shear zone during ductile displacements. At temperatures of 750 ± 50°C, the DI barometer of Newton and Perkins (1982) yielded pressures that average 10.9 kbar (unadjusted for the 1.6 kbar pressure correction). The clinopyroxene barometers of this study yield 12.9 (HD) and 11.7 (DI) kbar. It is difficult to evaluate the accuracy of these values without other petrologic constraints on pressure.

Ghent et al. (1983) have mapped a prograde Gt–Cpx isograd in sillimanite zone metabasites (Hbl–Pg–Ilm±Qz±Gt±Cpx±Cc±Ti) from Mica Creek, British Columbia. The Gt–Cpx isograd nearly coincides with a kyanite–sillimanite isograd, placing excellent constraints on maximum pressure of 7.8 ± 1 kbar at an upper temperature limit of 700°C (based on Gt–Cpx thermometry). The DI barometer of Newton and Perkins (with correction) yields pressures of 7.2±0.3 kbar at 650°C (Ghent et al. 1983, 8 samples). In lower grade rocks containing kyanite, Ghent et al. (1979) and Newton and Haselton (1981) quote pressures of 6.6 to 8.9 kbar at approximately 575±50°C using the reaction

Anorthite = Grossular + Kyanite + Quartz (18)

$$3\ CaAl_2Si_2O_8 = Ca_3Al_2Si_3O_{12} + 2\ Al_2SiO_5 + SiO_2$$

(Ghent 1976). The clinopyroxene barometers of the present study yield apparently high values of 9.8±0.9 (HD) and 10.5±0.6 (DI) kbar at 650°C. The reason for this discrepancy is not immediately apparent. Ghent et al. (1983) see no structural evidence for an increase in pressure for the higher grade rocks near the sillimanite isograd, relative to lower grade rocks below the Ky=Sill isograd and that yield

pressures approaching those calculated for the mafic gneisses. It appears for these rocks that the clinopyroxene barometers overestimate pressure by about 1 kbar, although the upper limit of pressure obtained from Reaction 18 overlaps the lower limit of pressure for the clinopyroxene barometers assuming an error estimate of about 1 kbar.

Sanders et al. (1987) describe high pressure granulite facies gneisses from the Northeast Ox Inlier of northwestern Ireland. Gt–Cpx–Pg–Qz–Ilm–Ru metabasites interpreted as decompressed eclogites occur with metapelites, metapsammites, and ultramafites. Sieve–texture intergrowths of clinopyroxene and plagioclase are interpreted to be a result of exsolution of an original omphacitic clinopyroxene. As with the Doubtful Sound, NZ samples, the presently preserved clinopyroxenes are magnesian (X_{HD}^{Cpx} = 0.03 to 0.10) and relatively high in Al_2O_3 (up to 8 wt % Al_2O_3). Peak temperatures are estimated at 850 – 900°C, based on Gt–Cpx thermometry and the presence of mesoperthite, and the occurrence of kyanite in pelites (Gt–Ky–Pg–Kfs–Qz–Ru) places a minimum constraint on pressure of 10.8 to 11.8 kbar at 850 – 900°C. Pressure estimates for the metabasites from Gt–Cpx core compositions range from 19 (HD) to 15 (DI) kbar, and 16 (HD) to 13 (DI) kbar for rim compositions. In view of the tendency of HD barometer to overestimate pressure for Mg–rich clinopyroxenes, the HD values are likely to be upper limits on pressure. However, pressures calculated from Reaction 18 for the Gt–Ky–Pg–Qz assemblage reported by Sanders et al. (1987), using the calibration of Newton and Haselton (1981) and Essene (1988), are also in excess of 15 kbars (at 800°C), in agreement with the DI barometer. Pressures calculated from Gt–Pg–Ilm–Ru–Qz assemblages in the metabasite (Reaction 8: Anovitz and Essene 1987a) yield minimum pressure estimates of 12 to 13 kbar (assuming $a_{FeTiO_3}^{Ilm}$ = 1). If equilibrium can be demonstrated for the sieve texture clinopyroxenes then the pressures indicated by the geobarometry are consistent as a whole with the extremely deep crustal history for these samples suggested by Sanders et al. (1987).

Wood (1975) presents analyses for coexisting garnet, clinopyroxene inclusions within garnet, and plagioclase from metagabbros from the South Harris, Scotland, Igneous Complex. The presence of kyanite in metapelites associated with the meta-igneous lithologies places a lower limit on pressure of 9 kbar. Pressures were estimated to range from 10 to 13 kbar at 800 to 860°C (two-pyroxene and Gt-Cpx thermometry), based on constraints from Gt-Ol-Pg and Gt-Opx-Pg-Qz barometry. We have recalculated the Gt-Cpx temperatures to be 750°C using the Ellis and Green (1979) thermometer, and these are likely to be lower limits on temperature as garnet and clinopyroxene in contact with one another tend to re-equilibrate with falling temperature after the peak of metamorphism (Johnson et al. 1983, Moecher et al. 1986). Pressures for three samples average 12.3 (HD) and 10.6 (DI) kbar. One sample with X_{Hd}^{Cpx} = 0.07 yields the highest pressure, and as with the samples from Doubtful Sound, NZ and the Northeast Ox Inlier, Ireland, this is likely to yield an overestimate of pressure. Excluding this sample the average HD pressure is 11.3 kbar. Metamorphic pressure for the South Harris area is likely to be 11 $\pm$ 1 kbar, essentially that predicted by Wood's earlier analysis.

Evaluation of the HD and DI barometers in previous sections indicated that the DI barometer tended to yield somewhat lower and more scattered pressures than the HD and FS barometers. The results from the six areas above indicate that the two clinopyroxene barometers are in better agreement with one another. This is not inconsistent with the former observation, as some of the garnet two-pyroxene granulites yield similar pressures for all three barometers. From the foregoing applications it is apparent that the clinopyroxene barometers of this study can yield reasonable pressures for most Gt-Cpx-Pg-Qz assemblages. In the absence of assemblages for which experimentally determined geobarometers are available, the HD and DI barometers can be applied with reasonable precision in the granulite facies. However, the thermodynamic, temperature, and compositional dependencies of these barometers, and the inherently less precise nature of empirical calibrations must be kept in mind when applying the barometers in natural settings. More accurate calibrations of these barometers will require careful experiments on

Reactions 1 and 2, or on the reactions that constrain the $\Delta G^{\circ}_{f,298}$ of hedenbergite and pyrope.

References

Anastasiou P, Seifert F (1972) Solid solubility of Al_2O_3 in enstatite at high temperature and 1-5 kbar water pressure. Contrib Mineral Petrol **34**:272-287

Anovitz LM (1987) Pressure and Temperature Constraints on Metamorphism in the Grenville Province of Ontario. PhD thesis, University of Michigan

Anovitz LM, Essene EJ (1987a) Compatibility of geobarometers in the system CaO-FeO-Al_2O_3-SiO_2-TiO_2: implications for garnet mixing models. J Geol **95**:633-645

Aranovich LYa, Kosyakova NA (1987) The cordierite = orthopyroxene + quartz equilibrium: laboratory data on and thermodynamics of ternary Fe-Mg-Al orthopyroxene solid solutions. Geochem Int **24**:111-131

Babuska V, Fiala J, Kumazawa M, Ohno I (1978) Elastic properties of garnet solid-solution series. Phys Earth Plan Int **16**:157-176

Bass JD, Weidner DJ (1984) Elasticity of single-crystal orthoferrosilite. J Geophys Res **89**:4359-4372

Bennington KO, Beyer RP, Brown RR (1984) Thermodynamic properties of hedenbergite, a complex silicate of Ca, Fe, Mn, and Mg. US Dept Int Rept Inv **8873**:19 p

Berman RG, Brown TH (1985) Heat capacity of minerals in the system Na_2O-K_2-O-CaO-MgO-FeO-Fe_2O_3-Al_2O_3-SiO_2-TiO_2-H_2O-CO_2: representation, estimation, and high temperature extrapolation. Contrib Mineral Petrol **89**:168-183

Berman RG, Engi M, Greenwood HJ, Brown TH (1986) Derivation of internally consistent thermodynamic data by the technique of mathematical programming: a review with application to the system MgO-SiO_2-H_2O. J Petrol **27**:1331-1364

Bhattacharyya, P.K. and Mukherjee, S., 1987. Granulite in and around the Bengal anorthosite, eastern India; genesis of coronal garnet, and evolution of the granulite-anorthosite complex. Geol Mag **124**:21-32

Birch F (1966) Compressibility: elastic constants. In: Clark SP Jr (ed) Handbook of Physical Constants, Geol Soc Am Mem **97**, pp 97-173

Boettcher AL (1970) The system CaO-Al_2O_3-SiO_2-H_2O at high pressure and temperature. J Petrol **11**:337-379

Bohlen SR (1979) Pressure, Temperature, and Fluid Composition of Adirondack Metamorphism as Determined in Orthogneisses, Adirondack Mountains, New York. PhD Thesis (unpubl) Univ Michigan.

Bohlen SR, Boettcher AL (1982) Experimental investigations and geological applications of orthopyroxene geobarometry. Am Mineral **66**:951-964

Bohlen SR, Essene EJ, Boettcher AL (1980) Reinvestigation and application of olivine-quartz-orthopyroxene barometry. Earth Planet Sci Lett **47**:1-10

Bohlen SR, Liotta JJ (1986) A new barometer for garnet amphibolites and garnet granulites. J Petrol **27**:1025-1034

Bohlen SR, Metz GW, Essene EJ, Anovitz LM, Westrum EF Jr, Wall VJ (1983) Thermodynamics and phase equilibria of ferrosilite: potential oxygen barometer in mantle rocks. Eos **64**:350

Bohlen SR, Wall VJ, Boettcher AL (1983a) Experimental investigation of model garnet granulite equilibria. Contrib Mineral Petrol **83**:52-61

Bohlen SR, Wall VJ, Boettcher AL (1983b) Experimental investigations and applications of equilibria in the system $FeO-TiO_2-Al_2O_3-SiO_2-H_2O$. Am Mineral **68**:1049-1058

Bohlen SR, Wall VJ, Boettcher AL (1983c) Geobarometry in granulites. In: Saxena SK (ed) Kinetics and Equilibrium in Mineral Reactions. Springer, New York, pp 141-171

Boyd FR, England JL (1964) The system enstatite-pyrope. Carnegie Inst Wash Yrbk **63**:157-161

Brace WF, Scholz CH, La Mori PN (1969) Isothermal compressibility of kyanite, andalusite, and sillimanite from synthetic aggregates. J Geophys Res **74**:2089-2098

Burton JC, Taylor LA, Chou I-M (1982) The fO_2-T and fS_2-T stability relations of hedenbergite and of hedenbergite-johannsenite solid solutions. Econ Geol **77**:764-783

Cameron M, Sueno S, Prewitt CT, Papike JJ, (1973) High temperature crystal chemistry of acmite, diopside, hedenbergite, jadeite, spodumene, and ureyite. Am Mineral **58**:594-618

Cameron M, Papike JJ (1980) Crystal chemistry of silicate pyroxenes. In: Prewitt CT (ed) Reviews in Mineralogy **7**, Pyroxenes. Mineralogical Society of America, Washington DC, pp 5-92

Chatillon-Colinet C, Newton RC, Perkins D III, Kleppa OJ, (1983). Thermochemistry of $(Fe^{2+},Mg)SiO_3$ orthopyroxene. Geochim Cosmochim Acta **47**:1597-1603

Coolen JJMMM (1980) Chemical petrology of the Furua Granulite Complex, southern Tanzania. GUA Papers Geol **1-13**:258 pp

Dal Negro A, Carbonin S, Molin GM, Cundari A, Piccirillo EM (1982) Intracrystalline cation distribution in natural clinopyroxenes of tholeiitic, transitional, and alkaline basaltic rocks. In: Saxena SK (ed) Advances in Physical Geochemistry, Vol 2 Springer, New York, pp 117-150

Danckwerth PA, Newton RC (1978) Experimental determination of the spinel peridotite to garnet peridotite reactions in the system $MgO-Al_2O_3-SiO_2$ in the range 900-1100°C and Al_2O_3 isopleths of enstatite in the spinel field. Contrib Mineral Petrol **66**:189-201

Davidson A (1984) Tectonic boundaries within the Grenville Province of the Canadian Shield. J Geodynam **1**:433-444

Davidson A (1986) New interpretations in the southwestern Grenville Province. In: Moore JM, Davidson A, Baer AJ (eds) The Grenville Province. Geol Assoc Can Spec Pap **31**:61-74

Davidson PM, Lindsley DH (1985) Thermodynamic analysis of quadrilateral pyroxenes Part II: model calibration from experiments and application to geothermometry. Contrib Mineral Petrol **91**:390-404

Devaraju TC, Coolen JJMMM (1983) Mineral chemistry and P-T conditions of formation of a basic scapolite-garnet-pyroxene granulite from Doddakanya, Mysore District. J Geol Soc India **24**:404-411

Ellis DJ, Green DH (1979) An experimental study of the effect of Ca upon garnet–clinopyroxene Fe–Mg exchange equilibria. Contrib Mineral Petrol 71:13–22

Essene EJ (1988) The current status of thermobarometry in metamorphic rocks. In: Daly S (ed) Evolution of Metamorphic Belts, Spec Pub Geol Soc London, in press.

Ganguly J, Saxena SK (1984) Mixing properties of aluminosilicate garnets: constraints from natural and experimental data, and applications to geothermobarometry. Am Mineral 68:88–97

Gasparik T (1984a) Experimental study of subsolidus phase relations and mixing properties in the system $CaO–AlO_2(2)O_3–SiO_2$. Geochim. Cosmochim. Acta 48:2537–2546.

Gasparik T (1984b) Experimentally determined stability of clinopyroxene + garnet + corundum in the system $CaO–MgO–Al_2O_3–SiO_2$. Am Mineral 69:1025–1035

Gasparik T, Newton RC (1984) The reversed alumina contents of orthopyroxene in equilibrium with spinel and forsterite in the system $MgO–Al_2O_3–SiO_2$. Contrib Mineral Petrol 85:186–196

Ghent ED (1976) Plagioclase–garnet–Al_2SiO_5–quartz: a potential geobarometer – geothermometer. Am Mineral 61:710–714

Ghent ED, Robbins DB, Stout MZ (1979) Geothermometry, geobarometry, and fluid compositions of metamorphosed calcsilicates and pelites, Mica Creek, British Columbia. Am Mineral 64:874–885

Ghent ED, Stout MV, Raeside RP (1983) Plagioclase–clinopyroxene–garnet–quartz equilibria and the geobarometry and geothermometry of garnet amphibolites from Mica Creek, British Columbia. Can J Earth Sci 20:699–706

Glassley WE, Sorensen K (1980) Constant P_s–T amphibolite to granulite facies transition in Agto (West Greenland) metadolerites: implications and applications. J Petrol 21:69–105

Griffin WL, Carswell DA, Nixon PH (1979) Lower–crustal granulites and eclogites from Lesotho, Southern Africa. In: Boyd FR, Meyer, HOA (eds) The Mantle Sample: Inclusions in Kimberlites and Other Volcanics. American Geophysical Union, Wash DC, pp 59–86

Gustafson WI (1974) The stability of andradite, hedenbergite, and related minerals in the system Ca–Fe–Si–O–H. J Petrol 15:455–496

Hansen EC, Newton, RC, Janardhan AS (1984) Pressures, temperatures and metamorphic fluids across an unbroken amphibolite facies to granulite facies transition in southern Karnataka, India. In: Kroner A, Hanson GN, Goodwin AM (eds) Archaean Geochemistry, Springer, Berlin, pp 161–181

Harris NBW, Holt RW, Drury SA (1982) Geobarometry, geothermometry, and late Archean geotherms from the granulite facies terrain of south India. J Geol 90:509–527

Haselton HT (1979) Calorimetry of synthetic pyrope–grossular garnets and calculated stability relations. PhD thesis (unpubl) Univ Chicago

Haselton HT, Newton RC (1980) Thermodynamics of pyrope–grossular garnets and their stabilities at high temperatures and high pressure. J Geophys Res 85B:6973–6982

Haselton HT, Westrum EF Jr (1980) Low temperature heat capacities of synthetic pyrope, grossular, and $pyrope_{60}grossular_{40}$. Geochim Cosmochim Acta **44**:701-709

Haselton HT, Robie RA, Hemingway BS (1987) Heat capacities of synthetic hedenbergite, ferrobustamite, and $CaFeSi_2O_6$ glass. Geochim Cosmochim Acta **51**:2211-2218

Hays JF (1967) Lime-alumina-silica. Carnegie Inst Wash Yrbk **65**:234-239

Hazen RM, Finger LW (1978) Crystal structures and compressibilities of pyrope and grossular to 60 kbar. Am Mineral **63**:297-303

Hazen RM, Finger LW (1981) Crystal structure of diopside at high temperature and pressure. Carnegie Inst Wash Yb **80**:373-376

Hazen RM, Prewitt CT (1977) Effects of temperature and pressure on interatomic distances in oxygen-based minerals. Am Mineral **62**:309-315

Helgeson HC, Delany JM, Nesbitt HW, Bird DK (1978) Summary and critique of the thermodynamic properties of rock-forming minerals. Am J Sci **278-A**:229 p

Hemingway BS (1987) Quartz: heat capacities from 340 to 1000 K and revised values for the thermodynamic properties. Am Mineral **72**:273-279

Hensen BJ, Essene EJ (1971) Stability of pyrope-quartz in the system $MgO-Al_2O_3-SiO_2$. Contrib Mineral Petrol **30**:72-83

Holdaway MJ (1971) Stability of andalusite and the aluminum silicate phase diagram. Am J Sci **271**:97-131

Holmes RD, O'Neill HSt-C, Arculus RJ (1986) Standard Gibbs free energy of formation for Cu_2O, NiO, CoO, and Fe_xO: high resolution electrochemical measurements using zirconia solid electrolytes from 900 - 1400 K. Geochim Cosmochim Acta **50**:2439-2452

Hormann PK, Raith M, Raase P, Ackermand D, Seifert F (1980) The granulite complex of Finnish Lapland: petrology and metamorphic conditions in the Ivalojoki-Inarijarvi area. Bull Geol Surv Finland **308**:95 pp

Huckenholz HG, Holz E, Lindhuber W (1975) Grossularite, its solidus and liquidus relations in the $CaO-Al_2O_3-SiO_2-H_2O$ system up to 10 kbar. Neues Jahrb Mineral Abh **124**:1-46

Huckenholz HG, Lindhuber W, Springer J (1974) The join $CaSiO_3-Al_2O_3-Fe_2O_3$ of the $CaO-Al_2O_3-Fe_2O_3-SiO_2$ system and its bearing on the formation of granditic garnets and fassaitic pyroxenes. Neues Jahr Mineral Abh **121**:160-207

Janardhan AS, Gopalkrishna D (1983) Pressure-temperature estimates of the basic granulites and conditions of metamorphism in Sargur Terrain, southern Karnataka and adjoining areas. J Geol Soc India **24**:219-228

Janardhan AS, Newton RC, Hansen EC (1982) The transformation of amphibolite facies gneisses to charnockite in southern Karnataka and northern Tamil Nadu, India. Contrib Mineral Petrol **79**:130-149

Johnson CA, Bohlen SR, Essene EJ (1983) An evaluation of garnet-clinopyroxene geothermometry in granulites. Contrib Mineral Petrol **84**:191-198

Koziol AM, Newton RC (1986) Redetermination of the arorthite breakdown reaction and improvement of the plagioclase-garnet-Al_2SiO_5-quartz geobarometer. Am Mineral **73**:216-223

Krupka KM, Hemingway BS, Robie RA, Kerrick DM, Ito J (1985a) Low-temperature heat capacities and derived thermodynamic properties of anthophyllite, diopside, enstatite, bronzite, and wollastonite. Am Mineral **70**:249-260

Krupka KM, Hemingway BS, Robie RA, Kerrick DM (1985b) High-temperature heat capacities and derived thermodynamic properties of anthophyllite, diopside, dolomite, enstatite, bronzite, talc, tremolite, and wollastonite. Am Mineral **70**:262-271

Lane DL, Ganguly J (1980) Al_2O_3 solubility of orthopyroxene in the system MgO-Al_2O_3: a reevaluation, and mantle geotherm. J Geophys Res **85B**:6963-6972

Levien L, Prewitt CT (1981) High-pressure structural study of diopside. Am Mineral **66**:315-323

Liebermann RC, Ringwood AE (1976) Elastic properties of anorthite and the nature of the lunar crust. Earth Planet Sci Lett **8**:361-374

Lindsley DH (1983) Pyroxene thermometry. Am Mineral **68**:477-493

Liou JG (1974) Stability relations of andradite-quartz in the system Ca-Fe-Si-O-H. Am Mineral **59**:1016-1025

MacGregor ID (1974) The system MgO-Al_2O_3-SiO_2: solubility of Al_2O_3 in enstatite for spinel and garnet peridotite compositions. Am Mineral **59**:110-119

Metz GW, Anovitz LM, Essene EJ, Bohlen SR, Westrum EF Jr (1983) The heat capacity and phase equilibria of almandine. Eos **64**:346-347

Moecher DP (1984) Determination of Late Archean Metamorphic Conditions, Granite Falls, Minnesota. MS Thesis (unpubl) Univ Wisconsin

Moecher DP (1988) Application of scapolite phase equilibria and carbon isotope systematics to high grade rocks: a test of the CO_2-flooding hypothesis. PhD Thesis (unpubl) Univ Michigan

Moecher DP, Perkins D III, Leier-Englehardt PJ, Medaris LG Jr (1986) Metamorphic conditions of late Archean high-grade gneisses, Minnesota River valley, U.S.A. Can J Earth Sci **23**:633-645

Mora CI, Valley JW (1985) Ternary feldspar thermometry in granulites from the Oaxacan Complex, Mexico. Contrib Mineral Petrol **89**:215-225

Newton RC (1966) Some calc-silicate equilibrium relations. Am J Sci **264**:204-222

Newton RC (1983) Geobarometry of high-grade metamorphic rocks. Am J Sci **283A**:1-28

Newton RC (1987) Thermodynamic analysis of phase equilibria in simple mineral systems. In: Carmichael ISE, Eugster HP (eds) Thermodynamic Modeling of Geological Materials: Minerals, Fluids, and Melts, Reviews in Mineralogy **17**, Mineralogical Society of America, Washingtion, D.C., pp 1-33

Newton RC, Charlu TV, Kleppa OJ (1980) Thermochemistry of the high structure state plagioclases. Geochim Cosmochim Acta **44**:933-941

Newton RC, Haselton HT (1981) Thermodynamics of the garnet-plagioclase-Al_2SiO_5-quartz geobarometer. In: Newton RC, Navrotsky A, Wood BJ (eds) Thermodynamics of Minerals and Melts, Springer, New York, pp 129-145

Newton RC, Perkins D III (1982) Thermodynamic calibrations of geobarometers for charnockites and basic granulites based on the assemblages garnet-plagioclase-orthopyroxene-(clinopyroxene)-quartz, with applications to high grade metamorphism. Am Mineral **67**:203-222

Nielson TH, Leipold MH (1965) Thermal expansion of NiO. J Am Ceramic Soc **48**:164

Oliver GJH (1977) Feldspathic hornblende and garnet granulites and associated anorthosite pegmatites from Doubtful Sound, Fiordland, New Zealand. Contrib Mineral Petrol **65**:111-121

Orville PM (1972) Plagioclase cation exchange equilibria with aqueous chloride solution: results at 700°C and 2000 bars in the presence of quartz. Am J Sci **272**:234-272

Paktunc AD, Baer AJ (1986) Geothermobarometry of the northwest margin of the Superior Province: implications for its tectonic evolution. J Geol **94**:381-394

Percival JA (1983) High-grade metamorphism in the Chapleau-Foleyet area, Ontario. Am Mineral **68**:667-686

Percival JA, McGrath PH (1986) Crustal structure of the northern Kapuskasing uplift of Ontario: an integrated petrological-geophysical study. Tectonics **5**:553-572

Perkins D III (1979) Application of New Thermodynamic Data to Mineral Equilibria. PhD Thesis (unpubl) Univ Michigan

Perkins D III (1983) The stability of Mg-rich garnet in the system CaO-MgO-Al_2O_3-SiO_2 at 1000-1300°C and high pressure. Am Mineral **68**:355-364

Perkins D III, Chipera SJ (1985) Garnet-orthopyroxene-plagioclase-quartz barometry: refinement and application to the English River Subprovince and the Minnesota River Valley. Contrib Mineral Petrol **89**:69-80

Perkins D III, Newton RC (1980) The composition of coexisting pyroxenes and garnet in the system CaO-MgO-Al_2O_3-SiO_2 at 900°-1100°C and high pressures. Contrib Mineral Petrol **75**:291-300

Perkins D III, Holland TJB, Newton RC (1981) The Al_2O_3 contents of enstatite in equilibrium with garnet in the system MgO-Al_2O_3-SiO_2 at 15-40 kbar and 900°-1600°C. Contrib Mineral Petrol **78**:99-109

Phillips GN (1978) Metamorphism and Geochemistry of the Willyama complex, Broken Hill. PhD Thesis (unpubl) Monash Univ (Melbourne)

Richardson SW, Bell PM, Gilbert MC (1968) Kyanite-sillimanite equilibrium between 700° and 1500°C. Am J Sci **266**:513-541

Robie RA, Bin Z, Hemingway BS, Barton MD (1987) Heat capacity and thermodynamic properties of andradite garnet, $Ca_3Fe_2Si_3O_{12}$, between 10 and 1000 K and revised values of $\Delta_f G^\circ_m$ (298.15) of hedenbergite and wollastonite. Geochim Cosmochim Acta **51**:2219-2224

Robie RA, Hemingway BS (1984) Entropies of kyanite, andalusite, and sillimanite: additional constraints on the pressure of the Al_2SiO_5 triple point. Am Mineral **69**:298-306

Robie RA, Hemingway BS, Fisher JR (1979) Thermodynamic properties of minerals and related substances at 298.15 K and 1 bar (10^5 pascals) and at higher temperatures. U.S Geol Surv Bull **1452**

Robinson GR Jr, Haas JL Jr, Schafer CM, Haselton HT (1982) Thermodynamic and thermophysical properties of selected phases in the $MgO-SiO_2-H_2O-CO_2$, $CaO-Al_2O_3-SiO_2-H_2O-CO_2$, and $Fe-FeO-Fe_2O_3-SiO_2$ systems, with special emphasis on the properties of basalts and their mineral components. U.S. Geol Surv Open-File Rept **83-79**

Robinson GR Jr, Haas JL Jr (1983) Heat capacity, relative enthalpy, and calorimetric entropy of silicate minerals: an empirical method of prediction. Am Mineral **68**:541-553

Sanders IS, Daly JS, Davies GR (1987) Late Proterozoic high pressure granulite facies metamorphism in the north-east Ox Inlier, north-west Ireland. J Meta Geol **5**:69-85

Sharp ZD (1988) Metamorphism and Oxygen Isotope Geochemistry of the Northern Wind River Range, Wyoming. PhD thesis (unpubl) Univ Michigan

Sharp ZD, Essene EJ, Anovitz LM, Metz GW, Westrum EF Jr, Hemingway BS, Valley JW (1986) The heat capacity of a natural monticellite and phase equilibria in the system $CaO-MgO-SiO_2-CO_2$. Geochim Cosmochim Acta **50**:1475-1484

Skinner BJ (1966) Thermal Expansion. (In) Clark SP Jr (ed) Handbook of Physical Constants, Geol Soc Am Mem **97**:75-96

Srikantappa C, Raith M, Ackermand D (1985) High-grade regional metamorphism of ultramafic and mafic rocks from the Archaean Sargur Terrane, Karnataka, south India. Precambrian Res **30**:189-219

Stoddard EF (1976) Granulite Facies Metamorphism in the Colton-Rainbow Falls Area, Northwest Adirondacks, New York. PhD Thesis (unpubl) Univ California Los Angeles

Suwa Y, Tami Y, Naka S (1976) Stability of synthetic andradite at atmospheric pressure. Am Mineral **61**:26-28

Tella S, Eade KE (1986) Occurrence and possible tectonic significance of high-pressure granulite fragments in the Tulemalu Fault Zone, District of Keewatin, N.W.T., Canada. Can J Earth Sci **23**:1950-1962

Thompson DL (1983) The nature of anorthosite-country rock interaction during granulite facies metamorphism: an example from the Whitestone Anorthosite. MS thesis (unpubl) McMaster University

Vaidya SN, Bailey S, Pasternack T, Kennedy GC (1973) Compressibility of fifteen minerals to 45 kilobars. J Geophys Res **78**:6893-6898

Wagner ME, Srogi L (1987) Early Paleozoic metamorphism at two crustal levels and a tectonic model for the Pennsylvania-Delaware Piedmont. Geol Soc Am Bull **99**:113-126

Wells PRA (1977) Chemical and thermal evolution of Archaean sialic crust, southern West Greenland. J Petrol **20**:187-226

Winter JK, Ghose S (1979) Thermal expansion and high-temperature crystal chemistry of the Al_2SiO_5 polymorphs. Am Mineral **64**:573-586

Wood BJ (1975) The influence of pressure, temperature and bulk composition on the appearance of garnet in orthogneisses - an example from South Harris, Scotland. Earth Plan Sci Lett **26**:299-311

Wood BJ, Banno S (1973) Garnet-orthopyroxene and orthopyroxene-clinopyroxene relationships in simple and complex systems. Contrib Mineral Petrol **42**:109-124

Wood BJ, Holloway JR (1984) A thermodynamic model for subsolidus equilibria in the system CaO-MgO-Al_2O_3-SiO_2. Geochim Cosmochim Acta **48**:159-176

CHAPTER III

SCAPOLITE PHASE EQUILIBRIA I: QUANTITATIVE PHASE RELATIONS IN THE SYSTEM $CaO-Al_2O_3-SiO_2-CO_2-H_2O$ (CASCH)

Introduction

Scapolite solid solutions involving marialite ($Na_4Al_3Si_9O_{24}Cl$), meionite ($Ca_4Al_6Si_6O_{24}CO_3$), and sulfate meionite ($Ca_4Al_6Si_6O_{24}SO_4$) are potential sensors of fluid composition in a wide variety of geologic environments. Provided that thermodynamic and thermobarometric data were available, one may calculate or limit the activities of NaCl, CO_2, and/or SO_2 in scapolite-bearing calc-pelites (Hietanen, 1967; Frank, 1983; Tuisku, 1985; Mora & Valley, 1988), hydrothermally metamorphosed metabasites (Vanko & Bishop, 1982), calc-silicate skarns, gneisses, and marbles (Shaw *et al.*, 1963a, 1963b; Misch, 1964; Trommsdorff, 1966; Kerrick *et al.*, 1973; Rollinson, 1980; Oterdoom & Wenk, 1983; Shenk, 1984; Perchuk *et al.*, 1985, Warren *et al.*, 1987), amphibolites (Kwak, 1977; Oliver & Wall, 1987), and mafic granulites and deep crustal xenoliths (von Knorring & Kennedy, 1958; Lovering & White, 1964; Wilkinson, 1974; Devaraju & Gowd Reddy, 1976; Edwards *et al.* 1979; Okrusch *et al.*, 1979; Coolen, 1980; Boivin & Camus, 1981; Devaraju & Coolen, 1983; Jones *et al.*, 1983; Austreim & Griffen, 1985; Srikantappa *et al.*, 1985; Thomas & Nixon, 1987; Stolz, 1987). This would provide a powerful tool in evaluating the presence and activity (fugacity) of some fluid species other than H_2O in metamorphic rocks.

The experiments of Ellis (1978) and Vanko & Bishop (1980) on sodic scapolite suggest that Na- and Cl-rich scapolites are indicative of highly saline metamorphic fluids. The high P-T stability of CO_3 and SO_4-rich calcic scapolites led Goldsmith (1976) to propose that scapolite would be a significant phase in lower crustal lithologies, being stabilized relative to plagioclase in the presence of CO_2 and SO_2. However, these hypotheses have yet to be quantitatively tested in natural systems by phase equilibrium calculations. As a result of calorimetric measurements on the scapolite solid solution series (Komada *et al.*, 1988) some of these calculations are now more feasible. Using the relevant experimental data on meionite and other phases as constraints, we have generated quantitative P-T and T-X equilibria for scapolite (meionite) phase relations in the system $CaO-Al_2O_3-SiO_2-CO_2-H_2O$ (CASCH). Work in the Grenville Province of southwestern Ontario (Chapter IV) and a survey of the literature reveal that scapolite often occurs in calc-silicate assemblages with quartz, calcite, wollastonite, clinopyroxene, plagioclase, garnet, and/or clinozoisite, and in metabasites and meta-anorthosite with garnet, plagioclase, quartz, amphibole, clinopyroxene, and orthopyroxene. Reactions involving quartz, calcite, wollastonite, anorthite, grossular, clinozoisite, meionite, and to a lesser extent corundum and gehlenite, were chosen as the most practical in evaluating fluid composition in natural systems. For these phase relations to be of practical significance, activity-composition (a-X) relations for the meionite component in scapolite were calculated based on natural scapolite-plagioclase-calcite assemblages. In a later publication we will discuss the application of these phase equilibrium and a-X relations to the calculation of CO_2 activities in high grade scapolite-bearing lithologies from a number of localities and in different geologic settings.

Re-examination of Al-Si and Anion Ordering in Scapolite

Application of new entropy data for the scapolite solid solution series (Komada *et al.* 1988) in phase equilibrium calculations on natural systems is limited by accurate estimates of the configurational entropy (S_{δ}) of end-member meionite.

Contributions from Al–Si disorder and CO_3 and SO_4–group disorder potentially comprise up to 12% of the total molar entropy of meionite at 298 K. Uncertainties of this magnitude in molar entropy may have serious consequences for calculation of reliable phase equilibria in this system. Therefore, a re–examination of available data that constrain S°_0 is warranted.

Crystal Chemical and Experimental Constraints

The scapolite crystal structure is comprised of two types of four–membered Si–Al tetrahedral rings oriented perpendicular to the c axis: two T_2–T_3 rings and one T_1 ring per formula unit (Z = 2) which links every second and third T_2–T_3 ring along c (Papike & Zoltai, 1965; Papike & Stephenson, 1966; Lin & Burley, 1972, 1973a, 1973b, 1973c, 1975; Ulbrich, 1973a; Levien & Papike, 1976; Peterson *et al.*, 1979; Aitken *et al.*, 1984). This linking of the tetrahedra in T_2–T_3 rings by T_1 tetrahedra results in five–membered tetrahedral rings oriented parallel to C and perpendicular to a. The Cl, CO_3 and SO_4 anions are centered immediately between successive T_1 rings, in cages formed by the Al–Si tetrahedra.

Single crystal X–ray diffraction studies of calcic scapolites have shown that the CO_3 and SO_4 groups are disordered over at least four and two orientations in the anion site, respectively (Papike & Stephenson, 1966; Peterson *et al.*, 1979). This would contribute 11.5 (Rln4) and 5.8 (Rln2) J/mol K to S°_0 for meionite and sulfate meionite. More recently Aitken *et al.* (1984) have refined a calcic, carbonate scapolite (Me_{84}: %Me = 100Ca/[Ca+Na+K]) with the carbonate group disordered over eight orientations in the anion site. This would contribute 17.3 (Rln8) J/mol·K to S°_0. The positional disorder of anions within the scapolite structure is required by symmetry constraints on the trigonal carbonate and tetragonal sulfate radical. We have assumed a model of long range disorder over eight and two positions respectively for the CO_3 and SO_4 groups in the meionite structure, consistent with the most recent single crystal refinements.

Oterdoom & Wenk (1983) summarized the available single-crystal XRD, TEM, and experimental data relative to Al-Si ordering, and concluded that ordering in scapolites is a function of composition, with Me_{33-37} (EqAn = 100([Al-3]/3) = 33) being the only composition for which complete long range Al-Si order is possible. The Al and Si are interpreted to be disordered over the T_2 and T_3 sites in marialite. With increasing substitution of the meionite component into marialite, Al partitions into the T_2 site until, at a composition of approximately Me_{33}, Al and Si alternate in an ordered arrangement in the $T_2(Al)-T_3(Si)$ ring. From Me_{37} to $Me_{90\pm2}$ (the most calcic scapolite studied) Al enters the T_1 ring. Between Me_{37} to Me_{90} the presence of five-membered tetrahedral rings makes it impossible to maintain an ordered Al-Si distribution without forming Al-O-Al bonds. Such bonds are generally unstable in silicate structures (Lowenstein, 1954) and have been shown to control Al-Si ordering in plagioclase (Ribbe, 1983) and cordierite (Gibbs, 1966; Putnis & Bish, 1983). The increase in meionite content is also accompanied by a change in the refined space group from $P4_2/n$ for Me_{37} to I4/m for samples of Me_{80-90}. This has been interpreted to reflect a change in the degree of Al-Si disorder and/or the extent of $Cl-CO_3$ substitution in the anion site. As the end members are approached the degree of Al-Si disorder increases until, presumably, complete disorder is attained for end-member meionite. This would result in maximum separation of Al-O-Al bonds throughout the structure. However, Oterdoom and Wenk concluded that natural scapolites are as ordered as is possible up to 1000°C, the onset of Al-Si disorder proposed by Levien & Papike (1976) in a single crystal study of scapolite (Me_{37}) at elevated temperature, and that the available single crystal data are not inconsistent with a short range ordered domain structure. Oterdoom and Wenk (1983) further concluded that synthetic meionite is metastably and completely disordered in terms of Al-Si, and that the reaction

Anorthite + Calcite = Meionite (1)

$$3\ CaAl_2Si_2O_8 + CaCO_3 = Ca_4Al_6Si_6O_{24}CO_3$$

has a positive slope in the range 850 to 875°C and 1 to 18 kbar. A positive slope for Reaction 1 necessitates a very high (nearly vertical) dP/dT in order to fit the experimental reversals of Goldsmith & Newton (Fig. 1). This in turn requires S°_{0} to be that for completely disordered meionite, or 80.8 J/mol·K, corresponding to complete Al–Si disorder over twelve sites and carbonate group disorder over four sites (Goldsmith & Newton, 1977; Oterdoom & Wenk, 1983, pg. 339).

Oterdoom & Wenk's conclusion of complete disorder in synthetic end-member meionite rests in part on the assumption of a positive slope for Reaction 1. Their analysis is based on the expansivity of a scapolite of composition Me_{37} (Levien & Papike, 1976). However, the expansivity data of Grazziani & Lucchessi (1982) for sodic scapolites yield a much higher dV/dT than calcic scapolites. If ΔV°_{T} for Reaction 1 were calculated using the dV/dT of a sodic scapolite one would indeed obtain a positive slope. Use of the measured expansivity for a scapolite of composition Me_{88} (Grazziani & Lucchessi, 1982) in the calculation of Reaction 1 yields a negative slope for all values of S°_{0} (meionite) over the temperature interval 850–875°C. The experimental reversals for Reaction 1 suggest a negative slope is entirely consistent with the experimental data (Fig. 1). In reality the reversals do not constrain the ordering state of meionite; the reaction can be made to fit the experimental reversals assuming a wide range of Al–Si disorder.

Experimental reversals for the reaction

Anorthite + Anhydrite = Sulfate–Meionite (2)

$$3\ CaAl_2Si_2O_8 + CaSO_4 = Ca_4Al_6Si_6O_{24}SO_4$$

provide additional constraints on the configurational entropy of end member meionite, as sulfate–meionite was synthesized under conditions similar to those for meionite ((Fig. 1: Goldsmith & Newton, 1977). The $S^{\circ}_{298} - S^{\circ}_{0}$ estimated for sulfate meionite (Komada *et al.*, 1988) is 703.7 J/mol·K, and S°_{298} is 778.6 J/mol·K for completely disordered sulfate–meionite (Al–Si and SO_4 group disorder over twelve and two sites, respectively). It was assumed that the heat-capacity function for

Figure 1. Experimental reversals and calculated position of Reactions 1 (◁) and 2 (○) (Goldsmith & Newton, 1977) assuming complete Al–Si order (dashed–dot lines), complete disorder (dashed lines), and intermediate ordering state (–6RIn2 for Al–Si, solid lines). The slope of Reaction 2 changes from positive to negative with increasing degrees of Al–Si disorder. A range of Al–Si disorder is allowed by the reversals for Reaction 1 (3 An + Cc = Me), but a high degree of disorder is required for Reaction 2 (3 An + Anhy = Me–SO_4).

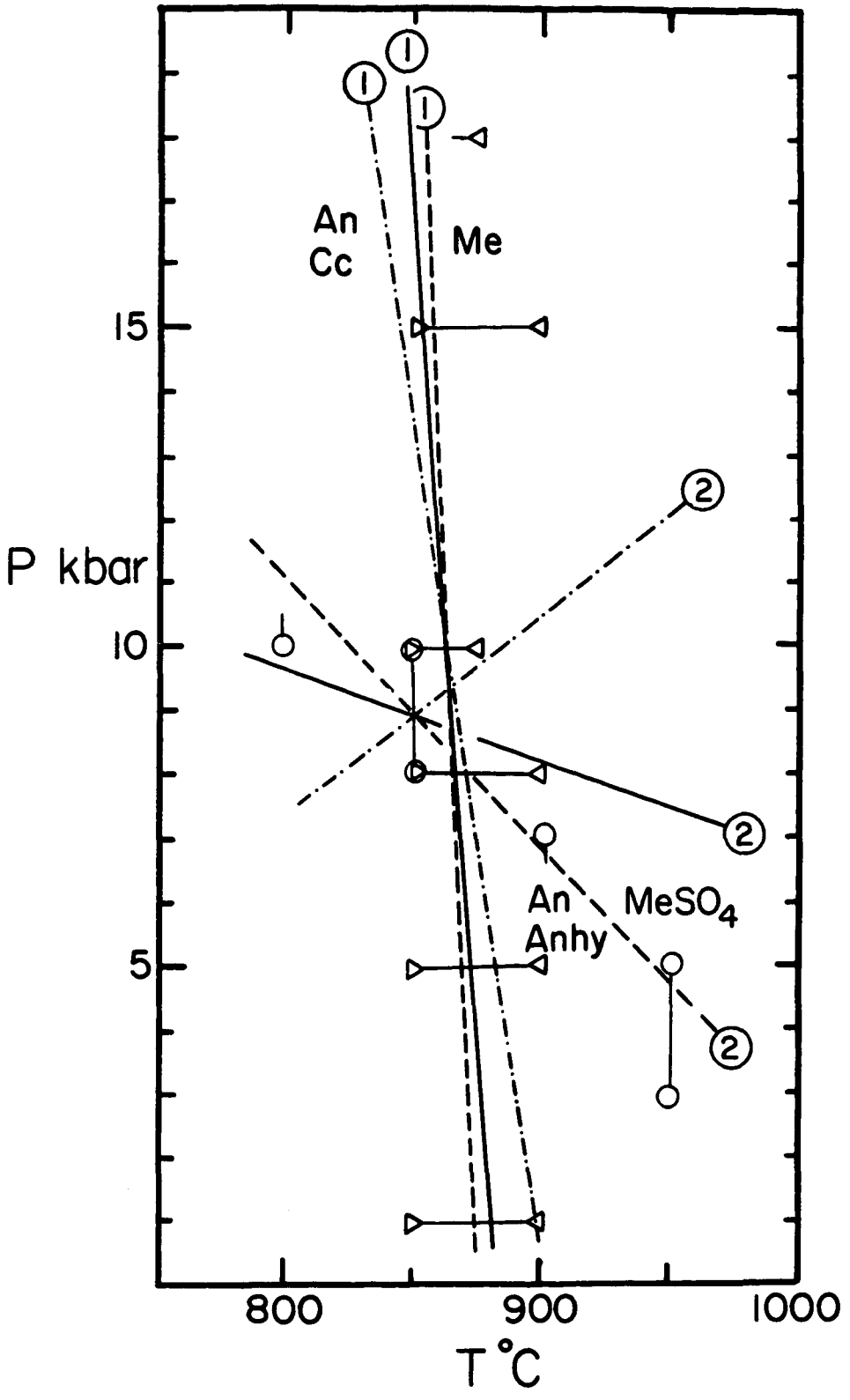
An
Cc
Me
15
P kbar
10
5
An
Anhy
MeSO4
800
900
1000
T °C

meionite adequately describes that of sulfate meionite. The reversals require a high degree of Al–Si and SO_4 disorder to adequately fit the reversals (Goldsmith & Newton, 1977) (Fig. 1), but not necessarily complete Al–Si disorder. If this analysis were performed assuming $\Delta S^{\circ}_{298} = \Delta S^{\circ}_{T})$ for Reaction 2, one would reach the erroneous conclusion that a wider range of intermediate ordering states would be possible, with completely ordered and completely disordered sulfate meionite being prohibited by the reversals for Reaction 2.

MASNMR Constraints

Recent MASNMR (magic angle spinning nuclear magnetic resonance) spectroscopic methods are an additional means of evaluating the Al–Si ordering state of scapolite (Sheriff *et al.*, 1987; see Klinowski *et al.*, 1981; Putnis & Angel, 1985; Yang *et al.*, 1986; and references therein for MASNMR theory and application). Sheriff *et al.* (1987) analyzed an extensive set of ^{29}Si MASNMR spectra for natural scapolites, including the samples used by Komada *et al.* (1988) in their heat capacity measurements. Systematic changes are evident in the spectra of the scapolite solid solution series as a function of composition. Sheriff *et al.* (1987) interpreted the spectra in terms of a model based on predictions of tetrahedral occupancies from the single crystal XRD data base, electrostatic energy considerations that are consistent with cation–anion ordering in Me_{33} (Chamberlain *et al.*, 1985), and ^{29}Si peak assignments based on previous empirical studies (Janes & Oldfield, 1985). The latter assumptions preclude a unique solution for the ordering state of scapolites. The spectra and models of Sheriff *et al.* (1987) are in good agreement with the prediction of Al–Si order in samples of Me_{33}, for which the predicted and observed tetrahedral structural formula are $[Si_4]^{T1}[Al_4]^{T2}[Si_4]^{T3}$. For Me_{70} the model predicts $[Si_{3.2}Al_{0.8}]^{T1}[Al_4]^{T2}[Si_{4.0}]^{T3}$, while the observed site occupancies from the deconvoluted NMR spectra are $[Si_{3.2}Al_{0.8}]^{T1}[Al_4]^{T2}[Si_{3.8}Al_{0.2}]^{T3}$, in good agreement considering the imprecision in measuring peak intensities of complex spectra consisting of several overlapping peaks (Sheriff *et al.*, 1987, Fig.

10). However, there are significant differences between the predicted and observed site occupancies for more calcic scapolites. For example, the model of Sheriff *et al.* predicts occupancies for a sample of Me_{91} to be $[Si_{0.8}Al_{3.2}]^{T1}[Si_{0.3}Al_{3.7}]^{T2}[Si_{3.8}Al_{0.2}]^{T3}$, while the observed NMR occupancies are $[Si_{0.8}Al_{3.2}]^{T1}[Si_{1.5}Al_{2.5}]^{T2}[Si_{4.0}]^{T3}$. Aside from the observation that the two occupancies are rather different, both indicate that the T_1 tetrahedral ring contains excess Al and the T_2–T_3 ring is Al deficient, relative to the commonly assumed distribution where T_2–T_3 cannot have more than four Si and four Al. Tetrahedral site occupancies for Me_{93}, calculated from mean T–O bond distances, are consistent with equal amounts (approximately 50%) of Al and Si in the T_2–T_3 ring, and 21 to 34% Al in the T_1 ring (Lin & Burley, 1973a; Ulbrich, 1973a). It is likely that the peak assignments are not valid for the more calcic scapolites. Sheriff *et al.* (1988, in press) report revised values of peak positions for a large number of silicates, and this may eventually change the interpretation of the spectra for more calcic scapolites (Sheriff pers. comm., 1988).

For intermediate scapolite (Me_{33} to Me_{75}) it appears that Al and Si are ordered in the tetrahedral framework, but more work is needed on the most calcic samples in order to constrain Al–Si disorder. Disorder that is not resolvable by MASNMR methods may still be present in calcic scapolite and MASNMR methods may not be sufficiently precise at present to calculate the amount of Al–Si disorder and configurational entropy in silicates, even for minerals less complex than scapolite (e.g., low and high albite, W.-H. Yang, 1987, writ. comm.). Small degrees of Al–Si disorder can contribute significant amounts of configurational entropy because of the rapid increase of S°_{0} at small degrees of disorder. In addition, the ordering state of scapolite at the elevated temperatures where natural scapolites form still needs to be evaluated, by collecting MASNMR spectra on quenched samples heated to approximately 600–900°C. The presence of domains imaged by TEM methods in natural scapolites ranging in composition from Me_{33} to Me_{78} (Phakey & Ghose, 1972; Oterdoom & Wenk, 1983; Hassan & Buseck, 1988) is consistent with the development of ordering upon cooling, and scapolites may

possess either cation or anion disorder at metamorphic temperatures. In addition, any Al–Si disorder indicated by NMR may be a result of disorder at domain boundaries in a short range–ordered structure (depending on the size of domains).

Based on the preceeding discussion, natural scapolite solid solutions, particularly the intermediate compositions, appear to be ordered at room temperature. Hassan & Buseck (1988) reached a similar conclusion based on HRTEM analysis of two intermediate natural scapolites. They deduced coupled ordering of Na–Ca with Si–Al and Cl–CO_3, producing compositional domains of marialite and meionite–rich components. This information places important constraints on ordering in scapolite solid solutions, however it will not have a similar bearing on end member meionite, nor does it provide information on the ordering state of scapolite at high temperature. The exact ordering state of *synthetic* scapolite remains unresolved, although the experiments are consistent with intermediate to high degrees of Al–Si disorder (Goldsmith & Newton, 1977, p.1076). Until MASNMR spectra on synthetic end–members are collected and tighter experimental reversals for Reactions 1 and 2 are obtained, one can only assume a particular ordering state consistent with the experiments and X–ray diffraction data on synthetic samples. We have assumed a model of partial Al–Si disorder (6Rln2 or one–half of total Al–Si disorder) for synthetic meionite as this is consistent with the experimental reversals for Reactions 1 and 2, and with the refined space group I4/m of synthetic scapolite (Me_{85}: I4/M, Aitken *et al.* 1984). The implication of this assumption and the effect of varying degrees of Al–Si disorder on scapolite phase equilibrium relations will be discussed in following sections.

Thermodynamic and Experimental Data Base

Low temperature (10–350 K) adiabatic calorimetry and high temperature (300 – 1000 K) DSC data for five natural scapolites ranging in composition from Me_{28} to Me_{88} are presented in Komada *et al.* (1988). These data were used to calculate

the lattice contribution to S°_{298} (S°_{298} - S°_0) for four scapolite end members: marialite ($Na_4Al_3Si_9O_{24}Cl$), an intermediate composition commonly referred to as mizzonite ($Ca_3NaAl_5Si_7O_{24}CO_3$), meionite, and sulfate-meionite ($Ca_4Al_6Si_6O_{24}SO_4$). The reader is referred to Komada *et al.* (1987) for a summary of the calorimetric data and the methods used to correct data on natural samples to the end-members. A value for S°_{298} - S°_0 of 697.9 J/mol·K was calculated for end-member meionite. Including 6Rln2 for Al-Si and Rln8 for CO_3 disorder, S°_{298} for meionite is 749.8 J/mol K. High temperature DSC data for Me_{88} from Komada *et al.*, adjusted to end-member meionite, were fit with a Meier-Kelley polynomial expansion yielding the coefficients in Table 2. Extrapolation of entropy above 1000 K was calculated from the method of Robinson & Haas (1982).

Because of the relatively steep slope of Reaction 1 in P-T space (due to a small ΔV_r), small variations in the volume of the anorthite and meionite will affect the interpretation of the experimental data. The value of V°_{298} for end-member meionite was obtained from a linear regression of molar volume versus percent Me for natural scapolite (Ulbrich, 1973). The value of V°_{298} calculated from this relation (340.36 cm^3) is nearly identical to that measured by Goldsmith & Newton (1977) for synthetic end-member meionite (340.39 cm^3). Thermal expansion for meionite (Table 2) was calculated from expansivity data on a sample of Monte Somma meionite (Grazziani & Lucchessi, 1982). The compressibility of meionite (Table 2) is that measured for a sample of Monte Somma meionite by the diamond anvil technique in the pressure range 1 bar to 30 kbar (Hazen & Sharp, 1988).

Values of V°_{298} and V°_T for anorthite are taken from Robie *et al.* (1978) and Skinner (1966), and the compressibility of anorthite was taken from Liebermann & Ringwood (1976) and Angel *et al.* (1988). The compressibility of anorthite should be used in calculations, rather than that of labradorite (Birch, 1966), as only slight variations in the volume of anorthite will change the calculated slope of Reaction 1 and affect the interpretation of the degree of Al-Si disorder in synthetic meionite.

TABLE 1. Entropy and Gibbs free energies (relative to elements) for phases used in thermodynamic calculations.

PHASE	S°_{298} J/mol K	ref.	A	B	C	D	ref.	ΔG°_{298} kJ/mol	ref.
Quartz (α)	41.5	1	55.414	18.863	7.141	-329.4	2	-856.3	1
Quartz (β)	47.3	2	65.616	6.074	14.665	-391.9	4,2	-854.4	2
Corundum	50.9	3	116.336	11.983	19.514	-688.3	3	-1582.2	3
Calcite	91.8	3	88.884	45.256	9.492	-530.6	3	-1131.2	3
Anhydrite	106.7	1	72.170	97.206	0.846	441.1	1	-1321.7	1
Wollastonite	81.7	3	102.238	28.446	13.444	-605.9	3	-1549.2	3
Kyanite	82.4	4	177.002	24.849	29.564	-1049.1	4	-2445.8	2
Ca-Tschermakite	141.1	3	232.052	24.860	35.780	-1369.5	3	-3127.1	2
Anorthite	199.3	3	278.255	47.694	38.295	-1642.6	3	-4010.9	2
Gehlenite	210.0	5	274.530	28.577	38.343	-1615.5	3	-3782.1	2
Zoisite	295.4	3	398.825	171.962	44.865	-2374.1	3	-6509.1	2
Clinozoisite	297.1	2	398.825	171.962	44.865	-2374.1	3	-6506.5	2
Grossular	256.3	3	463.212	463.212	70.651	-2731.3	3	-6282.3	7
Meionite(ord)	709.3	2	959.108	158.200	144.418	-5673.2	6		2
Meionite(int)	749.8	2	959.108	158.200	144.418	-5673.2	6	-13115.4	2
Meionite(dis)	778.3	2	959.108	158.200	144.418	-5673.2	6		2
SO_4 meionite	778.2	2	959.108	158.200	144.418	-5673.2	6	-13108.8	2

$S^{\circ}_T = S^{\circ}_{298} + A\ln T + B10^{-3}T + C10^{5}/T^{2} + D$

1: Robie et al. 1978; 2:this study; 3:Robinson et al. 1982; 4: Robie & Hemingway 1984

5: Hemingway & Robie 1984; 6:Komada et al. 1988; 7: Anovitz and Essene 1987

TABLE 2. Molar volume, compressibility, and expansivity for phases used in thermodynamic calculations

PHASE	V^0_{298} cm^3	ref.	a mbar-1	b mbar-2	ref.	cE-02	dE-03	eE-07	fE-10	ref.
Quartz (α)	22.69	1	2.76	24.00	11	11.414	4.877	-25.192	9.984	17
Quartz (β)	23.79	2	1.78	0.00	11	1.392	-0.452	-1.352	0.617	17
Corundum	25.57	3	0.38	0.00	11	-7.526	2.034	-8.758	-3.150	17
Calcite	36.92	3	1.37	3.90	11	-3.912	1.244	19.108	0.000	18
Anhydrite	45.94	1	1.84	0.00	11	-11.657	4.690	-11.271	14.033	19
Wollastonite	39.79	3	1.47	9.82	3	11 177	5.009	-41.664	15.535	3
Kyanite	64.21	4	0.79	5.00	12	5.427	2.144	8.100	-3.296	20
Ca-Tschermakite	63.58	3	0.78	1.38	3	-5.531	2.162	7.709	-2.334	3
Anorthite	100.79	1	1.11	2.48	13,14	-5.030	2.055	-17.795	12.376	17
Gehlenite	90.25	3	0.46	1.01	3	-6.947	2.753	0.043	0.020	3
Zoisite	135.80	5,6	1.13	0.00	3	-6.248	4.117	-7.597	3.295	3
Clinozoisite	136.45	7,8	1.13	0.00	3	-6.248	4.117	-7.597	3.295	3
Grossular	125.30	3	0.74	4.47	15	-4.359	1.721	9.114	-1.866	17
Meionite	340.36	9	1.14	2.07	16	-3.720	1.529	-16.389	9.631	21
SO_4 meionite	340.39	10	1.14	2.07	2	-3.720	1.529	-16.389	9.631	2

$V^P_{298} = V^0_{298} - V^0_{298}[aP - bP^2]$, P in mbars

$V^0_T = V^0_{298} + V^0_{298}/100[c + dT + eT^2 + fT^3]$, T in ^oC

1:Robie et al. 1978; 2:this study; 3:Robinson et al. 1982; 4:Robie & Hemingway 1984;
5:Perkins et al. 1980; 6:Dollase 1968; 7:Seki 1959; 8:Myer 1966; 9:Ulbrich 1973b;
10:Goldsmith & Newton 1977; 11:Birch 1966; 12:Bass & Weidner 1984; 13: Liebermann & Ringwood 1975;
14:Angell et al. 1988; 15: Hazen & Finger 1978; 16:Hazen & Sharp 1988; 17:Skinner 1966;
18:Markgraf & Reeder 1985; 19:Evans 1979; 20:Winter & Ghose; 21:Grazziani & Lucchessi 1983

The expansivity of anorthite is from Skinner (1966). The sources of the remaining thermodynamic data are listed in Tables 1 and 2.

Thermodynamic calculations were performed with a computer program (EQUILI, Wall & Essene unpbl.) that solves the relation

$$\Delta G^{P_2}_{T_2} - \Delta G^{P_1}_{T_1} = \int_{P_1}^{P_2} \Delta V_s dP - \int_{T_1}^{T_2} \Delta S_s dT + \Delta G_f(P_2, T_2, X_{H_2O}, X_{CO_2}) - \Delta G_f(P_1, T_1, X_{H_2O}, X_{CO_2})$$

using available standard volume, entropy, expansivity, compressibility and free energy data. Equilibria are adjusted to fit experimental reversals in order to obtain internally consistent values for free energy (ΔG°_{298}, Table 1). Additional equilibria can then be calculated at any P and T using 1 bar, 298 K as a starting point. Mixed volatile equilibria were calculated using the modified MRK equation of state for H_2O–CO_2 mixtures of Kerrick & Jacobs (1981).

The α–β quartz transition is involved in the location of reactions 3, 4, 5, and 6. Entropy and expansivity data for β–quartz from Hemingway (1987) and Skinner (1966) are valid only above the α–β quartz transition, but were empirically extrapolated to 298 K and 1 bar to yield fictive values of S°_{298} and V°_{298} for the purposes of calculation,. Using the compressibility for β–quartz in Birch (1966), the V°_T of α–quartz from Skinner (1966) empirically extrapolated above 844 K, and the compressibility of α–quartz from Birch (1966), the value of S°_T for α–quartz was obtained at T>844 K by solving the first derivative of the equation for the α–β transition (Mirwald & Massone 1980) to obtain $\Delta S^P_T / \Delta V^P_T$ at a series of temperatures from 1 to 20 kbar. Using the above data and S°_T obtained from this calculation, the transition can be fit to within ±15°C in the range of 1 to 20 kbar.

In addition to Reaction 1 the following experimentally reversed equilibria were selected as constraints on the Gibbs free energy of relevant phases:

Calcite + Quartz = Wollastonite + CO_2 (3)

$CaCO_3 + SiO_2 = CaSiO_3 + CO_2$

(Harker & Tuttle, 1956; Jacobs & Kerrick, 1981);

Grossular + Quartz = Anorthite + Wollastonite (4)

$Ca_3Al_2Si_3O_{12} + SiO_2 = CaAl_2Si_2O_8 + 2\ CaSiO_3$

(Newton, 1966; Boettcher, 1970; Huckenholz *et al.*, 1975);

Grossular + Kyanite + Quartz = Anorthite (5)

$Ca_3Al_2Si_3O_{12} + 2\ Al_2SiO_5 + SiO_2 = 3\ CaAl_2Si_2O_8$

(Goldsmith, 1980; Gasparik, 1984b; Koziol & Newton, 1988)

Zoisite + Quartz = Anorthite + Grossular + H_2O (6)

$4\ Ca_2Al_3Si_3O_{12}(OH) + SiO_2 = 5\ CaAl_2Si_2O_8 + Ca_3Al_2Si_3O_{12} + 2\ H_2O$

(Newton, 1966; Boettcher, 1970; Chatterjee *et al.*, 1984);

Zoisite + Kyanite + Quartz = Anorthite + H_2O (7)

$2\ Ca_2Al_3Si_3O_{12}(OH) + Al_2SiO_5 + SiO_2 = 4\ CaAl_2Si_2O_8 + H_2O$

(Newton & Kennedy, 1963; Goldsmith, 1981; Chatterjee *et al.*; 1984, Jenkins *et al.* 1985);

Zoisite = Anorthite + Grossular + Corundum + H_2O (8)

$2\ Ca_2Al_3Si_3O_{12}(OH) = CaAl_2Si_2O_8 + Ca_3Al_2Si_3O_{12} + Al_2O_3 + H_2O$

(Newton, 1965; Boettcher, 1970; Chatterjee *et al.*, 1984)

Grossular + Corundum = Anorthite + Gehlenite (9)

$Ca_3Al_2Si_3O_{12} + Al_2O_3 = CaAl_2Si_2O_8 + Ca_2Al_2SiO_7$

(Boettcher, 1970; Huckenholz *et al.*, 1975)

Grossular = Anorthite + Gehlenite + Wollastonite (10)

$2\ Ca_3Al_2Si_3O_{12} = CaAl_2Si_2O_8 + Ca_2Al_2SiO_7 + 3\ CaSiO_3$

(Boettcher, 1970, Huckenholz *et al.*, 1975);

Grossular + Corundum = Ca-Tschermakite (11)

$Ca_3Al_2Si_3O_{12} + 2\ Al_2O_3 = 3\ CaAl_2SiO_6$

(Gasparik 1981, 1984b);

Ca-Tschermakite = Anorthite + Gehlenite + Corundum (12)

$3CaAl_2SiO_6 = CaAl_2Si_2O_8 + Ca_2Al_2SiO_7 + Al_2O_3$

(Hays 1967).

Most of the resultant Gibbs energies were adjusted only slightly from Robinson *et al.* (1982), which is a statistical least squares fit of available experimental data. The experimental reversals and our calculated fits are shown in Figs. 2, 3, and 4. A reasonable fit to most of the reversals can be attained with our thermodynamic data set. However, there is an inconsistency between the calculated and experimental position for Reactions 9 and 10. Assuming a set of free energies that are consistent with Reactions 1 through 8, 11, and 12, one cannot simultaneously fit both sets of reversals for Reactions 9 and 10 (Chatterjee *et al.*, 1984). On the other hand, Robinson *et al.* (1982) derived a set of Gibbs energies consistent with reactions 9 and 10 that was inconsistent with the available reversals for Reaction 5. We have placed more weight on Reaction 5 because its location is now well established, and it appears that one of the gehlenite reactions is incorrectly located. There is considerable disagreement between the reversals of Boettcher (1970) and Huckenholz *et al.* (1975) for Reaction 10. The slope of Reaction 9 is consistent with a considerable amount of Al-Si disorder in gehlenite (2Rln2 = 11.5 J/mol·K, Ulbrich & Waldbaum, 1976), whereas the high temperature reversals of Huckenholz *et al.* (1975) for Reaction 10 suggest a greater slope than that calculated for Reaction 10. We have chosen to fit Reaction 9, because it is most consistent with the location of Reaction 12, which is derived from the intersection of Reactions 9 and 11, and our phase equilibrium analysis to follow rests on this assumption. Re-evaluation of the gehlenite equilibria are necessary in order to resolve the discrepancy.

The ΔG°_{298} of partially disordered meionite used in this study was calculated from ΔG°_{298} for Reaction 1, and ΔG°_{298} for anorthite and calcite:

ΔG°_{298} (Me) = ΔG°_{298} (Reaction 1) + $3\Delta G^\circ_{298}$ (An) + ΔG°_{298} (Cc)

Figure 2. Experimental constraints and calculated position of Reactions 3, 4, 6, 7, 9, 10 and 13, used to constrain thermodynamic data in Tables 1 and 2. The location of Reaction 10 (Gr = An + Ge + Wo), was calculated from the thermodynamic data assuming a fit to Reaction 9 (Gr + Co = An + Ge). The reversals for Reaction 10 are at a lower temperature than its calculated position. Symbols: ▽ : Harker & Tuttle, 1956; ■ : Newton, 1966; ● : Boettcher, 1970; ▲ : Huckenholz *et al.*, 1975; □ : Goldsmith, 1981; ▽ : Jacobs & Kerrick, 1981; ○ : Chatterjee *et al.*, 1984: ◇ (Reaction 7), and ◆ (Reaction 13): Jenkins *et al.*, 1985.

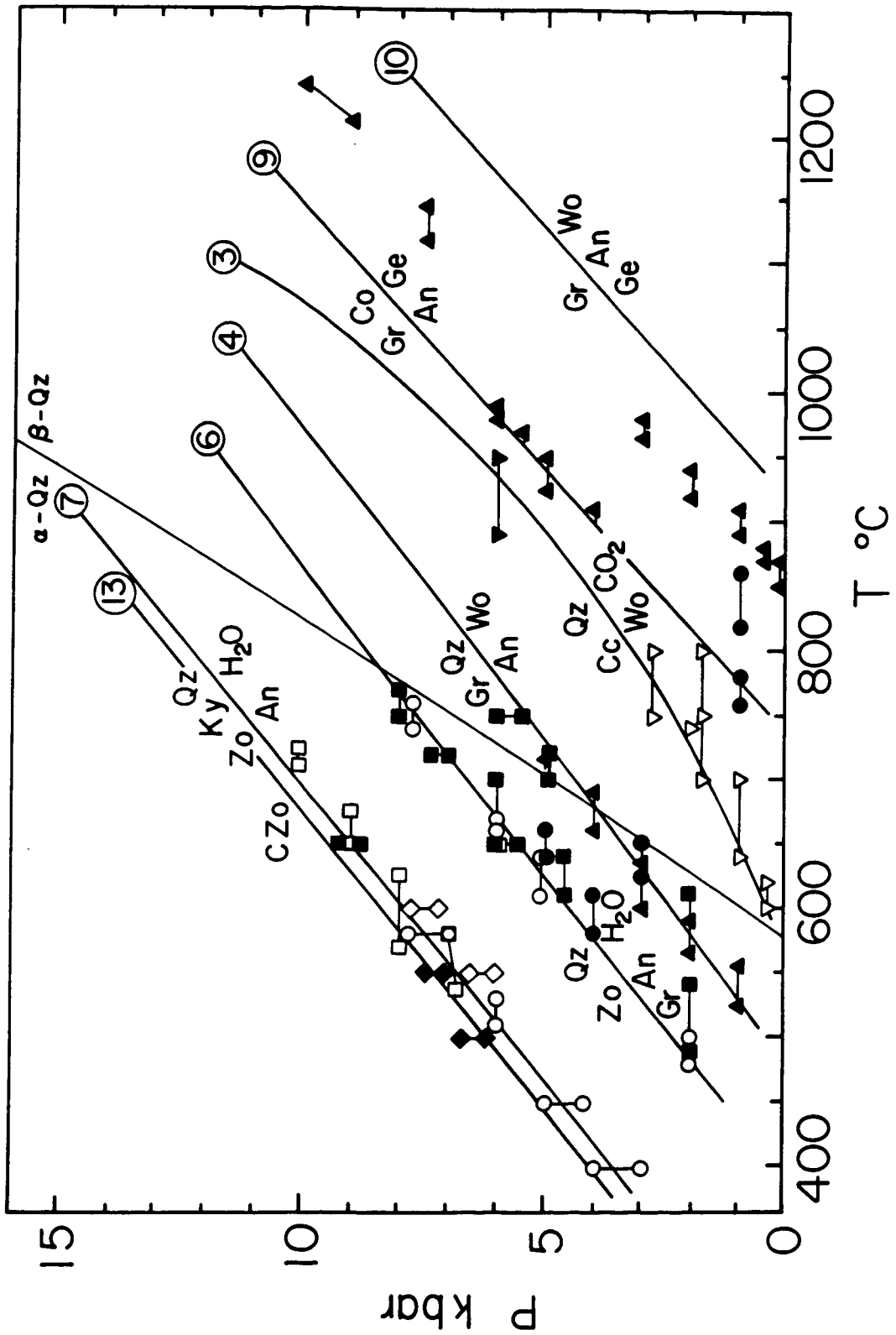
P kbar
T °C
0
5
10
15
400
600
800
1000
1200
α-Qz
β-Qz
(7)
(13)
(6)
(4)
(3)
(9)
(10)
Qz
Ky
H2O
An
Zo
CZo
Qz
Wo
Gr
An
Qz
H2O
Zo
An
Gr
Co
Ge
Gr
An
Qz
CO2
Cc
Wo
Gr
Wo
An
Ge

Figure 3. Experimental constraints and calculated positions of Reactions 5, 11, and 12. Symbols: ▲ : Hays, 1965: ■ : Goldsmith, 1980; ○ : Gasparik, 1984a; ● : Gasparik, 1984b: I : Koziol & Newton, 1986. The disagreement between the calculated and experimental locations of Reaction 12 may be related to systematic errors in pressure corrections of the piston cylinder.

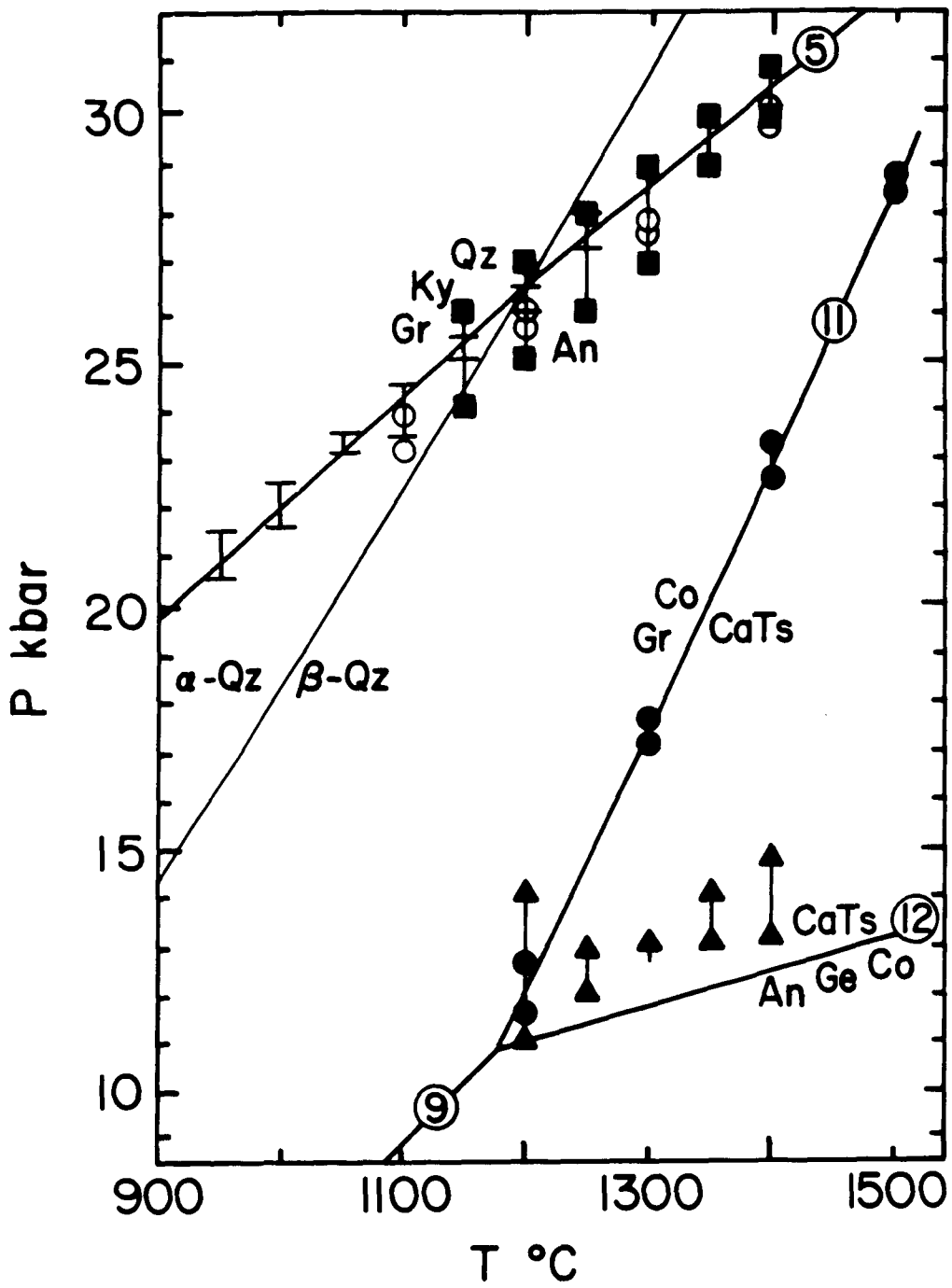
30
25
20
15
10
P kbar
900
1100
1300
1500
T °C
Qz
Ky
Gr
An
α-Qz
β-Qz
Co
Gr
CaTs
CaTs
An
Ge
Co
⑤
⑪
⑫
⑨

4. Experimental constraints and calculated positions of Reaction 8. Symbols: ■ : Newton, 1965; ● : Boettcher, 1970: ○ : Chatterjee *et al.* 1984.

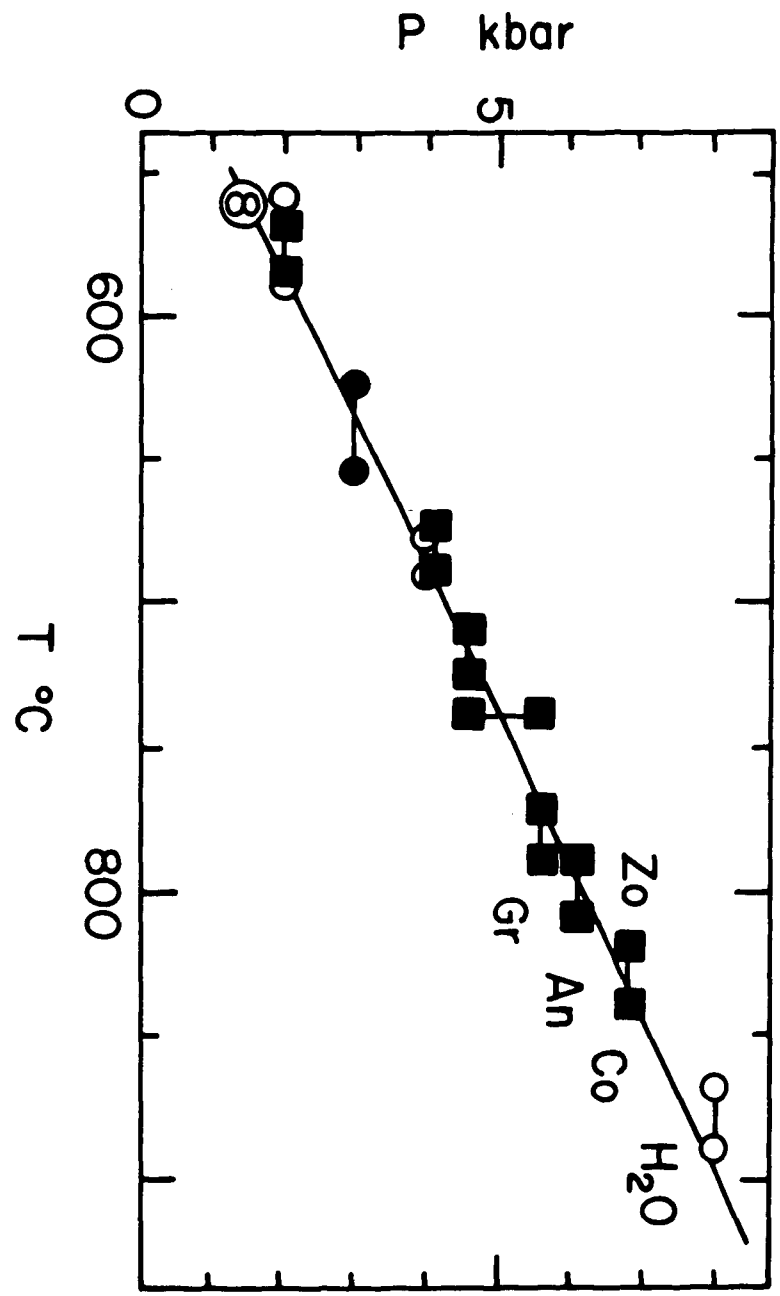
P kbar
0
5
600
800
T °C
Zo
Gr
An
Co
H2O

The ΔG°_{298} (Reaction 1) was calculated using the midpoint of the reversal at 10 kbar (863°C) as a starting point. The ΔG°_{298} for meionite with the intermediate disordering state assumed here is −13,115.4 kJ/mol. Also tabulated are the Gibbs energies for completely disordered and ordered meionite calculate relative to the ordering state assumed for this study. The reversals correspond to only one ordering state, and if the partially disordered state is the correct ordering state for the experiments, then the ordered reaction would lie at higher temperatures and the disordered reaction at lower temperature relative to the present reversals.

The thermodynamic data set derived here assumes that anorthite is ordered with respect to its Al–Si distribution. Gasparik (1984b) and Wood & Holloway (1984) concluded that synthetic anorthite may contain small but significant amounts of Al–Si disorder, and a configurational entropy term of approximately three to five J/mol K is required for anorthite in order to fit reversals for Reaction 5. However, Anovitz & Essene (1987) concluded that a satisfactory fit to experiments in the system $CaO–FeO–Al_2O_3–SiO_2–TiO_2$ can be obtained using alternative entropy data for grossular, and including expansivity and compressibility data in the calculation of the location of Reaction 5. For the present work we have accepted the conclusion of Anovitz & Essene (1987), obtaining a reasonable fit to the CASCH experimental data set. The effect on Reaction 1 of Al–Si disorder in anorthite is the opposite of that of Al–Si disorder in meionite. That is, it causes Reaction 1 to have a lower slope, requiring a greater configurational entropy for meionite to fit the reversals. The ratio of anorthite to meionite in Reaction 1 requires that the meionite entropy increase by 3-fold over the increase in anorthite entropy.

Epidote–group minerals coexisting with scapolite are usually monoclinic, therefore it is more appropriate to use clinozoisite reactions rather than zoisite reactions to model natural systems. Using experimental data for the reaction

Clinozoisite + Kyanite + Quartz = Anorthite + H_2O (13)

$2\ Ca_2Al_3Si_3O_{12}(OH) + Al_2SiO_5 + SiO_2 = 4\ CaAl_2Si_2O_8 + H_2O$

(Jenkins *et al.*, 1985), we have calculated ΔG°_{298} for clinozoisite in the same manner as that for meionite. The ΔG°_{298} for Reaction 13 was calculated from the mid-point of the experimental reversal at 7.35 kbar, 550°C to 1 bar, 25°C to obtain ΔG°_{298} (Cz) of −6506.5 kJ/mol. We have assumed the entropy for clinozoisite to be that of zoisite, corrected for a volume difference of 0.65 cm^3 (i.e, S°_{298} (Cz) = S°_{298} (Zo) + 1.4 J), and that thermal expansion and compressibility are the same for the two polymorphs. The molar volume for natural zoisite of Perkins *et al.* (1980) is consistent with the volume of natural zoisite obtained from Myer (1965, 1966) and that measured by Langar & Lattard (1980) and Chatterjee *et al.* (1984) for synthetic zoisite. The molar volume of clinozoisite was obtained from linear extrapolation of data on natural clinozoisite (Seki, 1959, Myer, 1966, Dollase, 1968) and is in agreement with the data on synthetic clinozoisite (Chatterjee *et al.*, 1984). Clinozoisite will be the polymorph used in the phase equilibrium calculations to follow.

Phase Equilibria

Scapolite parageneses from a wide range of metamorphic environments should provide valuable constraints on fluid composition. We have investigated occurrences of calcic, carbonate-rich scapolite in amphibolite and granulite facies gneisses in the Central Gneiss Belt of the southwestern Grenville Province of Ontario in order to constrain fluid compositions in high grade rocks. A detailed description of mineral assemblages and geologic setting of these rocks will described in Chapters IV and V. Briefly, carbonate-rich calcic scapolite occurs in high grade calc-silicate rocks, marble, garnet amphibolite, and garnet meta-anorthosite. The most common phases coexisting with carbonate scapolite in calc-silicates include grossular-rich garnet, intermediate to calcic plagioclase, salitic clinopyroxene, pistacitic clinozoisite, wollastonite, calcite, and quartz. In contrast, sulfate-bearing carbonate scapolite typically occurs in garnetiferous mafic granulites, amphibolites, and meta-anorthosites.

Geobarometric studies indicate the Central Gneiss Belt is a high pressure granulite terrain with peak metamorphic pressures in excess of 10 kbar (Anovitz, 1987). Other high pressure granulite terranes also contain scapolite-bearing granulites (*e.g.*, Furua Complex, Tanzania: Coolen 1980; Bergen Arcs, Norway: Austreim & Griffen, 1985; Southern India Archean Terrane: Devaraju & Coolen, 1983; Srikantappa *et al.*, 1985). Scapolite is also widely developed as a prograde index mineral in regional metamorphic terranes at intermediate pressures (*e.g.*, Trommsdorff, 1966; Heitenan, 1967; Kwak 1977). Therefore, scapolite decarbonation equilibria involving the above phases were calculated at 5 *and* 10 kbar in order to delineate phase relations over a range of crustal conditions and determine the effect of variable fluid pressure and composition on scapolite stability.

Previous studies of the CASCH system are numerous (Boettcher, 1970; Kerrick, 1970; Storre, 1970; Gordon & Greenwood, 1971; Hoschek, 1980; Perkins *et al.*, 1980; Halbach & Chatterjee, 1984; Kerrick & Ghent, 1984), and a number of other studies consider equilibria involving scapolite (Kerrick *et al.*, 1973; Ellis, 1978; Aitken, 1983; Schenk, 1984; Warren *et al.*, 1987). However none of these present a complete *quantitative* analysis of the stability of meionite relative to other CASCH phases. Our study takes the analysis of the CASCH system one step further by placing quantitative constraints on the limits of meionite stability.

At 5 kbar meionite is stable in the absence of quartz to water-rich conditions (Figs. 5a and 5b). The stability of meionite in T-X_{CO_2} space is delimited by Reaction 1 at 873°C and the reactions Me = Gr + An + Co + CO_2 and Me = Gr + An + Ge + CO_2 at X_{CO_2} = 0.94±0.01. Therefore, end member meionite has an extremely large stability field at intermediate pressure and high temperature. However, in the presence of quartz the stability of meionite is greatly reduced and is confined to $X_{CO_2} \geq 0.9$ at 5 kbar.

Reaction 1 is virtually independent of pressure, and at 10 kbar all other equilibria shift to higher temperature relative to Reaction 1, yielding a different

Figure 5a. Calculated meionite phase equilibria at 5 kbar. Dashed line is stability of Me_{90} relative to 3 Anorthite + Calcite calculated from assemblage reported by Schenk (1984). Meionite stability is further reduced in temperature for less calcic scapolite coexisting with calcic plagioclase (Me_{77}: $EqAn_{69}$ and An_{96}: Table 3). See Fig. 5b for detail of H_2O-rich region at high temperature.

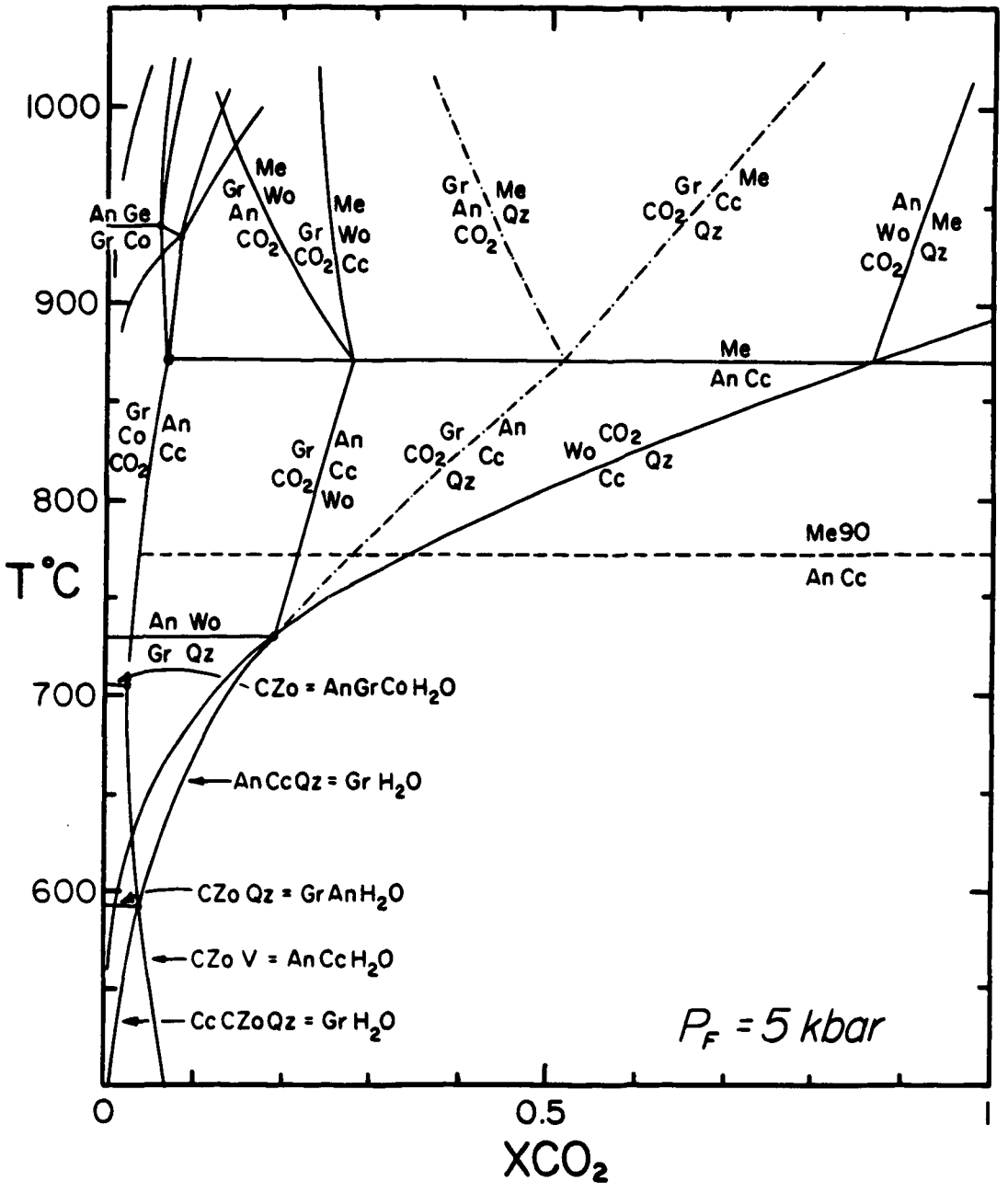
1000
900
800
700
600
T°C
0
0.5
1
XCO2
An Ge
Gr Co
Me
Gr
An
CO2
Wo
Gr
CO2
Me
Wo
Cc
Gr
An
CO2
Me
Qz
Gr
Me
CO2
Cc
Qz
An
Wo
Me
CO2
Qz
Me
An Cc
Gr
Co
CO2
An
Cc
Gr
CO2
An
Cc
Wo
Gr
An
CO2
Cc
Qz
CO2
Wo
Cc
Qz
Me90
An Cc
An Wo
Gr Qz
CZo = AnGrCo H2O
AnCcQz = Gr H2O
CZo Qz = GrAnH2O
CZo V = AnCcH2O
CcCZoQz = Gr H2O
PF = 5 kbar

Figure 5b. Detail of high temperature, H_2O-rich area of Fig. 5a. The reaction Me + Ge = Gr + Co + CO_2 is an example of a decarbonation reaction with a negative T-XCO_2 slope. This results from the assemblage Me + Ge having a higher entropy than the volatile-bearing assemblage.

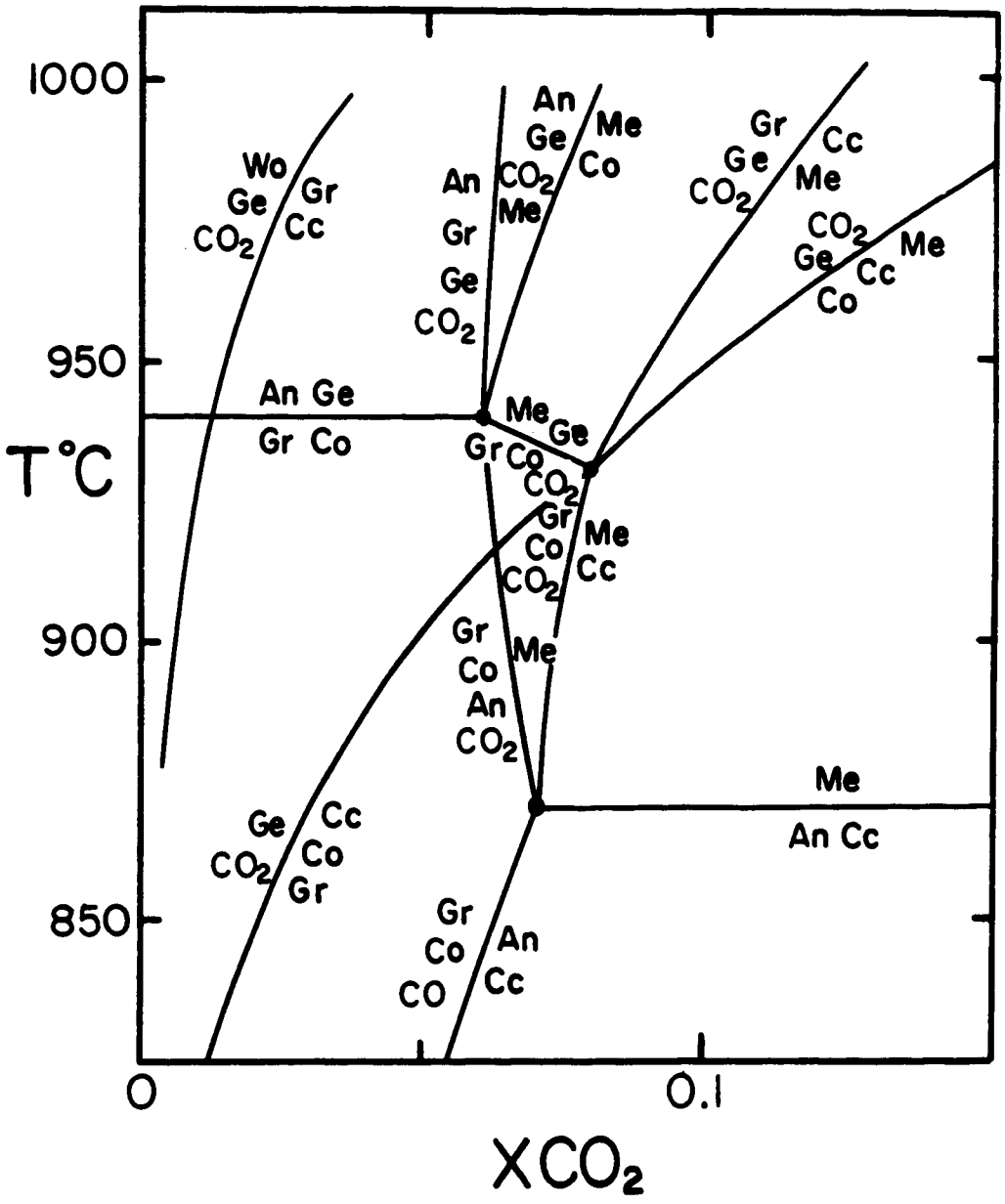
1000
950
900
850
T°C
0
0.1
XCO2
Wo
Ge
Gr
CO2
Cc
An
Ge
Me
Co
An
CO2
Me
Gr
Ge
CO2
Gr
Ge
Cc
CO2
Me
CO2
Ge
Me
Cc
Co
An Ge
Gr Co
Me
Ge
Gr
Co
CO2
Gr
Co
Me
CO2
Cc
Gr
Co
An
CO2
Me
Me
An Cc
Ge
Cc
CO2
Co
Gr
Gr
Co
An
CO
Cc

Figure 6. Calculated meionite phase equilibria at 10 kbar. All equilibria shift to higher temperature relative to 3 Anorthite + Calcite = Meionite. Terminal meionite reaction as a function of fluid composition is Me + H_2O = Czo + CO_2. The effect of increasing pressure on the phase relations is essentially the same as solid solutions in meionite.

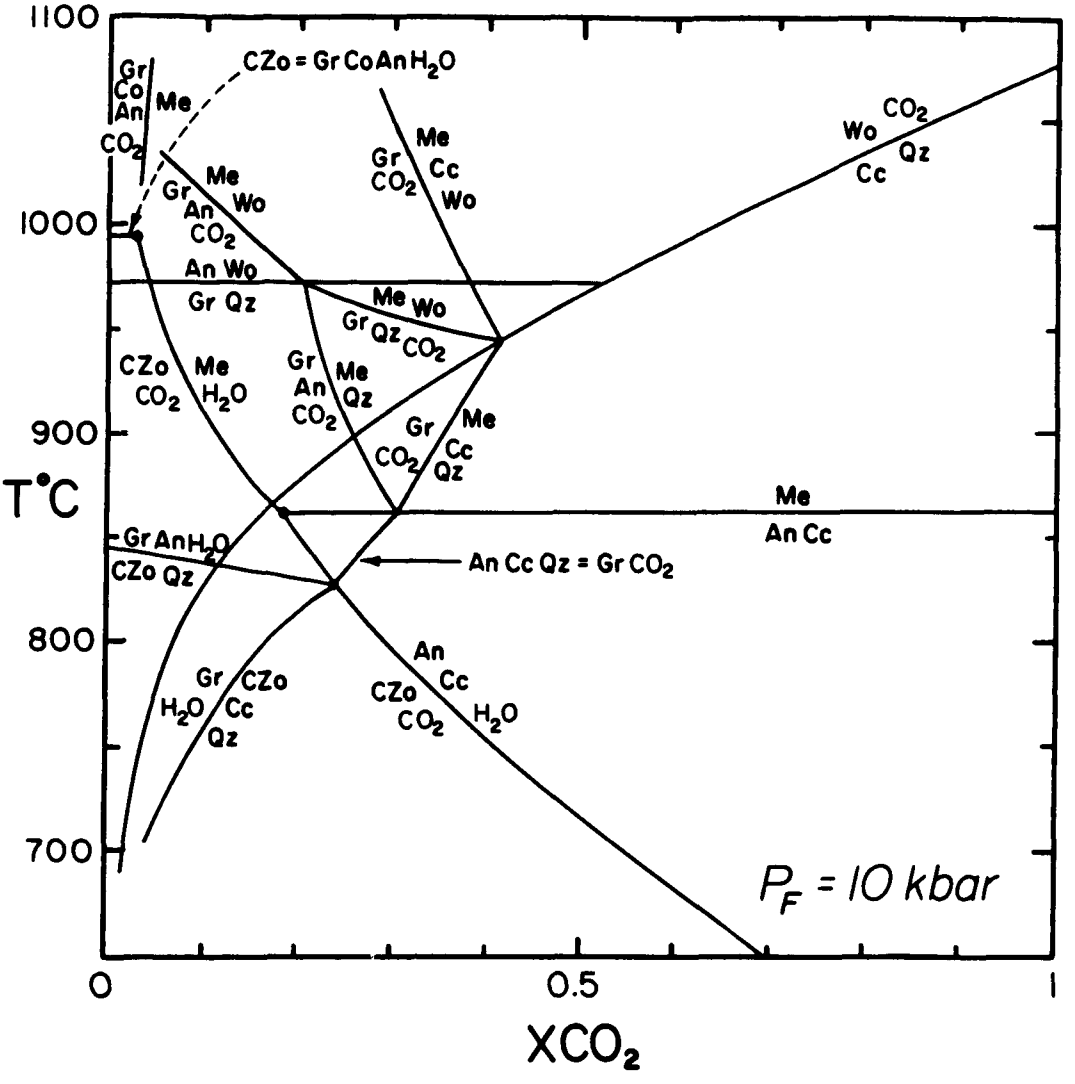
1100
1000
900
800
700
T°C
0
0.5
1
XCO2
CZo = Gr Co An H2O
Gr Co An
Me
CO2
Gr An CO2
Me Wo
An Wo
Gr Qz
Me Wo
Gr Qz CO2
CZo CO2
Me H2O
Gr An CO2
Me Qz
Gr CO2
Me Cc Wo
Wo CO2 Qz Cc
Gr CO2 Cc Qz
Me
An Cc
Gr An H2O
CZo Qz
An Cc Qz = Gr CO2
Gr CZo H2O Cc Qz
An Cc CZo CO2 H2O
PF = 10 kbar

topology (Fig. 6). The stability field of Me + Qz assemblages expands to much more water rich conditions, and meionite alone reacts to clinozoisite at $X_{CO_2} < 0.2$ and 865 to 1000°C. Reactions that were metastable at 5 kbar (e.g., An + Cc + Qz = Gr + CO_2, Me + Qz = Gr + An + CO_2) become stable at 10 kbar.

Ellis (1978) was the first to present a complete, detailed, qualitative topology of the same reactions shown in Figs. 5 and 6. Schenk (1984) deduced a phase diagram for selected meionite T–X equilibria at 6 kbar in the CASCH system that is similar to our T–X diagram (Fig. 5a). However, Ellis (1978) implied a much more restricted range of $T–X_{CO_2}$ stability for meionite than that calculated here. In addition, previous topologies were drawn with the meionite decarbonation equilibria as all having positive $T–X_{CO_2}$ slopes (relative to the common T–X diagram with XCO_2 increasing to the right, Figs. 5 and 6). Based on the model for Al–Si disorder assumed here, many of the meionite reactions have negative slopes in T–X space, and in P–T space. That is, meionite decarbonation reactions have negative slopes with meionite on the *high* temperature side of the reaction. The reaction

Meionite + Quartz = Anorthite + Grossular + CO_2 (14)

$2\ Ca_4Al_6Si_6O_{24}CO_3 + SiO_2 = 5\ CaAl_2Si_2O_8 + Ca_3Al_2Si_3O_{12} + 2\ CO_2$.

is used in Chapter IV to calculate CO_2 activities in high grade gneisses. This is unusual for decarbonation reactions, reactions that characteristically involve high volume and entropy changes, but a necessary consequence of the disordering model. A completely ordered model yields a slight positive slope, and an entropy of approximately 728 j/mol K (configurational entropy of 19 j/mol K) yields a slope of 0.

The phase relations depicted in Figs. 5 and 6 are essentially the same (with regard to locations of reactions in $T–XCO_2$ space) if one assumes an alternative ordering state for synthetic meionite. Phase relations were calculated for the hypothetical case of meionite with completely ordered and disordered Al–Si distribution, and although the slopes of meionite volatilization equilibria change, the

invariant points out of which the meionite reactions emanate do not change, as they are controlled by equilibria such as Reactions 1, 3 and 4.

Effects of Solid Solutions

The phase relations in Figs. 5 and 6 indicate that the stability of end-member meionite is restricted to unusually high temperatures for regional metamorphism (Goldsmith, 1976), and it would only be found in high temperature contact metamorphism of pure calc-silicates (Na and Cl free) adjacent to mafic or intermediate intrusions, or in high temperature granulite terranes. The tendency of scapolite to preferentially partition Na relative to plagioclase (Orville, 1974; Goldsmith & Newton, 1977) would further restrict the occurrence of meionite to an extremely pure protolith. In order to account for the common occurrence of calcic carbonate scapolite in quartz-bearing assemblages in metamorphic rocks, solid solutions are required as an alternative to the high pressures discussed above, in order to bring the stability of scapolite into the temperature and pressure range of the amphibolite and granulite facies. The effect of solid solutions on meionite phase relations is essentially identical to the shift observed with increasing pressure (i.e., Reaction 1 shifts to lower T relative to other equilibria; Ellis, 1978), with the ultimate stability of meionite limited by the intersection of Reaction 1 with

$$\text{Clinozoisite} + CO_2 = \text{Anorthite} + \text{Calcite} + H_2O \qquad (15)$$
$$2Ca_2Al_3Si_3O_{12}(OH) + CO_2 = 3CaAl_2Si_2O_8 + CaCO_3 + H_2O$$

to yield the equilibrium

$$\text{Clinozoisite} + CO_2 = \text{Meionite} + H_2O \qquad (16)$$
$$2Ca_2Al_3Si_3O_{12}(OH) + CO_2 = Ca_4Al_6Si_6O_{24}CO_3 + H_2O$$

(Kerrick *et al.*, 1973; Aitken, 1983) (Fig. 6). With increasing solid solution of Na, Cl, or SO_4 in scapolite, Reaction 1 will track along Reaction 14 to higher X_{CO_2} and lower temperature. For example, scapolite of composition Me_{90} (EqAn = 85) is the most calcic natural scapolite known (Shaw, 1960; Schenk, 1985; Perchuk *et al.*,

1985). The occurrence of nearly pure anorthite ($An_{97.5}$) with scapolite (Me_{90}) and calcite at 6 kbar and 750°C (Schenk, 1984: Table 3) defines the position of Reaction 1 for the most calcic scapolite known. Me_{90} would break down to grossular + anorthite + corundum + CO_2 at $X_{CO_2} < 0.1$, and the absence of scapolite–gehlenite assemblages may be due to the relative instability of end member meionite (Fig. 5a). The stability field of meionite + quartz is also greatly expanded with dilutions of meionite compared to the end member system in which a limited stability field for meionite is predicted in the presence of quartz at 5 kbar. Further dilution of the meionite component (e.g., assemblages reported by Oterdoom & Gunter, 1983; Table 3: Sc (Me_{80}) + Pg (An_{98}) + Cc) shifts the locus of the end member reaction to even lower temperature. Meionite alone would then break down to clinozoisite, and in the presence of quartz would break down to grossular at nearly the same X_{CO_2}.

An example of the effect of solid solutions in scapolite *and* coexisting phases on the location of scapolite reactions is exemplified by the assemblage Sc (Me_{73}) + Pg (An_{42}) + Gt ($Gr_{37}Py_5Alm_{55}Sp_3$) + Ep (Ps_{21}) + Cc + Qz + Hbl (Table 3, PS86E–31), found in a sheared meta–anorthosite in the southwestern Grenville Province of Ontario (Chapter IV). This is an invariant assemblage formed by the intersection of Reaction 1 with Reactions 7, 14, and 15. At 10 kbar and 700°C, a_{CO_2} was calculated using the equilibrium

$$\text{Anorthite} + \text{Calcite} + \text{Quartz} = \text{Grossular} + CO_2 \qquad (17)$$
$$CaAl_2Si_2O_8 + 2CaCO_3 + SiO_2 = Ca_3Al_2Si_3O_{12} + 2CO_2$$

to be 0.38, corresponding to X_{CO_2} of approximately 0.30 to 0.35 assuming $P_{fluid} = P_{total}$ (anorthite activity calculated from Newton *et al.*, 1980 (Table 3), and grossular activity from Anovitz & Essene, 1987). Because the activity of meionite is fixed by the presence of plagioclase and calcite in this assemblage, and the free energy of meionite is calculated relative to anorthite + calcite, one obtains the same value of

TABLE 3. Data used in calculation of activity-composition relations for carbonate scapolite. K is equilibrium constant for Reaction 1 defined in text.

				Plagioclase		Scapolite		
REFERENCE	P kbar	T°C	K	XAn	aAn	EqAn	aMe	γMe
Frank 1983 Crevola, Switz.	7	600	0.0923	0.50	0.743	0.71	0.441	0.6211
Ferry 1976 Maine, U.S.A.	3.5	600	0.0913	0.34	0.569	0.65	0.360	0.5538
Oterdoom & Gunter 1983	3	600	0.0912	0.94	0.940	0.73	0.525	0.7192
Val Schiesone, Switz.	3	600	0.0912	0.91	0.910	0.74	0.512	0.6919
Hayob, pers. comm Idaho, U.S.A.	7	600	0.0923	0.96	0.960	0.69	0.535	0.7754
Thompson, quoted in Oterdoom & Gunter E. Conn., U.S.A.	6	675	0.2037	0.95	0.950	0.74	0.646	0.8730
Mezger & Okrusch 1985 Samos, Greece	5	700	0.2570	0.59	0.720	0.64	0.556	0.8688
Moecher 1988	10	700	0.2655	0.42	0.598	0.62	0.488	0.7871
Parry Sound, Ont. Canada	10	700	0.2655	0.65	0.740	0.69	0.573	0.8304
Ellis 1978	4	750	0.3963	0.92	0.920	0.82	0.745	0.9085
experiments	4	750	0.3963	0.50	0.642	0.53	0.569	1.0736
Glassley 1983 W. Greenland	6	750	0.4027	0.83	0.830	0.67	0.693	1.0343
Schenk 1984 S. Calabria, Italy	6	750	0.4027	0.98	0.980	0.85	0.785	0.9235

a_{CO_2} for this sample from Reaction 16 if a_{CO_2} is calculated using meionite decarbonation equilibria such as Reaction 14. Therefore, in scapolite–calcite–bearing calc–silicates, meionite equilibria will not provide additional information with regard to fluid composition. It is in scapolite–bearing calc–silicates, orthogneisses and metabasites devoid of calcite that meionite equilibria will prove most useful in constraining fluid composition.

Activity–Composition (a–X) Relations

A reduction in activity of the meionite component in scapolite may arise from substitution of NaCl and $CaSO_4$ for $CaCO_3$, and NaSi for CaAl. The various substitutions are related as a result of local charge balance constraints (Chamberlain *et al.*, 1985; Hassan & Buseck, 1988), and complete modeling of activity–composition (a–X) relations for all scapolite solid solutions is likely to be extremely complex, and perhaps more realistically treated as mixing of marialite–mizzonite and mizzonite–meionite. Here, we will attempt to model only the NaSi–CaAl exchange for application to carbonate–rich scapolites. Oterdoom & Gunter (1983) have performed similar calculations based on the model for completely disordered end–member meionite of Oterdoom & Wenk (1983). The results of our calculations are similar to the model of Oterdoom & Gunter (1983), in that both models predict negative departures from ideality.

Natural scapolite–plagioclase–calcite assemblages buffer the activity of Me in scapolite (a^{Sc}_{Me}) according to Reaction 1. Knowing the pressure and temperature of equilibration of such an assemblage, the value of ln K (= $-\Delta G°/RT$) for the shift in Reaction 1 at this P and T can be calculated using **EQUILI**. Assuming an activity model for anorthite in plagioclase, one can then calculate the activity of meionite in natural scapolite (Oterdoom & Gunter, p. 983). For pure calcite, K for Reaction 1 reduces to

$$K = a^{Sc}_{Me} / (a^{Pl}_{An})^3.$$

For carbonate scapolite, mixing of Ca and Na occurs on four equivalent cation sites. Therefore, the activity of meionite based on mixing of one cation is obtained from the relation

$$a_{Me}^{Sc} = [K \cdot (a_{An}^{Pg})^3]^{0.25}.$$

One parameter is not sufficient to describe the composition of natural scapolite that may contain Cl in addition to CO_3, and the mole fraction of meionite calculated above (Me = Ca/[Ca+Na+K]) takes into account only the NaSi–CaAl solid solution. However, the mole fraction of meionite in pure carbonate scapolite is adequately described by the equivalent anorthite content (Orville, 1974; Ellis, 1978), or EqAn = 100[(Al–3)/3] for the meionite formula based on Si + Al = 12 (Shaw, 1960; Evans *et al.*, 1969). This convention will be used for calculating the mole fraction of meionite for the purposes of modeling a–X relations. The two end members are taken to be meionite ($Ca_4Al_6Si_6O_{24}CO_3$, EqAn = 100) and the hypothetical composition $CaNa_3Al_3Si_9O_{24}CO_3$ (EqAn = 0).

In the absence of experiments aimed at directly modeling a–X relations, one would ideally use well-characterized scapolite–plagioclase–calcite assemblages from a single regional metamorphic terrane for which there exists good temperature control and a wide range of scapolite and plagioclase compositions. Sc–Pg–Cc assemblages are reported from a number of metamorphic settings, however mineral chemistries are not always reported, analyses may be of questionable quality or are incomplete, or textural relations make identification of equilibrium equivocal. Using a variety of sources that do not all provide detailed petrographic and compositional data, and for which well calibrated geothermobarometers are not used, certainly introduces errors in the activity model. However, the data provide insight into the mixing properties of calcic carbonate–scapolites and allow a provisional model to be developed for the purposes of calculating CO_2 activities in scapolite–bearing gneisses.

Thermobarometric and compositional data compiled for natural scapolite–plagioclase–calcite assemblages, along with the calculated a^{Sc}_{Me} and γ^{Sc}_{Me} are summarized in Table 3. Activities of anorthite in plagioclase for $X_{An} < 0.80$ were calculated using the model of Newton *et al.* (1980). For $X_{An} > 0.80$ the latter model predicts $\gamma_{An} < 1$. However, ion exchange experiments on the plagioclase solid solution series predict γ_{An} equal to or slightly greater than 1 (Orville, 1972; Blencoe *et al.* 1982). For these anorthite rich plagioclases we have assumed $\gamma_{An} = 1$. A $\pm$25°C temperature uncertainty was included in the calculation of a^{Sc}_{Me} as temperature is the greatest source of uncertainty in the data on natural assemblages. An asymmetric regular solution was used to model the activity–composition relations, with the constraint that $a^{Sc}_{Me} = 1$ at $X^{Sc}_{Me} = 1$ and $a^{Sc}_{Me} = 0$ at $X^{Sc}_{Me} = 0$. Based on a least squares fit of the a–X data to the relation

$$RT \ln \gamma^{Sc}_{Me} = (1-X^{Sc}_{Me})^2[W_{GMe} + 2X^{Sc}_{Me}(W_{GMa} - W_{GMe})]$$

the following values are obtained for W_{GMe} and W_{GMa}, where Me is the $Ca_4Al_6Si_6O_{24}CO_3$ end member, Ma is the hypothetical $CaNa_3Al_3Si_9O_{24}CO_3$ end member ("carbonate marialite"), and $W_G = W_H - TW_S$:

$W_{GMe} = 21{,}761 - 33T(K)$ J/mol·cation, and
$W_{GMa} = -176{,}314 + 171T(K)$ J/mol·cation.

These values were used to calculate the distribution of isotherms in Fig. 7. The calculated activities are generally in good agreement with the observed activities except for the two 750°C samples at EqAn 82 and 85. This discrepancy may result from the assumption that for all temperatures $a^{Sc}_{Me} = 1$ at $X^{Sc}_{Me} = 1$, with the real mixing relations being more complex. It is evident that at 750°C, mixing is essentially ideal. Extrapolation to temperatures greater than 750°C indicates a marked positive deviation from ideality, consistent with the experiments of Goldsmith & Newton (1977) at 1100°C. Additional data on scapolite more calcic than EqAn = 0.75 in the temperature range 600 to 800°C are required in order to determine how a–X relations vary in this T–X field. The a–X relations are valid for

Figure 7. Activity–composition relations for carbonate scapolite. Vertical bars are variation in a^{Sc}_{Me} produced by a ±25°C variation in reported equilibration temperature. Symbols without bars are experimental data points of Ellis (1978), all others based on natural assemblages tabulated in Table 3.

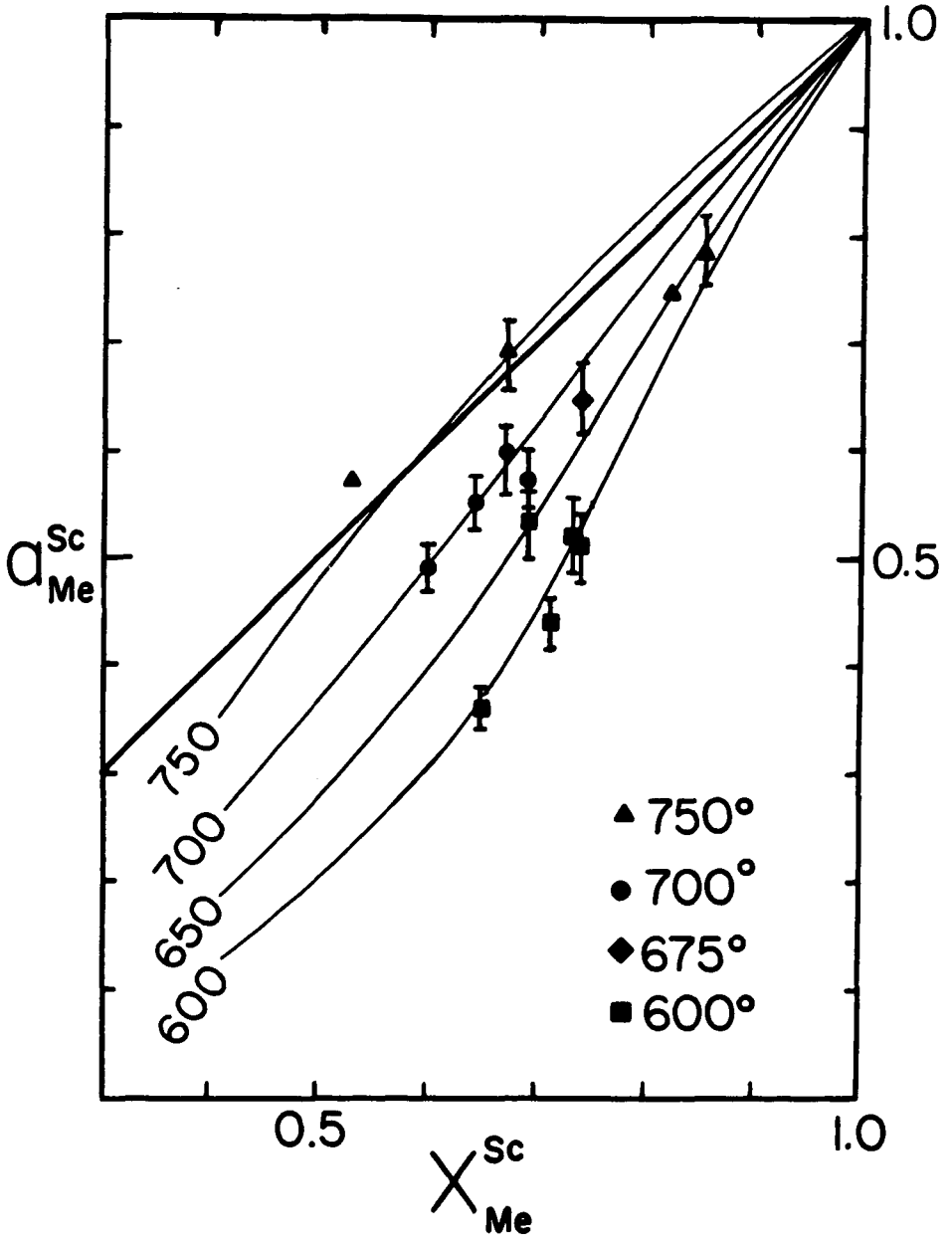
1.0
0.5
a^{Sc}_{Me}
750
700
650
600
▲ 750°
● 700°
◆ 675°
■ 600°
0.5
1.0
X^{Sc}_{Me}

carbonate scapolite only in the temperature and composition range of the data in Fig. 7 and Table 3, and should not be extrapolated outside this region.

The negative values of W_H and W_S obtained for Ma component are consistent with observations on the stability of intermediate scapolite solid solutions relative to the isostructural, partly disordered end member standard state assumed here. The scapolite solid solutions are much more stable than the end members, consistent with the lack of reported occurrences of meionite, marialite, or sulfate meionite in nature. Scapolites with compositions centered around mizzonite are an unusually common intermediate composition (Evans *et al.*, 1969; Orville, 1974; Aitken, 1983; Oterdoom & Gunter, 1983; Chapter 3), and mizzonitic scapolite with a limited compositional range in terms of EqAn and $CO_3/(CO_3+Cl)$ often coexists with an extremely wide range of plagioclase compositions (e.g., Frank, 1983). The stability of mizzonite is manifest by the relatively high molar entropy compared to more meionite and marialite-rich compositions, and its high heat of solution relative to oxide mixes (Komada *et al.* 1988). If the a-X relations are calculated assuming a less disordered end member than that used here, one obtains slightly less non-ideal behavior, and a completely disordered end member yields greater departures from ideality, particularly for the 600 and 700°C samples. Therefore, the mixing effects observed here are in part dependent on the modeling assumptions, but may have some physical basis in reality.

The activity of meionite calculated in this manner is directly dependent on the activity of anorthite, and therefore on the choice of anorthite activity model. The degree of model dependency was evaluated by comparing meionite activities obtained above with those calculated using the anorthite models of Orville (1972) and Blencoe *et al.* (1982) at 700°C. The calculated meionite activities are only slightly different from those obtained using the activity model of Newton *et al.* (1980) and yield a smaller variation than that produced by a $\pm$25°C variation in temperature for any of the models. However, there is no means of evaluating the isotherms at 600, 650, or 750°C for our scapolite model. The model for the

activity of anorthite in plagioclase of Newton *et al.* can be used to calculate anorthite activities at temperatures other than those at which the solution calorimetry was performed (970 K: Newton *et al.* 1980), but there is only one additional thermodynamic constraint on the calculated activities for the model of Newton *et al.* This limits the general validity of the meionite activity model developed here, and more reliable modeling of a–X relations in scapolite will depend on a more carefully calibrated activity model for anorthite in plagioclase and meionite in scapolite.

An artifact of the empirical method of calculating meionite activities based on anorthite activities from coexisting plagioclase is that its application to phase equilibrium calculations for systems based on alternative thermodynamic data will lead to erroneous conclusions involving the activity of meionite. For example, application of the activity model derived above (or that of Oterdoom & Wenk 1983) in the calculation of CO_2 activities using the thermodynamic data base of Berman *et al.* (1986), for example, will yield values that may be highly disparate and inaccurate. Both our model and that of Oterdoom and Gunter (1983) are based on different assumptions concerning the standard state of end member meionite, activity models for anorthite, and thermodynamic data for anorthite, calcite, and meionite. Future work should be directed at direct experimental determination of a–X relations for plagioclase and carbonate scapolite over a wide temperature range, and at obtaining better constraints on the ordering state of synthetic scapolites. It may prove more useful to experimentally constrain the stability of mizzonite (Me_{75})

$$\text{Anorthite} + \text{Albite} + \text{Calcite} = \text{Mizzonite} \qquad (18)$$

$$3\ CaAl_2Si_2O_8 + NaAlSi_3O_8 + CaCO_3 = Ca_3NaAl_5Si_7O_{24}CO_3$$

as it appears to be a relatively stable and common intermediate composition.

The presence of carbonate rich scapolite in calc–silicate assemblages has been inferred to indicate high CO_2 partial pressures in high grade calc–silicates (*e.g.*, Kumar & Chacko, 1986). Based on the phase relations quantified above, this is not

necessarily the case, and meionite is stable over virtually the entire range of fluid compositions. Intermediate scapolite solid solutions may eventually be found to be consistent with high CO_2 activities (e.g., Aitken 1983; Chapter IV). Clearly, the exact fluid composition will depend on temperature, pressure, and activities of components in the solid phases. In Chapter IV the thermodynamic data base and scapolite mixing model derived here will be applied to evaluation of the effects of solid solutions in scapolite and coexisting phases on fluid composition in upper amphibolite and granulite facies calc-silicates, garnet amphibolites, meta-anorthosites, and metabasites.

References

Aitken, B.G., 1983. T-XCO_2 stability relations and phase equilibria of a calcic carbonate scapolite. Geochim. Cosmochim. Acta **47**, 351-362.

Aitken, B.G., Evans, H.T., & Konnert, J.A., 1984. The crystal structure of a synthetic meionite. N. Jb. Miner. Abh. **149**, 309-324.

Angel, R.J., Hazen, R.M., McCormick, T.C., Prewitt, C.T., & Smyth, J.R., 1988. Comparative compressibility of end-member feldspars. Phys. Chem. Min., in press.

Anovitz, L.M., & Essene, E.J., 1987. Compatibility of geobarometers in the system $CaO-FeO-Al_2O_3-SiO_2-TiO_2$: implications for garnet mixing models. J. Geol. **95**, 633-645.

Anovitz, L.M., 1987. Pressure and Temperature Constraints on Metamorphism in the Grenville Province, Ontario. Ph.D. Thesis, University of Michigan.

Austreim, H., & Griffen, W.L., 1985. Shear deformation and eclogite formation within granulite-facies anorthosites of the Bergen Arcs, Western Norway. Chem. Geol. **50**, 267-281.

Bass, J.D. & Weidner D.J., 1984. Elasticity of single-crystal orthoferrosilite. J. Geophys. Res. **89**, 4359-4372.

Berman, R.G., Engi, M., Greenwood, H.J., & Brown, T.H., 1986. Derivation of internally consistent thermodynamic data by the technique of mathematical programming: a review with application to the system $MgO-SiO_2-H_2O$. J. Petrol. **27**, 1331-1364.

Birch, F., 1966. Compressibility: elastic constants. In: Clark, S.P., Jr., (ed.) Handbook of Physical Constants, Geol. Soc. Amer. Mem. **97**, 97-173.

Blencoe, J.G, Merkel, G.A., & Seil, M.K., 1982. Thermodynamics of crystal-fluid equilibria, with applications to the system $NaAlSi_3O_8-CaAl_2Si_2O_8-SiO_2-NaCl-CaCl_2-H_2O$. In: Saxena, S. (ed) Advances in Physical Geochemistry, vol 2. New York: Springer-Verlag, 191-222.

Boettcher, A.L., 1970. The system $CaO-Al_2O_3-SiO_2-H_2O$ at high pressure and temperature. J. Petrol. **11**, 337-379.

Boivin, P., & Camus, G., 1981. Igneous scapolite-bearing associations in the Chaine des Puys, Massif Central (France) and Atakor (Hoggar, Algeria). Contrib. Mineral. Petrol. **77**, 365-375

Chamberlain, C.P., Docka, J.A., Post, J.E., & Burnham, C.W., 1985. Scapolite: alkali atom configurations, antiphase domains, and compositional variations. Am. Mineral. **70**, 134-140.

Chatterjee, N.D., Johannes, W., & Leistner, H., 1984. The system $CaO-Al_2O_3-SiO_2-H_2O$: new phase equilibrium data, some calculated phase relations and their petrological applications. Contrib. Mineral. Petrol. **88**, 1-13.

Coolen, J.J.M.M.M., 1980. Chemical Petrology of the Furua Granulite Complex, Southern Tanzania. GUA Papers Geol. Ser. 1, No. **13-1980**, 258pp.

Devaraju, T.C., & Coolen, J.J.M.M.M., 1983. Mineral chemistry and P-T conditions of a basic scapolite-garnet-pyroxene granulite from Doddakanya, Mysore District. J. Geol. Soc. India **24**, 404-411.

Devaraju, T.C., & Gowd Reddy, K., 1976. Coexisting orthopyroxene and scapolite in certain basic granulites from Doddakanya, Mysore District. Indian Mineral. **17**, 5-11.

Dollase, W.A., 1968. Refinement and comparison of the structures of zoisite and clinozoisite. Am. Mineral. **53**, 1882-1898.

Edwards, A.C., Lovering, J.F., & Ferguson, J., 1979. High pressure basic inclusions from the Kayrunnera kimberlite diatreme in New South Wales, Australia. Contrib. Mineral. Petrol. **69**, 185-192.

Ellis, D.E., 1978. Stability and phase equilibria of chloride and carbonate scapolites at 750°C and 4000 bars. Geochim. Cosmochim. Acta **42**, 1271-1281.

Evans, B.W., Shaw, D.M., & Houghton, D.R., 1969. Scapolite stoichiometry. Contrib. Mineral. Petrol. **24**, 293-305.

Evans, H.T., Jr., 1979. The thermal expansion of anhydrite to 1000°C. Phys. Chem. Mins. **4**, 77-82.

Ferry, J.M., 1976. Metamorphism of calcareous sediments in the Waterville-Vassalboro area, south-central Maine: mineral reactions and graphical analysis. Am. J. Sci **276**, 841-882.

Frank, E., 1983. Alpine metamorphism of calcareous rocks along a cross-section in the Central Alps: occurrence and breakdown of muscovite, margarite, and paragonite. Schweiz. Mineral. Petrogr. Mitt. **63**, 37-93.

Gasparik, T., 1981. Mixing properties of the binary Jd-CaTs. Eos **62**, 412.

Gasparik, T., 1984a. Experimentally determined stability of clinopyroxene + garnet + corundum in the system $CaO-MgO-Al_2O_3-SiO_2$. Am. Mineral. **69**, 1025-1035.

Gasparik, T., 1984b. Experimental study of subsolidus phase relations and mixing properties of pyroxene in the system $CaO-Al_2O_3-SiO_2$. Geochim. Cosmochim. Acta **48**, 2537-2545.

Gibbs, G.V., 1966. The polymorphism of cordierite I: the crystal structure of low cordierite. Am. Mineral. **51**, 1068-1087.

Glassley, W.E., 1983. Deep crustal carbonates as CO_2 fluid sources: evidence from metasomatic reaction zones. Contrib. Mineral. Petrol. **84**, 15-24.

Goldsmith, J.R., 1976. Scapolites, granulites, and volatiles in the lower crust. Geol. Soc. Amer. Bull. **61**, 161-168.

Goldsmith, J.R., 1980. The melting and breakdown reactions of anorthite at high pressures and temperatures. Am. Mineral. **65**, 272-284.

Goldsmith, J.R., 1981. The join $CaAl_2Si_2O_8-H_2O$ (anorthite-water) at high pressures and temperatures. Am. Mineral. **66**, 1183-1188.

Goldsmith, J.R., & Newton, R.C., 1977. Scapolite-plagioclase stability relations at high pressure and temperatures in the system $NaAlSi_3O_8-CaAl_2Si_2O_8-CaCO_3-CaSO_4$. Am. Mineral. **62**, 1063-1081.

Gordon, T.M., & Greenwood, H.J., 1971. The stability of grossularite in H_2O–CO_2 mixtures. Am. Mineral. **56**, 1674–1688.

Grazziani, G., & Lucchessi, S., 1982. The thermal behavior of scapolites. Am. Mineral. **67**, 1229–1247.

Halbach, H., & Chatterjee, N.D., 1984. An internally consistent set of thermodynamic data for twentyone CaO–Al_2O_3–SiO_2–H_2O phases by linear parametric programming. Contrib. Mineral. Petrol. **88**, 14–23.

Harker, R.I., & Tuttle, O.F., 1956. Experimental data on the PCO_2–T curve for the reaction: calcite + quartz = wollastonite + carbon dioxide. Am. J. Sci. **254**, 239–256.

Hassan, I., & Buseck, P.R., 1988. HRTEM characterization of scapolite solid solutions. Am. Mineral. **73**, 119–134.

Hazen, R.M., & Finger, L.W., 1978. Crystal structures and compressibilities of pyrope and grossular to 60 kbar. Am. Mineral. **63**, 297–303.

Hazen, R.M., & Sharp, Z.D., 1988. Compressibility of the framework silicates sodalite and scapolite. Am. Mineral., in press.

Hays, J.F., 1967. Lime–alumina–silica. Carnegie Inst. Wash. Yrbk. **65**, 234–239.

Hemingway, B.S., 1987. Quartz: Heat capacities from 340 to 1000 K and revised values for the thermodynamic properties. Am. Mineral. **72**, 273–279.

Hemingway, B.S., & Robie, R.A., 1984. Heat capacity and thermodynamic functions for gehlenite and staurolite, with comments on the Schottky anomaly in the heat capacity of staurolite. Am. Mineral. **69**, 307–318.

Hietanen, A., 1967. Scapolite in the Belt Series in the St. Joe–Clearwater region, Idaho. Geol. Soc. Amer. Spec. Pap. **86**.

Hoschek, G., 1980. Phase relations of a simplified marly rock system with applications to the Western Hohe Tauern (Austria). Contrib. Mineral. Petrol. **73**, 53–68.

Huckenholz, H.G., Holzl, E., & Lindhuber, W., 1975. Grossularite, its solidus and liquidus relations in the $CaAl_2Si_2O_8$–H_2O system up to 10 kbar. N. Jb. Miner. Abh. **124**, 1–46.

Jacobs, G.K., & Kerrick, D.M., 1981. Devolatilization equilibria in H_2O–CO_2 and H_2O–NaCl fluids: an experimental and thermodynamic evaluation at elevated pressures and temperature. Am. Mineral. **66**, 1135–1153.

Janes, N., & Oldfield, E., 1985. Prediction of silicon–29 nuclear magnetic resonance chemical shifts using a group electronegativity approach: applications to silicate and aluminosilicate structures. J. Amer. Chem. Soc. **107**, 6769–6775.

Jenkins, D.M., Newton, R.C., & Goldsmith, J.R., 1985. Relative stability of Fe–free zoisite and clinozoisite. J. Geol. **93**, 303–325.

Jones, A.P., Smith, J.V., Dawson, J.B., Hansen, E.C., 1983. Metamorphism, partial melting, and K–metasomatism of garnet–scapolite–kyanite granulite xenoliths from Lashaine, Tanzania. J. Geol. **91**, 143–165.

Kerrick, D.M., (1970). Contact metamorphism in some areas of the Sierra Nevada, California. Geol. Soc. Am. Bull. **81**, 2913–2938.

Kerrick, D.M., Crawford, K.E., & Randazzo, A.F., 1973. Metamorphism of three roof pendants in the Sierra Nevada, California. J. Petrol. **14**, 303-325.

Kerrick, D.M., & Ghent, E.D., (1984). P-T-X_{CO_2} relations of equilibria in the system $CaO-Al_2O_3-SiO_2-CO_2-H_2O$. In: Fonarev, V.I., & Korikovskii, S.P., (eds.) Problems of Physico-Chemical Petrology **2**, 57-64. Moscow: Science.

Kerrick, D.M., & Jacobs, G.K., 1981. A modified Redlich-Kwong equation for H_2O, CO_2, and H_2O-CO_2 mixtures at elevated pressures and temperatures. Am. J. Sci. **281**, 735-767.

Klinowski, J., Thomas, J.M., Fyfe, C.M., & Hartman, J.S., 1981. Applications of magic angle-spinning silicon-29 nuclear magnetic resonance. Evidence for two different kinds of silicon-aluminum ordering in zeolitic structures. J. Phys. Chem. **85**, 2590-2594.

Komada, N., Moecher, D.P., Westrum, E.F. Jr., Hemingway, B.S., Zolotov, M.Yu., Semenov, Y.V., & Khodakovsky, I.L., 1988. Thermodynamics of scapolites. J. Chem. Thermo. in press.

Koziol, A.M., & Newton, R.C., 1988. Redetermination of the anorthite breakdown reaction and improvement of the plagioclase-garnet-Al_2SiO_5-quartz geobarometer. Am. Mineral. **73**, 216-223.

Kumar, G.R.R., & Chacko, T., 1986. Mechanisms of charnockite formation and breakdown in Southern Kerala: implications for the origin of the Southern Indian Granulite Terrain. J. Geol. Soc. India **28**, 277-288.

Kwak, T.A.P., 1977. Scapolite compositional change in a metamorphic gradient and its bearing on the identification of meta-evaporite sequences. Geol. Mag. **114**, 343-354.

Langer, K., & Lattard D., 1980. Identification of a low-energy OH-valence vibration in zoisite. Am. Mineral. **65**, 779-783.

Levien, L., & Papike, J.J., 1976. Scapolite crystal chemistry: aluminum-silicon distributions, carbonate group disorder, and thermal expansion. Am. Mineral. **61**, 864-877.

Liebermann, R.C., & Ringwood, A.E., 1976. Elastic properties of anorthite and the nature of the lunar crust. Earth Plan. Sci. Lett. **31**, 69-74.

Lin, S.B., & Burley, B.J., 1972. Crystal structure of a sodium and chlorine-rich scapolite. Acta Crystall. **29**, 1272-1278.

Lin, S.B., & Burley, B.J., 1973a. The crystal structure of meionite. Acta Crystall. **B29**, 2024-2026.

Lin, S.B., & Burley, B.J., 1973b. On the weak reflections violating body-centered symmetry in scapolites. Tscher. Mineral. Petrog. Mitt. **20**, 28-44.

Lin, S.B., & Burley, B.J., 1973c. Crystal structure of an intermediate scapolite - wernerite. Acta Crystall. **B31**, 1806-1814.

Lin, S.B., & Burley, B.J., 1975. Crystal chemistry and stoichiometry of the scapolite group. Acta Geol. Taiwanica **18**, 36-48.

Lovering, J.F., & White, A.J.R., 1964. The significance of primary scapolite in granulitic inclusions from deep-seated pipes. J. Petrol. **5**, 195-218.

Lowenstein, W., 1954. The distribution of aluminum in the tetrahedra of silicates and aluminates. Am. Mineral. 39, 92-96.

Markgraf, S.A., & Reeder, R.J., 1985. High temperature structure refinements of calcite and magnesite. Am. Mineral. 70, 590-600.

Mezger, K., & Okrusch, M., 1985. Metamorphism of the variegated sequence at Kallithea, Samos, Greece. Tscher. Mineral. Petrog. Mitt. 34, 67-82.

Mirwald, P.W., & Massone, H.-J., 1980. The low-high quartz and quartz-coesite transition to 40 kbar between 600° and 1600°C and some reconnaissance data on the effect of $NaAlO_2$ component in the low quartz-coesite transition. J. Geophys. Res. 85B, 6983-6990.

Misch, P., 1964. Stable association of wollastonite-anorthite, and other calc-silicate assemblages in amphibolite-facies crystalline schists of Nanga Parbat, northwest Himalayas. Contrib. Mineral. Petrol. 10, 315-356.

Moecher, D.P., 1988. Application of scapolite phase equilibria and carbon isotopes to high grade rocks: a test of the CO_2 flooding hypothesis. PhD thesis (unpublished) University of Michigan.

Moecher, D.P., & Essene E.J., 1985a. Scapolite as a potential sensor of fluid composition in calc-silicates and granulites. Geol. Soc. Amer. Abs. Progs. 17, 666.

Moecher, D.P., & Essene, E.J., 1986. Fluid composition in Grenville gneisses: constraints from scapolite equilibria. Geol. Assoc. Canada-Min. Assoc. Canada Prog. Abs. 11, 102.

Mora, C.I., & Valley, J.W., 1988. Halogen-rich scapolite and biotite: implications for metamorphic fluid-rock interaction. Am. Mineral., in submission.

Myer, G.H., 1965. X-ray determinative curve for epidote. Am. J. Sci. 263, 78-86.

Myer, G.H., 1966. New data on zoisite and epidote. Am. J. Sci. 264, 364-385.

Newton, R.C., 1965. The thermal stability of zoisite. J. Geol. 73, 431-441.

Newton, R.C., 1966. Some calc-silicate equilibrium relations. Am. J. Sci. 264, 204-222.

Newton, R.C., Charlu, T.V., & Kleppa, O.J., 1980. Thermochemistry of the high structure state plagioclases. Geochim. Cosmochim. Acta 44, 933-941.

Newton, R.C., & Kennedy, G.C., 1963. Some equilibrium relations in the join $CaAl_2Si_2O_8$-H_2O. J. Geophys. Res. 68, 2967-2983.

Okrusch, M., Schroder, B., & Schnutgen, A., 1979. Granulite facies metabasite ejecta in the Laacher See area, Eifel West Germany. Lithos 12, 251-270.

Oliver, N., & Wall, V.J., 1987. Metamorphic plumbing system in Proterozoic calc-silicates, Queensland, Australia. Geology 15, 793-796.

Orville, P.M., 1972. Plagioclase cation exchange equilibria with aqueous chloride solution: results at 700°C and 2000 bars in the presence of quartz. Am. J. Sci. 272, 234-272.

Orville, P.M., 1974. Stability of scapolite in the system Ab-An-NaCl-$CaCO_3$ at 4 kb and 750°. Geochim. Cosmochim. Acta 39, 1091-1105.

Oterdoom, H., & Gunter, W.D., 1983. Activity models for plagioclase and CO_3-scapolites: an analysis of field and laboratory data. Am. J. Sci. **283-A**, 255-282.

Oterdoom, H., & Wenk, H.-R., 1983. Ordering and composition of scapolite: field observations and structural interpretations. Contrib. Mineral. Petrol. **83**, 330-341.

Papike, J.J., & Stephenson, N.C., 1966. The crystal structure of mizzonite, a calcium- and carbonate-rich scapolite. Am. Mineral. **51**, 1014-1027.

Papike, J.J., & Zoltai, T., 1965. The crystal structure of a marialite scapolite. Am. Mineral. **50**, 641-655.

Perchuk, L.L., Aranovich, L.Ya., Podlesskii, K.K., Lavrent'eva, I.V., Gerasimov, V.Yu., Fed'kin, V.V., Kitsul, V.I., Karsakov, L.P., & Berdnikov, N.V., 1985. Precambrian granulites of the Aldan shield, eastern Siberia, USSR. J. Meta. Petrol. **3**, 265-310.

Perkins III, D., Westrum, E.F. Jr., & Essene, E.J., 1980. The thermodynamic properties and phase relations of some minerals in the system $CaO-Al_2O_3-SiO_2-H_2O$. Geochim. Cosmochim. Acta **44**, 61-84.

Peterson, R.C., Donnay, G., & LePage, Y., 1979. Sulfate disorder in scapolite. Can. Mineral. **17**, 53-61.

Phakey, P.P., & Ghose, S., 1972. Scapolite: observation of antiphase domain structure. Nature **238**, 78-80.

Putnis, A., & Angel, R.J., 1985. Al,Si ordering in cordierite using "Magic Angle Spinning" NMR. Phys. Chem. Min. **12**, 217-222.

Putnis, A., & Bish, D.L., 1983. The mechanism and kinetics of Al,Si ordering in Mg cordierite. Am. Mineral. **68**, 60-65.

Ribbe, P.H., 1983. Aluminum-silicon order in feldspars; domain textures and diffraction patterns. (In): Ribbe, P.H., (ed.) 1983, Feldspar Mineralogy, 2nd Ed., Min. Soc. Amer. Rev. Min **2**, 21-54.

Robie, R.A., & Hemingway, B.S., 1984. Entropies of kyanite, andalusite, and sillimanite: additional constraints on the pressure and temperature of the Al_2SiO_5 triple point. Am. Mineral. **69**, 298-306.

Robie, R.A., Hemingway, B.S., & Fisher, J.R., 1978. Thermodynamic properties of minerals and related substances at 298.15 K and 1 bar (10^5 pascals) pressure and at higher temperatures. U.S. Geol. Surv. Bull **1452**, reprinted with corrections, 1979.

Robinson, G.R., Jr., & Haas, J.L., 1983. Heat capacity, relative enthalpy, and calorimetric entropy of silicate minerals: an empirical method of prediction. Am. Mineral. **68**, 541-553.

Robinson, G.R., Jr., Haas, J.L., Jr., Schafer, C.M., & Haselton, H.T., Jr., 1982. Thermodynamic and thermophysical properties of selected phases in the $MgO-SiO_2-H_2O-CO_2$, $CaAl_2Si_2O_8-H_2O-CO_2$, and $Fe-FeO-Fe_2O_3-SiO_2$ chemical systems, with special emphasis on the properties of basalts and their mineral components. U.S. Geol. Surv. Open File Rept. **83-79**.

Rollinson, H.R., 1980. Mineral reactions in a granulite facies calc-silicate rock from Scourie. Scott. J. Geol. **16**, 153-164.

Schenk, V., 1984. Petrology of felsic granulites, metapelites, metabasics, ultramafics, and metacarbonates from Calabria (Italy): prograde metamorphism, uplift and cooling of a former lower crust. J. Petrol. 25, 255-298.

Seki, Y., 1959. Relation between chemical composition and lattice constants of epidote. Am. Mineral. 44, 720-730.

Shaw, D.M., 1960. The geochemistry of scapolite: part I. Previous work and general mineralogy. J. Petrol. 1, 218-260.

Shaw, D.M., Moxham, R.L., Filby, R.H., & Ladkowsky, W.W., 1963a. The petrology and geochemistry of some Grenville skarns, Part I: Geology and Petrography. Can. Mineral. 7, 420-442.

Shaw, D.M., Moxham, R.L., Filby, R.H., & Ladkowsky, W.W., 1963a. The petrology and geochemistry of some Grenville skarns, Part II: Geochemistry. Can. Mineral. 7, 578-616.

Sheriff, B.L., Grundy, H.D., & Hartmann, S.J., 1987. Occupancy of T sites in the scapolite series: a multinuclear NMR study using magic angle spinning. Can. Mineral., 25, 717-730.

Skinner, B.J., 1966. Thermal Expansion. In: Clark, S.P., (ed.), Handbook of Physical Constants, Geol. Soc. Am. Memoir 97, 78-96.

Srikantappa, C., Raith, M., & Ackermand, D., 1985. High-grade regional metamorphism of ultramafic and mafic rocks from the Archean Sargur Terrane, Karnataka, south India. Precamb. Res. 30, 189-219.

Storre, B., 1970. Stabilitatsbedingungen Grossular-fuhrender Paragenesen im System $CaO-Al_2O_3-SiO-(2)-CO_2-H_2O$. Contrib. Mineral. Petrol. 29, 145-162.

Stolz, A.J., 1987. Fluid activity in the lower crust and upper mantle: mineralogical evidence bearing on the origin of amphibole and scapolite in ultramafic and mafic granulite xenoliths. Min. Mag. 51, 719-732.

Thomas, C.W., & Nixon, P.H., (1987). Lower crustal granulite xenoliths in carbonatite volcanoes of the Western Rift of East Africa. Min. Mag. 51, 621-633.

Trommsdorff, V., 1966. Progressive Metamorphose kieseliger Karbonatgeshteine in den Zentralalpen zwischen Bernina und Simplon. Schweiz. Mineral. Petrog. Mitt. 46, 431-460.

Tuisku, P., 1985. The origin of scapolite in the Central Lapland schist area, Northern Finland: preliminary results. Bull. Geol. Surv. Finland 331, 159-173.

Ulbrich, H.H., 1973a. Structural refinement of Monte Somma scapolite, a 93% meionite. Schweiz. Mineral. Petrog. Mitt. 53, 385-393.

Ulbrich, H.H., 1973b. Crystallographic data and refractive indices of scapolites. Am. Mineral. 58, 81-92.

Ulbrich, H.H., & Waldbaum, D.R., 1976. Structural and other contributions to the third-law entropies of silicates. Geochim. Cosmochim. Acta 40, 1-24.

Vanko, D.A., & Bishop, F.C., 1980. Experimental determination of NaCl-rich scapolite stability. Geol. Soc. Amer. Abs. Progs. 12, 540.

Vanko, D.A., & Bishop, F.C., 1982. Occurrence and origin of marialitic scapolite in the Humboldt Lopolith, N.W. Nevada. Contrib. Mineral. Petrol. 81, 277-289.

von Knorring, O., & Kennedy, W.Q., 1958. The mineral paragenesis and metamorphic status of garnet–hornblende–pyroxene–scapolite gneiss from Ghana (Gold Coast). Min. Mag. **31**, 846–859.

Warren, R.G., Hensen, B.J., & Ryburn, R.J., 1987. Wollastonite and scapolite in Precambrian calc–silicate granulites from Australia and Antarctica. J. Meta. Geol. **81**, 277–289.

Wilkinson, J.F.G., 1974. Garnet clinopyroxenite inclusions from diatremes in the Gloucester area, New South Wales, Australia. Contrib. Mineral. Petrol. **46**, 275–299.

Winter, J.K., & Ghose, S., 1979. Thermal expansion and high–temperature crystal chemistry of the Al_2SiO_5 polymorphs. Am. Mineral. **64**, 573–586.

Wood, B.J., & Holloway, J.R. (1984) A thermodynamic model for subsolidus equilibria in the system $CaO–MgO–Al_2O_3–SiO–(2)$. Geochim. Cosmochim. Acta **48**, 159–176.

Yang, W.–H., Kirkpatrick, R.J., & Henderson, D.M., 1986. High–resolution ^{29}Si, ^{27}Al, and ^{23}Na NMR spectroscopic study of Al–Si disordering in annealed albite and oligoclase. Am. Mineral. **71**, 712–726.

CHAPTER IV

SCAPOLITE PHASE EQUILIBRIA. II: CO_2 ACTIVITIES IN HIGH GRADE ROCKS

Introduction

The role of fluids in the petrogenesis of high grade rocks and the granulite facies in particular has received considerable attention during the last decade. Although long recognized as the distinguishing feature of granulites (e.g., Eskola 1939), it has become increasingly apparent, based on quantitative petrologic, phase equilibrium and stable isotopic studies, that the granulite facies is characterized by its relatively anhydrous nature relative to lower grade equivalents. The role of a fluid phase in high grade metamorphism can be distilled into two salient questions: 1) is a free fluid phase actually present during high grade metamorphism?; and, 2) is the low H_2O activity (a_{H_2O}) commonly calculated for high grade rocks necessarily balanced by a high CO_2 activity (a_{CO_2}) in order to maintain $P_{fluid} = P_{total}$? In order to address these questions one needs to know the activities of the dominant fluid species typically assumed to be present during metamorphism of high grade rocks (H_2O and CO_2). The a_{H_2O} in high grade rocks is usually calculated from biotite (phlogopite or annite) or amphibole (tremolite) dehydration equilibria such as

Phlogopite + Quartz = Enstatite + Sanidine + H_2O (1)

$KMg_3AlSi_3O_{10}(OH)_2 + 3\ SiO_2 = 3\ MgSiO_3 + KAlSi_3O_8 + H_2O$,

Annite + Quartz = Ferrosilite + Sanidine + H_2O (2)

$KFe_3AlSi_3O_{10}(OH)_2 + 3\ SiO_2 = 3\ FeSiO_3 + KAlSi_3O_8 + H_2O$,

or

$$\text{Tremolite} = \text{Enstatite} + \text{Diopside} + \text{Quartz} + H_2O \qquad (3)$$

$$Ca_2Mg_5Si_8O_{22}(OH)_2 = 3\ MgSiO_3 + 2\ CaMgSi_2O_6 + SiO_2 + H_2O.$$

In most cases the a_{H_2O} has been shown to be considerably less than unity in natural assemblages, and often in the range 0.1 to 0.3 (Wells, 1979; Bohlen *et al.*, 1980; Phillips, 1980; Percival, 1983; Valley *et al.*, 1983; Bhattacharya & Sen, 1986; Aranovich *et al.*, 1987; Hansen *et al.*, 1987; Edwards & Essene, 1988; Lamb & Valley, in press). Except in the unusual occurrence of nearly pure end-member phases (*e.g.*, Valley *et al.*, 1983), application of these equilibria is generally complicated by strong dilutions of the end-member hydrous phase. Lack of a realistic solution model for the mixing relations, and a poorly constrained correspondence between the material on which the experimental or thermodynamic data were collected and the natural phase (*c.f.* Clemens *et al.*, 1987), complicate the issue. Although the precision of such calculations may be low, the general pattern of low a_{H_2O} is consistent with the interpretation that granulites represent relatively dry lithologies, and this has become an established tenet of metamorphic petrology.

The implication of $a_{H_2O} < 1$ has usually been interpreted as resulting from either 1) the presence of some other fluid species with dilution of H_2O, but maintaining $P_{Fluid} = P_{Total}$ and leading to low H_2O activities; or 2) low volatile contents *before* the high grade metamorphism, either as inherently dry igneous protoliths or as rocks having experienced multiple or protracted metamorphic events. In support of 1), fluid inclusion studies of granulites have demonstrated that CO_2-rich inclusions are characteristic of many granulite facies gneisses relative to their lower grade equivalents, which commonly have H_2O-rich inclusions (Touret, 1971; Coolen, 1982; Schreurs, 1984; Hansen *et al.*, 1984; Rudnick *et al.*, 1985; Santosh, 1986). Thus the logical conclusion has been that CO_2 is the major diluent in the granulite facies fluid. This then implies that either the CO_2 was preferentially left behind in the rock during prograde dehydration or by partitioning of H_2O into a granitic partial melt, or that the CO_2 was introduced from an external source.

Recent studies have attempted to evaluate quantitatively the hypothesis that CO_2 is the dominant component of the fluid phase in the granulite facies, and some conflicting evidence has been presented. For example, Lamb & Valley (1985) emphasized that the stability of CO_2 is restricted to rocks with fO_2 greater than that corresponding to the FMQ buffer, and that CO_2 cannot be a major fluid component in some rocks with low a_{H_2O}, implying fluid absent metamorphism. Lamb *et al.* (1987) demonstrated that CO_2-rich fluid inclusions in granulite facies calc-silicates are often inconsistent with peak metamorphic fluid compositions calculated from wollastonite-calcite-quartz equilibria or from constraints on f_{CO_2} based on calculations of fluid speciation in the C-O-H system. This would imply late entrapment of a CO_2-rich fluid phase for these rocks, or post-metamorphic modification of fluid inclusions. Vry *et al.* (1988) have shown by carbon isotope measurements and calculations of fluid-rock ratios that many cordierite-bearing gneisses could not have experienced interaction with a CO_2-rich fluid phase possessing a heavy carbon isotopic signature (greater than or equal to the assumed average upper mantle value of approximately -6 per mil), or resetting of the cordierite carbon isotope compositions to the heavier values would have occurred at the fluid-rock ratios required by models of large-scale CO_2 infiltration (e.g., Touret, 1971; Newton *et al.*, 1980).

The purpose of the present study is to extend the quantitative evaluation of fluid compositions in high grade rocks, by applying a reasonably well constrained scapolite decarbonation equilibrium to directly calculate a_{CO_2}. An analysis of the thermodynamics, phase equilibria, and mixing relations of calcic, carbonate scapolite (meionite) were presented in Chapter III. This chapter is an application of these relations to natural systems. Although the intent is not to evaluate mechanisms for the generation of low H_2O activities in high grade rocks, the results presented here have important implications for models of granulite genesis that invoke open system interaction via a CO_2-rich fluid as the means of reducing the a_{H_2O}.

Scapolite Compositions in High Grade Settings

Shaw (1960) reviewed the chemical variation of scapolite in metamorphic rocks, and included available analyses of scapolite from high grade terranes (*e.g.*, von Knorring & Kennedy, 1958). Numerous studies since then have demonstrated that scapolite from the upper amphibolite and some granulite facies occurrences tends to be more calcic and carbonate-rich than that from lower grade settings, the latter tending to be more sodic and chlorine-rich (*e.g.*, Hietanen, 1967; Kwak, 1977; Tuisku, 1985). Furthermore, scapolite in the granulite facies proper, i.e., coexisting with orthopyroxene, has been shown to be sulfate-rich ($SO_4/(SO_4+CO_3+Cl)$ in the anion site = 0.25 to 0.75) as is scapolite in garnet-clinopyroxene granulite facies gneisses and deep-crustal xenoliths (von Knorring & Kennedy, 1958; Lovering & White, 1964; Wilkinson, 1974; Devaraju & Gowd Reddy, 1976; Edwards *et al.*, 1979; Okrusch *et al.*, 1979; Coolen, 1980; Devaraju & Coolen, 1982; Jones *et al.*, 1983; Austreim & Griffin, 1985; Srikantappa *et al.*, 1985; Stolz, 1987; Thomas & Nixon, 1987). These observations are consistent with the relatively high temperature and pressure stability of calcic, sulfate-carbonate scapolite solid solutions (Goldsmith & Newton, 1977). The most prolific occurrence of sulfate rich scapolite is in the Furua Granulite Complex of Tanzania (Coolen, 1980), where scapolite with $SO_4/(SO_4+CO_3)$ ranging from 0.27 to 0.77 is encountered. A characteristic feature of the Furua Complex is the widespread development of sulfate-rich scapolite in all calcium-rich lithologies (calc-silicates, amphibolites, felsic to mafic granulites). Scapolite-bearing lithologies in the Central Gneiss Belt (CGB) of the Grenville Province of Ontario and other localities were investigated for the present study. A wide range of scapolite compositions were encountered, with the same general pattern observed above. The range of anion and cation compositional variation of scapolite in high grade lithologies from this and other studies is summarized in Fig. 1. Scapolite compositions approaching mizzonite (EqAn = 100(Al-3)/3 = 67, $CO_3/(SO_4+CO_3+Cl)$ = 1) are very common in these occurrences. This intermediate member of the scapolite solid solution series has been inferred to be stable relative

Figure 1. Compositional range of natural scapolites expressed in terms of EqAn (100(Al−3)/3) and anion site composition X_{CO_3} (CO_3/[CO_3+SO_2+Cl]). Samples falling along the trend between Mz (mizzonite, $NaCa_3Al_5Si_7O_{24}CO_3$) and Ma (marialite, $Na_4Al_3Si_9O_{24}Cl$) are CO_3−Cl solid solutions. Field of points between Mz field and EqAn 55 at intermediate X_{CO_3} are sulfate−rich scapolites from granulites and high grade gneisses.

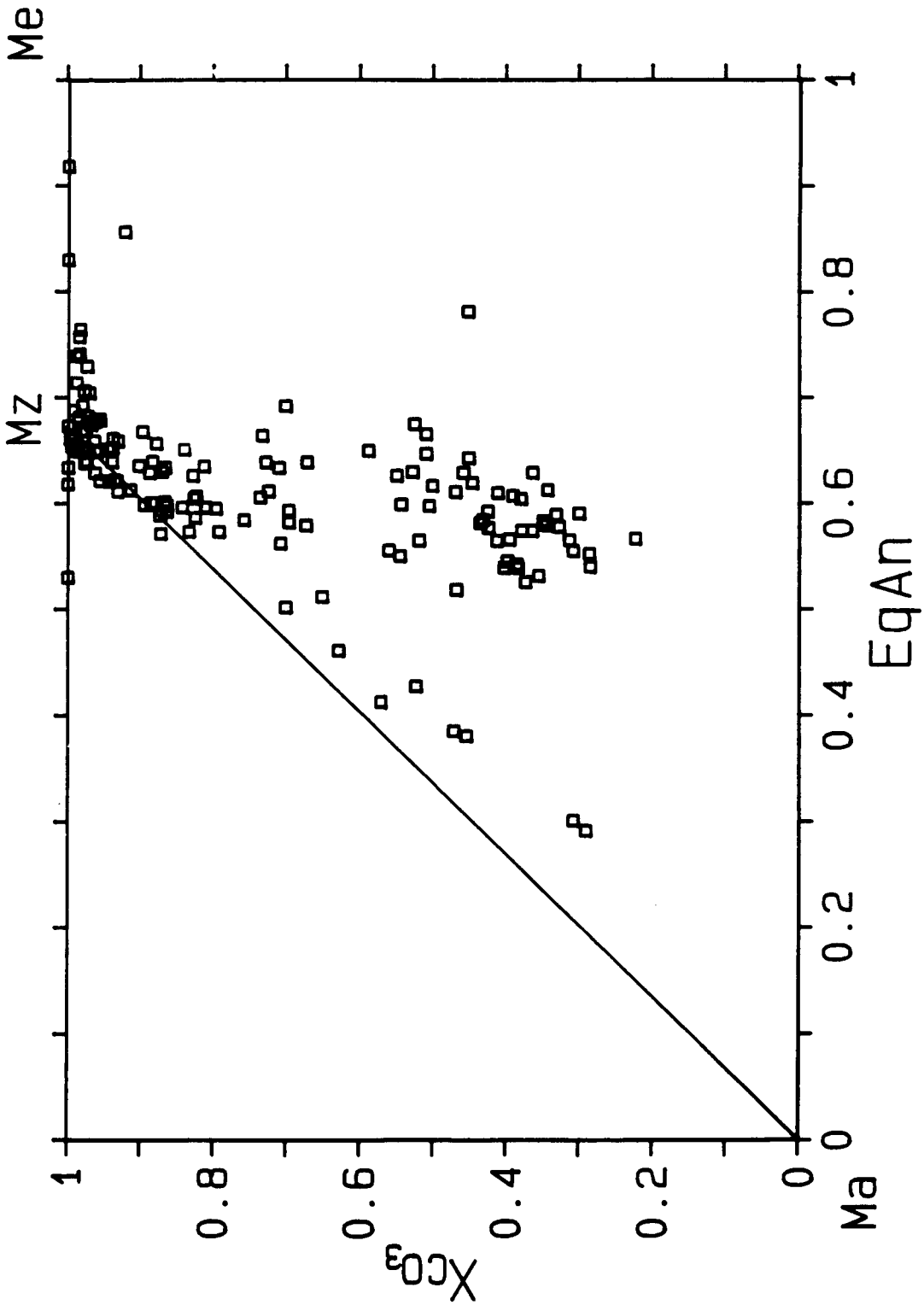
Me
Mz
EqAn
Ma
X_{CO_3}
0
0.2
0.4
0.6
0.8
1

to other scapolite compositions, probably as a result of Al–Si ordering within the silicate framework (Oterdoom & Gunter, 1983; Oterdoom & Wenk, 1983; Komada *et al.*, 1988; Chapter III). Sulfate–bearing scapolite tends to be slightly less calcic than mizzonite, but these compositions also cluster within a limited compositional range (Fig. 1). This study will deal with carbonate and sulfate solid solutions in the upper amphibolite and granulite facies. Chlorine–carbonate solid solutions, and constraints they place on fluid composition are discussed in various detail by Hietanen (1967), Ellis (1977), Kwak (1977), Vanko & Bishop (1982), and Mora & Valley (1988).

The partitioning of Ca and Na between scapolite and plagioclase has been proposed as a geothermometer (Goldsmith & Newton, 1977) for calcic plagioclase–scapolite assemblages. The reaction

Anorthite + Calcite = Meionite (4)

$$3\ CaAl_2Si_2O_8 + CaCO_3 = Ca_4Al_6Si_6O_{24}CO_3$$

has a large dP/dT (Goldsmith & Newton, 1977; Chapter III), making it a potentially ideal geothermometer. A provisional experimental calibration was presented by Goldsmith & Newton (1977). However, application of the thermometer to natural assemblages has yielded mixed results, in some cases giving temperatures consistent with other thermometers, and in others often resulting in erroneously high temperatures (Goldsmith & Newton, 1977; Rollinson, 1980). A reason for this may be seen in the $K_{DSc\text{-}Pg}^{Ca\text{-}Na}$ relationship for naturally occurring scapolite and plagioclase pairs. For carbonate and/or sulfate–bearing scapolite, the relevant exchange reaction is essentially:

Anorthite + "Carbonate marialite" = Albite + Meionite (5)

$$3\ CaAl_2Si_2O_8 + CaNa_3Al_3Si_9O_{24}CO_3 = 3\ NaAlSi_3O_8 + Ca_4Al_6Si_6O_{24}CO_3$$

where carbonate marialite is a hypothetical endmember, and $K_{DSc\text{-}Pg}^{Ca\text{-}Na}$ was calculated as

$$K_{DSc\text{-}Pg}^{Ca\text{-}Na} = [X_{Ca}^{Sc}/X_{Na}^{Sc}]/[X_{Ca}^{Pg}/X_{Na}^{Pg}] \quad (6)$$

Figure 2a. $K_{D_{Sc-Pg}}^{Ca-Na}$ vs. An content of plagioclase for coexisting scapolite–plagioclase in high grade gneisses (this study) and data compiled from literature. Data are plotted irrespective of anion site composition. Open symbols: natural parageneses; filled symbols: experimental scapolite–plagioclase pairs at quoted temperatures (Goldsmith & Newton, 1977; Ellis, 1978). Range of $K_{D_{Sc-Pg}}^{Ca-Na}$ at a given X_{An} content is due in part to compositional variability of plagioclase coexisiting with scapolite and to disequilibrium partitioning between scapolite and plagioclase. Points falling below trend at $X_{An} < 0.20$ are chlorine–rich scapolites from amphibolite facies calc–sililcates and amphibolites encountered in the southwestern Grenville Province.

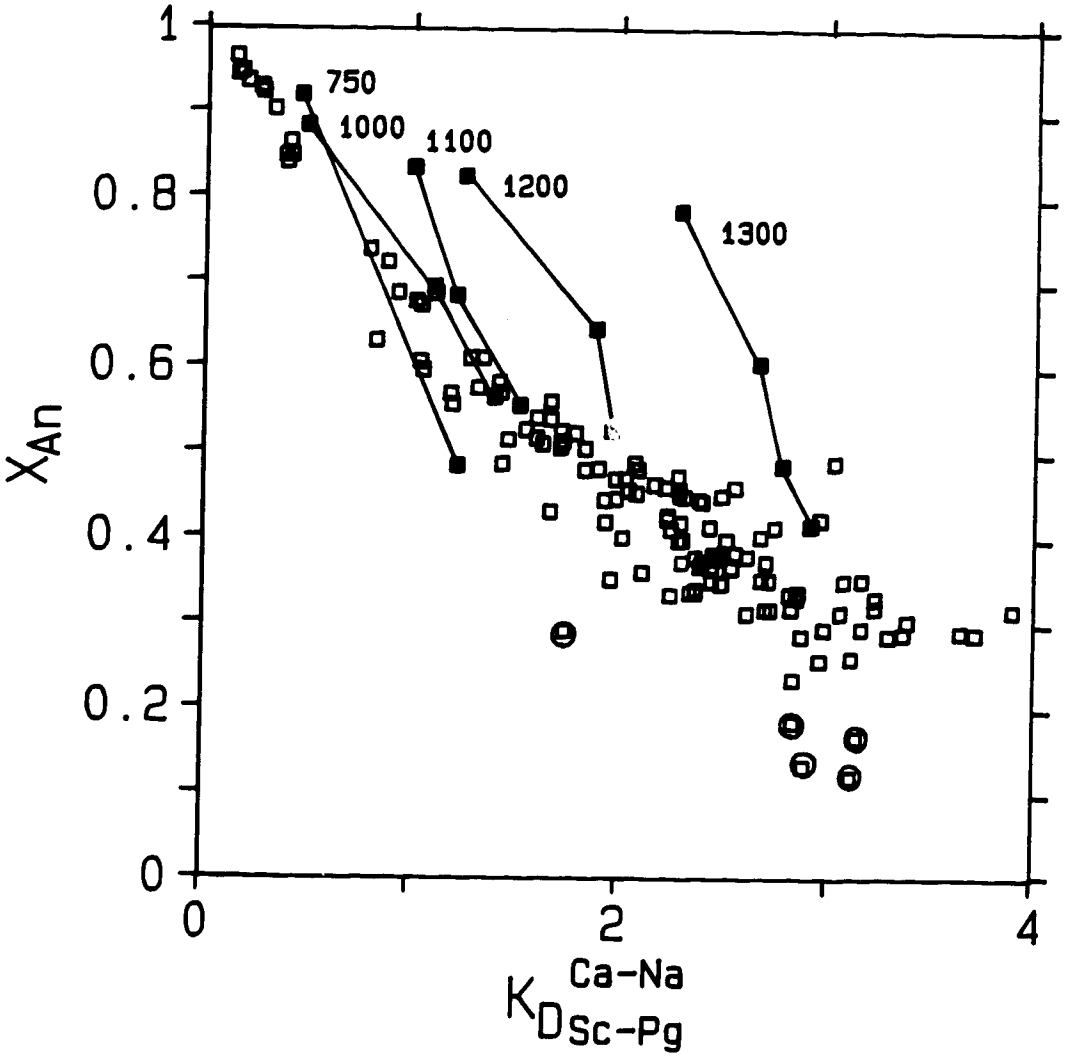
1
0.8
0.6
0.4
0.2
0
X_{An}
750
1000
1100
1200
1300
0
2
4
$K_{D\,Sc-Pg}^{Ca-Na}$

Figure 2b. $K_{D_{Sc\text{-}Pg}}^{Ca\text{-}Na}$ vs X_{An} content for scapolite with $X_{SO_4} \geq 0.10$ in the anion site. Symbols as in Fig. 2a. The field of these samples is indistinguishable from that of all available scapolites compiled in 2a.

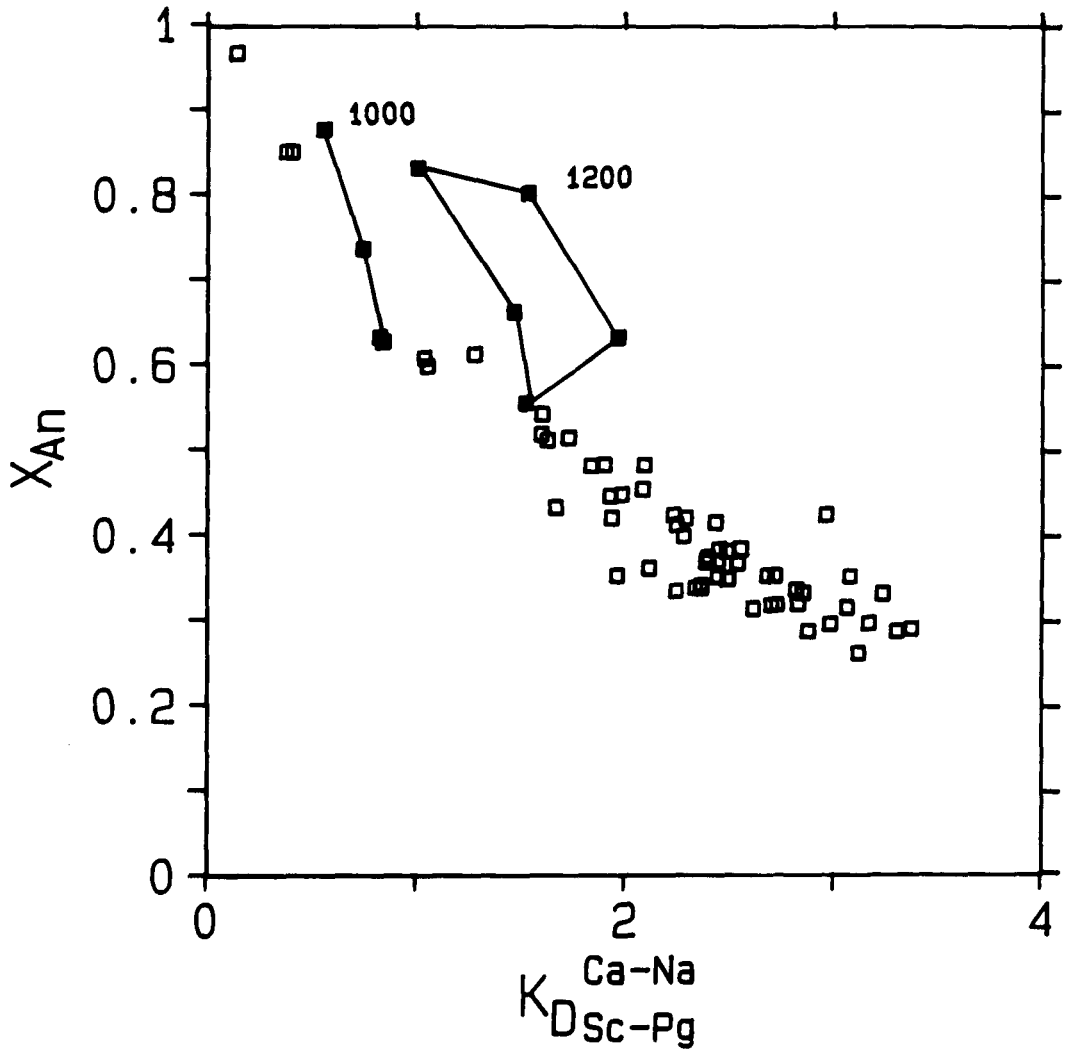
1
0.8
0.6
0.4
0.2
0
0
2
4
X_{An}
$K_{D\,Sc-Pg}^{Ca-Na}$
1000
1200

where X_{Ca}^{Sc} is defined as the EqAn content of scapolite, X_{Na}^{Sc} is 1-EqAn of scapolite, and X_{Ca}^{Pg} and X_{Na}^{Pg} are the anorthite and albite contents of plagioclase (abbreviations in Appendix 5). Fig. 2 was compiled from data in Appendix 3, and includes samples from the present study and available literature sources. The analyses mainly represent coexisting carbonate/sulfate scapolite and plagioclase from calc-silicate and mafic gneisses that are estimated to have equilibrated in the temperature range 550 to 800°C. Some samples coexist with calcite, and some contain up to 15 mol % Cl in the anion site. Experimental data points for carbonate/sulfate scapolite are also included for comparison. For the natural assemblages, there is a distinct curvilinear relationship within a restricted range between $K_{D_{Sc-Pg}}^{Ca-Na}$ and plagioclase composition (a best fit line, $K_D = 4.923 - 7.363\ X_{An} + 2.507\ X_{An}^2$, with $R^2 = 0.83$ and standard error = 0.37, was calculated for the distribution) indicating that the composition of scapolite is primarily dependent on the plagioclase composition, and that $K_{D_{Sc-Pg}}^{Ca-Na}$ is only slightly dependent on temperature. An_{27} is the approximate lower limit for which coexisting carbonate-sulfate scapolite has been reported, and An_{65} is the composition at which the scapolite EqAn composition is the same as the anorthite content of the coexisting plagioclase. The experimental data of Goldsmith & Newton (1977) are consistent with a marked temperature-dependent fractionation at temperatures greater than 1000°C, but apparently not in the temperature range of high grade regional metamorphism where the 1000°C isotherm of Goldsmith & Newton merges with the natural assemblages (Fig 2). Unfortunately, the data are not consistent with coexisting scapolite and plagioclase being a reliable geothermometer. Goldsmith & Newton (1977) inferred that this may be due to ordering of natural scapolite relative to the experimental phases. Based on a thermodynamic analysis, ordering of intermediate compositions relative to the end members is highly likely (Oterdoom and Wenk 1983; Oterdoom & Gunter 1983; Chapter III).

The analyses plotted in Fig. 2a represent all available scapolite solid solutions. Of these the sulfate-rich scapolites are indistinguishable from the other scapolite samples (mainly CO_3 scapolites) in terms of X_{An} versus K_D (Fig. 2b), consistent with

nearly ideal mixing of carbonate and sulfate anions in the scapolite structure. A limited number of points for chlorine-rich scapolite coexisting with sodic plagioclase fall well below the trend for calcic scapolite-plagioclase pairs, possibly as a result of disequilibrium, lower temperature, and/or a different equilibrium partitioning relation (Fig. 2a). Despite the lack of direct useful thermometric information, analysis of scapolite-bearing assemblages can provide important constraints on a_{CO_2}, given reliable temperatures obtained from other equilibria.

Calculation of CO_2 Activities

Thermodynamic Data and Activity Models

Thermodynamic data and activity-composition (a-X) relations for scapolite are necessary in order to calculate a_{CO_2} in high grade rocks using scapolite equilibria. An internally consistent thermodynamic data set for meionite and other calc-silicate phases in the system $CaO-Al_2O_3-SiO_2-CO_2-H_2O$ (CASCH) has been derived based on recently acquired thermodynamic data for scapolite and published experiments in the CASCH system. The a-X relations for carbonate scapolite were calculated from natural scapolite-plagioclase-calcite assemblages. The reader is referred to Chapter III for the details of these calculations. Briefly, the a-X relations for meionite in scapolite approach ideality at 750°C and exhibit increasingly negative departures from ideality below 750°C. The only constraints above 750°C are the experiments of Goldsmith & Newton (1977) which indicate positive departures from ideality at 1000 to 1300°C, consistent with our model.

Assumptions concerning the mixing of carbonate and sulfate in the anion site need to be made in order to apply the scapolite a-X relations based on pure carbonate scapolite to natural carbonate-sulfate-chlorine solid solutions. Based on the K_D relations discussed above, it appears that the carbonate and sulfate groups mix ideally in the anion site in calcic scapolite. In addition, Ellis (1977) presented evidence for ideal mixing between CO_3 and Cl in the anion site for intermediate carbonate-chlorine solid solutions. Therefore the activity of carbonate meionite in a

carbonate–sulfate solid solution with less than 10 mol percent Cl in the anion site will be calculated from the mixing relations for carbonate scapolite presented in Chapter III, but reduced by the factor $X_{CO_3} = CO_3/(CO_3+SO_4+Cl)$ for that particular scapolite.

Thermodynamic data for anorthite, grossular, and quartz comprise part of the internally consistent data set used in the derivation of scapolite phase equilibria in the CASCH system (Chapter III). The equation of state for CO_2 by Shmonov & Shmulovich (1974) was used to calculate end member decarbonation equilibria. The data of Burnham *et al.* (1969) was used to calculate end member dehydration equilibria. Thermodynamic calculations were performed with a computer program (**EQUILI**, Wall & Essene, unpublished) that solves the relation

$$\Delta G^{P_2}_{T_2} - \Delta G^{P_1}_{T_1} = \int_{P_1}^{P_2} \Delta V_s dP - \int_{T_1}^{T_2} \Delta S_s dT + \Delta G(P,T,X)_{H_2O} + \Delta G(P,T,X)_{CO_2}$$

using available volume, entropy, expansivity and compressibility data.

In the calculations to follow, anorthite activities were calculated using the plagioclase activity model of Newton *et al.* (1980). The same model was used in the derivation of meionite activities from natural Sc–Pg–Cc assemblages (Chapter III), and is used here in order to maintain internal consistency. The model of Newton *et al.* (1980) predicts that the activity coefficient (γ) for anorthite becomes less than one at compositions more calcic than An_{80}. In fact, based on a comparison of various studies of plagioclase mixing, it is unlikely that activity coefficients are less than one for these compositions (see Carpenter & Ferry (1984) for a critique and summary of available constraints on plagioclase mixing). For plagioclase with compositions more calcic than An_{80} we have assumed ideal mixing, that is $\gamma = 1$. Grossular activities for quaternary Gr–Py–Alm–Sp garnets were calculated using the quaternary mixing model of Anovitz & Essene (1987) which is a modification of the model of Ganguly & Saxena (1984), and incorporates updated mixing parameters for the grossular–almandine exchange. Explicit analytical expressions for calculating activity coefficients for the garnet components are presented in Appendix 4.

Volatile Equilibria

A number of scapolite equilibria are potential CO_2-barometers, particularly for calc-silicate lithologies (e.g., Jones *et al.*, 1983; Chapter III). A survey of the reported scapolite-bearing assemblages and our investigation in the CGB of Ontario reveal that the sub-assemblage scapolite-plagioclase-garnet-quartz is common to the range of bulk compositions discussed above. This assemblage monitors a_{CO_2} by the reaction

Meionite + Quartz = Anorthite + Grossular + CO_2 (7)

$2\ Ca_4Al_6Si_6O_{24}CO_3 + SiO_2 = 5\ CaAl_2Si_2O_8 + Ca_3Al_2Si_3O_{12} + 2\ CO_2$)

In the absence of quartz in the mineral assemblage, Reaction 7 places an upper limit on a_{CO_2}. This allows constraints on a_{CO_2} to be placed on many quartz undersaturated lithologies that contain scapolite-garnet-plagioclase, *e.g.*, deep crustal xenoliths.

Although direct experimental studies of Reaction 7 are lacking, constraints on its position are provided by the intersection of Reaction 4 and

Anorthite + Calcite + Quartz = Grossular + CO_2 (8)

$CaAl_2Si_2O_8 + 2\ CaCO_3 + SiO_2 = Ca_3Al_2Si_3O_{12} + 2\ CO_2$

whose position in turn is derived from addition of the reactions

Anorthite + Wollastonite = Grossular + Quartz (9)

$CaAl_2Si_2O_8 + 2\ CaSiO_3 = Ca_3Al_2Si_3O_{12} + SiO_2$

Calcite + Quartz = Wollastonite + CO_2 (10)

$CaCO_3 + SiO_2 = CaSiO_3 + CO_2$

for which experimental constraints are available (see Chapter III).

In Chapter III it was seen that the configurational entropy arising from Al-Si disorder in meionite had a marked effect on the dP/dT slope of Reactions 4 and 7, and on the degree of departure from ideality of a-X relations for meionite in scapolite. However, if an internally consistent set of data is used to derive the

Gibbs free energy of meionite and to model mixing relations of meionite (defined by Reaction 4), the same value of a_{CO_2} is obtained for a given sample no matter what value of configurational entropy one allows for meionite, as long as the entropy of meionite is consistent with experimental constraints on Reaction 7. In addition to using Reaction 7, a_{CO_2} was calculated for calcite-bearing meta-anorthosite and mafic gneisses using Reaction 8. In rocks that contain the assemblage Sc-Pg-Gt-Cc-Qz, one may calculate a_{CO_2} from both Reactions 7 and 8, however the same value of a_{CO_2} should be obtained from each reaction for a given Sc-Pg-Gt-Qz-Cc assemblage because of the dependence of the Gibbs free energy and mixing relations for meionite on thermodynamic data for calcite and anorthite. This was found to be the case in all samples for which this calculation was performed (see following sections and Table 2).

The locus of Reaction 7 in P-T space is displayed in Fig. 3. The unusual orientation of this reaction, that is , the negative slope with meionite on the high T side and CO_2 on the low T side of the reaction, is due to the high entropy of meionite. In contrast to other volatilization reactions, in which the energetics of the reaction are dominated by the higher entropy and volume of the volatile-bearing assemblage, Reaction 7 is dominated by the entropy contribution from a phase with a large number of atoms that also has a significant configurational entropy, and that produces a relatively low mole fraction of CO_2 per formula weight of the carbonate-bearing silicate phase. This is in contrast to calcite, which has a large mole fraction of CO_2 per mole of a carbonate-bearing phase with few atoms. By comparison, Reaction 10 is a reaction dominated by the energetics of the high entropy and molar volume of CO_2.

Based on Reaction 7 values of $\log_{10}K$ were calculated at various P and T using **EQUILI** (Fig. 3), and the expression

$$K = [(a^{Gt}_{Ca_3Al_2Si_3O_{12}})\cdot(a^{Pg}_{CaAl_2Si_2O_8})^5\cdot(a_{CO_2})^2] \;/\; (a^{Sc}_{Ca_4Al_6Si_6O_{24}CO_3})^2 \qquad (11)$$

Figure 3. Locus and values of $\log_{10}K$ for Reaction 7. See text for discussion.

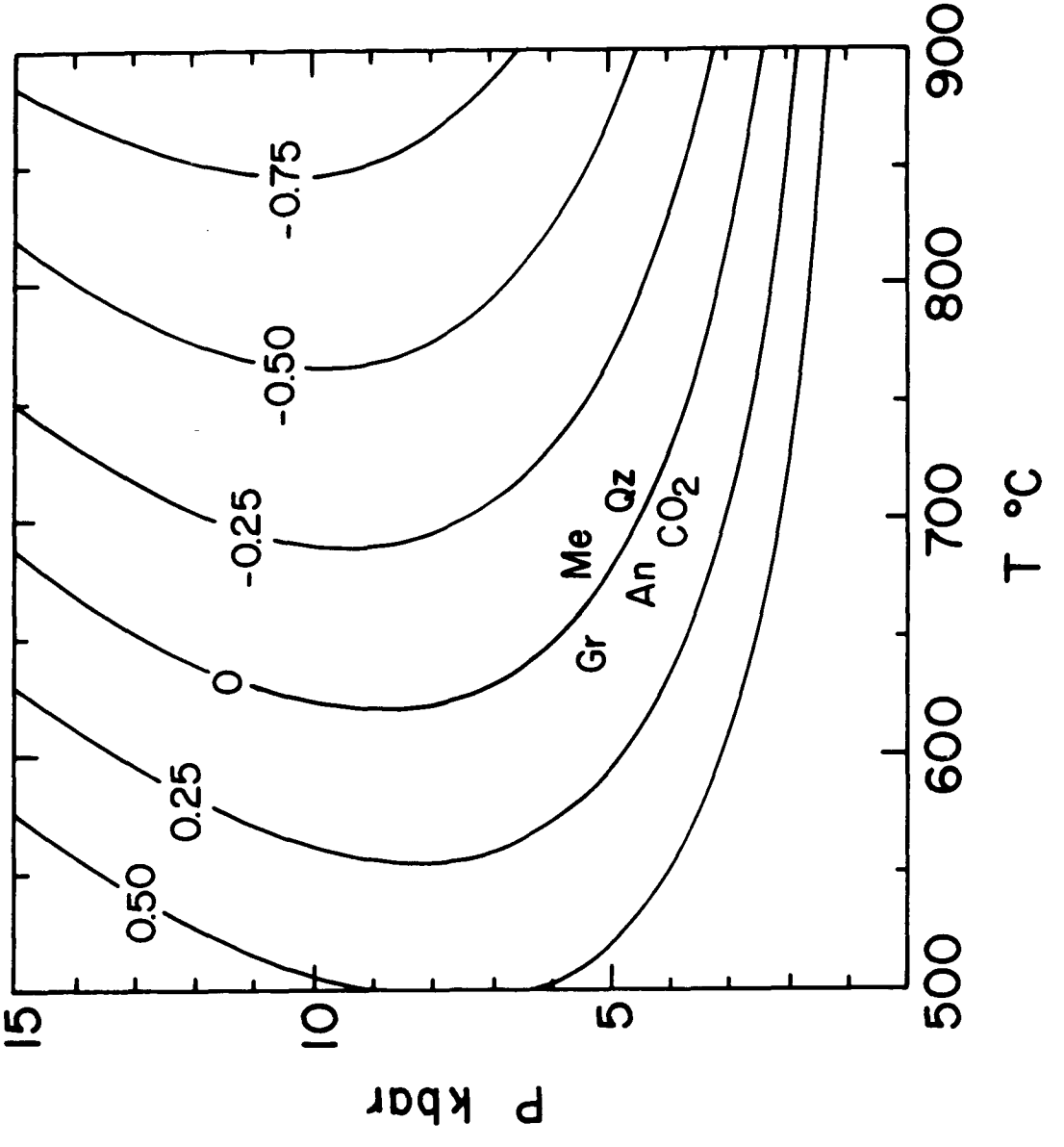
-0.75
-0.50
-0.25
0
0.25
0.50
Gr
Me
Qz
An
CO_2
15
10
5
P kbar
500
600
700
800
900
T °C

was solved for a_{CO_2} using the appropriate activity models. Explicit expressions for calculating the activity of grossular and meionite are outlined in Appendix 5 and Chapter III, respectively.

The a_{CO_2} calculated in the above manner is relative to a standard state of pure CO_2 at the pressure and temperature of interest. An a_{CO_2} of unity implies a pure CO_2 fluid phase with $P_{Fluid} = P_{Total}$ at the equilibrium P and T. An a_{CO_2} less than one results from either a mixed H_2O–CO_2 fluid with $P_{Fluid} = P_{Total}$, or fluid absence ($P_{Fluid} < P_{Total}$). Alternatively, the fugacity of CO_2 may be calculated using a 1 bar, T standard state and thermodynamic data. From this a partial pressure of CO_2 is determined from $P_{CO_2} = f_{CO_2}/\gamma_{CO_2}$, where γ_{CO_2} is the fugacity coefficient of CO_2 obtained from the data of Shmulovich & Shmonov (1975). Where possible, calculation of the partial pressures of all gas species allows evaluation of fluid absence of fluid presence.

The final data required to calculate a_{CO_2} are accurate P–T estimates for the conditions of equilibration of the scapolite-bearing assemblage. Initial calculations showed that temperature is the most critical factor in obtaining precise values of a_{CO_2}. Typically, a temperature variation of ±50°C, a commonly quoted estimate of precision for geothermometry, will double or halve the resultant value of a_{CO_2}. This is less of a problem when working with samples that equilibrated at apparently low a_{CO_2} (e.g., $a_{CO_2} \leq 0.2$). For intermediate fluid activities it means the difference between realistic ($a_{CO_2} \leq 1.0$) and erroneous ($a_{CO_2} \geq 1.0$) estimates of a_{CO_2}. Therefore the most precise value of temperature possible is necessary for accurate CO_2 barometry. The a_{CO_2} was calculated over a range of T for all settings to evaluate the effect of T on a_{CO_2}. Values of a_{CO_2} are quoted to two decimal places for rounding purposes. However, the precision of the values may approach +100%/–50% of the calculated value for +50/–50°C temperature difference.

The temperature sensitivity of Reaction 7 arises primarily from two factors. First, the activity of meionite increases rapidly from 650 to 800°C, while the

activities of anorthite and grossular decrease with increasing temperature, though not as markedly as that of meionite. This results in rapid changes in calculated K (Eq. 11) with changing T, compared to using an ideal model for all species that would result in little variation of K (and therefore a_{CO_2}) with T (e.g., Reaction 1). In the calculation of meionite and grossular activities, mole fractions are raised to the 8th, and 3rd powers, and anorthite activities are raised to the 5th power, accentuating even small shifts in composition of these phases. Secondly, the free energy of Reaction 7 does not change markedly with temperature (Fig. 3), so that small shifts in the composition or activity of any component will result in major shifts in a_{CO_2} of the magnitude quoted above. Therefore the calculation of a_{CO_2} using Reaction 7 is highly model dependent.

The effect of overestimating the equilibrium temperature is to yield erroneously high values of a_{CO_2}, such as a_{CO_2} greater than unity, which implies $P_{CO_2} > P_{Total}$, a structurally unsustainable condition in rocks. The temperature may be overestimated as a result of retrograde metamorphism in which the scapolite assemblage is secondary after and replaces a higher grade assemblage. Examples of such a condition will be noted in later sections. Pressure, which is presently more accurately determined than temperature (Essene, 1988), has much less of an effect on a_{CO_2} than temperature, and precision of ± 1 kbar results in only a $\pm 2\%$ variation in a_{CO_2}. However, partial pressures are more sensitive to total pressure as the fugacity coefficient of CO_2 is highly pressure dependent.

The a_{H_2O} was calculated for selected scapolite-bearing samples when appropriate mineral assemblages are present. The reaction

$$\text{Clinozoisite} + \text{Quartz} = \text{Anorthite} + \text{Grossular} + H_2O \qquad (9)$$

$$4\ Ca_2Al_3Si_3O_{12}(OH) + SiO_2 = 5\ CaAl_2Si_2O_8 + Ca_3Al_2Si_3O_{12} + 2\ H_2O$$

is applicable to many calc-silicates and some scapolite-bearing meta-anorthosite for calculating a_{H_2O}. Reaction 1 was also used to calculate a_{H_2O}. Thermodynamic data for clinozoisite are compiled in Chapter III. The activity model of Bird & Helgeson

(1980) was used to calculate the activity of clinozoisite in epidote solid solutions. For the epidotes encountered in this study the activity model of Bird & Helgeson (1980) yields ideal activities, that is $a^{Ep}_{Ca_2Al_3Si_3O_{12}(OH)} = X_{Ca_2Al_3Si_3O_{12}(OH)}$.

Microprobe Analyses

Microprobe analyses of phases for CO_2 barometry and P–T calculations were obtained on a Cameca CAMEBAX microprobe. All phases were analyzed at an accelerating potential of 15 kV and sample current of 10 nA, using natural or synthetic silicates and oxides. A slightly defocussed or rastered beam was used to analyze plagioclase and scapolite to prevent Na and volatile loss. Core compositions were generally used in the calculation of a_{CO_2}, although core and rim analyses were commonly collected to evaluate compositional zonation and its effect on a_{CO_2}. Mineral formulae were calculated on the basis of 8 (garnet and epidote), 5 (plagioclase), or 4 (pyroxene) cations, and Fe^{3+} was calculated for garnet and pyroxene on the basis of charge balance and stoichiometry. Scapolite formulae were calculated on the basis of Si + Al = 12 (Evans *et al.* 1969), and CO_3 + Cl + SO_4 = 1.00. Mineral analyses are compiled in Appendix 2.

Application and Interpretation

Sample Localities and Description

The majority of samples for this study were collected in upper amphibolite to granulite facies gneisses from the Central Gneiss Belt (CGB) of Ontario, a major section of the Grenville Province bounded by the Grenville Front Tectonic Zone (GFTZ) to the northwest and the Central Metasedimentary Belt Boundary Tectonic Zone (CMBBTZ) to the southeast (Figs. 4 and 5). The CGB is comprised of distinct lithotectonic domains which are bounded by km–wide to 100's km long zones of high strain and ductile shearing (Davidson, 1984a, 1984b; Davidson *et al.*, 1979, 1982). The ductile shearing has been dated to have been syn– to slightly post peak–metamorphic (van Breemen *et al.*, 1986). The domains are interpreted to

Figure 4. Sample localities and lithotectonic domains (inset 1) for southwestern Grenville Province, Ontario. Boxes 2 and 3 outline area of Whitestone Anorthosite (shaded) detailed in Figs. 5 through 7. PSSZ = Parry Sound shear zone.

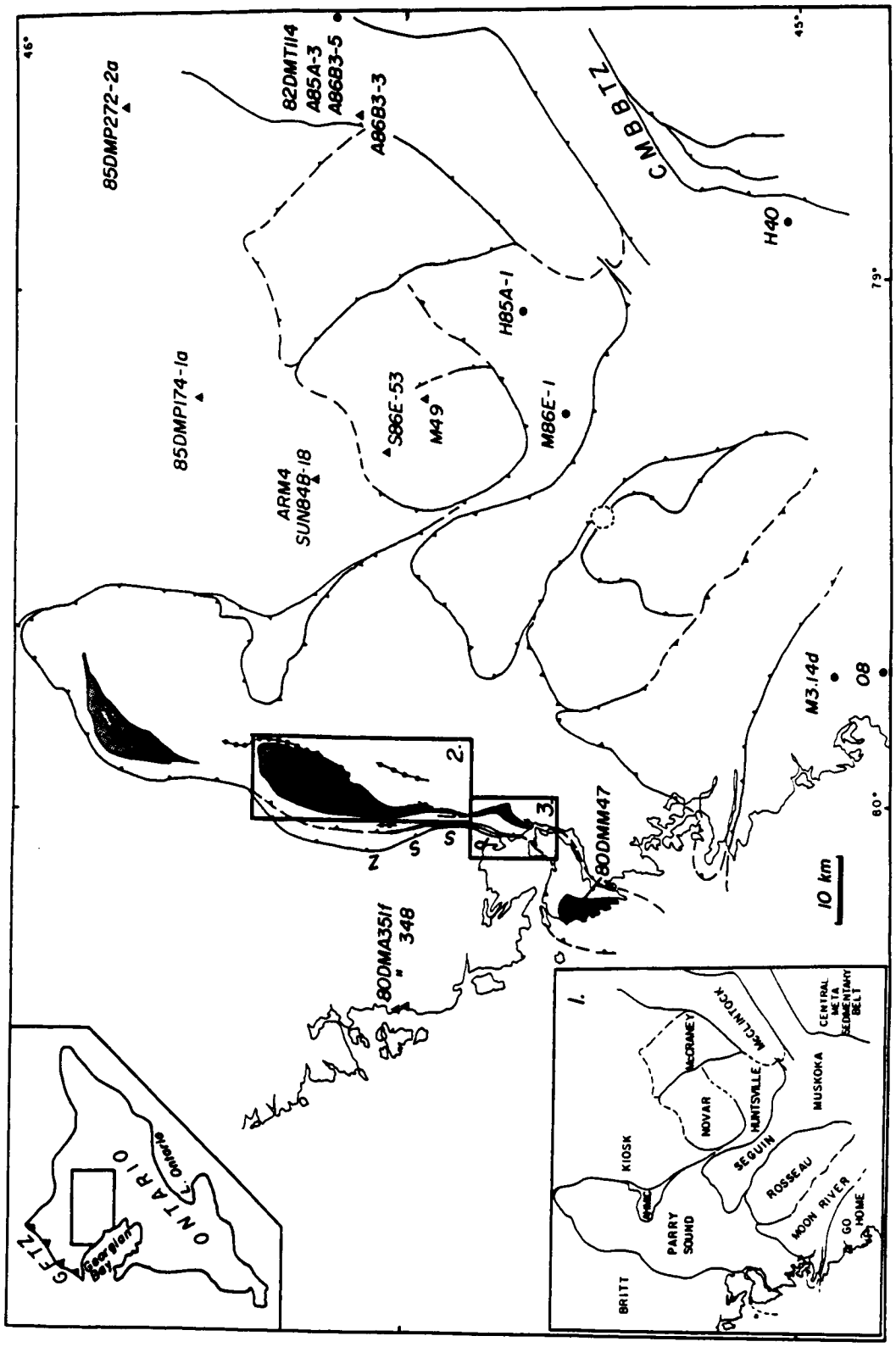
85DMP272-2a
82DMT114
A85A-3
A86B3-5
A86B3-3
CMBBTZ
H40
85DMP174-1a
H85A-1
S86E-53
M49
M86E-1
ARM4
SUN848-18
M3.14d
08
80DMM47
80DMA351f
348
10 km
Z
S
S
2.
3
1.
KIOSK
BRITT
PARRY SOUND
NOVAR
McCRANEY
McCLINTOCK
HUNTSVILLE
SEGUIN
ROSSEAU
MOON RIVER
GO HOME
MUSKOKA
CENTRAL METASEDIMENTARY BELT
ONTARIO
Georgian Bay
Ontario
46°
45°
80°
79°

represent large scale segments of deep crust, transported via thrusting toward the northwest during the Grenville Orogeny. Each domain is characteristically of a single, consistent metamorphic grade and each is underlain by lithologies distinct from neighboring domains. Thermobarometric studies have outlined a wide expanse of high pressures rocks within the CGB, with pressures approaching 11 kbar toward the GFTZ and decreasing to 7 kbar toward the CMBBTZ (Anovitz, 1987). Peak temperatures are in excess of 800°C in the vicinity of Parry Sound and decrease to 700°C near the CMBBTZ. The scapolite-bearing lithologies sampled for this study are primarily in granulite facies Parry Sound and McCraney domains of the CGB, (Figs. 4 through 7).

Within the Parry Sound Domain (PSD), scapolite is widely developed in the Whitestone Anorthosite (WSA), a 170 km^2 leucocratic gabbroic anorthosite to anorthositic gabbro sill (Mason, 1969; Nadeau, 1983; Thompson, 1983; Bright, 1987) that was emplaced at approximately 1.35 Ga and underwent granulite facies metamorphism within Parry Sound Domain at approximately 1.15 Ga (van Breemen *et al.*, 1986). Contemporaneous with the waning stages of Grenville metamorphism, the WSA experienced a protracted episode of ductile shearing that was most pervasive within the Parry Sound Shear Zone (PSSZ), which delineates the western boundary of the PSD (Fig. 4). Detailed descriptions of the development of scapolite within the WSA and PSSZ are presented by Mason (1969), Nadeau (1983), and Thompson (1983). An upper amphibolite facies metamorphic aureole is developed within the outer 75% of the WSA, characterized by a modal increase in scapolite, hornblende, epidote and garnet toward the pluton margin. The aureole is developed around a core of relict granulite facies Cpx-Gt-Opx meta-anorthosite. Toward the center of the aureole, where relict igneous textures are preserved (Mason, 1969), scapolite and hornblende are seen to replace and mantle plagioclase and clinopyroxene, and garnet porphyroblasts are commonly embayed and resorbed. In contrast to the core of the WSA, the margin exhibits a foliation concordant to enclosing lithologies, and

Figure 5. Location of samples from main body and southern extension of WSA.

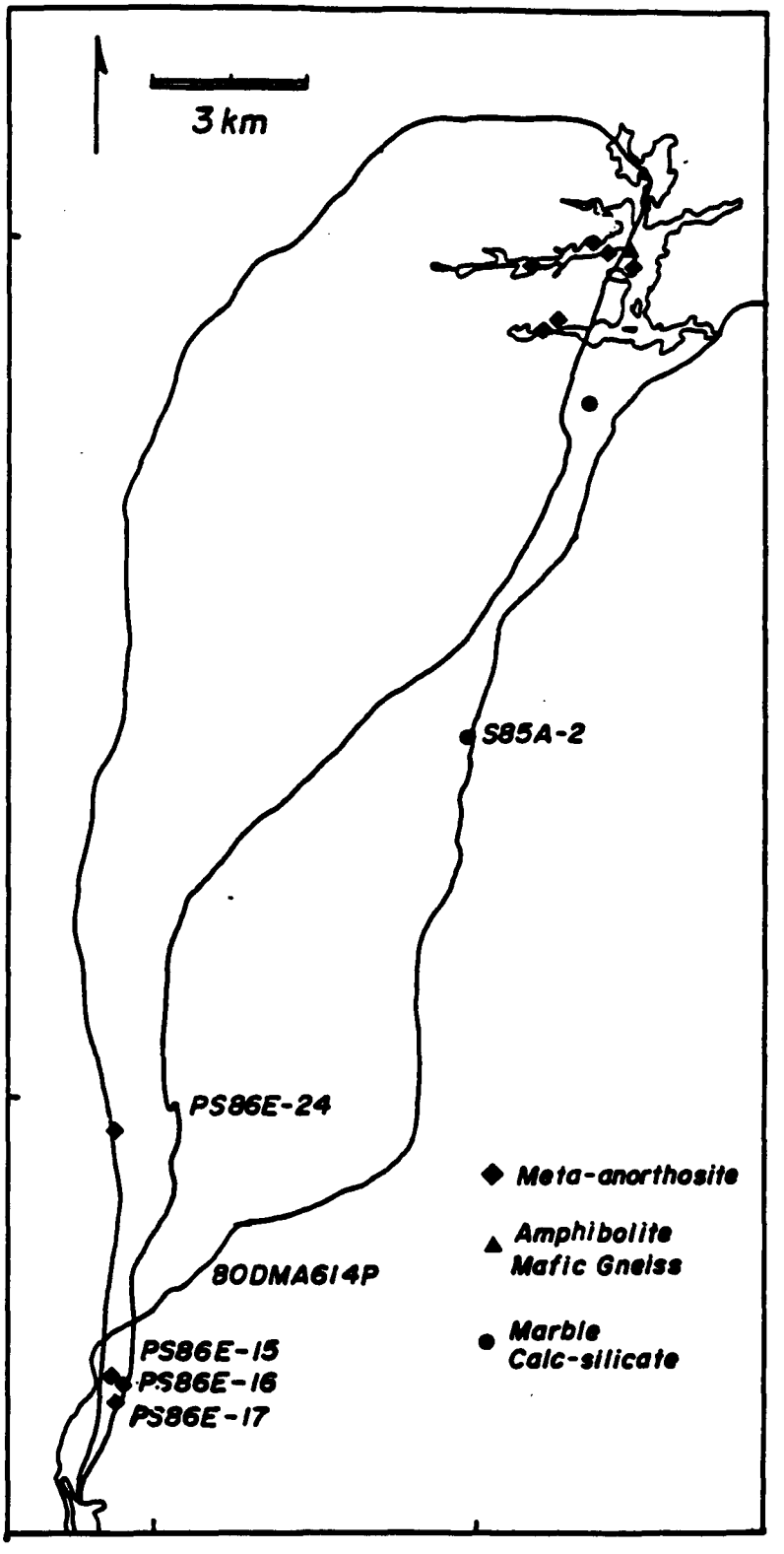
3 km
S85A-2
PS86E-24
80DMA614P
PS86E-15
PS86E-16
PS86E-17
Meta-anorthosite
Amphibolite
Mafic Gneiss
Marble
Calc-silicate

Figure 6. Detail of sample localities along east margin of WSA adjacent to marble breccia (hatchured), in vicinity of Whitestone Lake. Inset outlines area shown in Figure 6.

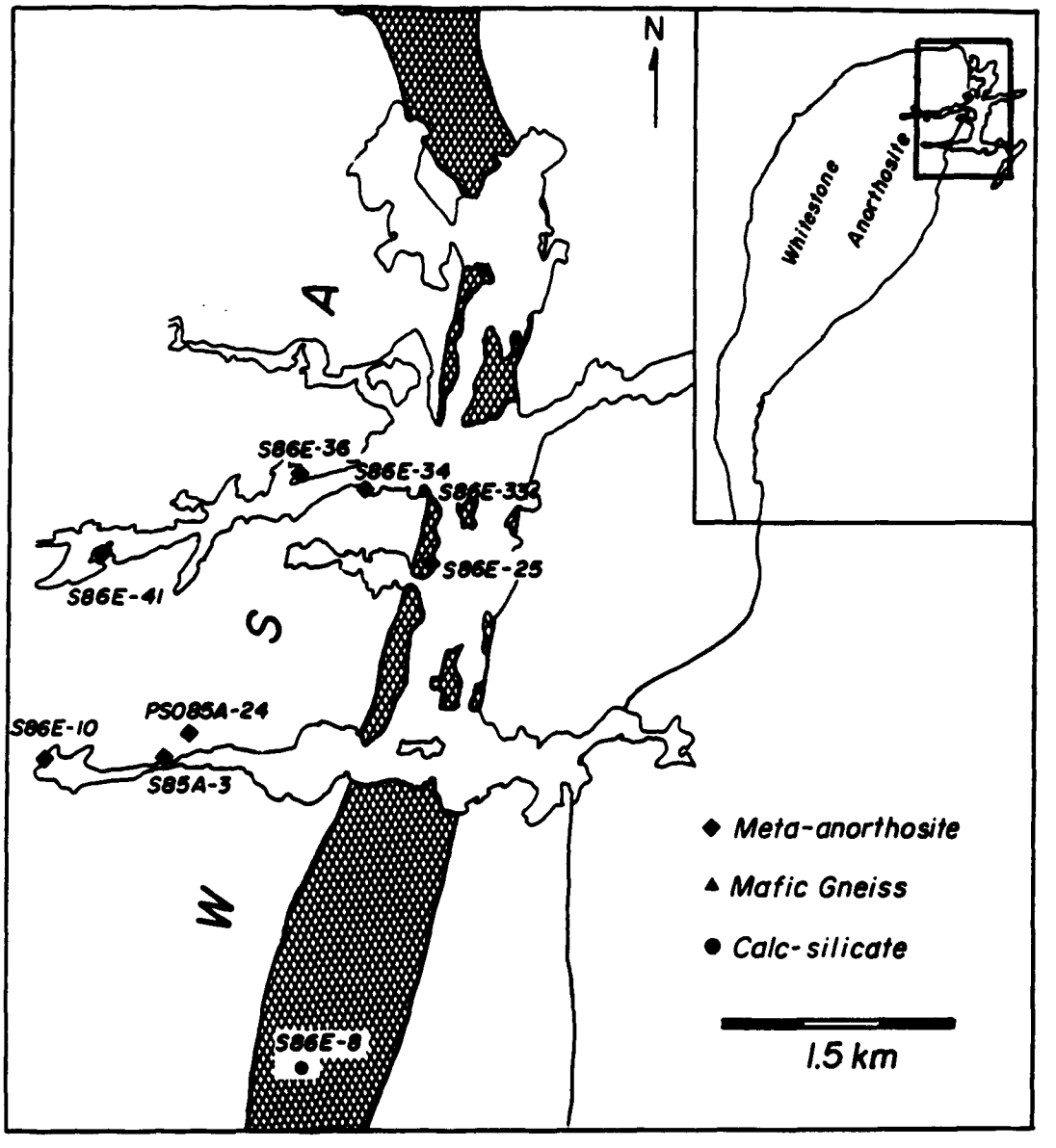
N
Whitestone
Anorthosite
S86E-36
S86E-34
S86E-33
S86E-25
S86E-41
S
A
PS085A-24
S86E-10
S85A-3
W
S86E-8
◆ Meta-anorthosite
▲ Mafic Gneiss
● Calc-silicate
1.5 km

Figure 7. Detail of sample localities in WSA in vicinity of Parry Sound Shear Zone. PS: town of Parry Sound.

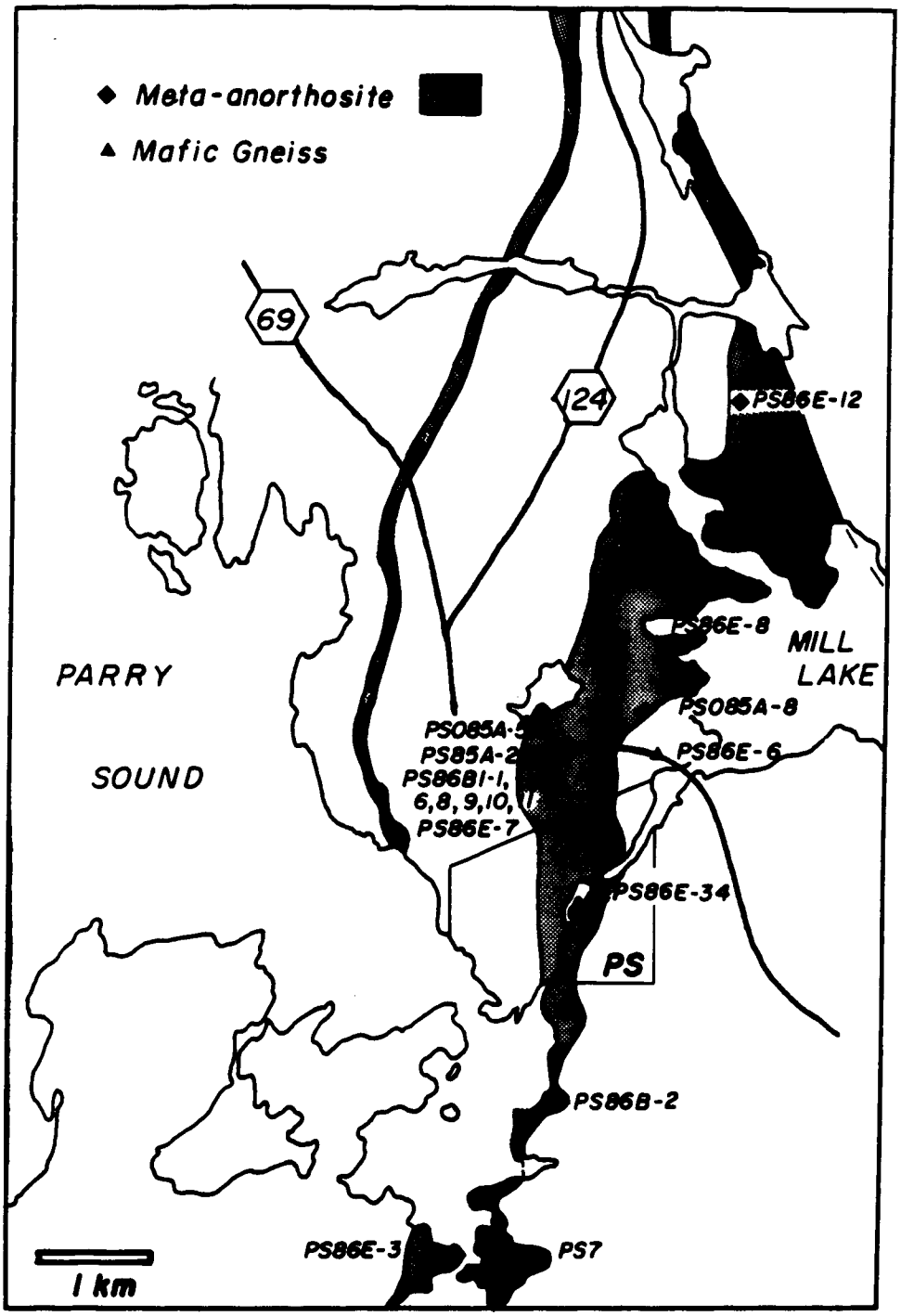
◆ Meta-anorthosite
▲ Mafic Gneiss
69
124
◆PS86E-12
PS86E-8
MILL
LAKE
PARRY
SOUND
PS085A-8
PS86E-6
PS085A-5
PS85A-2
PS86B1-1,
6,8,9,10,11
PS86E-7
PS86E-34
PS
PS86B-2
PS86E-3
PS7
1 km

Sc–Hbl–Pg–Cpx–Gt mineral assemblages exhibit granoblastic equilibrium textures. The WSA is in tectonic contact with a marble tectonite breccia on the east, and Gt–Cpx amphibolite on the west. In the southern extension of the WSA where it is intersected by the PSSZ, mineral assemblages are identical to those in the aureole of the anorthosite.

Regional metamorphic temperature for the peak of granulite facies metamorphism in PSD is in excess of 800°C (including Gt–Cpx thermometry, (Anovitz, 1987). However, Gt–Cpx temperatures for gneisses in the aureole, for Gt–Cpx amphibolites along the western margin of the WSA and that bound the PSSZ, and for sheared meta–anorthosite in the PSSZ, range from 650 to 750°C, consistent with movement of the PSSZ and WSA during cooling of the PSD.

Fluid composition was calculated for Sc–Gt–Pg–Qz±Ep±Cc assemblages along the entire length of the WSA, from the eastern margin of the main body to the PSSZ. The range of temperatures calculated from lithologies within the variably tectonized western margin of PSD make precise CO_2 barometry difficult for this area. The western PSD was probably a dynamic system during scapolite formation in the WSA. As ductile shearing proceeded during cooling of the PSD, its likely that retrograde diffusion continued to varying degrees, which would account for the range of Gt–Cpx temperatures calculated for this area.

Sulfate–bearing carbonate scapolite was identified in mafic garnet–clinopyroxene gneisses, mafic garnet granulites *sensu strictu* (containing orthopyroxene and generally with clinopyroxene), and garnet–amphibolites from Algonquin and Parry Sound Domains of the CGB. The amphibolites are distinguished from the mafic gneisses by the preponderance of hornblende over other mafic phases, and often by the presence of biotite. The mafic gneisses are generally Pg–Cpx–Gt–Sc assemblages with 5 to 10% hornblende and lacking biotite.

Carbonate–rich scapolite with up to 20 mol% Cl occurs in high grade calc–silicates with any or all of grossular–rich garnet, calcic plagioclase, salitic

clinopyroxene, epidote, wollastonite, quartz, titanite, and calcite. Calc-silicate lithologies usually occur as conformable units interlayered with pelitic or mafic gneisses. Equilibrium textures and equilibrium compositional relations are common among the phases in such units.

Samples of scapolite-bearing granulites and mafic gneisses, collected and donated by other workers or taken from the literature, were also analyzed. Microprobe analyses of samples donated for CO_2 barometry and thermobarometry were obtained at the University of Michigan. Samples usually contained mineral assemblages that allowed calculation of P and T using Gt-Cpx thermometry and Cpx-Opx-Gt-Pg-Qz barometry.

Grenville Province

Granulites, Mafic Gneisses and Amphibolites

Values of a_{CO_2} average range 0.09 to 0.68 (Table 1, Fig. 8) for the granulites and mafic gneisses. The garnet amphibolites are from widely separated localities and yield a range of values: 0.05 to 0.97. ARM 4 and SUN84B-18 are two samples from the same outcrop in the Kiosk domain that yield essentially the same a_{CO_2} (average 0.85), high values for a lithology that might be expected to be relatively hydrous. Unfortunately the samples do not contain mineral assemblages for which a_{H_2O} could be calculated. The third sample is from Parry Sound Domain, and in contrast to the previous amphibolites, yields comparatively low a_{CO_2} (0.09).

For the granulites it would appear that $P_{Fluid} < P_{Total}$ if a_{H_2O} is correspondingly low, as has been calculated for many granulites and charnockites. Although CO_2 may have a finite activity in these samples, it certainly does not have a high enough activity to yield a partial pressure that would be equal to $P_{Total} - p_{H_2O}$, assuming a_{H_2O}/p_{H_2O} is low (approximately less than 0.5)

TABLE 1. P, T, Mineral compositions, calculated component activities, and CO_2 activities for granulites and gneisses calculated from Reaction 7. 1: equilibrium constant for Reaction 7 relative to standard state for CO_2 at P and T of interest, used to calculate a_{CO_2}. 2: equilibrium constant for Reaction 7 relative to 1 bar, T standard state used to calculate f_{CO_2}. 3: activity of meionite calculated from scapolite activity model in Chapter III, reduced by factor X_{CO_3} (see text). * = grain to grain variability in any one or all of plagioclase, scapolite, or garnet.

SAMPLE	P	T°C	K^1	$\log K_f{}^2$	X_{An}	EqAn	X_{CO_3}	X_{Gr}	a_{An}	a_{Me}	$a_{Me}{}^3$	a_{Gr}	a_{CO_2}	$\log f_{CO_2}$	P_{CO_2}
Southwestern Grenville Province															
Granulites (G), Mafic Gneisses (M), Amphibolites (A)															
80DMA614p(G)	10	800	0.2455	5.076	0.510	0.643	0.45	0.187	0.628	0.775	0.351	0.220	0.23	4.749	2314
85DMP272-2a(G)	11	800	0.2489	5.245	0.415	0.619	0.45	0.208	0.540	0.753	0.338	0.263	0.22	4.898	3031
85DMP174-1a(M)	11	800	0.2544	5.245	0.314	0.565	0.52	0.201	0.409	0.695	0.362	0.243	0.68	5.373	9053
S86E-53a(M)	10	800	0.2455	5.076	0.394	0.597	0.51	0.275	0.515	0.731	0.371	0.327	0.26	4.801	2608
A86B3-3B-3(G)	10	800	0.2455	5.076	0.443	0.612	0.34	0.129	0.570	0.747	0.256	0.156	0.14	4.530	1397
M49(M)	10	800	0.2455	5.076	0.419	0.617	0.50	0.440	0.544	0.751	0.377	0.483	0.14	4.516	1353
80DMA348c(A)	10	800	0.2455	5.076	0.407	0.607	0.39	0.288	0.531	0.741	0.291	0.337	0.09	4.325	872
ARM4(A)	10	800	0.2455	5.076	0.413	0.579	0.68	0.254	0.537	0.711	0.480	0.305	0.74	5.249	7317
SUN84B-18(A)	10	750	0.3532	5.206	0.365	0.584	0.76	0.239	0.504	0.591	0.449	0.267	0.97	5.417	9594
Calc-silicates															
A85A-3b	10	800	0.2455	5.076	0.713	0.694	0.980	0.372	0.733	0.814	0.798	0.444	1.47	5.549	13559
A85A-3a*	10	800	0.2455	5.076	0.680	0.669	0.980	0.355	0.720	0.796	0.780	0.433	1.47	5.548	13526
	10	800	0.2455	5.076	0.840	0.669	0.980	0.355	0.840	0.796	0.780	0.433	1.00	5.380	9185

TABLE 1, continued

SAMPLE	P	T°C	K[1]	logK$_f$[2]	X_{An}	EqAn	X_{CO_3}	X_{Gr}	a_{An}	a_{Me}	a_{Me}[3]	a_{Gr}	a_{CO_2}	logf_{CO_2}	P_{CO_2}
H85A-1b	10	750	0.3532	5.206	0.724	0.686	0.989	0.710	0.750	0.709	0.701	0.617	0.61	5.216	6040
H85A-1d-1	10	750	0.3532	5.206	0.676	0.706	0.978	0.833	0.733	0.730	0.714	0.741	0.53	5.153	5224
H85A-1e(2)	10	750	0.3532	5.206	0.513	0.659	0.964	0.817	0.654	0.679	0.655	0.771	0.47	5.099	4613
H85A-1e(1)	10	750	0.3532	5.206	0.441	0.649	0.988	0.809	0.593	0.668	0.660	0.639	0.82	5.344	8110
M86E-1c-2	10	750	0.3532	5.206	0.280	0.598	0.865	0.964	0.378	0.608	0.526	0.930	0.58	5.192	5715
M86E-1b	10	750	0.3532	5.206	0.253	0.502	0.702	0.972	0.335	0.483	0.339	0.921	0.14	4.571	1368
08e	10	750	0.3532	5.206	0.513	0.661	0.906	0.838	0.654	0.682	0.618	0.816	0.34	4.962	3365
S85A-2a	10	750	0.3532	5.206	0.390	0.621	0.933	0.946	0.536	0.636	0.593	0.846	0.45	5.084	4457
S85A-2b	10	750	0.3532	5.206	0.285	0.596	0.844	0.952	0.386	0.606	0.511	0.871	0.54	5.163	5346
S85A-2d	10	750	0.3532	5.206	0.395	0.601	0.868	0.925	0.542	0.612	0.531	0.862	0.27	4.867	2704
S86E-8c	10	700	0.5200	5.344	0.315	0.598	0.895	0.542	0.459	0.495	0.443	0.650	0.37	4.767	4188
Meta-anorthosite															
PS7a	10	700	0.5200	5.344	0.485	0.661	0.939	0.324	0.662	0.579	0.544	0.396	0.71	5.338	7051
PS7b	10	700	0.5200	5.344	0.440	0.668	0.898	0.340	0.622	0.589	0.529	0.435	0.65	5.296	6401
PS7c	10	700	0.5200	5.344	0.433	0.653	0.979	0.340	0.615	0.569	0.557	0.433	0.82	5.404	8208
PS85A-2c	10	700	0.5200	5.344	0.573	0.638	0.977	0.340	0.714	0.548	0.536	0.417	0.51	5.195	5073
PS085A-5*	10	700	0.5200	5.344	0.363	0.568	0.834	0.267	0.530	0.456	0.381	0.317	0.41	5.102	4095
	10	700	0.5200	5.344	0.363	0.612	0.914	0.267	0.530	0.514	0.470	0.317	0.96	5.468	9511

TABLE 1, continued

SAMPLE	P	T°C	K[1]	logK$_f$[2]	X_{An}	EqAn	X_{CO_3}	X_{Gr}	a_{An}	a_{Me}	a_{Me}[3]	a_{Gr}	a_{CO_2}	logf_{CO_2}	P_{CO_2}
PS085A-8b	10	700	0.5200	5.344	0.466	0.639	0.884	0.328	0.646	0.550	0.486	0.395	0.48	5.170	4789
PS085A-13	10	700	0.5200	5.344	0.410	0.656	0.988	0.365	0.590	0.573	0.566	0.443	0.94	5.458	9294
PS085A-24	10	700	0.5200	5.344	0.538	0.651	0.841	0.252	0.697	0.565	0.476	0.310	0.53	5.209	5239
PS86B1-1	10	700	0.5200	5.344	0.375	0.611	0.932	0.339	0.546	0.513	0.478	0.430	0.60	5.267	5987
PS86B1-11''	10	700	0.5200	5.344	0.502	0.649	0.961	0.286	0.674	0.563	0.541	0.343	0.82	5.402	8170
PS86B2-1	10	700	0.5200	5.344	0.397	0.571	0.873	0.339	0.575	0.460	0.402	0.419	0.28	4.928	2743
PS86B2-3	10	700	0.5200	5.344	0.466	0.634	0.867	0.325	0.646	0.543	0.471	0.399	0.42	5.108	4152
PS86E-7e	10	700	0.5200	5.344	0.445	0.650	0.963	0.356	0.627	0.565	0.544	0.439	0.70	5.329	6906
PS86E-8	10	700	0.5200	5.344	0.478	0.657	0.879	0.351	0.656	0.574	0.504	0.422	0.49	5.174	4833
PS86E-15	10	700	0.5200	5.344	0.510	0.605	0.828	0.310	0.680	0.505	0.418	0.373	0.25	4.890	2513
PS86E-16a	10	700	0.5200	5.344	0.536	0.659	0.932	0.295	0.696	0.576	0.537	0.358	0.69	5.327	6874
PS86E-24f	10	700	0.5200	5.344	0.478	0.635	0.814	0.323	0.656	0.544	0.443	0.396	0.32	4.991	3171
PS86E-31	10	700	0.5200	5.344	0.424	0.621	0.956	0.367	0.605	0.526	0.503	0.465	0.51	5.193	5049
PS86E-34	10	700	0.5200	5.344	0.374	0.586	0.826	0.285	0.545	0.480	0.396	0.340	0.41	5.096	4039
S85A-3a(C)	10	700	0.5200	5.344	0.594	0.607	0.825	0.150	0.723	0.507	0.418	0.211	0.51	5.196	5084
S85A-3a(R)	10	700	0.5200	5.344	0.566	0.606	0.837	0.204	0.711	0.506	0.423	0.278	0.37	5.053	3658
S85A-3b(C)	10	700	0.5200	5.344	0.560	0.651	0.976	0.259	0.708	0.566	0.553	0.317	0.89	5.437	8856
S85A-3b(R)	10	700	0.5200	5.344	0.560	0.651	0.976	0.304	0.708	0.566	0.553	0.374	0.70	5.329	6906

TABLE 1, continued

SAMPLE	P	T°C	K[1]	logK$_f$[2]	X_{An}	EqAn	X_{CO_3}	X_{Gr}	a_{An}	a_{Me}	a_{Me}[3]	a_{Gr}	a_{CO_2}	logf_{CO_2}	P_{CO_2}
S85A-3c-1(C)	10	700	0.5200	5.344	0.557	0.677	0.968	0.175	0.707	0.601	0.582	0.215	1.97	5.781	19553
S85A-3c-1(R)	10	700	0.5200	5.344	0.557	0.677	0.968	0.232	0.707	0.601	0.582	0.279	1.33	5.611	13220
S86E-25a	10	700	0.5200	5.344	0.522	0.652	0.940	0.311	0.688	0.567	0.533	0.374	0.65	5.299	6445
S86E-25c(C)	10	700	0.5200	5.344	0.456	0.651	0.946	0.304	0.637	0.566	0.535	0.368	0.82	5.399	8114
S86E-34	10	700	0.5200	5.344	0.472	0.626	0.829	0.292	0.651	0.532	0.441	0.558	0.19	4.769	1902
S86E-36b	10	700	0.5200	5.344	0.496	0.635	0.903	0.288	0.670	0.544	0.492	0.346	0.56	5.237	5588
S86E-41	10	700	0.5200	5.344	0.573	0.661	0.997	0.221	0.714	0.579	0.578	0.272	1.31	5.605	13038
Furua Complex, Tanzania (Coolen, 1983). All granulites except 1 = calc-silicate and 2 = amphibolite.															
MF-283.2	10	800	0.2455	5.076	0.323	0.583	0.35	0.174	0.422	0.716	0.251	0.207	0.18	4.637	1788
MF-268.1	10	800	0.2455	5.076	0.322	0.581	0.44	0.171	0.420	0.714	0.312	0.206	0.44	5.024	4358
MF-283.1	10	800	0.2455	5.076	0.339	0.589	0.33	0.174	0.444	0.722	0.240	0.209	0.13	4.497	1295
WE-322.3	10	800	0.2455	5.076	0.405	0.629	0.46	0.174	0.528	0.762	0.351	0.212	0.38	4.960	3761
ZC-8	10	800	0.2455	5.076	0.340	0.564	0.41	0.176	0.446	0.694	0.287	0.214	0.26	4.791	2549
MF-266.3	10	800	0.2455	5.076	0.306	0.552	0.29	0.163	0.397	0.679	0.195	0.196	0.08	4.301	825
C-247.1	10	800	0.2455	5.076	0.327	0.542	0.39	0.173	0.427	0.667	0.258	0.196	0.21	4.707	2101
C-112	10	800	0.2455	5.076	0.327	0.539	0.40	0.179	0.427	0.663	0.268	0.213	0.22	4.719	2159
C-311.1	10	800	0.2455	5.076	0.352	0.578	0.33	0.177	0.462	0.710	0.233	0.213	0.10	4.393	1019

TABLE 1, continued

SAMPLE	P	T°C	K[1]	$\log K_f$[2]	X_{An}	EqAn	X_{CO_3}	X_{Gr}	a_{An}	a_{Me}	a_{Me}[3]	a_{Gr}	a_{CO_2}	$\log f_{CO_2}$	P_{CO_2}
SC-157	10	800	0.2455	5.076	0.330	0.545	0.40	0.171	0.432	0.670	0.268	0.217	0.21	4.697	2053
C-54.1	10	800	0.2455	5.076	0.277	0.531	0.36	0.170	0.353	0.652	0.232	0.213	0.20	4.675	1951
C-52.2	10	800	0.2455	5.076	0.276	0.565	0.31	0.186	0.352	0.695	0.218	0.211	0.16	4.579	1564
SC-156.1	10	800	0.2455	5.076	0.304	0.579	0.35	0.198	0.394	0.711	0.246	0.224	0.18	4.626	1743
C-57	10	800	0.2455	5.076	0.351	0.540	0.29	0.181	0.461	0.664	0.190	0.249	0.04	3.937	357
C-217	10	800	0.2455	5.076	0.286	0.566	0.40	0.188	0.367	0.696	0.276	0.236	0.31	4.872	3071
C-180.1	10	800	0.2455	5.076	0.334	0.557	0.37	0.166	0.438	0.687	0.254	0.207	0.16	4.590	1604
ZC-6.2[1]	10	800	0.2455	5.076	0.337	0.567	0.22	0.644	0.441	0.697	0.156	0.220	0.02	3.726	219
MF-274.2[1]	10	800	0.2455	5.076	0.961	0.781	0.45	0.848	0.961	0.864	0.392	0.695	0.02	3.732	222
C-42.1[2]	10	700	0.5200	5.076	0.425	0.555	0.56	0.223	0.606	0.440	0.247	0.268	0.07	4.049	429
BERGEN ARCS, NORWAY (Austreim, pers. comm., 1987) All granulite facies meta-anorthosite.															
HA10/83	11.5	900	0.1253	5.069	0.502	0.626	0.551	0.150	0.582	1.020	0.562	0.233	1.22	5.606	12017
HA54/83	12	900	0.1268	5.146	0.500	0.629	0.365	0.173	0.580	1.021	0.373	0.242	0.22	4.946	2295
HA46/85	14.5	900	0.1536	5.526	0.322	0.525	0.375	0.154	0.383	0.953	0.357	0.205	0.76	5.813	10780
HA53/80	14.5	900	0.1536	5.526	0.307	0.555	0.309	0.150	0.362	0.984	0.304	0.204	0.46	5.596	6535
SARGUR TERRANE, INDIA (Devaraju, pers. comm., 1987) Granulites (33A, 39) and calc-silicates (5, 25)															
TCD33A	10	800	0.2455	5.076	0.369	0.584	0.433	0.173	0.485	0.717	0.311	0.217	0.28	4.828	2775
TCD39	10	800	0.2455	5.076	0.379	0.610	0.413	0.169	0.497	0.744	0.307	0.217	0.25	4.781	2491

TABLE 1, continued

SAMPLE	P	T°C	K^1	$\log K_f^2$	X_{An}	EqAn	X_{CO_3}	X_{Gr}	a_{An}	a_{Me}	a_{Me}^3	a_{Gr}	a_{CO_2}	$\log f_{CO_2}$	P_{CO_2}
TCD5	10	800	0.2455	5.076	0.945	0.739	0.989	0.894	0.945	0.842	0.833	0.596	0.60	5.157	5920
TCD25	10	800	0.2455	5.076	0.927	0.764	0.983	0.902	0.927	0.856	0.841	0.612	0.63	5.179	6228
Devaraju & Coolen (1983) Granulite															
K21	10	800	0.2455	5.076	0.386	0.601	0.342	0.168	0.506	0.735	0.251	0.216	0.11	4.417	1077
Srikantappa (pers. comm., 1988) Granulite															
285	10	800	0.2455	5.076	0.380	0.574	0.38	0.158	0.498	0.706	0.268	0.209	0.15	4.566	1518
New South Wales (Wilkinson, 1973) Gt-Cpx-Pg-Hbl-Sc xenolith															
R30241	14	850	0.2109	5.594	0.378	0.599	0.545	0.243	0.474	0.868	0.473	0.298	0.92	5.894	12880
LASHAINE, TANZANIA (Jones et al., 1983) GA = Gt anorthosite, GPC= Gt-Pg-clinopyroxenite															
533 GA	14	800	0.3119	5.7485	0.419	0.681	0.985	0.307	0.544	0.805	0.793	0.370	4.50	6.655	48402
526 GPC	14	800	0.3119	5.7485	0.290	0.550	0.546	0.233	0.374	0.677	0.370	0.321	0.67	5.828	7215
528* GPC	14	800	0.3119	5.7485	0.326	0.611	0.611	0.275	0.426	0.745	0.455	0.352	0.97	5.987	10385
	14	800	0.3119	5.7485	0.480	0.611	0.611	0.275	0.604	0.745	0.455	0.352	0.40	5.608	4345
727a GPC	14	800	0.3119	5.7485	0.348	0.512	0.652	0.221	0.457	0.626	0.408	0.312	0.63	5.800	6753
798* GPC	14	800	0.3119	5.7485	0.347	0.621	0.944	0.227	0.455	0.755	0.712	0.304	6.14	6.790	66008
	14	800	0.3119	5.7485	0.347	0.606	0.778	0.227	0.455	0.740	0.576	0.304	2.62	6.420	28188
EIFEL, W. GERMANY (Okrusch et al. 1979) Granulite															
AS-K-3	10	850	0.1741	4.9545	0.702	0.718	0.592	0.196	0.717	0.919	0.544	0.243	0.70	5.178	6913
	10	850	0.1741	4.9545	0.537	0.718	0.592	0.196	0.627	0.919	0.544	0.243	0.98	5.324	9676

TABLE 1, continued

SAMPLE	P	T°C	K^1	$\log K_f^2$	X_{An}	EqAn	X_{CO_3}	X_{Gr}	a_{An}	a_{Me}	a_{Me}^3	a_{Gr}	a_{CO_2}	$\log f_{CO_2}$	P_{CO_2}
LESOTHO (Griffin et al.), 1978) All granulites or mafic gneisses															
K-2	10	800	0.2455	5.076	0.200	0.627	0.604	0.213	0.234	0.760	0.459	0.310	4.82	6.064	47789
PHN2852	10	800	0.2455	5.076	0.190	0.568	0.443	0.165	0.219	0.698	0.309	0.244	1.68	5.606	16647
PHN1670	10	800	0.2455	5.076	0.230	0.459	0.428	0.166	0.281	0.546	0.234	0.264	0.26	4.798	2590
PHN3017	10	800	0.2455	5.076	0.270	0.408	0.176	0.233	0.343	0.461	0.081	0.295	0.00	2.672	19
L-12A	10	800	0.2455	5.076	0.190	0.392	0.352	0.199	0.219	0.434	0.153	0.283	0.08	4.284	793
LQ-2	10	800	0.2455	5.076	0.320	0.533	0.55	0.174	0.417	0.654	0.360	0.275	0.51	5.090	5074
LT-2	10	800	0.2455	5.076	0.270	0.506	0.443	0.163	0.343	0.618	0.274	0.218	0.40	4.982	3957

Figure 8. Histogram summarizing results of calculations of a_{CO_2} as a function of lithology and setting, including values that exceed unity.

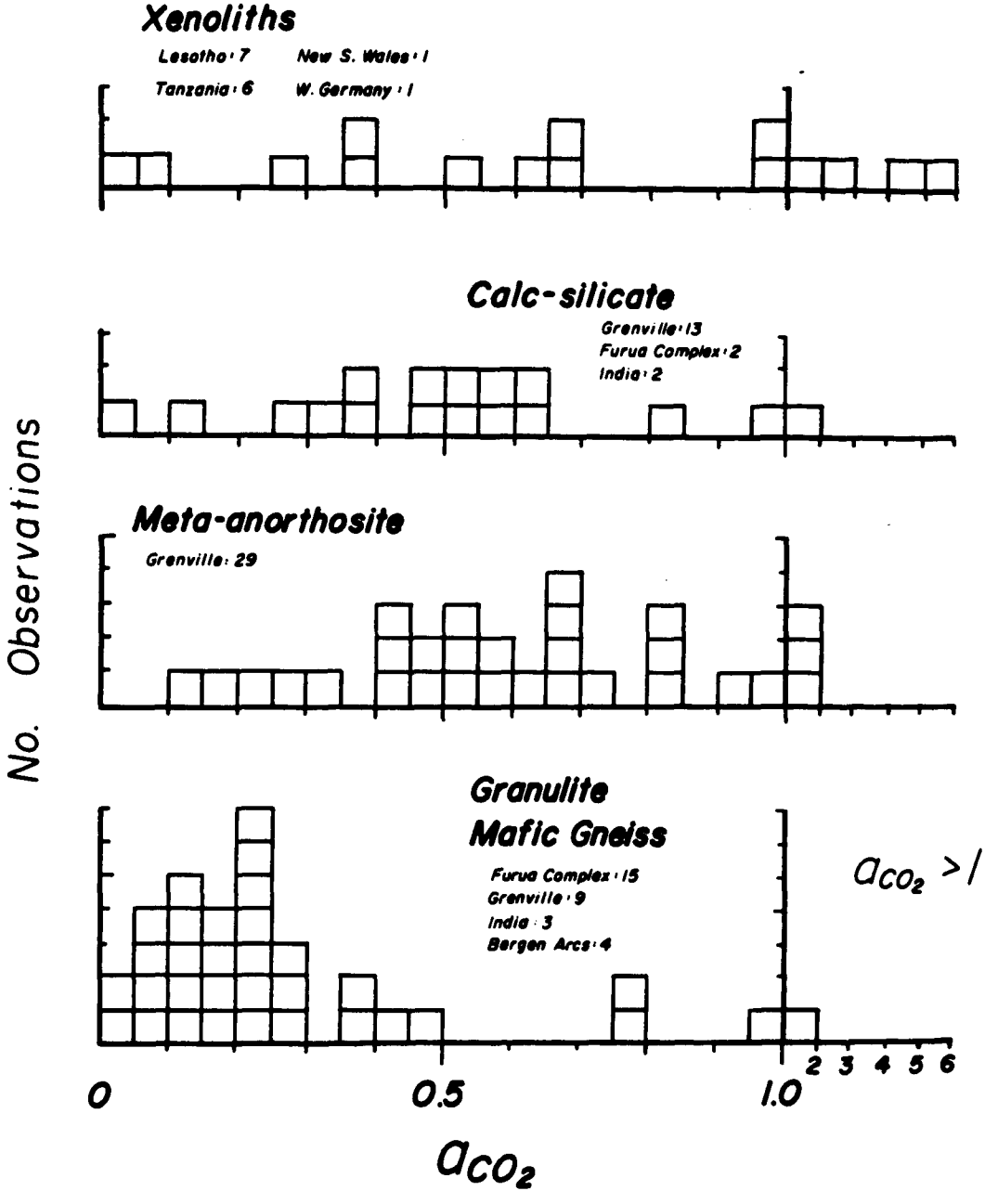
Xenoliths
Lesotho: 7
New S. Wales: 1
Tanzania: 6
W. Germany: 1
Calc-silicate
Grenville: 13
Furua Complex: 2
India: 2
Meta-anorthosite
Grenville: 29
Granulite
Mafic Gneiss
Furua Complex: 15
Grenville: 9
India: 3
Bergen Arcs: 4
$a_{CO_2} > 1$
No. Observations
0
0.5
1.0
2 3 4 5 6
a_{CO_2}

Whitestone meta-anorthosite

The calculation of a_{CO_2} for scapolite bearing samples of the WSA was done at 650, 700, and 750°C. Most of the temperatures are in the range 675 to 700°C, and therefore only the results of calculations at 700°C are summarized in Table 1. For some of these samples, an $a_{CO_2} > 1.0$ was obtained at temperatures above 700°C. The highest value of a_{CO_2} was calculated for sample S86E-41 (1.3), in which secondary scapolite and hornblende after plagioclase, clinopyroxene, and garnet are extensively developed. As with other samples of WSA with late scapolite, garnet in this sample is depleted in grossular component relative to those exhibiting equilibrium textures and values of $a_{CO_2} < 1.0$ (Table 1). The high a_{CO_2} is a manifestation of the retrograde disequilibrium. The results at 700°C are considered the most reasonable estimates of fluid activity for the aureole of the WSA and WSA in the PSSZ. Geobarometry in the same area indicates that pressure was 10±1 kbar during ductile shearing and tectonic displacement (Chapter II), essentially the same as peak regional P.

In general, Sc-Gt-Pg-Qz equilibria indicate that a_{CO_2} was in the range 0.2 to 0.8 in the WSA aureole and in sheared WSA (Table 1, Fig. 8), with the majority of samples exceeding 0.5. Using Reaction 8 calculation of a_{CO_2} for samples that are primarily from the PSSZ yields a similar range (Table 2). The samples of WSA represent a suite of lithologically similar rocks with limited mineral chemistry from the same tectonic setting. The range of activities and partial pressures is likely to mainly represent inherent imprecision in the calculation due to the limited chemical variation. Temperature imprecision is also a likely source for the range of a_{CO_2}. Where appropriate mineral assemblages were present, calculations of a_{H_2O} (Table 3) where performed using Reaction 9. A range of a_{H_2O} are obtained and indicate local fluid-present conditions, and that the fluid was a mixed H_2O-CO_2 fluid with CO_2 the dominant fluid component in the scapolite-bearing meta-anorthosite. Although the

TABLE 2. CO_2 activities for calc-silicate (C), meta-anorthosite (MA) and mafic gneisses (MG) from Parry Sound Domain calculated from Reaction 8 (An + 2Cc + Qz = Gr + $2CO_2$).

SAMPLE	P	T°C	logK[1]	$logK_f$[2]	X_{An}	X_{Gr}	a_{An}	a_{Gr}	a_{CO_2}	$logf_{CO_2}$	P_{CO_2}
M86E-1c-2 (C)	10	750	-1.212	9.650	0.280	0.964	0.378	0.930	0.17	4.661	1683
M86E-1b (C)	10	750	-1.212	9.650	0.253	0.972	0.335	0.921	0.16	4.641	1607
08e (C)	10	750	-1.212	9.650	0.513	0.838	0.654	0.816	0.27	4.865	2693
S86E-8c (C)	10	700	-1.437	9.536	0.315	0.542	0.459	0.650	0.25	4.880	2456
PS86B1-6 (MA)	10	700	-1.437	9.536	0.151	0.280	0.182	0.397	0.33	5.000	3238
PS86B1-9b (MA)	10	700	-1.437	9.536	0.156	0.280	0.190	0.345	0.41	5.101	4055
PS86B1-8 (MA)	10	700	-1.437	9.536	0.151	0.280	0.182	0.264	0.60	5.266	5973
PS86E-6b (MG)	10	700	-1.437	9.536	0.331	0.333	0.484	0.404	0.52	5.200	5131
PS86E-31 (MA)	10	700	-1.437	9.536	0.424	0.367	0.605	0.465	0.47	5.157	4648
S86E-33 (MA)	10	700	-1.437	9.536	0.152	0.205	0.184	0.226	0.77	5.370	7590

1: $log_{10}K$ relative to standard state of CO_2 at P and T of interest, used to calculate a_{H_2O}.
2: $log_{10}K$ relative to standard state of CO_2 at 1 bar, T, used to calculate f_{H_2O}.

TABLE 3. H_2O activities and fugacities for meta-anorthosite calculated from Reaction 9 (4Czo + Qz = 5An + Gr + H_2O).

Sample	P	T°C	$\log K^1$	$\log K_f^2$	X_{An}	X_{Ps}	X_{Gr}	a_{An}	a_{Czo}	a_{Gr}	a_{H_2O}	$\log f_{H_2O}$	P_{H_2O}
PS85A-2c	10	700	-1.425	6.887	0.573	0.195	0.340	0.714	0.415	0.417	0.29	3.614	2871
PS86B1-11''	10	700	-1.425	6.887	0.502	0.200	0.286	0.674	0.399	0.343	0.41	3.770	4112
PS86E-7e	10	700	-1.425	6.887	0.445	0.201	0.356	0.627	0.397	0.439	0.34	3.685	3381
PS86E-8	10	700	-1.425	6.887	0.478	0.218	0.351	0.656	0.346	0.422	0.24	3.542	2433
PS86E-12	10	700	-1.425	6.887	0.492	0.199	0.381	0.667	0.402	0.404	0.33	3.681	3350
PS86E-15	10	700	-1.425	6.887	0.510	0.193	0.310	0.680	0.420	0.373	0.40	3.753	3794
PS86E-16a	10	700	-1.425	6.887	0.536	0.215	0.295	0.696	0.357	0.358	0.28	3.610	2845
PS86E-17	11	700	-2.051	6.600	0.545	0.210	0.335	0.701	0.370	0.456	0.10	3.333	1277
PS86E-24f	10	700	-1.425	6.887	0.478	0.193	0.323	0.656	0.420	0.396	0.39	3.751	3936
S86E-25a	10	700	-1.425	6.887	0.522	0.169	0.311	0.688	0.493	0.374	0.53	3.877	5261
PS86E-31	10	700	-1.425	6.887	0.424	0.214	0.367	0.605	0.358	0.465	0.27	3.595	2748

1: $\log_{10}K$ relative to standard state of H_2O at P and T of interest.

2: $\log_{10}K$ relative to standard state of H_2O at 1 bar, T.

precision of these calculations are low, fluid present conditions are likely in some of the samples (Table 4), where $P_{CO_2} + P_{H_2O}$ is within 1 kbar of P_{Total} at 700°C.

Calc-silicates

The calc-silicates generally yield intermediate to high a_{CO_2} (Table 1). Four samples from a two meter thick calc-silicate lens in which the scapolite, plagioclase, and garnet exhibit variable composition (H85A-1 sample series) shows the range of values obtained as a result of variable mineral chemistry at constant P and T (0.47 to 0.82). The values of a_{CO_2} for this occurrence indicate either a CO_2-rich mixed CO_2-H_2O fluid, or fluid absent metamorphism. Other calc-silicates yield similar results except for the A85A-3 samples. At the temperature inferred for the McCraney domain, where the A85A-3 samples were collected (800°C) $a_{CO_2} = 1.47$, another example of either overestimating T or retrograde equilibration of the mineral assemblage. Petrographic examination of the samples indicated no textural evidence of retrogression. However, the plagioclase compositions were found to be highly variable within sample A85A-3a (not uncommon in scapolite-bearing rocks, *c.f.* Frank 1985). Based on the K_D relations discussed above, the samples that yield $a_{CO_2} > 1$ contain plagioclase that is less calcic than the scapolite (in terms of An content), and these samples are likely to represent disequilibrium resetting of the plagioclase composition. The most calcic plagioclase in this sample, one that is consistent with the K_D relations, yields a_{CO_2} of 1.0 at the equilibrium P and T, consistent with a pure CO_2 fluid phase and essentially $P_{Fluid} = P_{Total}$ for this sample. It would be interesting to compare the calculated fluid composition with that determined from fluid inclusion analysis.

TABLE 4. Comparison of activities and partial pressures of CO_2 and H_2O for samples of Whitestone Anorthosite at 700°C and 10,000 bars total pressure. Pressure in bars.

SAMPLE	a_{CO_2}	P_{CO_2}	a_{H_2O}	P_{H_2O}	P_{Total}
PS85A-2c	0.51	5073	0.29	2871	7944
PS86E-7e	0.70	6906	0.34	3381	10287
PS86E-8	0.49	4833	0.24	2433	7266
PS86E-11"	0.82	8170	0.41	4112	12282
PS86E-15	0.25	2513	0.40	3794	6307
PS86E-16a	0.69	6874	0.53	2845	9719
PS86E-24f	0.32	3171	0.39	3936	7107
S86E-25a	0.65	6445	0.53	5261	11706
PS86E-31	0.51	5049	0.27	2748	7797

Other Granulite Terranes

Furua Complex, Tanzania

Coolen (1980) presented a detailed discussion of the petrology and geochemistry of the Furua Complex, a 700 km² granulite terrane in the Pan-African Mozambique Belt of Tanzania. Sulfate scapolite occurs in quartz-bearing felsic to mafic two-pyroxene garnet granulites, garnet-clinopyroxene granulites, calc-silicate gneisses, and garnet-clinopyroxene amphibolites. P and T estimates for the granulite metamorphism cluster tightly around 10 kbar and 800°C (Coolen, 1980). We have recalculated P and T from Coolen's data using the pyroxene-garnet-plagioclase-quartz geobarometers of Chapter II and the garnet-clinopyroxene geothermometer of Ellis & Green (1979) and Pattison & Newton (1988), obtaining precisely the values determined by Coolen. As a result of the good control and limited variability in P and T, the Furua Complex provides a good opportunity to evaluate fluid composition in a well constrained setting, and to estimate precision based on compositional variation within this setting.

The a_{CO_2} was calculated for 15 samples of garnet two-pyroxene and clinopyroxene-garnet granulites from throughout the complex, two calc-silicate gneisses, and one garnet-clinopyroxene amphibolite. The a_{CO_2} ranges from 0.02 to 0.44 for the Furua granulites (Table 1). Values of 0.02 to 0.10 were obtained for the calc-silicates, and 0.07 for the amphibolite.

Several of the scapolite-bearing granulites from the Furua Complex also contain the assemblage Phl-Kfs-Opx-Qz which were used to evaluate a_{H_2O} by Reaction 1. The experimental reversal for Reaction 1 of Bohlen *et al.* (1983) (5 kbar, 790°C, and X_{H_2O} = 0.35) was used as a starting point for the calculation of a_{H_2O}. Entropy and volume data for phlogopite are from Robie and Hemingway (1984) and Hewitt and Wones (1975), respectively. Complete Al-Si disorder was assumed for phlogopite (Clemens *et al.*, 1987). Thermodynamic data for sanidine are

from Robie *et al.* (1978), and data for enstatite and quartz are from a number of sources summarized in Chapter II. The position of the pure H_2O reaction was determined using the activity coefficient for H_2O at X_{H_2O} = 0.35 calculated from the MRK equation of state of Kerrick & Jacobs (1981). Ideal mixing models were used for enstatite (Wood & Banno 1973) and phlogopite (Bohlen *et al.*, 1980). Biotite in the Furua Complex granulites was not analyzed for F or Cl, so calculation of a_{H_2O} will be an upper limit as F or Cl would reduce the activity of phlogopite and therefore reducing the a_{H_2O}. The a_{H_2O} and p_{H_2O} of four samples are uniformly low (0.14 to 0.18, Table 5). The results of the calculations indicate that p_{CO_2} is less than p_{H_2O}, and the two gases do not sum to P_{Total}. The presence of magnetite and pyrite in these samples allows calculation of fO_2 and fS_2 by the reactions

$$\text{Ferrosilite} + O_2 = \text{Magnetite} + \text{Quartz} \qquad (9)$$
$$6\ FeSiO_3 + O_2 = 2\ Fe_3O_4 + 6\ SiO_2)$$

$$\text{Magnetite} + S_2 = \text{Pyrite} + O_2 \qquad (10)$$
$$Fe_3O_4 + 3\ S_2 = 3\ FeS_2 + 2\ O_2$$

and from these values the fugacities of various fluid species in the C–O–H–S system can be calculated (French, 1966; Eugster, 1977; Holloway, 1977; Ohmoto & Kerrick, 1977; Lamb & Valley, 1985). Thermodynamic data for the various gases are taken from Robie *et al.* (1978). These calculations show that at the fO_2–fS_2 calculated for these four samples, most other gas species have low fugacities, and CO_2 and H_2O are the dominant gases (Table 5). SO_2 and H_2S have the next highest fugacities. Based on fugacity coefficients for H_2S and SO_2 calculated from the data of Ryzhenko & Volkov (1971), the two species have partial pressures on the order of 10 and 150 bars, respectively. The results for these samples from the Furua complex are consistent with fluid absent metamorphism. The limited range of mineral compositions determined for these lithologies suggests that this conclusion will hold for other samples in the Furua Complex once further characterization of the samples is performed.

TABLE 5. Activities and fugacities (log_{10}) of gas species, and activity (log_{10}) of graphite activity in C-O-H-S system for Furua Complex granulites at 800°C and 10 kbar. a_{H_2O} calculated from Reaction 1, a_{CO_2} calculated from Reaction 7.

SAMPLE	a_{CO_2}	f_{CO_2}	P_{CO_2}	a_{H_2O}	f_{H_2O}	P_{H_2O}	f_{O_2}	f_{H_2}	a_C	f_{CO}	f_{CH_4}	f_{S_2}	f_{H_2S}	f_{SO_2}	f_{SO_3}
MF-283.2	0.18	4.64	1788	0.18	3.86	4407	-11.13	0.25	-3.76	-1.00	-4.34	1.29	2.70	3.24	-2.36
MF-268.1	0.44	5.02	4358	0.17	3.84	4268	-11.18	0.25	-3.33	-1.26	-3.92	1.26	2.68	3.20	-2.42
MF-283.1	0.13	4.50	1295	0.17	3.83	4171	-11.11	0.20	-3.92	-0.85	-4.59	1.30	2.66	3.27	-2.32
ZC-8	0.26	4.79	2549	0.14	3.73	3313	-11.07	0.09	-3.66	-1.12	-4.57	1.33	2.56	3.32	-2.25
C-180.1	0.16	4.59	1604	0.14	3.76	3550	-10.80	-0.05	-4.15	-1.80	-5.32	1.51	2.52	3.69	-1.75

Coolen (1982) performed a fluid inclusion study of a mafic gneiss from the Furua Complex (sample C-180.1), documenting CO_2-rich fluid inclusions in quartz, plagioclase, and garnet. The calculated fluid compositions for this sample are not consistent with the presence of a pure CO_2 or CO_2-rich fluid inclusions. The pressure determined by Coolen from the CO_2 isochore and inferred metamorphic temperature was lower than that calculated from mineral equilibria. This is consistent with the interpretation that the fluid inclusions were trapped or modified after the peak of metamorphism and the fluid they contain does not represent that of peak metamorphism.

The results from the Furua Complex are intriguing with regard to the consistency of mineral compositions and calculated fluid activities, origin of the scapolite, and the geologic setting of the Complex in East Africa. The presence of scapolite in a wide range of differing bulk compositions, many that are not likely to contain significant pre-metamorphic carbon, might be taken as evidence that at some stage in the history of the complex there occurred an episode of fluid infiltration and interaction with the gneisses. The calculated fluid compositions are consistent with fluid absent metamorphism, indicating this infiltration would had to have occurred before the peak of granulite facies metamorphism. Although the scapolite is a mixed sulfate-carbonate variety, both volatile components need not both be externally derived. Based on geochemical data, Coolen (1980) proposes that the protoliths for the complex were sulfide-rich felsic to mafic volcanics and sediments. Stable S and C isotope analysis of the scapolite is consistent with an igneous source for the sulfur (Hoefs *et al.*, 1981), but the source of the carbon is equivocal (Hoefs *et al.*, 1981; Chapter V). Therefore the sulfur could have been a component of the sulfides in the igneous protoliths of the felsic to mafic gneisses and amphibolites, later oxidized by infiltrating CO_2-bearing fluids (Coolen, 1980). The area of East Africa is rich with active carbonic volcanism and scapolite-bearing deep crustal xenoliths are common. The Furua Complex and other granulite complexes of

Tanzania and East Africa deserve further study. If a case can be made for carbonic metamorphism, this would be the area in which it should be evaluated.

Bergen Arcs, Norway

Sulfate-rich scapolite is reported in coronitic granulite facies meta-anorthosite of the Bergen Arcs, Norway (Griffin, 1972; Austreim & Griffin, 1985; Austreim, 1987), which was locally subjected to ductile shearing under eclogite facies conditions. Using Gt-Cpx geothermometry (Ellis & Green 1979) and Gt-Opx geobarometry (Harley & Green, 1982), Austreim & Griffin (1985) report equilibration conditions of 775 to 850°C and P = 7.8 to 9.4 kbar for the granulites from the Bergen Arcs. In contrast, coronitic gneisses from the Bergen Arcs yield consistently higher temperatures (875 to 1015°C) and pressures (8.6 to 12.4 kbar; Austreim & Griffin, 1985). Four samples of the Sc-Gt±Cpx±Opx granulites and meta-anorthosites obtained from Austreim (pers. comm., 1988) were analyzed for this study. Pressures were recalculated to be 13±1.5 kbar using Cpx-Opx-Gt-Pg barometry, which are maximum pressure limits as quartz is absent in these lithologies. Values of a_{CO_2} were calculated at 800 and 900°C (Table 1). At 900°C one sample yields a_{CO_2} = 1.2 while the other three ranger from 0.2 to 0.8. At 850°C the four samples yield a_{CO_2} of 0.1 to 0.6.

South India

Scapolite granulites and calc-silicates are reported from a number of localities in Archean terranes of southern India (Devaraju & Gowd Reddy, 1976; Devaraju & Coolen, 1983; Srikantappa *et al.*, 1985; Kumar & Chacko, 1986; Mukherjee *et al.*, 1986). This area has been proposed as an example where the granulite facies fluid phase has been diluted by CO_2 influx and where the presence of scapolite has been taken to indicate high CO_2 partial pressures (Srikantappa *et al.*, 1985). Four mafic granulites from the Sargur area yield consistently low a_{CO_2} (0.11 to 0.28, Table 1). If a_{H_2O} is as low in these mafic granulites as it is in charnockites, for which a_{H_2O} is

usually much less than 0.5, and if other gas species are of minor importance, the results of our calculations argue for fluid absent metamorphism. Two calc-silicates from this area yield intermediate values of a_{CO_2} and $p_{CO_2} < P_{Total}$ (a_{CO_2} = 0.6), similar to the Grenville samples, and consistent with fluid absence or a mixed CO_2-H_2O fluid. The calc-silicates we evaluated contain no hydrous phases and a_{H_2O} cannot be evaluated from mineral equilibria.

Crustal Xenoliths

Sulfate-carbonate scapolite has be found to be a common phase in deep-crustal granulite facies xenoliths (see previous section on Scapolite Compositions). Calculation of precise fluid activities in crustal xenoliths is hampered by equivocal estimates of metamorphic temperature, more so than in a regional metamorphic setting. The requisite assemblage for geothermometry is often present in the scapolite xenoliths, however a suite of xenoliths may or may not represent a single metamorphic event, with the xenoliths being a sample from a range of levels in the crust or of different metamorphic events. Retrograde resetting of temperatures may also occur under static conditions in the deep crust, so that peak metamorphic temperatures are not preserved. However, a suite of xenoliths from a single volcanic vent may represent a coherent group of rocks sampled from the same crustal level. With this caveat in mind we have calculated a_{CO_2} in xenoliths from four settings (Table 1, Fig 8). We have recalculated P and T for most of these samples using Gt-Cpx thermometry (Ellis & Green, 1979; Pattison & Newton, 1988) and Cpx-Gt-Pg-Qz geobarometry (Chapter II).

Mineral analyses are reported for the requisite assemblage in single xenoliths from each of the occurrences at New South Wales, Australia (Wilkinson 1973) and Eifel, West Germany (Okrusch *et al.* 1979). These samples yield high a_{CO_2} ($\leq$0.83 and $\leq$0.79, respectively, quartz absent) at the inferred temperatures.

A suite of crustal xenoliths from Lashaine, Tanzania (Jones *et al.*, 1983) were interpreted to represent a relict suite of mafic igneous rocks metamorphosed to

granulite facies, and include a sample of meta-anorthosite (533, Table 1). The samples yield a range of Gt-Cpx temperatures (610-1035°C), and variably high values of a_{CO_2} with several exceeding 1.0. It is possible that there has been considerable resetting of mineral compositions at lower temperatures, resulting in the unrealistic values of $a_{CO_2} > 1.0$. However, considering even a 100°C decrease in estimated T the results are consistent with a CO_2-rich fluid phase if $P_{Fluid} = P_{Total}$.

A suite of xenoliths from the Kaapvaal Craton in Lesotho were analyzed by Griffin *et al.* (1978). Temperatures for all but one sample (1098°C) ranged from 650 to 770°C. Values of a_{CO_2} were calculated at 50° intervals between 650 and 800°C, with the 800°C values reported in Table 1. The values of a_{CO_2} are uniformly low, except for K-2 and PHN2852, which yield $a_{CO_2} > 1.0$ even at 700°C. Sample PHN3017 yields the lowest a_{CO_2} calculated for this study (<0.0), a result of the extremely sulfate rich scapolite. This is the most sulfate-rich natural scapolite that has been described to date.

Discussion

The results presented above indicate that scapolite mineral assemblages may be used to obtain reasonable estimates of a_{CO_2}. Improvements in the precision of the calculations are certainly possible, particularly in the experiments on scapolite stability and in the scapolite a-X relations. Variations on the order of 0.1 to 0.3 in a_{CO_2} for a given locality are likely to be due to the sensitivity of the calculations to local variations in mineral composition or resetting of equilibria. The results also illustrate a number of features of the mechanics of calculating fluid composition in high grade settings and the uncertainties inherent its calculation. There is a critical need for accurate geothermometry and determination of metamorphic conditions that correspond to the equilibration of fluid with solid phases. The erroneous conclusion that P_{Fluid} is less than P_{Total} may be reached if peak temperature is actually greater than that where thermometric equilibria are "frozen-in" (Pattison & Newton, 1988).

The equilibrium used here (Reaction 7) demonstrates that the presence of scapolite in a mineral assemblage may indicate a range of fluid composition. High a_{CO_2} is characteristic of carbonate-rich scapolite assemblages in meta-anorthosite and some calc-silicates and sulfate-rich scapolite assemblages in xenoliths, whereas low a_{CO_2} was calculated for most granulites and mafic gneisses. However, the results are equally sensitive to the anorthite content of plagioclase and grossular content of garnet. Higher grossular and anorthite contents will yield lower a_{CO_2}, by Reaction 7, for a constant scapolite composition. The point to be made is that the entire mineral assemblage monitors the fluid composition, and that the presence of scapolite alone does not correlate with CO_2-rich fluid composition. Similarly, the presence of amphibole, biotite, or calcite in any other mineral assemblage does not by itself imply H_2O or CO_2-rich fluid composition.

If even moderate or low a_{CO_2} are recorded by scapolite equilibria in meta-anorthosite and granulites, one might consider what implications the *absence* of scapolite has in these same lithologies in other high grade settings. In response to influx of a CO_2-rich fluid phase during post-granulite facies ductile shearing, a scapolite-bearing metamorphic aureole (up to 4 km wide) developed around the Whitestone Anorthosite. If other occurrences of anorthosite experienced the same processes, why should they not also develop scapolite-bearing mineral assemblages? Anorthosite massifs that have experienced granulite facies metamorphism are characteristic features of the Grenville Province, and smaller masses similar to the WSA have been reported in other high grade terrains. By analogy with the WSA, these intrusions should be the locus of scapolite formation if anorthosite-fluid interaction has occurred within the stability field of scapolite. For example Subramaniam (1956a) describes the occurrence of scapolite in meta-anorthosite of the Sittampundi Complex, an arcuate mafic layered intrusion in the Salem district, Madras, India. The highly aluminous composition of the anorthosite is reflected in the anorthite-rich plagioclase (An_{70} to An_{100}), grossular-rich garnet, clinozoisite-rich epidote, and the presence of corundum. Scapolite in the meta-anorthosite was not analyzed, however refractive indices correspond to values approaching EqAn 60.

Subramaniam (1956b) also describes a smaller metamorphosed anorthosite-gabbro mass from Kadavur, Madras, with mineralogic variation and structure remarkably similar to the WSA. Modal scapolite content increases from 0.5% in the core to 5% in the periphery of the body. Manna & Sen (1974) also report scapolite in the Bengal granulite-anorthosite complex at Saltora, W. Bengal, India (the complex is also described by Bhattacharyya & Mukherjee (1987) but they do not describe scapolite occurrences). These occurrences of scapolite merit further investigation as to fluid composition and the source of carbon in scapolite. In contrast to these latter two occurrences, the Bolangir granulite facies anorthosite massif and related mafic granulite gneisses near Orissa, eastern Ghats Belt, India have no reported scapolite (Mukherjee *et al.*, 1986). Except for the marginal facies and demonstrably retrograde occurrences (Valley *et al.*, 1978; Morrison, 1988), primary high grade scapolite is noticeably absent from the Adirondack (Buddington, 1939), and the Morin anorthosite massif of Quebec (Martignole & Schrijver, 1971), both massifs metamorphosed under granulite facies conditions.

As with calculations of a_{H_2O} based on hydrous phase equilibria (Reactions 1 to 3), scapolite equilibria are potentially a powerful tool in recording peak fluid compositions in a wide range of geologic settings and rock types. This would be preferred to using fluid inclusions in high grade rocks which require interpretation as to what fluids they have trapped, and often yield equivocal results. Perhaps as important, scapolite equilibria allow a means of evaluating the critical assumption of $P_{Fluid} = P_{Total}$ in high grade settings.

References

Anovitz, L.M., 1987. Pressure-Temperature Constraints on Metamorphism in the Grenville Province, Ontario. Ph.D. Thesis, Univ. Michigan.

Anovitz, L.M., Essene, E.J., 1987. Compatibility of geobarometers in the system CaO-FeO-Al_2O_3-SiO_2-TiO_2: implications for garnet mixing models. J. Geol. **95**, 633-645.

Aranovich, L.Ya., Schmupovich, K.I., & Fed'kin, V.V., 1987. The H_2O and CO_2 regime in regional metamorphism. Inter. Geol. Rev. **29**, 1379-1401.

Austreim, H., 1986. Eclogitization of lower crustal granulites by fluid migration through shear zones. Earth Plan. Sci. Lett. **81**, 221-232.

Austreim, H., Griffin, W.L., 1985. Shear deformation and eclogite formation within granulite-facies anorthosites of the Bergen Arcs, western Norway. Chem. Geol. **50**, 267-281.

Bhattacharya, A., Sen, S.K., 1986. Granulite metamorphism, fluid buffering, and dehydration melting in the Madras charnockites and metapelites. J. Petrol. **27**, 1119-1141.

Bhattacharyya, P.K., Mukherjee, S., 1987. Granulites in and around the Bengal anorthosite, eastern India; genesis of coronal garnet, and evolution of the granulite-anorthosite complex. Geol. Mag. **124**, 21-32.

Bird, D.K., Helgeson, H.C., 1980. Chemical interaction of aqueous solutions with epidote-feldspar mineral assemblages in geologic systems. I. Thermodynamic analysis of phase relations in the system CaO-FeO-Fe_2O_3-Al_2O_3-SiO_2-H_2O-CO_2. Am. J. Sci. **280**, 907-941.

Bohlen, S.R., Peacor, D.R., Essene, E.J., 1980. Crystal chemistry of a metamorphic biotite and its significance in water barometry. Am. Mineral. **65**, 55-62.

Bohlen, S.R., Boettcher, A.L., Wall, V.J., Clemens, J.D., 1983. Stability of phlogopite-quartz and sanidine-quartz: a model for melting in the lower crust. Contrib. Mineral. Petrol. **83**, 270-277.

van Breemen, O,, Davidson, A., Loveridge, W.D., Sullivan, R.W. 1986. U-Pb geochronology of Grenville tectonites, granulites and igneous precursors, Parry Sound, Ontario. (In) The Grenville Province (eds Moore JM, Davidson A, Baer AJ) Geol Assoc Can Spec Pap 31:191-207

Bright, E.G., 1987. Precambrian geology of the Whitestone Lake Area, District of Parry Sound. Ont. Geol. Surv. Map P.3095.

Buddington, A.F., 1939. Adirondack Igneous Rocks and their Metamorphism. Geol. Soc. Amer. Mem. **7**.

Burnham, C.W., Holloway, J.R., & Davis, N.F., 1969. Thermodynamic properties of water to 1,000°C and 10,000 bars. Geol. Soc. Amer. Spec. Pap. **132**, 96 pp.

Carpenter, M.A., Ferry, J.M., 1984. Constraints on the thermodynamic mixing properties of plagioclase feldspars. Contrib. Mineral. Petrol. **87**, 138-148.

Clemens, J.D., Circone. S, Navrotsky A, McMillan PF, Smith BK, Wall, V.J., 1987. Phlogopite: high temperature solution calorimetry, thermodynamic properties, Al-

Si and stacking disorder, and phase equilibria. Geochim. Cosmochim. Acta **51**, 2569-2578.

Coolen, J.J.M.M.M., 1980. Chemical Petrology of the Furua Granulite Complex, southern Tanzania. PhD dissertation, Vrije University.

Coolen, J.J.M.M.M., 1982. Carbonic fluid inclusions in granulites from the Tanzania - a comparison of geobarometric methods based on fluid density and mineral chemistry. Chem. Geol. **37**, 59-77.

Davidson, A., 1984a. Tectonic boundaries within the Grenville Province of the Canadian Shield. Geodynam. **1**, 433-444.

Davidson, A., 1984b. Identification of ductile shear zones in the southwestern Grenville Province of the Canadian Shield. In Precambrian Tectonics Illustrated (eds. A. Kroner and R. Greiling), 263-279. E. Schweizerbart'sche Verlagsbuchhandlung.

Davidson, A., Britton, J.M., & Bell, K., 1979. Regional synthesis of the Grenville Province of Ontario and western Quebec. Curr. Res., Geol. Surv. Canada Pap. **78-1B**, 153-172.

Davidson, A., Culshaw, N.G., & Nadeau, L., 1982. A tectono-metamorphic framework for part of the Grenville Province, Parry Sound Region, Ontario. Curr. Res., Geol. Surv. Canada Pap. **82-1A**, 175-190.

Devaraju, T.C., & Coolen, J.J.M.M.M., 1983. Mineral chemistry and P-T conditions of formation of a basic scapolite-garnet-pyroxene granulite from Doddakanya, Mysore District. J. Geol. Soc. India. **24**, 404-411.

Devaraju, T.C., & Gowd Reddy, K., 1976. Coexisting orthopyroxene and scapolite in certain basic granulites from the Doddakanya, Mysore District. Ind. Mineral. **17**, 5-11.

Edwards, A.C., Lovering J.F., & Ferguson, J., 1979. High pressure basic inlcusions from the Kayrunnera kimberlitic diatreme in New South Wales, Australia. Contrib. Mineral. Petrol. **69**, 185-192.

Edwards, R.L., & Essene, E.J., 1988. Pressure, temperature and C-O-H fluid fugacities across the amphibolite-granulite transition, northwest Adirondack Mountains, New York. J. Petrol. **29**, 39-72.

Ellis, D.E., 1978. Stability and phase equilibria of chloride and carbonate scapolite at 750°C and 4000 bars. Geochim. Cosmochim. Acta **42**, 1271-1281.

Ellis, D.J., & Green, D.H., 1979. An experimental study of the effect of Ca upon garnet-clinopyroxene Fe-Mg exchange equilibria. Contrib. Mineral. Petrol. **71**, 13-22.

Eskola, P., 1939. Die metamorphen Gesteine, "Die Entstehung der Gesteine" (Barth TFW, Correns TW, Eskola P) 263-407, Springer, Berlin.

Essene, E.J., (1988). The current status of thermobarometry in metamorphic rocks. In: Daly, S. (ed.), The Evolution of Metamorphic Belts, Spec. Pub. Geol. Soc., in press.

Eugster, H.P., 1977. Compositions and thermodynamics of metamorphic solutions. In: Fraser, D.G. (ed.), Thermodynamics in Geology, Reidel, Dordrecht-Holland, 183-202.

French, B.M., 1966. Some geological implications of equilibrium between graphite and a C-H-O gas phase at high temperatures and pressures. Rev. Geophys. **4**, 223-253.

Ganguly, J., & Saxena, S.K., 1984. Mixing properties of aluminosilicate garnets: constraints from natural and experimental data, and applications to geothermobarometry. Am. Mineral. **68**, 88-97.

Goldsmith, J.R., & Newton, R.C., 1977. Scapolite-plagioclase stability relations at high pressures and temperatures in the system $NaAlSi_3O_8$-$CaAl_2Si_2O_8$-$CaCO_3$-$CaSO_4$. Am. Mineral. **62**, 1063-1081.

Griffin, W.L., 1972. Formation of eclogites and the coronas in anorthosites, Bergen Arcs, Norway. Geol. Soc. Am. Mem. **135**, 37-63.

Hansen, E.C., Newton, R.C., & Janardhan, A.S. 1984. Fluid inclusions in rocks from the amphibolite-facies gneiss to charnockite progression in southern Karnataka, India: Direct evidence concerning the fluids of granulite metamorphism. J. Meta. Geol. **2**, 249-264.

Hansen, E.C., Janardhan, A.S., Newton, R.C., Prame, W.K.B.N., & Ravindra Kumar, G.R., 1987. Arrested charnockite formation in southern India and Sri Lanka. Contrib. Mineral. Petrol. **96**, 225-244.

Harley, S.L., & Green, D.H., 1982. Garnet-orthopyroxene barometry for granulites and peridotites. Nature **300**, 697-701.

Hietanen, A., 1967. Scapolite in the Belt Series in the St. Joe-Clearwater region, Idaho. Geol. Soc. Amer. Spec. Pap. **86**.

Hoefs, J., Coolen, J.J.M., & Touret, J., 1981. The sulfur and carbon isotope composition of scapolite-rich granulites from southern Tanzania. Contrib. Mineral. Petrol. **78**, 332-336.

Holloway, J.R., 1977. Fugacity and activity of molecular species in supercritical fluids. In: Fraser, D.G. (ed), Thermodynamics in Geology, Reidel, Dordrecht-Holland, 161-181.

Jones, A.P., Smith, J.V., Dawson, J.B., & Hansen, E.C. (1983) Metamorphism, partial melting, and K-metasomatism of garnet-scapolite-kyanite granulite xenoliths from Lashaine, Tanzania. J. Geol. **91**, 143-165.

Kerrick, D.M., & Jacobs, G.K., 1981. A modified Redlich-Kwong equation for H_2O, CO_2, and H_2O-CO_2 mixtures at elevated pressures and temperatures. Am. J. Sci. **281**, 735-767.

von Knorring, O., & Kennedy, W.Q., 1958. The mineral paragenesis and metamorphic status of garnet-hornblende-pyroxene-scapolite gneiss from Ghana (Gold Coast). Min. Mag. **31**. 846-859.

Komada, N., Moecher, D.P., Westrum, E.F., Jr., Hemingway, B.S., Zolotov, M.Yu., Semenov, Y.V., & Khodakovsky, I.L., 1988. Thermodynamics of scapolite. J. Chem. Therm., in submission.

Kumar, G.R.R., & Chacko, T., 1986. Mechanisms of charnockite formation and breakdown in Southern Kerala: implications for the origin of the Southern Indian Granulite Terrain. J. Geol. Soc. Ind. **28**, 277-288.

Kwak, T.A.P., 1977. Scapolite compositional change in a metamorphic gradient and its bearing on the identification of meta-evaporite sequences. Geol. Mag. **114**, 343-354.

Lamb, W,M,, & Valley, J.W., 1985. C-O-H fluid calculations and granulite genesis. In: Tobi AC, Touret J.L.R. (eds.), The Deep Proterozoic Crust in the North Atlantic Provinces, Reidel, 119-131.

Lamb, W.M., Valley, J.W., & Brown, P.E., 1987. Post-metamorphic CO_2-rich fluid inclusions in granulites. Contrib. Mineral. Petrol. **96**, 485-495.

Lovering, J.F., & White, A.R.J., 1964. The significance of primary scapolite in granulitic inclusions from deep-seated pipes. J. Petrol. **5**, 195-218.

Moecher, D.P., Essene, E.J., Anovitz, L.M., 1988. Calculation and application of clinopyroxene-garnet-plagioclase-quartz geobarometers. Contrib. Mineral. Petrol., in press.

Mora, C.I., & Valley, J.W., 1988. Halogen-bearing scapolite and biotite. Am. Mineral., in prep.

Morrison, J., 1988. Stable Isotope Geochemistry of the Marcy Anorthosite Massif, Adirondack Mts., N.Y. Ph.D. Thesis, Univ. Wisconsin.

Mukherjee, A., Bhattacharya, A., & Chakraborty, S.C., 1986. Convergent phase equilibria at the massif anorthosite-granulite interface near Bolangir, Orissa, India and thermal evolution of a part of the Indian Shield. Precambrian Res. (**34**, 69-104.

Newton, R.C., Charlu, T.V., & Kleppa, O.J., 1980. Thermochemistry of the high structural state plagioclases. Geochim. Cosmochim. Acta **44**, 933-941.

Newton, R.C., Smith, J.V., & Windley, B.F., 1980. Carbonic metamorphism, granulites and crustal growth. Nature **288**, 45-49.

Ohmoto, H., & Kerrick, D., 1977. Devolatilization equilibria in graphitic systems. Am J Sci **277**, 1013-1044.

Okrusch, M., Schroder, B., & Schnutgen, A., 1979. Granulite-facies metabasite ejecta in the Laacher See area, Eifel, West Germany. Lithos **12**, 251-270,

Oterdoom, H., & Gunter, W.D., 1983. Activity models for plagioclase and CO_3-scapolites: an analysis of field and laboratory data. Am. J. Sci. **283-A**, 255-282.

Oterdoom, H., & Wenk, H.-R., 1983. Ordering and composition of scapolite: field observations and structural interpretations. Contrib. Mineral. Petrol. **83**, 330-341.

Pattison, D., & Newton, R.C., 1988. Reversed experimental calibration of the garnet-clinopyroxene Fe-Mg exchange thermometer. Contrib. Mineral. Petrol., in press.

Percival, J.A., 1983. High grade metamorphism in the Chapleau-Foleyet area, Ontario. Am. Mineral. **68**, 667-686.

Phillips, G.N., 1980. Water activity changes across an amphibolite-granulite facies transition, Broken Hill, Australia. Contrib. Mineral. Petrol. **75**:377-386.

Robie, R.A., Hemingway, B.S., & Fisher, J.R., 1978. Thermodynamic properties of minerals and related substances at 298.15 K and 1 bar (10^5 pascals) pressure and at higher temperatures. U.S. Geol. Surv. Bull. **1452**, reprinted with correctionss, 1979.

Robie, R.A., & Hemingway, B.S., 1984. Heat capacities and entropies of phlogopite ($KMg_3[AlSi_3O_{10}](OH)_2$) and paragonite ($NaAl_2[AlSi_3O_{10}](OH)_2$) between 5 and 900 K and estimates of the enthalpies and Gibbs free energies of formation. Am. Mineral. **69**, 858-868.

Rollinson, H.R., 1980. Mineral reactions in a granulite facies calc-silicate rock from Scourie. Scott. J. Geol. **16**, 153-164.

Rudnick, R.L., Ashwal, L.D., & Henry, D.J., 1985. Fluid inclusions in high-grade gneisses of the Kapuskasing structural zone, Ontario: metamorphic fluids and uplift/erosion path. Contrib. Mineral. Petrol. **87**, 399-406.

Ryzhenko, B.N., & Volkov, V.P. 1971. Fugacity coefficients of some gases in a broad range of temperatures and pressures. Geochem. Intl. **8**, 468-481.

Santosh, M., 1986. Carbonic metamorphism of charnockites in the southwestern Indian Shield: a fluid inclusion study. Lithos **19**, 1-10.

Schreurs, J., 1984. The amphibolite-granulite facies transition in West Uusimaa, S.W. Finland. A fluid inclusion study. J. Meta. Geol. **2**, 327-341.

Shaw, D.M., 1960.) The geochemistry of scapolite Part I. Previous work and general mineralogy. J. Petrol. **1**, 218-260.

Shmonov, V.M., & Shmulovich, K.I., 1974. Molal volumes and equation of state of CO_2 at temperatures from 100 to 1000°C and pressures from 2000 to 10,000 bars. Doklady Akad. Nauk SSSR **217**, 206-209.

Shmulovich, K.I., & Shmonov, V.M., 1975. Fugacity coefficients for CO_2 from 1.0132 to 10,000 bars and 450 - 1300 K. Geochem. Int. **12**, No. 2, 202-206.

Srikantappa, C., Raith, M., & Ackermand, D., 1985. High-grade regional metamorphism of ultramafic and mafic rocks from the Archaean Sargur Terrane, Karnataka, South India. Precambrian Res. **30**, 189-219.

Stolz, A.J., 1987. Fluid activity in the lower crust and upper mantle: mineralogical evidence bearing on the origin of amphibole and scapolite in ultramafic and mafic granulite xenoliths. Min. Mag. **51**, 719-732.

Subramaniam, A.P., 1956a. Mineralogy and petrology of the Sittampundi Complex, Salem District, Madras State, India. Bull. Geol. Sci. Am. **67**, 317-390.

Subramaniam, A.P., 1956b. Petrology of the anorthosite-gabbro mass at Kadavur, Madras, India. Geol. Mag. **93**, 287-301.

Thomas, C.W., & Nixon, P.H., 1987. Lower crustal granulite xenoliths in carbonatite volcanoes of the Western Rift of East Africa. Min. Mag. **51**, 621-633.

Touret, J., 1971. Le facies granulite en Norwege Meridionale. Lithos **4**, 239-249.

Valley, J.W., Bohlen, S.R., & Essene, E.J., 1978. Comment to Gressens, R.L. 'Evaporites as presursors of massif anorthosite', Geology **6**, 582-583.

Valley, J.W., McLelland, J., Essene, E.J., & Lamb, W., 1983. Metamorphic fluids in the deep crust: evidence from the Adirondacks. Nature **301**, 226-228.

Vanko, D.A., & Bishop, F.C., 1982. Occurrence and origin of marialitc scapolite in the Humboldt Lopolith, N.W. Nevada. Contrib. Mineral. Petrol. **81**, 277-289.

Vry, J., Brown, P.E., Valley, J.W., & Morrison, J., 1988. Constraints on granulite genesis from carbon isotope compositions of cordierite and graphite. Nature **332**, 66–68.

Wells, P.R.A., 1979. Chemical and thermal evolution of Archaean sialic crust, southern West Greenland. J. Petrol. **20**, 187–226.

Wilkinson, J.F.G., 1974. Garnet clinopyroxenite inclusions from diatremes in the Gloucester area, New South Wales, Australia. Contrib. Mineral. Petrol. **46**, 275–299.

CHAPTER V

THE CARBON ISOTOPE SYSTEMATICS OF HIGH-GRADE SCAPOLITE: CONSTRAINTS ON FLUID SOURCES IN GRENVILLE GNEISSES

Introduction

Scapolite is unique among the more common rock-forming silicates because it may contain one or all of the volatile species Cl, CO_2, and SO_2, (marialite: $Na_4Al_3Si_9O_{24}Cl$; meionite: $Ca_4Al_6Si_6O_{24}CO_3$; sulfate meionite: $Ca_4Al_6Si_6O_{24}SO_4$). As such it is potentially a sensor of fluid source and composition in a variety of rocks. Scapolite from the upper amphibolite and granulite facies is typically $Ca_4Al_6Si_6O_{24}CO_3/Ca_4Al_6Si_6O_{24}SO_4$ solid solutions (*e.g.*, von Knorring and Kennedy, 1958; Lovering and White, 1964; Wilkinson, 1974; Coolen, 1980; Devaraju and Coolen, 1983; Srikantappa *et al.*, 1985), whereas those from the greenschist and amphibolite facies are usually $Na_4Al_3Si_9O_{24}Cl/Ca_4Al_6Si_6O_{24}CO_3$ solid solutions (Shaw, 1960; Hietanen, 1967; Kwak, 1977; Vanko and Bishop, 1982; Frank, 1983; Tuisku, 1985; Oliver and Wall, 1987). Many lithologies containing scapolite would not be expected to have significant quantities of pre-metamorphic carbon, sulfur, or chlorine, and therefore fluid interaction or metasomatic introduction of volatile species may often be inferred from the presence of scapolite-bearing rocks. Massive introduction of fluid may be inferred from heavily scapolitized rocks that are virtually monomineralic scapolite rock, or a bimineralic scapolite-diopside or scapolite-biotite skarn. More subtle evidence of fluid interaction is indicated by granulite facies meta-anorthosites, metabasites, calc-silicates, and amphibolites that contain up to 40 modal percent CO_3 and SO_4 scapolite (*e.g.*, Mason, 1969; Coolen, 1980). Alternatively, many occurrences of scapolite are more realistically interpreted

in terms of isochemical metamorphism of an evaporitic protolith, without significant fluid–rock interaction (*e.g.*, Serdyuchenko 1973; Mora and Valley, 1988). Because virtually all scapolite contains some CO_3, carbon isotope analysis may provide evidence of fluid sources and scales of fluid movement involved in the formation of scapolite–bearing rocks. This would be a particularly useful tool in rocks devoid of another carbonate bearing phase. The carbon isotope data may be used in conjunction with oxygen isotope data to provide additional constraints on the amount and extent of fluid–rock interaction. However, there has been only one attempt to constrain fluid sources using scapolite (Hoefs *et al.*, 1981).

The work presented here is a detailed study of the carbon isotope systematics of scapolite from high grade metamorphic settings. Methods for extracting CO_2 from scapolite were evaluated in order to determine the most accurate and efficient means for extraction and analysis. In addition, the fractionation of ^{13}C between coexisting scapolite and calcite ($\Delta^{13}C_{Sc\text{-}Cc}$) was measured in high grade marbles and calc–silicates. Knowledge of the fractionation between scapolite and calcite allows calculation of the fractionation between scapolite and CO_2 ($\Delta^{13}C_{Sc\text{-}CO_2}$), and in turn constrains the isotopic composition of fluid that led to formation of scapolite. These methods are then applied to scapolite–bearing rocks from the Central Gneiss Belt of the Grenville province of southwestern Ontario, Canada, and other localities. In Ontario, carbonate–rich scapolite occurs in a wide variety of rock types and geologic settings, permitting demonstration of the utility of scapolite as a sensor of fluid sources, and isotopic composition.

Experiments on Extraction of CO_2 from Scapolite

Previous study of scapolite carbon isotopes indicated that extraction of CO_2 from scapolite may not be a straightforward procedure (Hoefs *et al.*, 1981). In order to evaluate methods for extraction of CO_2 from scapolite, and to better obtain control on the reaction of scapolite with phosphoric acid, a series of simple experiments were carried out using separates of well characterized scapolite. These

experiments were intended to evaluate the extent of reaction of the carbonate group in scapolite with phosphoric acid as a function of time and temperature. Different methods were used for pretreating the sample in order to remove additional carbon sources such as calcite. Thermal decomposition of scapolite was also evaluated as a means of collecting CO_2.

Hoefs *et al.* (1981) used phosphoric acid methods to extract CO_2 from scapolite in whole-rock, granulite facies gneisses. Two generations of CO_2 were obtained as a function of temperature. A low temperature generation of CO_2 was interpreted to be a result of reaction with phosphoric acid at 25°C with carbonate inclusions that were assumed to be present in the granulites, but not a result of reaction of phosphoric acid with the carbonate group in scapolite. A second generation of CO_2 was obtained by reaction in 200-400°C phosphoric acid, with the CO_2 produced by this reaction being precipitated as $BaCO_3$ in $Ba(OH)_2$ solution, which was then reacted in 25°C phosphoric acid. The second, high temperature, generation was inferred to represent CO_2 obtained from the scapolite. The high temperature fraction of CO_2 was isotopically distinct and lower in $\delta^{13}C$ relative to the low temperature fraction by up to 11.8‰.

Preliminary analysis of scapolite for this study indicated that the high temperatures used by Hoefs *et al.* (1981) may not be necessary to extract CO_2 from scapolite. Two scapolite mineral samples were chosen to serve as controls on the extraction of CO_2 from scapolite, based on availability of adequate material, purity, and chemical composition. The first scapolite is a coarse-grained aggregate of violet scapolite collected at Bolton, Massachusetts, and donated by Dr. C.A. Francis of the Harvard Mineralogical Museum. The other sample is a 0.5 kg single crystal of gray scapolite collected from a giant scapolite crystal near Ganonogue Park, Quebec, by Dr. D.C. Hogarth of the University of Ottawa. The samples were characterized by optical, X-ray diffraction, back-scattered electron imaging, cathodoluminescence, and microprobe methods in order to determine the composition and homogeneity of the scapolite, and the presence of carbonate

minerals which would contaminate the sample. The theoretical yield of CO_2 for calcite is ten times that of the scapolites used here (approximately 10 vs. 1 µmol CO_2/mg mineral, respectively). Therefore, small amounts of carbonate contamination could seriously affect analytical results, particularly if the calcite has an isotopic composition significantly different from the host scapolite. In hand sample the two materials appeared inclusion free. However upon closer inspection the Bolton sample ("BOLT") [$Na_{1.22}Ca_{2.79}K_{0.02}Si_{7.11}Al_{4.89}O_{24.02}Cl_{0.12}(CO_3)_{0.88}$] was found to contain 50 to 100 µm-sized inclusions of calcite intergrown with epidote inclusions, and 10 to 100 µm-wide veins of calcite associated with secondary sericitization along fractures (Fig. 1). The Ganonoque sample ("GAN") [$Na_{0.96}Ca_{2.89}K_{0.03}Si_{7.10}Al_{4.90}O_{23.95}Cl_{0.02}(CO_3)_{0.98}$] contained 50 µm inclusions of calcite with epidote, calcite concentrated along planar brittle fractures, 30 µm to mm-sized flakes of graphite, and various silicate inclusions.

Mineral separates of BOLT and GAN were prepared for extraction experiments by crushing and sieving coarse grains to a size range of 75 to 150 µm, followed by a rinse in distilled water. The samples were then immersed in dilute (1 M) hydrochloric acid solution at 23°C for 10 minutes in order to dissolve any calcite. A thin section of the BOLT sample, containing veins and inclusions of calcite as described above, was immersed half-way in 1M HCl to determine if calcite was leached by such a treatment. Cathodolumiscence showed that the calcite was completely dissolved in the immersed half of the thin section, with a sharp interface at the level where the thin section sat in the acid (Fig. 1). Reaction of scapolite in the dilute hydrochloric acid solution is undetectable for this short reaction time. The polished thin section of the coarse, single scapolite crystal showed no indications of etching or dissolution. Following a second elutriation in distilled water, samples were ground to 45µ in order to increase surface area and facilitate reaction of scapolite with acid. The finely ground scapolite powder was then reacted at 25°C or 75°C with 100% phosphoric acid for varying lengths of time in evacuated sidearm flasks. Yields of CO_2 were measured manometrically for all runs. The results of these experiments are compiled in Tables 1 and 2.

Figure 1. Cathodoluminescence photomicrographs of scapolite BOLT and GAN, showing nature of included calcite (Cc). Field of view 1.35 mm. a: BOLT with calcite-filled fracture and inclusions of calcite around elliptical epidote inclusion (left); b: HOG with ragged vein-filling calcite (yellow) and scattered calcite inclusions (orange); c: BOLT, calcite inclusions along fracture; d: same as c, showing effect of leaching in 1M HCl. Calcite is entirely dissolved in part of thin section that was immersed in acid (black hole at left in d.

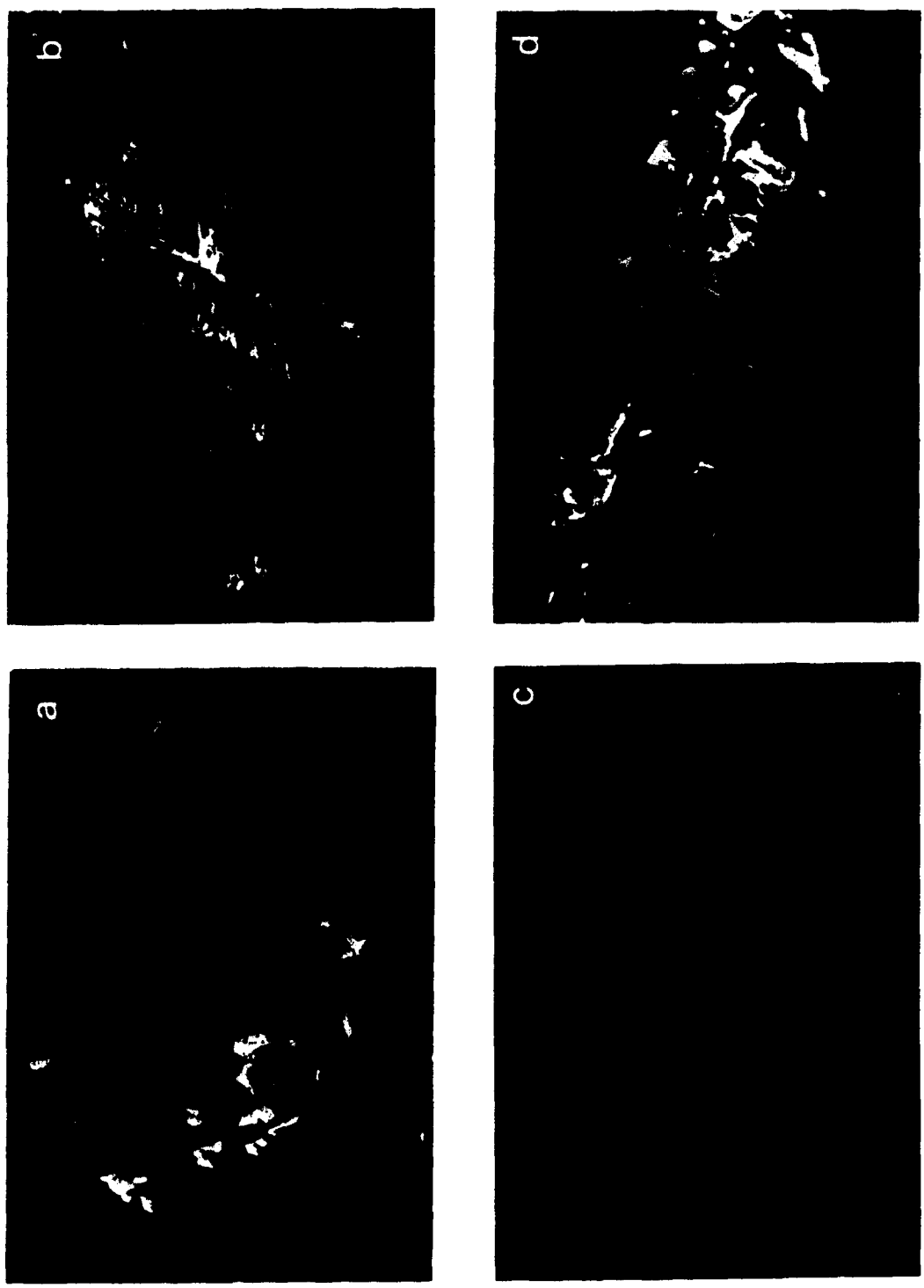
b
d
a
c

TABLE 1: Experimental data for BOLT scapolite mineral separate.

Scapolite leached in 1M HCl at 23°C for 10 minutes and reacted at 75°C in 100% phosphoric acid.

T°C	%Yield	Time hrs	$\delta^{13}C$
25	1	12	-6.80
75	35	4	-6.88
75	56	12	-7.01
75	76	34	-6.97
75	82	59	-7.07
75	86	83	-7.02
75	87	115	-7.01
Average	75°C		-6.99

Scapolite treated same as above but without leaching in HCl.

75	41	13	-7.30
75	65	34	-7.40
75	76	59	-7.37
75	84	83	-7.34
75	82	116	-7.34
Average			-7.35

Scapolite finely ground in air without out acid leaching.

75	47	16	-7.59
75	77	90	-7.51
Average			-7.55

Scapolite leached in HCl, ground in distilled water and thermally decomposed at 1050°C

1050	93	0.5	-7.53
1050	97	0.5	-7.59
1050	92	0.5	-7.69
Average			-7.60

TABLE 2: Experimental data for GAN scapolite mineral separate.

Scapolite leached in 1M HCl at 23°C for 10 mins and reacted at 75°C in 100% phosphoric acid

T°C	%Yield	Time hrs	$\delta^{13}C$
25	9	60	-0.58
75	50	11	-0.47
75	66	18	-0.53
75	40	22	-0.56
75	56	36	-0.58
75	74	41	-0.59
75	84	58	-0.51
75	65	60	-0.56
75	75	82	-0.57
75	81	82	-0.58
75	80	154	-0.54
75	85	203	-0.75
Average	75°C		-0.56

Scapolite leached in 1M HCl, ground in air and thermally decomposed at 1050°C

1050	93		-1.94
1050	91		-1.34

Thermal decomposition of scapolite at 1050°C was evaluated as an alternative method of CO_2 extraction. Measured quantities of the two scapolites with the same grain size and having been leached in dilute hydrochloric acid as above, were finely ground and mixed with CuO in order to prevent reduction of CO_2 to CO during the heating process. Care was taken to hand-pick grains of sample B that were free of visible graphite. The powders were loaded in 1/4"X1" Vycor glass tubes, fused at one end, with a loose plug of silica wool at the other end to prevent sample spillage. Sample tubes were then placed in a 3/4" X 10" quartz tube, evacuated, and heated at 1050°C for 30 minutes. Yields were measured manometrically. Data for the thermal decomposition runs are summarized in Tables 1 and 2.

Results of the extraction experiments on scapolite mineral separates are summarized in Fig. 2, which presents values of $\delta^{13}C$ as a function of extraction method and experimental yield. Reaction of scapolite in 25°C phosphoric acid is sluggish compared to that at 75°C. In 25°C phosphoric acid, 60 hours reaction time was required to obtain approximately 10% of expected CO_2, whereas yields of up to 90% of were obtained in 75°C acid, albeit for longer reaction times. At 75°C yields are higher for longer reaction times and for finer grinding. Values of $\delta^{13}C$ are virtually constant as a function of yield, indicating that the reaction of scapolite in phosphoric acid at 75°C is congruent (Fig. 2). Sharma and Clayton (1965) reached the same conclusion concerning $\delta^{13}C$ and $\delta^{18}O$ for other carbonates that are slow to react at 25°C in phosphoric acid. Values of $\delta^{13}C$ obtained for samples reacted in 25°C acid are virtually identical to those for samples reacted in 75°C acid. If $\delta^{13}C$ at 75°C is taken as the best representation of the carbon isotope composition of scapolite, it is concluded that structural CO_2 is extractable from scapolite at 25°C, although yields are small.

Values of $\delta^{13}C$ for both the BOLT and GAN samples obtained by thermal decomposition are consistently 0.5 to $1\,^{o}/_{oo}$ lower than those reacted in phosphoric acid (Fig. 2). This is also true for a calcite standard analyzed by acid and thermal decomposition methods, however with a less marked effect (Table 3). The lower

Figure 2. $\delta^{13}C$ of scapolites BOLT and GAN as a function of temperature and experimental yield of CO_2 liberated by reaction in phosphoric acid. Data compiled in Table 1. Squares: reaction in 25°C phosphoric acid; circles: reaction in 75°C phosphoric acid; diamonds: thermal decomposition at 1050°C in CuO. For both samples $\delta^{13}C$ remains constant at 25 and 75°C as a function of % yield, indicating the reaction of scapolite in phosphoric acid is congruent, and that complete quantitative yields of CO_2 need not be acquired in order to obtain a precise value for the carbon isotopic composition of scapolite. Lower $\delta^{13}C$ values at high yields is interpreted to be due to contamination by carbonate or reduced carbon for BOLT and by graphite for GAN. Dashed lines are averages for BOLT and GAN.

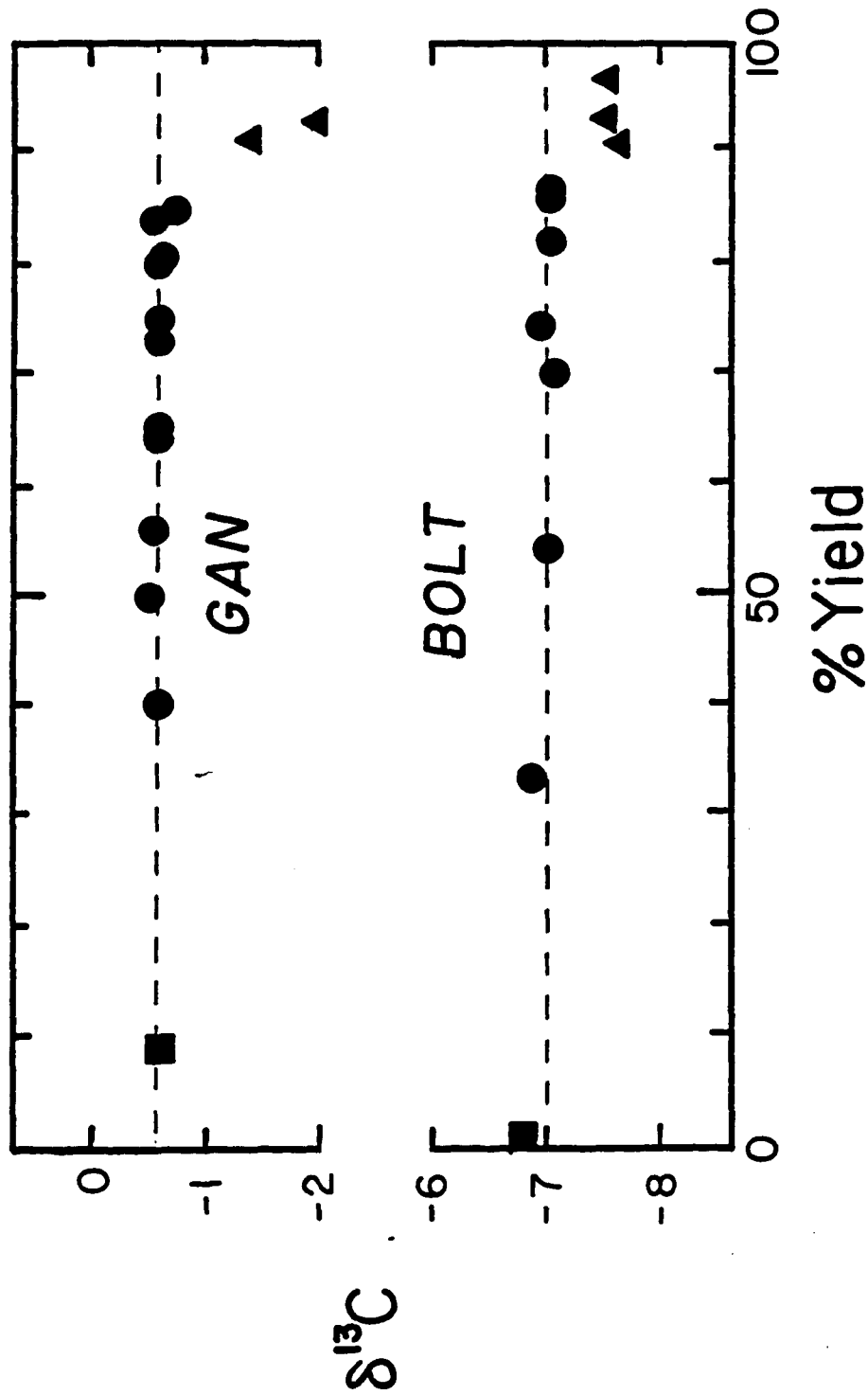
GAN
BOLT
0
-1
-2
-6
-7
-8
0
50
100
% Yield
δ13C

TABLE 3: UW calcite laboratory standard

T°C	%Yield	$\delta^{13}C$ PDB	$\delta^{18}OCO_2$ PDB	$\delta^{18}OCc$ SMOW
Reaction with 100% phosphoric acid				
75	102	-15.95	-3.10	18.98+
75	101	-15.96	-3.13	18.95+
75	100	-15.96	-3.11	18.98+
Average		-15.90	-3.11	18.97
Thermal decomposition				
1050	102	-15.99		na
1050	102	-15.99		na
1050	103	-16.04		na
1050	102	-16.05		na
Average		-15.98		
Reaction with 100% phosphoric acid at 25°C				
25	99	-15.89		18.94
25	99	-15.90		18.99
25	100	-15.88		18.92
25	95	-15.92		19.01
25	98	-15.91		18.91
25	96	-15.96		18.92
25	91	-15.94		18.85
25	96	-15.98		19.07
25	96	-15.99		18.94
25	96	-15.97		18.95
25	95	-15.95		18.94
25	97	-15.96		18.95
Average		-15.93		18.97

na: not applicable due to exchange with CuO.
+: calculated using 75°C acid-Cc fractionation factor derived in text

values may result from graphite contamination (*e.g.*, the GAN sample), however graphite was not evident in all the samples. The discrepancy between combustion and phosphoric acid extractions may be due to contamination by a carbon species with low $\delta^{13}C$, either within the sample and not leachable in dilute hydrochloric acid, from extremely light CO_2 in fluid inclusions, or from CO_2 adsorbed onto the powdered CuO (Hoefs, 1973) and the Vycor reaction tube. The deviation could also be a result of incomplete leaching of extraneous carbonate in the sample preparation. Samples of the BOLT scapolite that were reacted in phosphoric acid, but not leached with dilute hydrochloric acid, have the same lowering of $\delta^{13}C$ relative to the leached samples (Table 1). This isotopic pattern is consistent with the existence of secondary calcite in BOLT and GAN that is considerably lighter than the scapolite, as the secondary calcite comprises a small fraction of each sample. Because of the interference of any extraneous carbon, that is exacerbated by the thermal decomposition method which combusts all carbon species in a sample, the preferred method of CO_2 extraction for this study is reaction in 75°C phosphoric acid as it provides consistent and precise values of $\delta^{13}C$ along with large yields of CO_2 in a reasonable amount of time. Samples in which secondary carbon sources are absent or thoroughly leached from the rock should yield accurate analysis by the combustion extraction method (Hoefs, 1973). Further tests are required in order to constrain the cause of the isotopic discrepancy for the combustion method.

The results summarized in previous paragraphs permit an alternative interpretation to be made based on the data of Hoefs *et al.* (1981) for extraction of CO_2 from scapolite. The low temperature generation of CO_2 that Hoefs *et al.* proposed as being due to carbonate inclusions in the Furua granulites, could alternatively be derived from partial reaction of scapolite in 25°C acid. Alternatively, the low temperature generation could be a mixture of gas derived from the carbonate inclusions or other extraneous carbonate as seen in samples examined for this study, with a $\delta^{13}C$ near $0^{o}/_{oo}$, and the lighter carbon derived from the scapolite structure.

Analytical Methods

In order to extract CO_2 from scapolite in high grade gneisses, whole rock powders (mafic phases removed magnetically) were analyzed. Whole rock samples were utilized because it is extremely difficult to separate scapolite from plagioclase, as the two phases have similar densities and magnetic susceptibilities for the range of compositions studied here. Two size fractions (106 to 150 µm and 150 to 300 µm) from each sample were first treated with dilute hydrochloric acid at 23°C to remove extraneous carbonate. These relatively coarse powders were then ground in air to a 45 to 88µm grain size, and reacted at 75°C in 100% phosphoric acid for at least 48 to 72 hours. Depending on the modal abundance of scapolite present, up to 5 grams of sample were run in this manner.

High grade gneisses may contain significant secondary calcite along grain boundaries and fractures. This carbonate may not be visible under the polarizing microscope, but is very evident under cathodoluminescence (Morrison and Valley, 1988). Inspection of the samples analyzed for this study revealed variable amounts of secondary calcite. Some samples contained no visible evidence of calcite, whereas others contained pervasive grain boundary calcite and calcite-filled brittle fractures (Fig. 3). Mafic phases such as clinopyroxene and garnet typically contain the most calcite, which is concentrated along fractures, in contrast to plagioclase and quartz which contained few unhealed fractures with calcite. All samples were examined optically and by cathodoluminescence to ascertain approximate modal abundances of scapolite and the presence of secondary calcite. As with the scapolite mineral separates, a mafic gneiss with pervasively developed calcite was immersed in 1M HCl for 10 minutes to demonstrate the efficacy of the leaching process (Fig. 3). Also, samples of scapolite-free gneisses with traces of calcite occurring in a similar mode as in scapolite-bearing gneisses were analyzed as blanks to evaluate the HCl leaching process. The calcite-bearing gneisses that served as blanks yielded either no measurable amounts of CO_2 (PS7g) or only small quantities of gas (PS86E-22, 1 µmole CO_2 for three grams of powdered whole rock

Figure 3. Cathodoluminescence evaluation of mafic gneiss 85DMP174-1a. Field of view in all photos is 1.35 mm. a: cathodoluminescence photo of secondary calcite concentrated along fractures in clinopyroxene; b: same area, plane light; c: same sample, different area, with left half of sample leached in 1M HCl. Calcite is dissolved from fractures; d: same area, plane light. Abbreviations: hbl: hornblende; cpx; clinopyroxene; gt: garnet; pg: plagioclase; sc: scapolite.

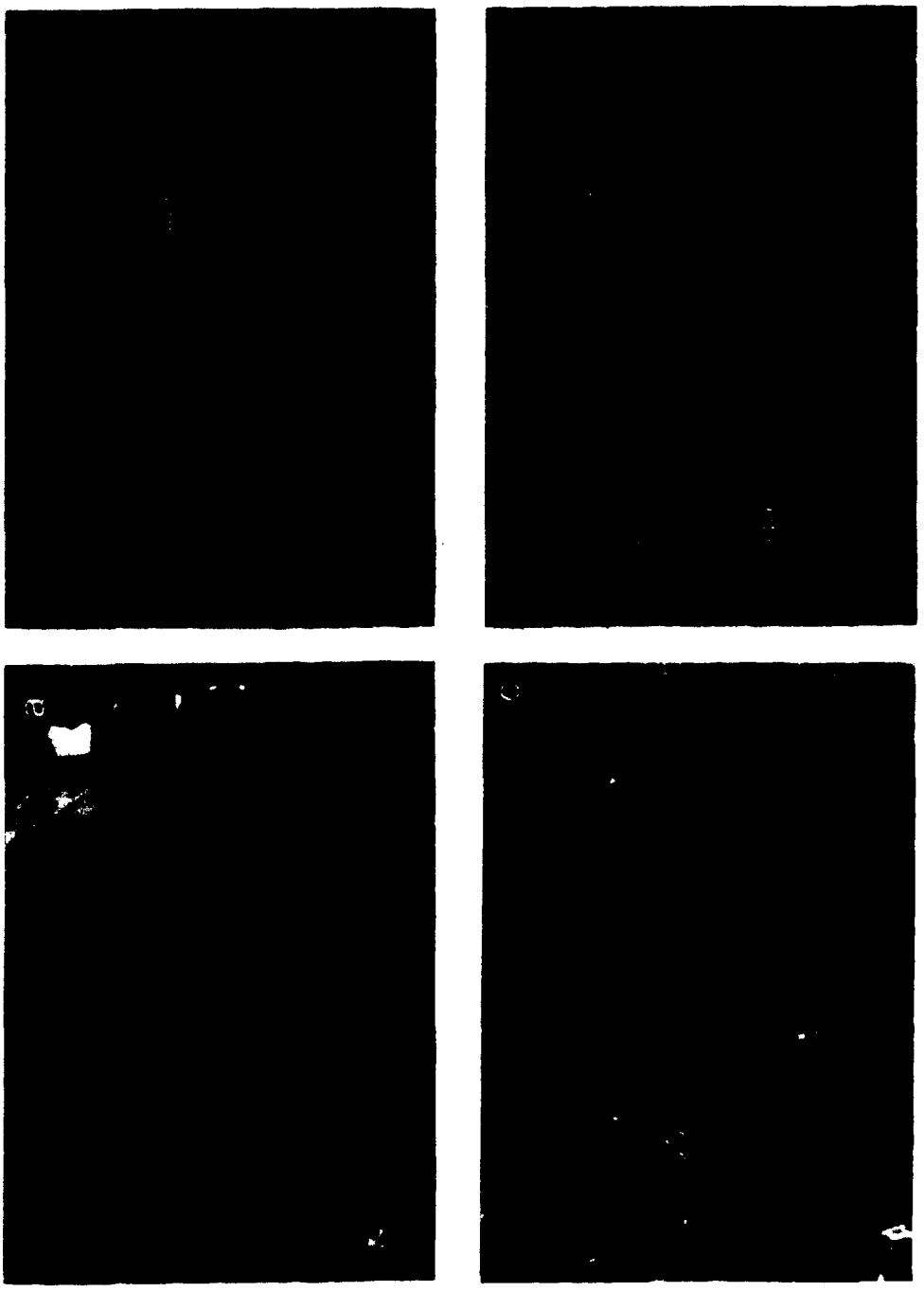

sample). The samples provide a test of the efficacy of hydrochloric acid leaching process, as they initially contained 1 modal % secondary calcite before leaching. The $\delta^{13}C$ value of the latter sample is $-3.3^{o}/_{oo}$, identical to values from nearby lithologies with similar occurrences of calcite (see discussion on meta-anorthosite to follow).

Oxygen was extracted from some whole rock samples and converted to CO_2 for isotopic analysis using the method of Clayton and Mayeda (1963). Analyses of the NBS 28 quartz standard in the University of Wisconsin isotope laboratory average $9.5^{o}/_{oo}$. Calcite was analyzed according to the method of McCrea (1950).

Isotopic analysis of CO_2 was performed on a Finnigan/MAT 251, dual inlet, triple collector mass spectrometer at the University of Wisconsin-Madison. Values of $\delta^{13}C$ and $\delta^{18}O$ are reported in the standard per mil notation relative to PDB (carbon) and SMOW (oxygen). Analytical precision for a clean sample of CO_2 and standard gases is typically $0.01^{o}/_{oo}$ for carbon and on the order of $0.1^{o}/_{oo}$ for oxygen. However, reproducibility of $\delta^{13}C$ is highly variable for scapolite-bearing whole rock samples. Scapolite mineral separates that yield relatively large volumes of CO_2 (>100 µmoles) are reproducible to $0.1^{o}/_{oo}$. Reaction of whole rock samples with only traces of scapolite often yields smaller volumes of CO_2 (< 10 µmoles) and poorer reproducibility (+/- $0.5^{o}/_{oo}$). Scapolite with high Cl and SO_4 contents (> 10 mol% in the anion site) typically yield extraneous gas species (HCl and SO_2) that can also lower the reproducibility of a given measurement, and cause systematic lowering of $\delta^{13}C$ by up to $10^{o}/_{oo}$.

Acid extraction of SO_4- and Cl-bearing scapolites yields SO_2 and HCl, which have serious effects on the mass spectrometric analyses, causing systematic errors in $\delta^{13}C$. For example, scapolite with approximately 10% or greater of Cl in the anion site would cause machine errors manifested by drifting sample voltage, and 45/44 mass ratios that systematically increase during the analysis, yielding values that are clearly too high. Routine microprobe analysis of all scapolites for isotopic work

allowed identification of samples for which this may be a problem, and these samples were not analyzed. Gases collected from reaction of SO_4-bearing scapolites in 75°C phosphoric acid were scrubbed of SO_2 by successive distillations in a n-pentane slush. Mass spectrometer scans indicated that significant quantities of SO_2 can be removed in this manner, yielding clean CO_2. Treatment of CO_2 collected from a calcite standard with the n-pentane slush indicated no fractionation by this distillation. Isotopic analysis of chlorine-rich scapolite using phosphoric acid extraction will require an additional scrubbing step to remove HCl.

Fractionation of ^{13}C Between Scapolite and Calcite

The fractionation of ^{13}C between scapolite and calcite was determined by analyzing the isotopic composition of coexisting scapolite and calcite from high grade marbles, calc-silicates, and skarns. Knowledge of $\Delta^{13}C_{Sc\text{-}Cc}$ allows calculation of $\Delta^{13}C_{Sc\text{-}CO_2}$, which constrains the isotopic composition of any fluids.

Based on crystal chemical parameters and fractionations among simple carbonates, one may predict the equilibrium fractionation of ^{13}C befween scapolite and calcite. Table 4 lists coordination numbers (CN), densities, and average M-O bond distances between oxygen atoms in the carbonate group (O) and the cations (M) to which oxygen is coordinated for calcite and aragonite (M = Ca), dolomite (M = Ca and Mg), and a scapolite with the composition Me_{84} (M = 84% Ca, 16% Na; Aitken *et al.* 1984). The average M-O bond distance for dolomite is less than that for calcite, and the $\Delta^{13}C_{Do\text{-}Cc}$ is 2.1 at 25°C and approximately $0.5‰$ at T > 600°C (Sheppard and Schwarcz, 1970). The average M-O bond length in aragonite is greater than in calcite, but the coordination number and density are higher in aragonite. The fractionation between aragonite and calcite is less than that of dolomite-calcite at 25°C. Estimates of $\Delta^{13}C_{Arag\text{-}Cc}$ range from 0.8 (Sommer and Rye, 1978) to 1.8 $‰$ (Rubinson and Clayton, 1969). The crystal chemical environment of CO_3 in scapolite is more similar to aragonite than calcite, and one might predict that the fractionation of ^{13}C between scapolite and calcite would be similar to that

TABLE 4: Crystal chemical parameters and ^{13}C fractionations between calcite and aragonite, dolomite, and scapolite.

	Mean M-O A	CN	ref.	$\Delta^{13}C$* 25°C	$\Delta^{13}C$* 700°C	ref.	Density g/cm3	ref
Calcite	2.36	6	1	0	0	-	2.712	6
Aragonite	2.53	9	2	0.8-1.8	na	-	2.930	6
Dolomite	Ca Mg 2.38 2.08	6	1	2.1	0.5	4	2.866	6
Scapolite**	2.47	8	3	-	0.5	5	2.740	3

CN: coordination number;
1: Markgraf and Reeder (1985); 2: de Villiers (1971);
3: Aitken et al. (1984); 4: Sheppard and Schwarcz (1970)
5: this study; 6: Robie et al. (1966).
*: $\Delta^{13}C$ between calcite and mineral at quoted T.
**: Me_{84}

TABLE 5: Data relevant to calculation of ^{13}C fractionation between scapolite and calcite from calc-silicates, marbles, and skarns. All samples are from this study except UK-1 and X27 (D. Mogk, pers. comm. 1987).

SAMPLE	Lith.	X_{Ca} Sc	X_{CO_3} Sc	$\delta^{13}C$ Sc	$\delta^{18}O$ Sc*	$\delta^{13}C$ Cc	$\delta^{18}O$ Cc	$\Delta^{13}C$
A85A-1	M	0.70	0.80	-4.0	9.1	-6.6	9.1	2.6
A85A-3c	CS	0.79	0.98	-8.7	11.9	-8.2	12.8	-0.5
A86B3-5	CS	na	na	-9.5	11.8	-9.9	12.2	0.4
H40d	CS	0.76	0.94	-3.7	11.2	-3.1	11.4	-0.6
M3.14D	SK	0.66	0.85	-8.1	12.3	-8.2	11.8	0.1
M86E-1C-2	CS	0.60	0.87	-1.9	15.4	-3.7	15.1	1.8
O8e	CS	0.74	0.91	-2.6	11.3	-2.2	11.8	-0.4
PSO85A-5	MA	0.73	0.90	-0.2	8.9	-1.3	15.1	1.1
PS85A-7	M	0.78	0.96	0.7	15.3	-0.7	15.6	1.4
S4d	SK	0.65	0.86	1.7	20.5	1.4	20.9	0.3
S86E-8c	M	0.69	0.90	0.9	15.4	-0.6	15.9	1.5
S86E-27B	M	0.76	0.93	0.1	17.6	-0.1	17.6	0.2
UK-1	M	0.78	0.98	-1.1	18.9	-1.4	21.1	0.3
X27	M	0.76	0.95	-1.5	15.3	-1.4	17.5	-0.1
82DMT114a	CS	0.79	0.98	-7.9	10.0	-8.1	10.5	0.2
Additional data on scapolite from high-grade calc-silicates in Ontario.								
A85A-3d	CS	0.75	0.95	-10.1	12.0			
H85A-1d	CS	0.81	0.98	-9.0	5.2			
M3.14b	SK	0.68	0.82	0.3	16.2			
82DMT114d	CS	na	na	-8.4	9.9			

M: marble; CS: calc-silicate; SK: skarn; MA: meta-anorthosite

*: see text for assumptions concerning calculation of $\delta^{18}O_{SMOW}$ for scapolite.

for aragonite–calcite. The average $\Delta^{13}C_{Sc\text{-}Cc}$ for 15 scapolite–calcite pairs (Table 5) is $+0.5\pm0.9‰$ (1σ), consistent with a small fractionation.

As Na substitutes for Ca in the scapolite structure the density of the scapolite changes (Shaw, 1960), so that $\Delta^{13}C_{Sc\text{-}Cc}$ may be compositionally dependent. Sodic scapolite is less dense than calcic scapolite, and one would predict that scapolite of composition Me_{90} (density closer to calcite) would yield higher $\delta^{13}C$ than Me_{70} for a given calcite composition, and a $\Delta^{13}C_{Sc\text{-}Cc}$ closer to zero than Me_{70}–calcite, which should be slightly negative. The spread of values obtained for $\Delta^{13}C_{Sc\text{-}Cc}$ may be due in part to this compositional dependence, as the more sodic and chlorine–rich scapolites tend to yield the greatest fractionation (Table 4). However, the shift in $\delta^{13}C$ is opposite to that expected from density considerations, with sodic scapolites yielding more *positive* values of $\Delta^{13}C_{Sc\text{-}Cc}$. The relative increase in $\delta^{13}C$ of these sodic, chlorine–bearing scapolites may instead be an artifact of the contamination by HCl gas, which produces erroneously high values of $\delta^{13}C$. Disregarding samples with $X_{Cl} > 0.10$, in which $\delta^{13}C_{Scap}$ is often systematically in error, the fractionation reduces to $+0.1\pm0.6‰$. This value is within the analytical precision of many of the analyses performed on scapolite gneisses. Primarily carbonate–rich scapolites will be analyzed for this study, and therefore the latter fractionation is taken as the most appropriate value. For practical purposes the average value of $\Delta^{13}C_{Sc\text{-}Cc}$ will be taken as $0‰$, with the understanding that there is a considerable range in the observed values. Based on this value and $\Delta^{13}C_{Cc\text{-}CO_2} = -2.5‰$ (Friedman & O'Neil, 1977), $\Delta^{13}C_{Sc\text{-}CO_2}$ is approximately $-2.5‰$ in the temperature range 600 to 800°C. Although the equilibrium fractionation of ^{13}C is small, the secondary carbonate common in many rocks may be much lower in $\delta^{13}C$ than the primary scapolite. The experimental data on unleached samples of the BOLT scapolite (Table 1) are consistent with this interpretation, as they yield slightly lighter values than leached samples.

Hoering and Hart (1964) analyzed coexisting scapolite–graphite ($\Delta^{13}C_{Sc\text{-}Gr} = 5.5‰$) and calcite–graphite ($\Delta^{13}C_{Cc\text{-}Gr} = 2.2‰$) pairs from two samples of marble

metamorphosed to approximately 750°C in the Adirondack Mts., New York. Coexisting scapolite and calcite samples were not analyzed. From these latter fractionations they calculated $\Delta^{13}C_{Sc\text{-}Cc} = +3.3^{o}/_{oo}$, higher than any of the $\Delta^{13}C_{Sc\text{-}Cc}$ values measured for this study. We have also analyzed a number of scapolite–calcite pairs from Adirondack marbles, but the scapolite in these samples is Na and Cl–rich, and not amenable to accurate or reliable analysis until the problem with HCl gas contamination is resolved.

Oxygen Isotope Composition of CO_3 in Scapolite

The fractionation of ^{18}O between the framework and carbonate oxygen in scapolite is a potential single mineral geothermometer. Precise estimates of the oxygen isotope composition of the carbonate group extracted from scapolite ($\delta^{18}O^{Scap}_{CO_3}$) cannot be made because the fractionation factor between CO_2 liberated from the reaction between phosphoric acid and scapolite is not known. However, by assuming that the acid fractionation factor ($\alpha_{Cc\text{-}acid}$) is the same for calcite and scapolite one can obtain *approximate* values for $\delta^{18}O^{Scap}_{CO_3}$ that can be used on a comparative basis. Sharma and Clayton (1965) showed that this not a valid assumption in precise work for other carbonates, however considerably more work would be required to determine a precise value following the method of Sharma and Clayton (1965), as scapolite has both framework *and* carbonate oxygen. One could combust the scapolite *in vacuuo* in the absence of CuO, and compare these $\delta^{18}O^{Scap}_{CO_3}$ values with those obtained in 25°C phosphoric acid. However, reduction of CO_2 to CO and exchange between the carbonate and framework oxygens during the combustion may occur. Most of the scapolite samples were reacted in 75°C acid, and therefore $\alpha_{acid\text{-}Cc}$ needs to be known at 75°C. The average $\delta^{18}O_{PDB}$ for CO_2 liberated from the UW calcite laboratory standard at 75°C is −3.11 (Table 3). The fractionation factor at 75°C can be calculated from the relation

$$[\delta^{18}O^{Cc}_{PDB} + 1000]/[\delta^{18}O^{CO_2}_{PDB} + 1000] = \alpha_{Cc\text{-}acid,75^{o}}$$

where $\delta^{18}O^{Cc}_{PDB}$ is of $\delta^{18}O$ for calcite at 25°C relative to the PDB standard. By convention, this considered the standard oxygen isotope composition of calcite. The relation yields $\alpha_{Cc\text{-}acid,75^{o}}$ of 1.00825. This value was used in calculation of $\delta^{18}O^{Sc}_{PDB}$ for scapolites analyzed in Tables 5, 6 and 9, from which values were converted to $\delta^{18}O^{Sc}_{SMOW}$ for the carbonate group in scapolite. The BOLT scapolite sample consistently yields a $\delta^{18}O^{Sc}_{SMOW}$ = 11.6°/$_{oo}$ for the carbonate oxygen when reacted at 75°C in phosphoric acid. A whole mineral oxygen isotope composition of 11.0 °/$_{oo}$ (10.9 when corrected for the fraction of the heavier carbonate oxygen present) was obtained from oxygen extracted by BrF_5 methods, is consistent with a small, positive fractionation of ^{18}O between the carbonate group and framework oxygen for this sample. In scapolite gneisses the carbonate oxygen is consistently enriched in ^{18}O relative to whole rock oxygen (see following section). For the scapolite–calcite samples in Table 5, the scapolite oxygen is the same as or slightly lighter than that in the coexisting calcite, consistent with variable exchange of the carbonate oxygen of scapolite with the framework silicate oxygen upon formation of scapolite from plagioclase and calcite.

Isotopic Analysis of Scapolite Gneisses

Samples of scapolite-bearing gneisses were collected from a variety of localities in the Central Gneiss Belt (CGB) of the southwestern Grenville Province, Ontario, Canada (Fig. 4). Sampling throughout the region allowed delineation of localities and lithologies likely to contain scapolite. A variety of lithologies were found to contain scapolite, and some of these units were sampled on a more detailed scale (Figs. 5, 6, and 7). The tectonic setting of the southwestern Grenville Province is described in Davidson (1984a, 1984b, 1986) and Davidson *et al.* (1979, 1982). Briefly, the region consists of discrete lithotectonic domains separated by km-wide zones of high strain and ductile shearing (Fig. 4). Metamorphic grade is consistent throughout a given domain, but the grade and the dominant lithologies may vary from one domain to another. For example, the Parry Sound Domain, consisting of granulite facies mafic orthogneisses, marble and amphibolite, tectonically overlies

Figure 4. Index map for scapolite–bearing gneisses and associated marbles in southwestern Grenville Province of Ontario, showing boundaries between regard to lithotectonic domains mapped by Davidson et al. (1979, 1982) (inset 1). Boxes 2 and 3 outline Whitestone Anorthosite (shaded) detailed in following figures.

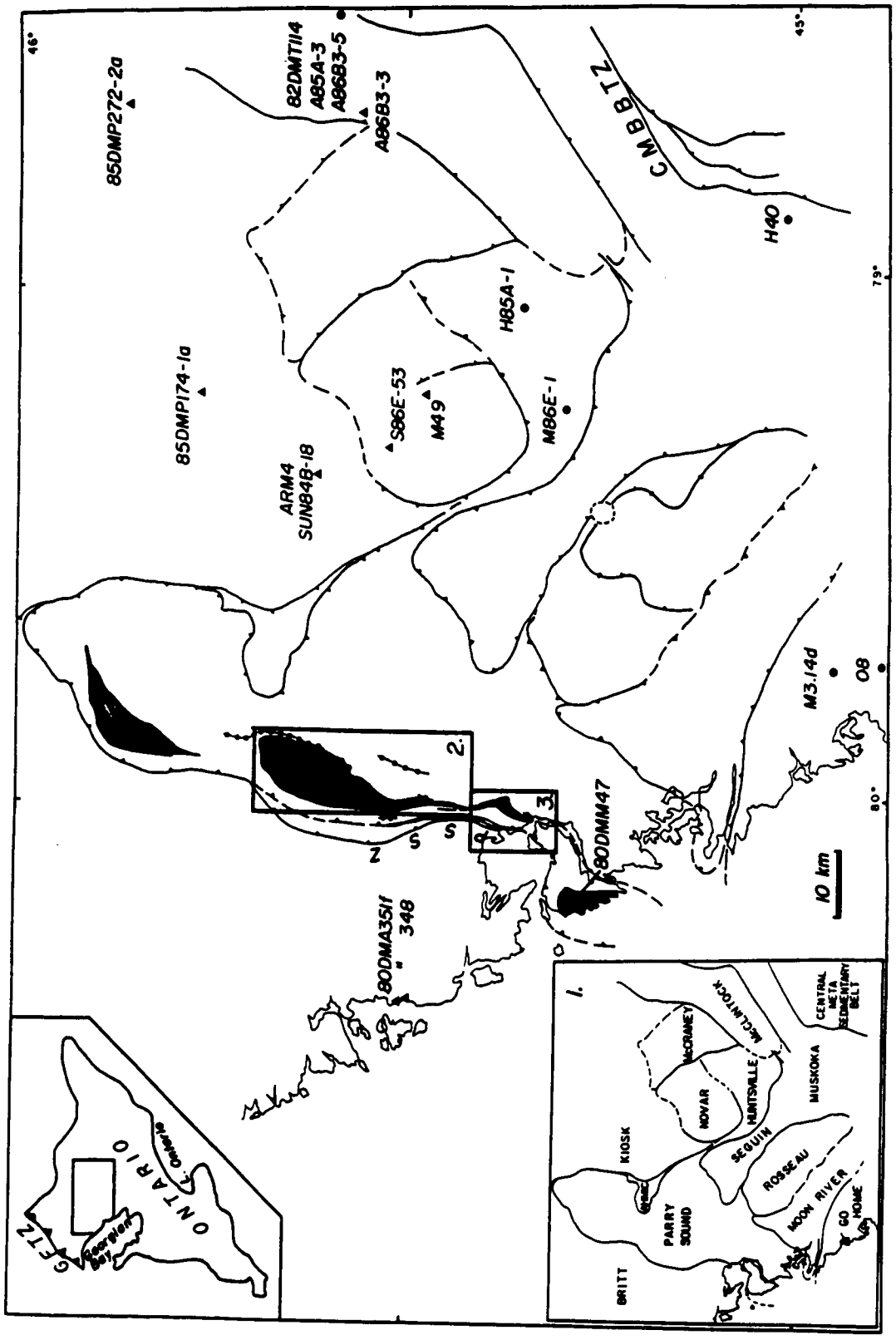
46°
45°
79°
80°
85DMP272-2a
82DMT114
A85A-3
A8683-5
A8683-3
85DMP174-1a
ARM4
SUN848-18
S86E-53
M49
H85A-1
M86E-1
CMBBTZ
H40
M3.14d
08
80DMM47
80DMA351
348
2.
3.
N
S
S
10 km
ONTARIO
Ontario
Georgian Bay
1.
BRITT
PARRY SOUND
KIOSK
NOVAR
McCRAMEY
HUNTSVILLE
SEGUIN
ROSSEAU
MOON RIVER
GO HOME
MUSKOKA
KOOTENAY
CENTRAL META SEDIMENTARY BELT

Figure 5. Disposition of samples within and around main body of WSA. East margin of Whitestone Anorthosite is detailed in Fig. 6.

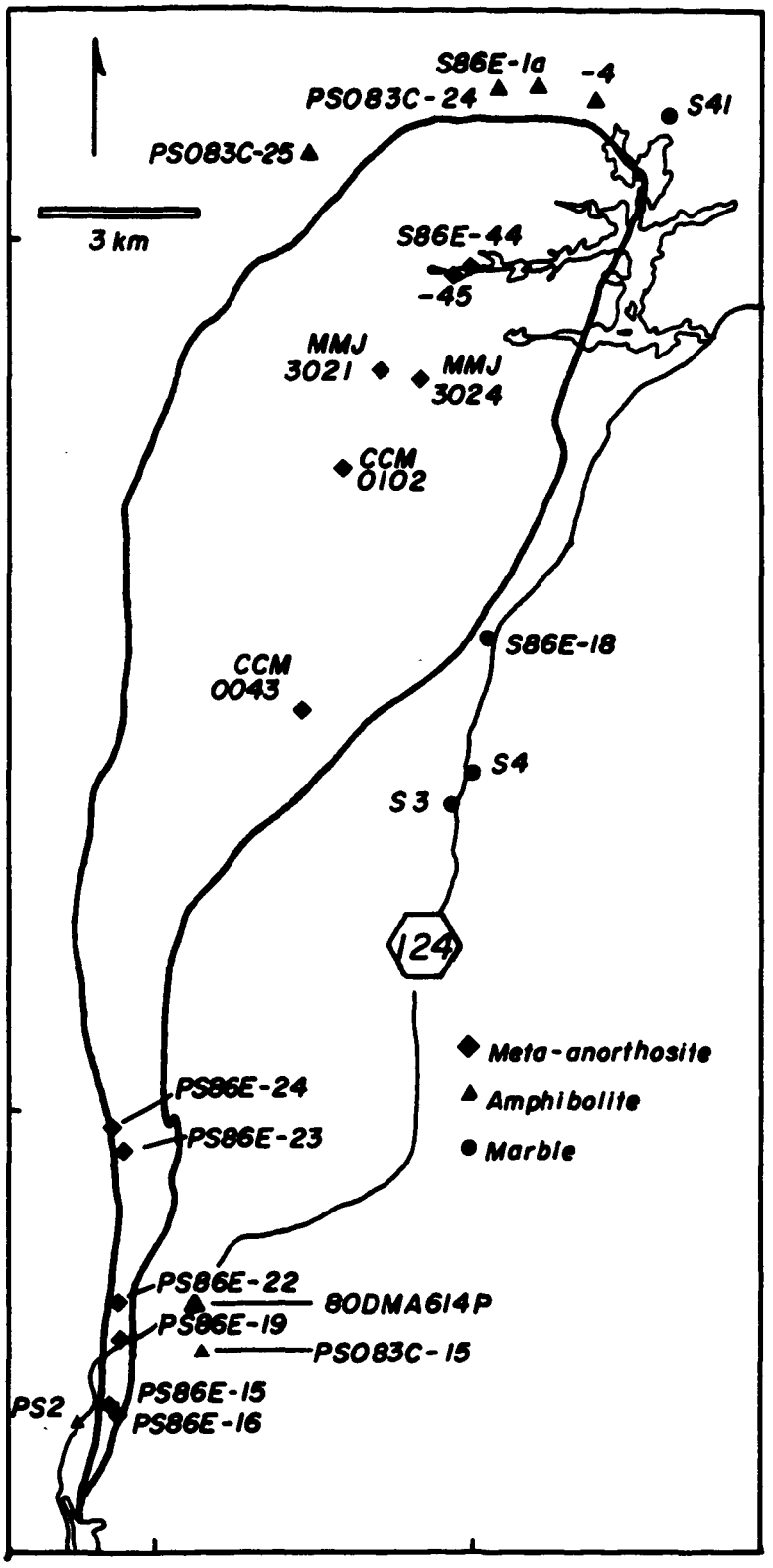
S86E-1a
-4
PS083C-24
S41
PS083C-25
3 km
S86E-44
-45
MMJ
3021
MMJ
3024
CCM
0102
S86E-18
CCM
0043
S4
S3
124
Meta-anorthosite
Amphibolite
Marble
PS86E-24
PS86E-23
PS86E-22
80DMA614P
PS86E-19
PS083C-15
PS86E-15
PS2
PS86E-16

Figure 6. Detail of east margin of WSA adjacent to marble breccia in vicinity of Whitestone Lake.

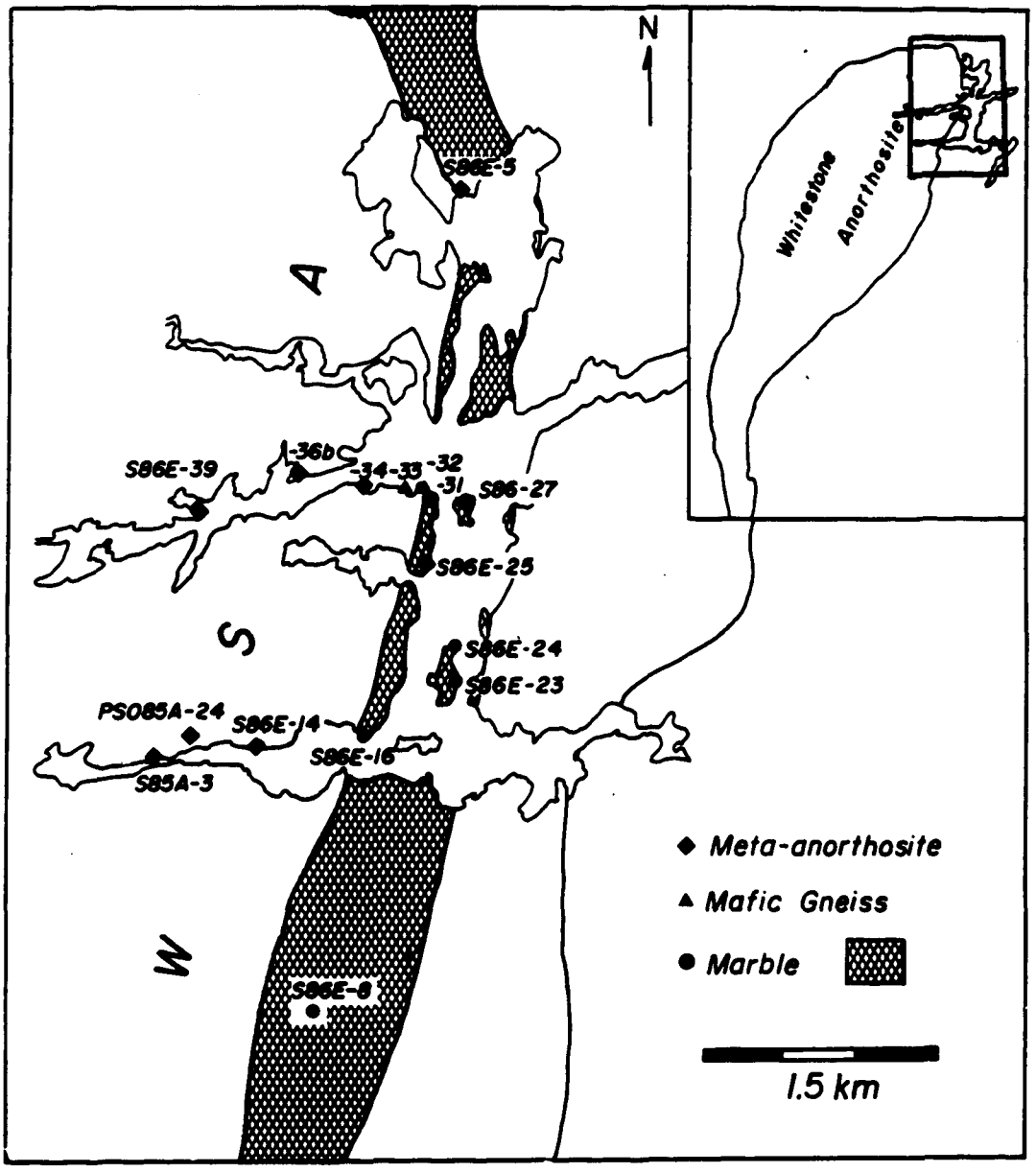
N
Whitestone
Anorthosite
S86E-5
S86E-39
-36b
-34
-33
-32
-31
S86-27
S86E-25
S86E-24
S86E-23
PS085A-24
S86E-14
S86E-16
S85A-3
S86E-8
Meta-anorthosite
Mafic Gneiss
Marble
1.5 km

Figure 7. Sample localities in vicinity of southern extension of WSA and Parry Sound Shear Zone. PS = town of Parry Sound. Shaded: sheared WSA.

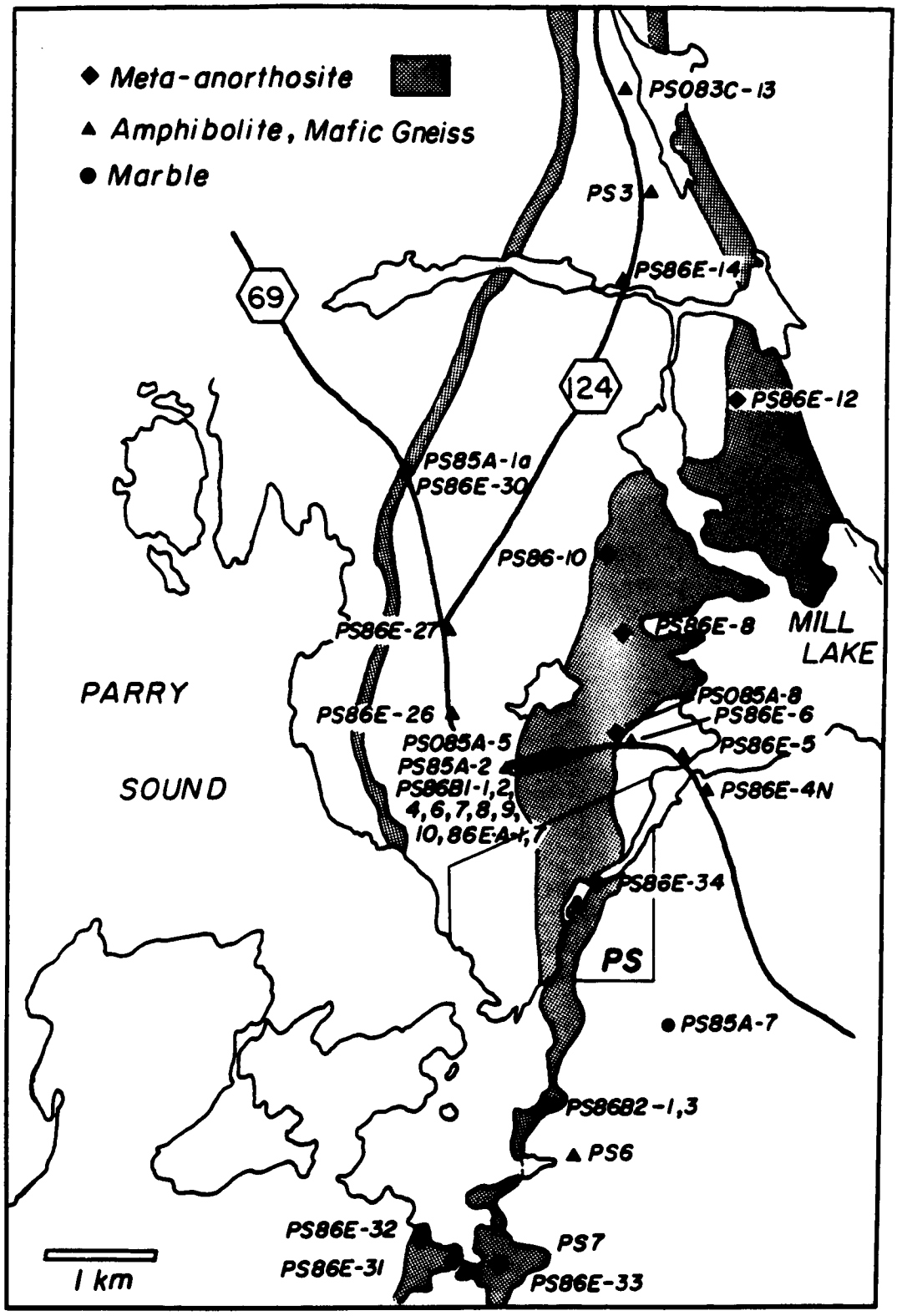
◆ Meta-anorthosite
▲ Amphibolite, Mafic Gneiss
● Marble
PS083C-13
PS3
PS86E-14
69
124
PS86E-12
PS85A-1a
PS86E-30
PS86-10
PS86E-27
PS86E-8
MILL LAKE
PARRY SOUND
PS085A-8
PS86E-6
PS86E-26
PS085A-5
PS86E-5
PS85A-2
PS8681-1,2,4,6,7,8,9,10,86E-A-1,7
PS86E-4N
PS86E-34
PS
PS85A-7
PS8682-1,3
PS6
PS86E-32
PS7
PS86E-31
PS86E-33
1 km

the Britt Domain which consists dominantly of upper amphibolite facies granitic to mafic orthogneisses and pelitic paragneisses. The Moon River Domain is dominantly composed of migmatitic paragneiss juxtaposed against the Parry Sound Domain. Thermobarometric studies indicate that a large part of the CGB of Ontario has experienced metamorphic pressures of at least 10 kbar (Anovitz and Essene, 1988), making it one of the largest known tracts of exposed deep crust in the world.

Shieh and Schwarcz (1974) analyzed orthogneisses, paragneisses, and migmatites collected along a 200 mile traverse across the CGB, from the Grenville Front Tectonic Zone to the Central Metasedimentary Belt. At the time of their study many of the lithologies they studied were interpreted to be migmatitic gneisses. The small range in $\delta^{18}O$ they obtained for this large expanse of high grade rocks (80% of their samples were within the range 6.5 to 8.4$^{o}/_{oo}$ was interpreted to be due to pervasive exchange on a regional scale with a mafic or ultramafic reservoir via a water rich pore fluid. This process was interpreted to be aided by widespread anatexis. Recently, Wu and Kerrich (1986) performed an extensive isotopic and geochemical study of Grenville granitoid plutons, including two from the CGB. They corroborated the limited range of values observed by Shieh and Schwarcz (1974). However, Wu and Kerrich (1986) concluded that the meta-plutonic rocks retained their primary igneous oxygen isotopic signatures, and that open system exchange with a fluid phase was limited.

Calc-silicate Gneisses

In the southwestern Grenville Province calcic scapolite commonly occurs in calc-silicate gneisses, marbles or skarns with quartz, calcite, calcic plagioclase, grossular/andradite garnet, wollastonite, epidote, and salitic/hedenbergitic clinopyroxene. The calc-silicate gneisses themselves usually occur as conformable layers and lenses within upper amphibolite to granulite facies granitic, pelitic, and mafic gneisses. Scapolite and calcite also coexist with the above phases in meta-anorthosite. Samples for this study were collected from the CGB of Ontario, and

represent diverse localities and settings. Because calc-silicates are likely to contain significant quantities of pre-metamorphic carbon within calcite, isotopic analysis of carbon in calc-silicates would likely provide constraints on prograde metamorphic volatilization processes rather than on external carbon sources. However, characterization of the carbon isotopic composition of calcite and scapolite in calc-silicates is necessary to constrain the characteristic carbon isotopic signature of calc-silicates as they may be sources of CO_2 in high grade terranes (*e.g.*, Glassley, 1983; Kumar and Chacko, 1985), and to determine how well scapolite records the carbon isotopic composition of rocks in which it forms.

Scapolite in calc-silicates, marbles, and skarns ranges widely in $\delta^{13}C$ and $\delta^{18}O$ (+1.7 to $-10.1^{o}/_{oo}$, Table 5), and $\delta^{13}C$ are generally very similar to those of the coexisting calcite (see previous section on $\Delta^{13}C_{Sc\text{-}Cc}$). Therefore, scapolite is providing a precise record of the isotopic composition of its host lithology, nearly as precisely as calcite. The range of isotopic values for scapolite and calcite in the calc-silicates may be a manifestation of several processes. Many of the samples in Table 5 have $\delta^{13}C$ and $\delta^{18}O$ characteristic of typical Grenville marbles and calc-silicates, which were interpreted to be indiscernible from primary sedimentary isotopic signatures (Valley and O'Neil, 1984). Therefore, the range of values could be an original bulk chemical effect. For calc-silicate samples that presently lack calcite or graphite and have relatively low $\delta^{13}C$ (*e.g.*, A85A-3d ($-10.1^{o}/_{oo}$), H85A-1d ($-9.0^{o}/_{oo}$), 82DMT114d ($-8.4^{o}/_{oo}$); samples that were likely to have contained calcite at lower grades that was consumed in scapolite or grossular-forming reactions) the ^{13}C depletion may be interpreted in terms of a Rayleigh distillation process whereby CO_2 evolved during prograde metamorphism left an isotopically light carbon residue that was incorporated in scapolite at high grades. These same samples also have very low $\delta^{18}O$ values for calc-silicates (12.0, 5.2, 9.9, respectively), consistent with a Rayleigh process. Alternatively, the pattern could result from varying degrees of interaction with a low ^{18}O, H_2O-rich fluid, the influx of which drove decarbonation reactions to completion, yielding an isotopically light carbon residue which was incorporated into scapolite when the latter formed at high grades. The wide

distribution of the samples precludes any detailed analysis of such processes until more detailed and extensive sampling is performed for each locality. An important feature to note from the scapolite data is the heterogeneity of the values, consistent with the lack of regional exchange of a single pervasive and isotopically homogeneous fluid. A second feature of the $\delta^{13}C$ values for scapolite is the of the range of low values of $\delta^{13}C$ (down to -10.1). If the carbonate group of calcite was incorporated directly into scapolite from calcite or CO_2 without an intervening process such as decarbonation, the range of scapolite $\delta^{13}C$ would be expected to overlap with the range of $\delta^{13}C$ observed in carbonates from Grenville marbles (-7.2 to 5.6$^{o}/_{oo}$: Valley, 1986). The observation that the scapolites measured so far are depleted in ^{13}C is consistent with a relatively complex history leading to the formation of scapolite in calc-silicates.

Meta-anorthosite

Carbonate scapolite occurs throughout the Whitestone Anorthosite (WSA), a 170 km^2 gabbroic-anorthosite body found along the western margin of the Parry Sound Domain in the CGB of Ontario (Mason, 1969; Thompson, 1983; Davidson *et al.* 1982; Nadeau 1983) (Fig. 4 through 7). Scapolite is particularly well developed around the margins of the WSA where the anorthosite is in contact with garnet$\pm$clinopyroxene amphibolite along the west, and marble tectonite breccia, a melange of mafic clasts and boudins entrained within a Cc-Cpx-Hbl$\pm$Ol$\pm$Do marble, along its east margin (Mason, 1969; Mummery, 1973; Thompson, 1983). Meta-diorite and mafic granulites occur immediately east of the marble breccia. Mason (1969) delineated a modal increase in scapolite and hornblende from the center of the WSA outward, accompanied by an increase in modal garnet toward the east and north margin, and an increase in modal epidote at the general exclusion of garnet along the west margin. These mineralogic variations exhibit a roughly concentric pattern around the core of the WSA. The WSA provides an opportunity to test the utility of scapolite in sensing fluid sources in a controlled geologic setting where there exists a known source of carbon in the marble breccia. Scapolite is also

found within southern extensions of the WSA where the WSA is cut by the Parry Sound Shear Zone (PSSZ), a high grade ductile shear zone that separates granulite facies rocks of the Parry Sound Domain on the east from upper amphibolite facies assemblages of the Britt Domain to the west (Fig. 4; Davidson *et al.*, 1982; Nadeau, 1983; Davidson, 1984b).

Scapolite may comprise up to 41 modal percent of the meta-anorthosite (Mason, 1969), with the scapolite ranging from 3.5 to 4.7 wt % CO_2 (*e.g.*, sample S86E-25a, Appendix 3). Whole rock analyses range up to 1 wt % CO_2 in the main body of the WSA and 1.6% in the PSSZ (Mason, 1969; Nadeau, 1983), but greater amounts are required by samples with 40 modal percent scapolite having 4 wt % CO_2. Most anorthosite does not have significant quantities of dissolved CO_2 (Morse, 1982), and the presence of carbonate scapolite in the WSA implies the addition of significant quantities of externally derived fluid as a result of assimilation or fluid interaction. The marbles directly adjacent to the east margin of the WSA are likely sources for this CO_2, however marbles are rare along the western margin of the WSA and in the PSSZ where scapolite is also developed. The WSA was continuously sampled from the apparent core to the east margin adjacent to marble, in order to test the hypothesis that the marbles were a source for CO_2 leading to the formation of scapolite.

Stable isotopic data were also collected for southern extensions of the WSA where it is intersected by the PSSZ. U-Pb zircon dating of sheared pegmatite dikes within the PSSZ are consistent with syn-metamorphic movement along the PSSZ, relative to the peak of regional metamorphism (van Breemen *et al.*, 1986). Deformation of the WSA within the PSSZ is heterogeneous, with large blocks of less strained gabbroic anorthosite entrained within an anastomosing network of more intensely strained gneiss (Nadeau, 1983). Mineral assemblages within the sheared WSA span the range encountered in the marginal facies of the main body of the WSA, but without the distinct spatial zoning in the latter. Mineral assemblages typically developed in the samples of sheared WSA examined for this study are

subassemblages of Pg–Hbl–Sc–Gt–Qz–Cpx–Ep–Bi–Ti–Ilm. Samples exhibit varying degrees of grain size reduction and recrystallization as a result of ductile shearing. In general, annealed, equilibrium granoblastic textures predominate in the sheared rocks. Other effects developed locally are relict plagioclase phenocrysts in a fine-grained plagioclase–hornblende matrix, neoblast formation around clinopyroxene porphyroclasts, and recrystallization of clinopyroxene to hornblende.

The WSA is bounded on the west (structurally underlain in the shear zone) by amphibolite, and on the east (structurally overlain) by mafic gneiss and granulite that are sheared and retrograded to varying degrees, with local preservation of ductily strained orthopyroxene. The Gt–amphibolite is structurally continuous with that along the west margin of the WSA. Localized masses of marble breccia occur within the overlying mafic gneisses, and coarse marble blocks have been found in sheared anorthosite. The stratigraphy within the PSSZ grossly approximates that for a west to east traverse across the main body of the WSA and enclosing lithologies to the north, but without the large layer of marble breccia occurring east of the WSA.

The margins of the WSA exhibit a marked foliation, manifested by a compositional layering of mafic phases, and locally by evidence of ductile shearing (Mason, 1969). This is in contrast to the center of the WSA where relict igneous textures are often preserved with minor recrystallization (glomeropoikiolitic clinopyroxene enclosing relict plagioclase phenocrysts, block structure, igneous layering: Mason, 1969). The core of the WSA also contains orthopyroxene in equilibrium with clinopyroxene, garnet, plagioclase, and traces of sulfate–rich scapolite. The interpretation of equilibrium mineral assemblages in the WSA is complicated by varying textural relations and mineral chemistry. In the marginal facies of the WSA scapolite and hornblende appear to be in textural equilibrium with garnet, plagioclase, and clinopyroxene, exhibiting annealed granoblastic textures. The same phases from the interior of the WSA, between the apparent core and the margins, display varying degrees of replacement textures, with scapolite after plagioclase and hornblende after clinopyroxene (Mason, 1969; Thompson, 1983; this

study). In any one outcrop, equilibrium (i.e., granoblastic) textures may be observed, and in another sample from the same outcrop the scapolite can be seen to embay and replace plagioclase. The volatile composition of scapolite from the two samples may also differ by up to 20 mol% in $CO_3/[CO_3+SO_4+Cl]$. The introduction of fluid components and equilibration of Sc–Hbl–Pl–Cpx±Ep±Gt assemblages may not be a single event, being modified by differential pre– to post–peak metamorphic movement, recrystallization, and fluid interaction.

Garnet amphibolites and mafic gneisses (Gt–Pg–Hbl–Qz±Bi±Cpx±Opx) that occur around the margins of the WSA often contain calcite, usually appearing as a secondary phase with ragged grain boundaries but in some cases appearing primary in granoblastic aggregates and having smooth, slightly curved grain boundaries. Whole rock samples of these lithologies were analyzed for $\delta^{13}C$ in order to compare it with WSA values.

Carbon isotope analyses of calcite from marbles and scapolite in WSA, and oxygen isotope analyses of calcite from marbles and whole–rock samples of the scapolite–bearing WSA, are presented as a function of distance to the WSA–marble contact (Figs. 8a and 8b), and compared with calcite from marbles and mafic gneisses (Figure 9, Tables 6, 7, and 8). The marbles exhibit a typical Grenville signature for $\delta^{13}C$ (-0.4 ± 0.3‰, 1σ, n=10) and $\delta^{18}O$ ($+19.4\pm2.4$ ‰, Table 7). Scapolite from the inner aureole of the anorthosite has a $\delta^{13}C$ value of -3.4‰, and as the marble contact is approached the values become systematically higher, approaching the $\delta^{13}C$ of the marble. Calcite in mafic gneisses at the east contact also have values of $\delta^{13}C$ approaching marble values (*e.g.*, S86E–5b, –14, –32, –33: Table 6). Whole rock $\delta^{18}O$ values of the anorthosite increase from 6.6 ‰ in the core to 11.5 at the marble contact.

Whole rock oxygen isotope analyses of samples at the southwestern margin of the WSA adjacent to garnet amphibolite are more similar to those of the inner aureole of the anorthosite than to values observed along the east margin. The values at the southwest margin range from 7.3 to 7.7‰. Values of $\delta^{18}O$ for the

Figure 8a. $\delta^{13}C$ of scapolite in the Whitestone Anorthosite (WSA) and of calcite in marble breccia as a function of distance to the eastern WSA–marble contact.

Figure 8b. Whole rock $\delta^{18}O$ values for scapolite-bearing WSA and associated mafic gneisses as a function of distance to the WSA–marble contact.

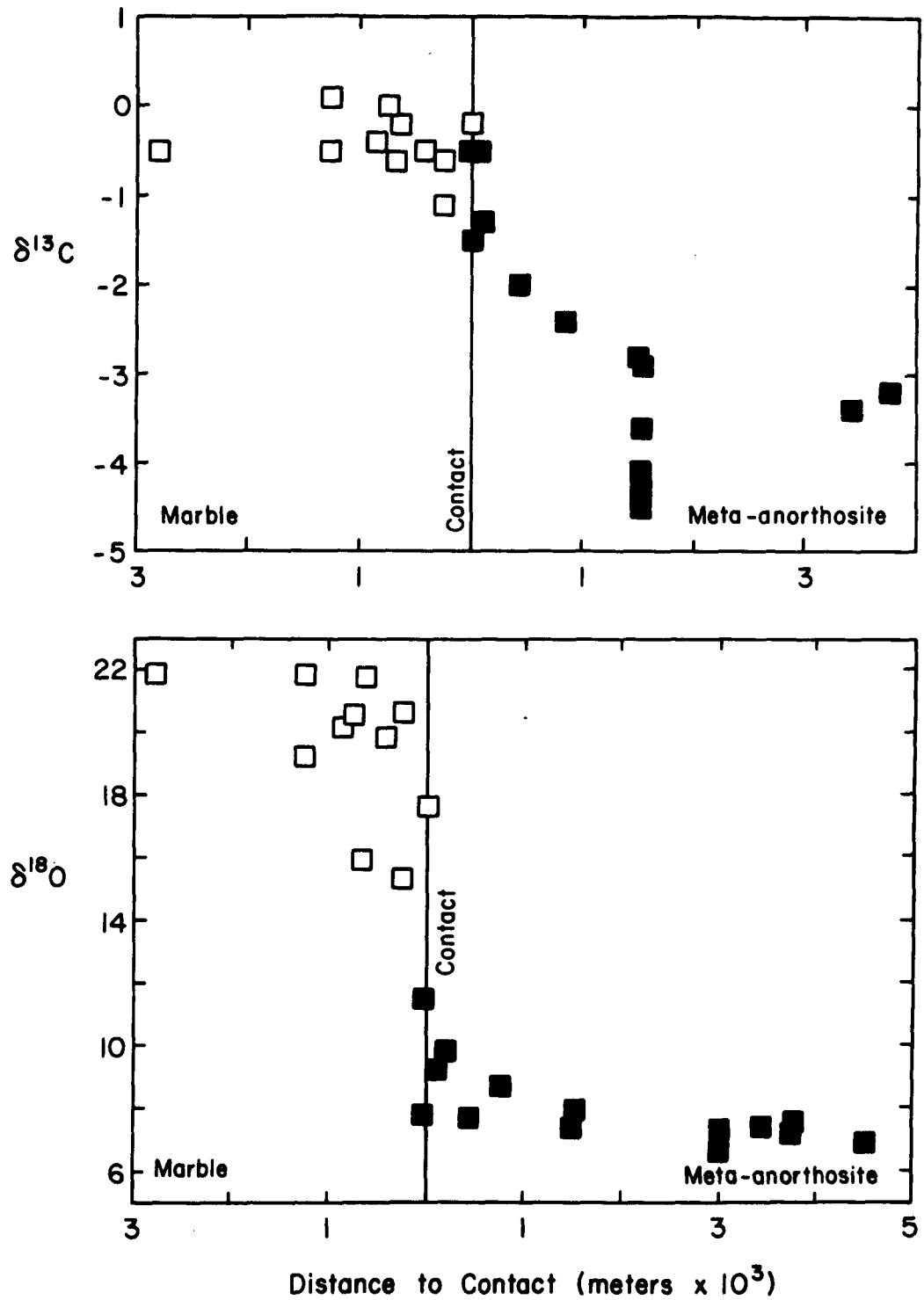
1
0
-1
-2
-3
-4
-5
δ13C
Marble
Contact
Meta-anorthosite
3
1
1
3
22
18
14
10
6
δ18O
Marble
Contact
Meta-anorthosite
3
1
1
3
5
Distance to Contact (meters x 10^3)

TABLE 6: Carbon and oxygen isotope analyses of scapolite and calcite from WSA and spatially associated garnet amphibolites and mafic gneisses. GA: garnet amphibolite; MA: meta-anorthosite; GMA: garnetiferous meta-anorthostie; EMA: epidote meta-anorthosite; GMG: garnetiferous mafic gneiss; WR: whole-rock silicate analysis.

SAMPLE	ROCK TYPE	PHASE	$\delta^{13}C$	$\delta^{18}O$	$\delta^{18}O$ WR	COMMENTS
PS2	GA	Cc	-7.0	14.4	-	retrograde Cc
PS3	GA	Cc	-2.4	11.0	-	retrograde Cc
PS6	GA	Cc	-2.6	11.2	-	PSSZ
PS7a	GMA	Sc	-1.4	9.6	7.9	sheared WSA, PSSZ
PS7b	GMA	Sc	-1.2	9.9	8.4	sheared WSA, PSSZ
PS7c	GMA	Sc	-1.1	9.6	8.0	sheared WSA, PSSZ
PS7e	GMA	Sc	-1.7	11.9		sheared WSA, PSSZ
PS7g	GMA	-	-	-	8.5	sheared WSA, PSSZ
PS85A-1a	EMA	Sc	-7.5	10.4	-	PSSZ
PS85A-2c	GMA	Sc	-0.1	10.5	-	sheared WSA, PSSZ
PSO85A-5	GMA	Sc Cc	-0.2 -1.3	8.9 15.1	-	sheared WSA, PSSZ
PSO85A-8	GMA	Sc	-0.5	9.4	8.1	sheared WSA, PSSZ
PSO85A-13	GMA	Sc	-1.4	10	-	sheared WSA, PSSZ
PSO83C-13	GA	Cc	-4.5	13.7	-	retrograde Cc
PSO83C-15	GA	Cc	-4.3	13.8	-	retrograde Cc
PSO85A-24	GMA	Sc	-3.6	10.3	-	WSA, retrograde Sc
PSO83C-24	GA	Cc	-2.6	10.5	-	retrograde Cc
PSO85A-25	GMA	Sc	-4.1	9.9	-	WSA, retro Sc
PSO83C-25	GA	Cc	-3.7	10.2	-	retrograde Cc
PS86B1-1	GMA	Sc	-1.2	9.1	-	sheared WSA, PSSZ
PS86B1-2	GA	-	-	-	6.4	PSSZ
PS86B1-4	GMA	-	-	-	7.8	sheared WSA, PSSZ
PS86B1-6	GMA	Cc	-3.0	9.4	8.6	sheared WSA, PSSZ
PS86B1-7	GMA	-	-	-	8.9	sheared WSA, PSSZ
PS86B1-8	GMA	Cc	-3.6	10.0	8.8	sheared WSA, PSSZ

PS86B1-10	GMA	Sc	-1.1	8.8	7.5	sheared WSA, PSSZ
PS86B-11a	GA	-	-	-	6.8	PSSZ
PS86B2-1	GMA	Sc	0.7	9.6	-	sheared WSA, PSSZ
PS86B2-3	GMA	Sc	-0.6	9.6	8.1	sheared WSA, PSSZ
PS86EA-1	GMA	Sc	-0.8	9.1	7.7	sheared WSA, PSSZ
PS86E-4Nd	GA	Cc	-5.1	14	-	sheared, PSSZ
PS86E-5c	GMG	-	-	-	6.8	sheared, PSSZ
PS86E-6a	GMG	Cc	-4.6	9.6	8.0	sheared, PSSZ
PS86E-6b	GA	Cc	-2.3	10.8	8.5	sheared, PSSZ
PS86E-7e	GMA	Sc	-1.7	8.8	-	sheared WSA, PSSZ
PS86E-8	GMA	Sc	-3.7	9.2	-	PSSZ
PS86E-10	GMA	Sc	-3.3	9.4	8.1	PSSZ
PS86E-12	MA	Cc	-4.3	14.1	7.4	retrograde Cc
PS86E-14	GA	Cc	-8.2	10.3	-	retrograde Cc
PS86E-15	GMA	Sc	-2.3	10.2	7.5	"tail of WSA"
PS86E-16a	GMA	Sc	-3.4	9.3	7.4	"tail of WSA"
PS86E-19b	EMA	- Pg Ep Bi	-	-	7.7 8.2 6.9 5.0	"tail of WSA"
PS86E-22	EMA	Cc	-3.3	12.8	-	retrograde Cc, southwest margin WSA
PS86E-23	EMA	Sc	-2.9	9.8	-	southwest margin WSA
PS86E-24a	MA	Sc	-	-	7.6	southwest margin WSA
PS86E-24b	EMA	Sc	-2.4	9.9	-	southwest margin WSA
PS86E-24f	GMA	Sc	-	-	7.7	southwest margin WSA
PS86E-24g	GMA	-	-	-	7.3	southwest margin WSA
PS86E-26c	GA	Cc	-4.6	14.4	6.3	retrograde Cc, PSSZ
PS86E-27	GA	Cc	-8.3	10.7	-	PSSZ
PS86E-30b	EMA	-	-	-	8.5	
PS86E-30c	EMA	Sc	-8.3	12.1	8.8	
PS86E-31	GMA	Cc	-1.0	10.0	-	sheared WSA, PSSZ
PS86E-32	GMA	-	-	-	7.5	sheared WSA, PSSZ

PS86E-33	GMA	Cc	-	-	8.4	sheared WSA, PSSZ
PS86E-34	GMA	Sc	-0.6	9.2	7.5	sheared WSA, PSSZ
S86E-1a	GA	Cc	-3.4	10.1	7.7	
S85A-3a	GMA	Sc	-4.5	9.2	7.9	retrograde Sc
S85A-3b	GMA	Sc	-4.3	9.1	-	retrograde Sc
S85A-3c	GMA	Sc	-2.9	9.1	-	
S86E-4	GA	-	-	-	7.1	
S86E-5b	GMA	Cc	-1.3	10.8	9.2	retrograde Cc
S86E-14	GMA	-	-	-	8.7	
S86E-18b	GMA	Cc	0.7	16.3	-	
S86E-18c	MG	Cc	-1.5	16.9	-	retrograde Cc
S86E-25a	GMA	-	-	-	7.8	east margin WSA
S86E-25c	GMA	Sc	-0.5	10.7	-	east margin WSA
S86E-25i	GMA	-	-	-	11.5	east margin WSA
S86E-25f	GMA	Cc	0.2	15.5	10.8	amphibolite clast in marble breccia
S86E-31c	GMA	Sc	-1.5	10.5	-	east margin WSA
S86E-31e	GMG	-	-	-	8.5	east margin WSA
S86E-32	GMG	Cc	-0.5	12.6	-	east margin WSA
S86E-33	GMG	-	-	-	9.8	east margin WSA
S86E-34	GMA	Sc	-2.0	9.4	7.7	aureole in WSA, retrograde Sc
S86E-36b	GMA	Sc	-2.4	9.6	-	aureole in WSA, retrograde Sc
S86E-39	GMA	Sc	-2.8	9.5	7.4	aureole in WSA, retrograde Sc
S86E-44	MA	Sc	-3.4	9.9	7.4	aureole in WSA
S86E-45	MA	Sc	-3.2	10.2	7.5	aureole in WSA
MMJ3024	MA	-	-	-	7.2	inner aureole of WSA
MMJ3011	MA	-	-	-	7.3	inner aureole of WSA
MMJ0043	MA	-	-	-	6.6	granulite facies core WSA
MMJ0102	MA	-	-	-	6.9	granulite facies core WSA

TABLE 7: Carbon and oxygen isotope composition of calcite in marble and marble breccia along east margin of WSA.

	$\delta^{13}C$	$\delta^{18}O$
PS85A-7	-0.6	15.7
S3a	-0.5	21.8
S41b	0.1	21.8
S41c	-0.5	19.2
S86E-8c	-0.6	15.9
S86E-16d	-0.6	15.3
S86E-16g	-1.1	20.6
S86E-18a	-0.4	20.1
S86E-23	0.0	20.5
S86E-24c	-0.2	21.7
S86E-27a	-0.5	19.8
S86E-31c	-0.2	17.6
Average	-0.4	19.4

mafic gneisses along the west and east margin of the WSA are similar to those of the WSA, and are not likely to provide constraints for the additional fluid source in the WSA as provided by the carbon isotopic data for scapolite.

The carbon and oxygen isotope data from the WSA and associated mafic gneisses are consistent with a model invoking marble as a local source of high ^{13}C and ^{18}O material along the east margin of the WSA. CO_2 in equilibrium with calcite at 700°C is enriched in ^{13}C relative to calcite by approximately 2.5 $^{o}/_{oo}$, which would equilibrate with a scapolite that is approximately the same isotopic composition as the calcite from marble (*e.g.*, east margin of WSA). However, the lower values of $\delta^{13}C$ recorded in samples of meta-anorthosite from the inner aureole of the WSA argue for a second carbon fluid source, or a much lower temperature for the fluid-rock interaction. The lower values are more similar to $\delta^{13}C$ from calcite in the regional country rock garnet amphibolites and mafic gneisses (*e.g.*, PS3, S86E-1a: Table 6). The fractionation of ^{13}C between CO_2 and calcite undergoes a crossover at approximately 190°C, where CO_2 is lower in ^{13}C relative to coexisting calcite (Friedman and O'Neil, 1977). Textural relations discussed above are consistent with a syn- to post-peak metamorphic crystallization for the scapolite, but certainly not at temperatures approaching the CO_2-calcite crossover. Garnet-clinopyroxene thermometry for the scapolite-bearing WSA yields temperatures in excess of 650°C (Chapter II). If the CO_2 is externally derived, the $\delta^{13}C$ data for the interior of the WSA require that the CO_2 be derived from marble with a similar composition to the scapolite, assuming production of CO_2 from the marble and incorporation into the scapolite occurred at a constant temperature (approximately -3 to $-4^{o}/_{oo}$), or an some other source $2.5^{o}/_{oo}$ higher than the scapolite. The data are not consistent with an igneous or mantle source of carbon (CO_2) with $\delta^{13}C$ = -5 to $-7^{o}/_{oo}$ because of the negative fractionation of ^{13}C between scapolite and CO_2. An igneous or mantle source would produce a scapolite with $\delta^{13}C$ of approximately -7.5 to $-9.5^{o}/_{oo}$.

Figure 9. Summary of $\delta^{13}C$ and $\delta^{18}O$ for scapolite WSA, calcite–bearing amphibolites and mafic gneisses, and marbles in vicinity of WSA in Parry Sound Domain.

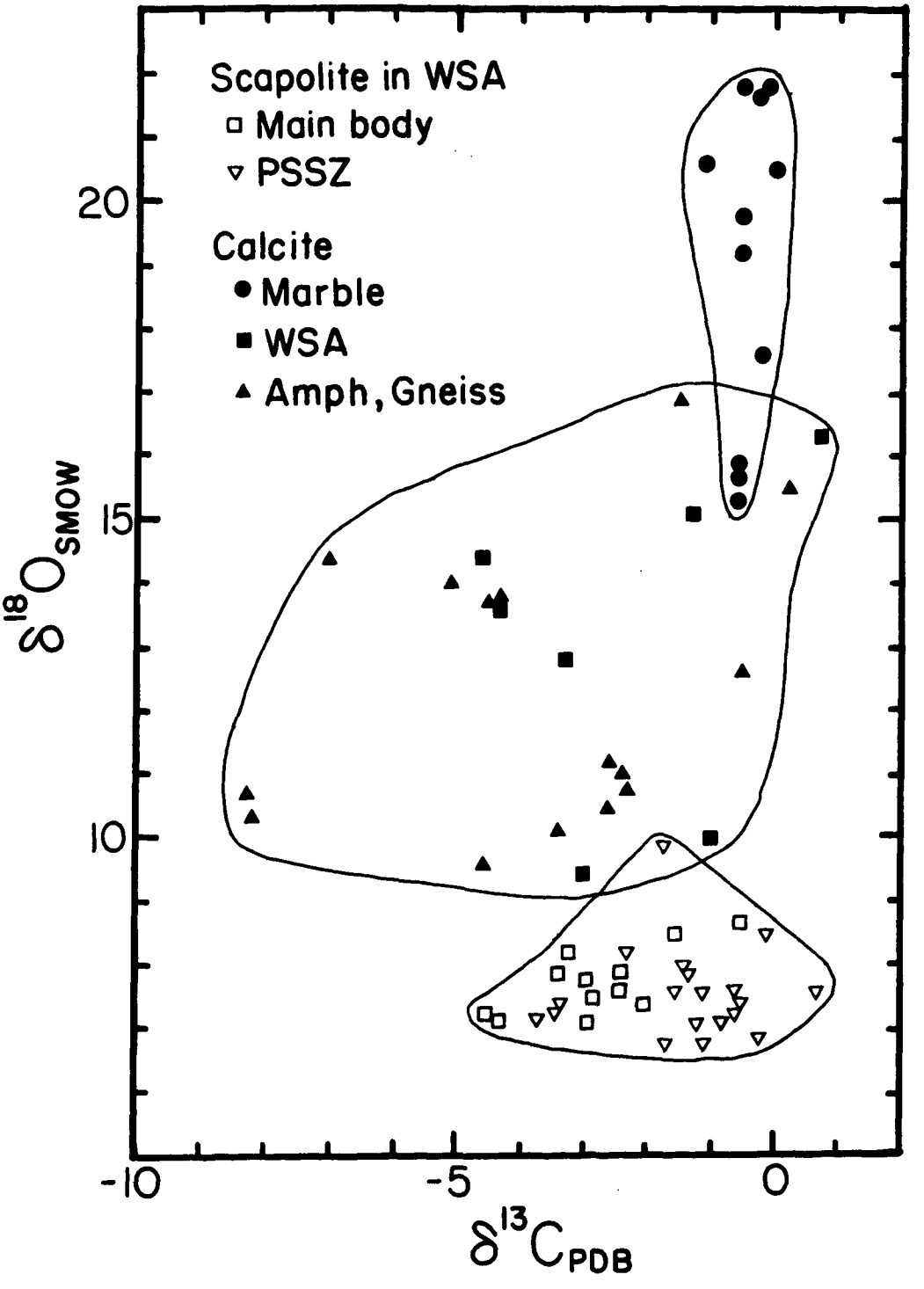
Scapolite in WSA
Main body
PSSZ
Calcite
Marble
WSA
Amph, Gneiss
20
15
10
-10
-5
0
$\delta^{18}O_{SMOW}$
$\delta^{13}C_{PDB}$

TABLE 8: Carbon isotope analyses of scapolite and calcite, and whole-rock oxygen analyses of WSA as a function of distance from WSA-marble contact. Distance in meters: negative values of distance are for marble samples and for a 1000 X 100 m xenolith of WSA in marble breccia. Scapolite analyzed in samples of GMA, MA, and GMG (see Table 6 for abbreviations), and calcite analyzed in marble samples.

Sample	Lithology	Distance	$\delta^{13}C$ Sc	$\delta^{18}O$ WR	Comments
S85A-3A	GMA	1530	-4.5	7.9	retrograde Sc
S85A-3B	GMA	1530	-4.3	-	retrograde Sc
S85A-3C	GMA	1530	-2.9	-	Sc-bearing WSA
PS085A-24a	GMA	1530	-3.6	-	retrograde Sc
PS085A-24b	GMA	1530	-4.1	-	retrograde Sc
S86E-5B	GMG	100	-1.3	9.2	retrograde Cc
S86E-14	GMG	770	-	8.7	retrograde Cc
S86E-25a	GMA	-30	-	7.8	Sc-bearing WSA
-25c	GMA	-30	-0.5		Sc in WSA margin
-25i	GMA	-30	-	11.5	Sc-bearing WSA
-31a	MA	0	-1.5	-	Sc-bearing WSA
-32	GMG	66	-0.5	-	Cc-bearing granulite
-33	GMG	200	-	9.8	Cc-bearing granulite
-34	GMA	433	-2.0	7.7	retro Sc
-36B	GMA	850	-2.4	-	retro Sc
-39	GMA	1500	-2.8	7.4	retro Sc
-44	GMA	3430	-3.4	7.4	Sc-bearing WSA
-45	GMA	3770	-3.2	7.5	Sc-bearing WSA
CCM0043	MA	3000	-	6.6	opx-bearing, core facies
CCM0102	MA	4500	-	6.9	core facies
MMJ3011	MA	3000	-	7.3	retro Sc
MMJ3024	MA	3750	-	7.2	retro Sc
Marble samples from east margin of WSA					
S3a		-2800	-0.5	21.8	
S41b		-1260	0.1	21.8	
S41c		-1260	-0.5	19.2	
S86E-8c		-670	-0.6	15.9	
S86E-16d		-250	-0.6	15.3	
S86E-16g		-250	-1.1	20.6	
S86E-18a		-850	-0.4	20.1	
S86E-23		-750	0.0	20.5	
S86E-24c		-640	-0.2	21.7	
S86E-27a		-420	-0.5	19.8	
S86E-31c		0	-0.2	17.6	

The amount of fluid–rock interaction for the east margin of the WSA can be constrained assuming a model of closed system fluid interaction using the relation

$$F/R = [\delta_R^f - \delta_R^i] / [\delta_F^i - (\delta_R^f - \Delta)]$$

(Taylor, 1977), where f and i are the final and initial isotopic composition of rock (R) and fluid (F), respectively, and Δ is the calculated fractionation between rock and fluid. The marbles at the anorthosite margin locally contain the assemblage Cc–Do–Fo–Di. In the absence of tremolite, this restricts the fluid composition derived from marble to approximately $X_{CO_2} > 0.5$ at 10 kbar (Eggert and Kerrick, 1985). Scapolite and epidote volatile equilibria for the east margin are consistent with a CO_2–rich, mixed H_2O–CO_2 vapor phase (Chapter IV). Assuming a fluid of $X_{CO_2} = 0.5$ in equilibrium with calcite with $\delta^{18}O = 20.3‰$, the initial isotopic composition of the CO_2–H_2O fluid is 24.1‰. The initial composition of the gabbroic anorthosite (δ_R^i) is taken as 6.6‰, the value observed in the WSA core facies. The final rock values (δ_R^f) are taken as the least and most altered values for meta–anorthosite at the east margin (7.8 and 11.5‰), allowing a range of fluid/rock values to be calculated relative to the least altered anorthosite. The value of Δ was calculated from plagioclase (An_{50}) –H_2O and H_2O–CO_2 fractionations at 700°C (Friedman and O'Neil 1977), assuming $X_{CO_2} = 0.50$. Based on the above parameters, minimum values of F/R range from 0.1 for the least enriched to 0.3 for the most enriched meta–anorthosite. The same calculations at 750°C and $X_{CO_2} = 0.75$ do not significantly change the values of F/R. This range of values is for samples in a single outcrop at the east margin of the WSA directly adjacent to marble breccia, indicating varying degrees of fluid interaction on an outcrop scale.

Scapolite from the sheared garnet meta–anorthosite in the PSSZ exhibits a range of $\delta^{13}C$, from −0.1 to −3.6, with a pronounced maximum about $-1\pm1‰$ (Table 6, Fig. 10). One sample of epidote–scapolite meta–anorthosite from a thin layer approximately 2 km west of the main mass of sheared WSA yields

Figure 10. Histogram summarizing carbon isotopic composition of samples for this study.

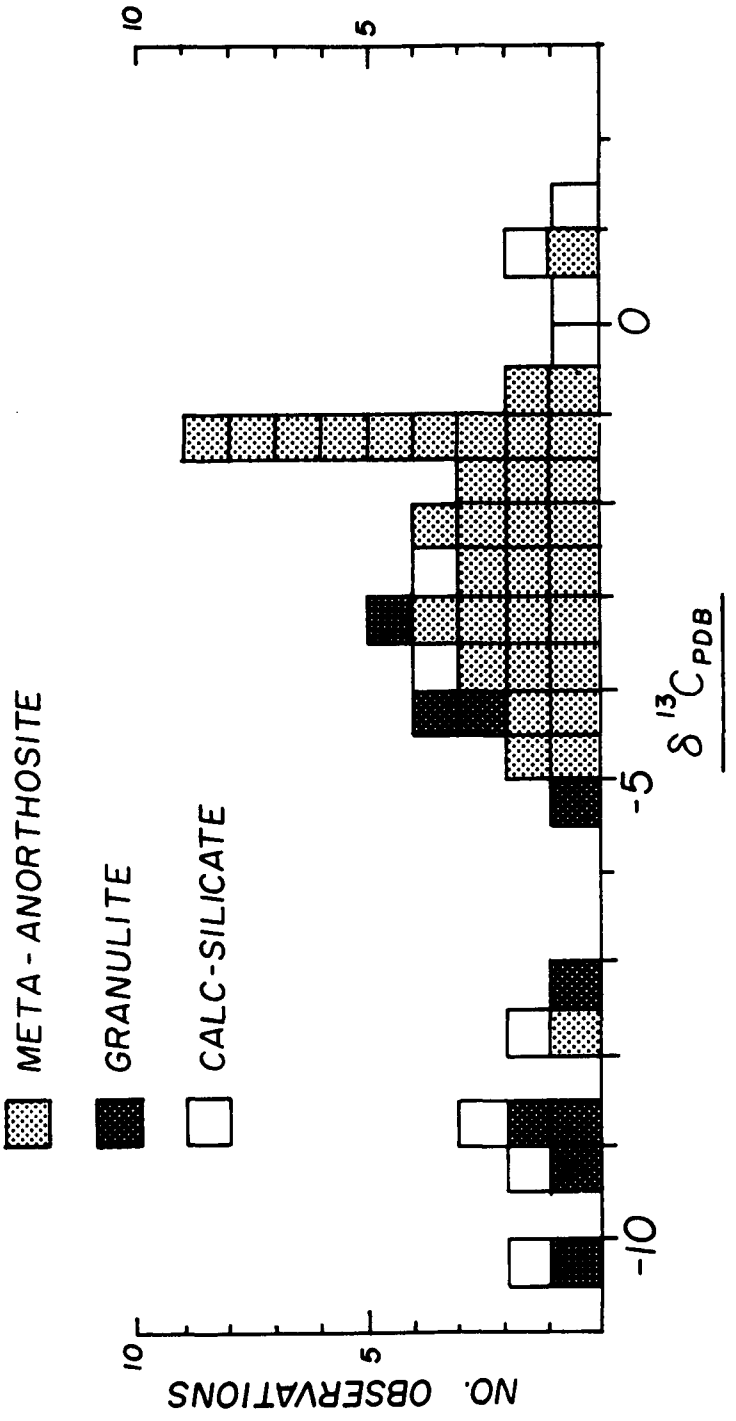
META - ANORTHOSITE
GRANULITE
CALC-SILICATE
NO. OBSERVATIONS
10
5
10
5
0
-5
-10
$\delta^{13}C_{PDB}$

significantly lighter carbon (−8.0‰). Calcite from meta-anorthosite, mafic gneisses (Pg-Gt-Cpx-Hbl-Cc) and amphibolite (Pg-Hbl-Bi±Gt±Cpx-Cc) overlaps the lower end of the range of scapolite values, but is generally significantly lower ($\delta^{13}C_{Cc}$ = −1.0 to −8.3; $\delta^{18}O_{Cc}$ = 10.2 to 16.1). A sample of silicate-rich marble breccia from a 20 m long outcrop east of (structurally above) the axis of the PSSZ has $\delta^{13}C$ = −0.6 and $\delta^{18}O$ = 15.6‰. Whole rock $\delta^{18}O$ values for the sheared WSA span a narrow range from 7.4 to 8.9‰. Garnet amphibolite at the west contact of the WSA has $\delta^{18}O$ = 6.5 − 6.8‰, and $\delta^{18}O$ values of mafic gneiss along the east contact range from $\delta^{18}O$ = 5.8 − 8.5‰. On the scale at which we have sampled there does not appear to be any systematic variation of $\delta^{13}C$ or $\delta^{18}O$ along the length of, or across the WSA in the PSSZ.

The carbon and oxygen isotope data for the PSSZ essentially span the same range of values displayed by the main body of the WSA. The isotopic and mineralogic data for the PSSZ are consistent with the WSA in the PSSZ being the sheared equivalent of the east and west margins of the main body of the WSA, having undergone ductile shearing following fluid-rock interaction to form the scapolite-hornblende-epidote-garnet meta-anorthosite assemblages. The variation of $\delta^{13}C$ and $\delta^{18}O$ values, and similarity with WSA values, indicate that there has not been significant, additional introduction of fluids through rocks in the PSSZ. This does not preclude the possibility of localized, closed system retrograde hydration, which is evident in both the PSSZ and WSA. The lack of a high fluid flux in the PSSZ is consistent with observations from other ductile shears where stable isotope evidence and mass balance calculations are consistent with low F/R ratios (e.g., Kerrich *et al.*, 1984). The granulite facies, deep crustal environment of the PSSZ and Parry Sound Domain (Anovitz, 1987; Chapter II) would not be a likely source for significant amounts of fluid. Therefore the dry nature of the PSSZ is not surprising considering its geologic setting.

Mafic Gneisses, Granulites, and Amphibolites

Solid solutions of carbonate–sulfate scapolite occur in amphibolite (Sc+Pg+Hbl+Qz±Gt±Cpx±Bi±Ti±Ilm) and mafic granulite (Sc+Pg+Hbl+Cpx±Gt±Opx±Qz) at a number of localities in the southwestern Grenville Province. The samples are located in four different lithotectonic domains in southwestern Ontario (Davidson *et al.*, 1982) (Fig 4). These occurrences of scapolite–bearing granulites are similar to lithologies and scapolite–bearing assemblages from the Furua Complex in Tanzania (Coolen, 1980) analyzed by Hoefs *et al.* (1981). The igneous protoliths (basalt, diabase) inferred for such lithologies would not be expected to contain significant pre–metamorphic carbon, and as with the meta–anorthosite, the presence of carbonate/sulfate scapolite is consistent with introduction of externally derived C at some point in the rock's history.

$\delta^{13}C$ values of CO_2 extracted from scapolite in mafic gneisses are all relatively low, ranging from −2.9 to −10.0‰ (Table 9). Samples 80DMA614P and 80DMM47b are both from the Parry Sound domain, and have $\delta^{13}C$ that are broadly consistent with values from meta–anorthosite (WSA) and mafic gneisses from the same domain (Table 9). The A86B granulite samples occur in the same domain (McCraney) and within 20 km of the A85A and A86B calc–silicate localities (Table 5). Scapolite in the granulites is distinctly enriched in ^{13}C relative to scapolite and calcite from calc–silicates in this domain. Scapolite derived from a calc–silicate should record the same isotopic composition as the calc–silicate source: the east margin of the WSA is an example of such a process. Therefore, carbon in scapolite from the McCraney domain granulites must record an alternative source or process resulting in the formation of scapolite.

If a simple scenario is adopted to account for the formation of scapolite in these rocks (introduction of CO_2 into a mafic gneiss without fractionation of carbon during the process of scapolite formation), the data in Table 9 are consistent with a range of sources for the carbon, having distinct isotopic signatures for each domain.

TABLE 9: Carbon and oxygen isotope data for scapolite amphibolite and granulites, southwestern Ontario. Domains as in Fig. 3.

SAMPLE	ASSEMBLAGE	$\delta^{13}C$	$\delta^{18}O$ Sc*	$\delta^{18}O$ WR**	DOMAIN
A86B3-3a	Sc-Pg-Opx-Cpx-Hbl	-8.6	9.1	6.5	McCraney
A86B3-3c'	Sc-Pg-Cpx-Opx-Hbl-Bi-Mt-Ilm-Ap	-7.0	9.3	6.8	McCraney
85DMP272-2a	Sc-Pg-Gt-Cpx-Opx-Hbl-Qz-	-4.0	8.7	-	Kiosk
85DMP174-1a	Sc-Pg-Gt-Cpx-Hbl-Qz-Bi-Mt-Ap	-5.4	10.2	-	Kiosk
80DMA348d	Sc-Pg-Gt-Hbl-Bi-Qz-Ilm-Ap	-8.8	9.7	-	Britt
80DMA351f	Sc-Pg-Cpx-Hbl	-9.4	12.2	-	Britt
S86E-53	Sc-Pg-Gt-Cpx-Hbl-Qz-Bi	-10.0	9.7	6.6	Novar
80DMA614P	Sc-Pg-Gt-Cpx-Opx-Hbl-Ap-Mt-Ilm	-4.1	7.0	-	Parry Sound
80DMP47b	Sc-Pg-Hbl-Bi-Ti	-2.9	9.3	-	Parry Sound

*: $\delta^{18}O$ calculated for CO_2 extracted from scapolite using fractionation factor for calcite-acid at 75°C; see text for discussion.

**: oxygen extracted from whole rock samples using BrF_5 methods.

Although based on a limited data set, this model precludes large scale pervasive equilibration among the various lithotectonic domains of the Central Gneiss Belt of southwestern Ontario, which would have resulted in homogenization of the scapolite isotopic compositions. This model has implications for carbonic metamorphism (e.g., Touret, 1971; Janardhan *et al.* 1979; Newton *et al.*, 1980) which invokes pervasive infiltration of a CO_2-rich, mantle derived fluid into high grade terranes, resulting in lowered H_2O activities and stabilization of granulite facies (Opx-bearing) mineral assemblages. One might predict that if such a pervasive process occurred, scapolite would record the isotopic composition of the fluid with which it equilibrated. Mantle carbon, as recorded in diamonds, carbonatites, and CO_2 in fluid inclusions in basalt glass, has a range of isotopic compositions from -3 to $-30^{o}/_{oo}$, with a pronounced mode at approximately $-6^{o}/_{oo}$ (Mattey, 1987). A carbonic fluid with $\delta^{13}C = -6^{o}/_{oo}$ would equilibrate under granulite facies conditions with a scapolite of $\delta^{13}C = -8.5^{o}/_{oo}$. Scapolite in the CGB of Ontario spans a wide range from approximately 0 to $-11^{o}/_{oo}$. This range is not inconsistent with a mantle or igneous source of carbon for some of the samples, however more than a single source appears to be indicated, or else the mantle below the Grenville Province in Ontario is heterogeneous with respect to its carbon isotopic composition.

The volatile components (C and S) present in the mafic gneisses could have been introduced during an early high temperature alteration event by interaction of mafic protoliths with sea water, resulting in the formation of calcite, sulfides, and/or anhydrite. Such a high temperature process was invoked to account for the anomalously light oxygen isotope composition of granulites from Australia (Wilson and Baksi, 1983). Three mafic scapolite gneisses from this study do not have unusual oxygen isotope compositions, having values approximately $1^{o}/_{oo}$ higher than those for a pristine mafic igneous rock (Table 9). The lack of such ^{18}O depletions is generally true for all the scapolite gneisses analyzed for this study, consistent with the lack of *extensive* interaction with hot sea water. Lowering of $\delta^{18}O$ that would occur during interaction with meteoric water have also not been observed in

the mafic gneisses and WSA. However interaction with seawater could precipitate calcite and elevate the whole-rock $\delta^{18}O$ by varying degrees.

Livnat (1983) reports calcite in prehnite/pumpellyite facies metabasalts from the Keweenaw volcanic system, northern Michigan, with $\delta^{13}C$ in the range observed for the Grenville gneisses ($-3.6\pm1.6^{o}/_{oo}$, 1σ). The Keweenaw system has been interpreted to have experienced an episode of hydrothermal interaction with heated seawater that led to extensive Cu mineralization. Thus, carbon in mafic rocks need not be introduced during high grade metamorphism. If basalts that have experienced an early carbon infiltrating event such as the Keweenawan system undergo later high grade metamorphism, this range of carbon compositions in calcite may or may not be later modified to varying degrees by prograde decarbonation reactions.

Application of the carbon isotope systematics of scapolite in high grade settings has been shown to yield reliable estimates of $\delta^{13}C$, particularly in controlled settings such as the Whitestone anorthosite and adjacent marble. However the overlap in isotopic signatures of the various carbon reservoirs makes it difficult to identify carbon sources unequivocally in rocks where there is no immediate source of carbon, such as the scapolite granulites and mafic gneisses investigated here and in the Furua Complex by Hoefs *et al.* (1981). The pattern of carbon isotope composition of scapolite may be more useful in identifying sources and processes leading to introduction of CO_2 into a rock and subsequent formation of scapolite. A limited range of $\delta^{13}C$ might be expected for models that invoke open system exchange (the system is here defined as the regional metamorphic terrane) and influx of mantle or subcrustally derived CO_2. The alternative model would involve decarbonation of crustal calc-silicates or marbles within a given system, having varying isotopic signatures as a result of original isotopic heterogeneity, or from having undergone varying degrees of Rayleigh distillation and depletion of ^{13}C. This process would be manifested in a wide range of isotopically light carbon values. However both alternatives assume that the gneissic protoliths initially contained no significant pre-metamorphic carbon.

References

Aitken B.G., Evans H.T. and Konnert J.A. (1985) The crystal structure of a synthetic meionite. *Neues J. Mineral. Abh.* **149**, 309–324.

Anovitz L.M. and Essene E.J. (1988) Pressure–temperature constraints on the metamorphism of the Grenville Province, Ontario. *J. Petrol.* in press.

Clayton R.M. and Mayeda T.K. (1963) The use of bromine pentafluoride in the extraction of oxygen from oxides and silicates for isotopic analysis. *Geochim. Cosmochim. Acta* **27**, 43–52.

Coolen J.J.M.M.M. (1980) Chemical petrology of the Furua Granulite Complex, southern Tanzania. GUA (Univ. of Amsterdam) Papers of Geology, series 1, no. 13, 258pp.

Davidson A. (1984a) Tectonic boundaries within the Grenville Province of the Canadian Shield. *Geodynam.* 1, 433–444.

Davidson A. (1984b) Identification of ductile shear zones in the southwestern Grenville Province of the Canadian Shield. In *Precambrian Tectonics Illustrated* (eds. A. Kroner and R. Greiling), pp. 263–279. E. Schweizerbart'sche Verlagsbuchhandlung.

Davidson A., (1986) New interpretations in the southwestern Grenville Province. In *The Grenville Province* (eds. J.M. Moore, A. Davidson, A.J. Baer), pp 61–74, Geol. Soc. Canada Spec. Pap. 31.

Davidson A., Britton J.M. and Bell, K. (1979) Regional synthesis of the Grenville Province of Ontario and western Quebec. *Curr. Res., Geol. Surv. Canada Pap.* **78-1B**, 153–172.

Davidson A., Culshaw N.G. and Nadeau, L. (1982) A tectono–metamorphic framework for part of the Grenville Province, Parry Sound Region, Ontario. *Curr. Res., Geol. Surv. Canada Pap.* **82-1A**, 175–190.

Devaraju T.C. and Coolen J.J.M.M.M. (1983). Mineral chemistry and P–T conditions of a basic scapolite–garnet–pyroxene granulite from Doddakanya, Mysore District. *J. Geol. Soc. India* **24**, 404–411.

de Villiers J.P.R. (1971) Crystal structures of aragonite, strontianite and witherite. *Amer. Mineral.* **56**, 758–767.

Frank E. (1983) Alpine metamorphism of calcareous rocks along a cross–section in the Central Alps: occurrence and breakdown of muscovite, margarite, and paragonite. *Schweiz. Mineral. Petrogr. Mitt.* **63**, 37–93.

Friedman I. and O'Neil J.R. (1977) Compilation of stable isotope fractionation factors of geochemical interest. In *Data of Geochemistry Sixth Edition* (ed. M. Fleischer), Chap KK, Geol. Surv. Prof. Pap. 440–KK.

Glassley W.E. (1983) Deep crustal carbonates as CO_2 fluid sources: evidence from metasomatic reaction zones. *Contrib. Mineral. Petrol.* **84**, 15–24.

Heitanen A.L. (1967) Scapolite in the Belt Series in the St. Joe–Clearwater region, Idaho. *Geol. Soc. Amer. Spec. Pap.* **86**.

Hoefs J. (1973) Ein Beitrag zur isotopengeochemie des Kohlenstoffs in magmatischen Gesteien. *Contrib. Mineral. Petrol.* **41**, 277–300.

Hoefs J., Coolen, J.J.M.M.M. and Touret J. (1981) The sulfur and carbon isotope composition of scapolite–rich granulites from southern Tanzania. *Contrib. Mineral. Petrol.* **78**, 332–336.

Hoering T.C. and Hart R. (1964) A geochemical study of some Adirondack graphites. *Carnegie Inst. Washington Yearbk.* **63**, 265–267.

Janardhan A.S., Newton R.C. and Smith J.V. (1979) Ancient crustal metamorphism at low p_{CO_2}: charnockite formation at Kabbaldurga, south India. *Nature* **278**, 511–514.

Kerrich R., La Tour T.E. and Willmore L. (1984) Fluid participation in deep fault zones: evidence from geological, geochemical, and $^{18}O/^{16}O$ relations. *J. Geophys. Res.* **89B**, 4331–4343.

Kumar G.R.R. and Chacko T. (1986). Mechanisms of charnockite formation and breakdown in Southern Kerala: implications for the origin of the Southern Indian Granulite Terrain. *J. Geol. Soc. India* **28**, 277–288.

Kwak T.A.P. (1977) Scapolite compositional change in a metamorphic gradient and its bearing on the identification of meta–evaporite sequences. *Geol. Mag.* **114**, 343–354.

Livnat A (1983) Metamorphism and Copper Mineralization of the Portage Lake Lava Series, Northern Michigan. PhD thesis, University of Michigan

Lovering J.F. and White A.J.R. (1964) The significance of primary scapolite in granulitic inclusions from deep–seated pipes. *J. Petrol.* **5**, 195–218.

Markgraf S.A. and Reeder R.J. (1985). High temperature structure refinements of calcite and magnesite. *Am. Miner.* **70**, 590–600.

Mason I.M. (1969) Petrology of the Whitestone anorthosite. Ph.D. dissertation, McMaster Univ.

Mattey D.P. (1987) Carbon isotopes in the mantle. *Terra Cognita* **7**, 31–36.

McCrea J.M. (1950) The isotopic chemistry of carbonates and a paleotemperature scale. *Jour. Chem. Phys.* **18**, 849–857.

Moecher D.P., Essene E.J. and Anovitz L.M. (1988) Calculation and application of clinopyroxene–garnet–plagioclase–quartz geobarometers. *Contrib. Mineral. Petrol.* in press.

Mora C.I. and Valley J.W. (1988) Halogen rich scapolite and biotite: implications for fluid rock interaction. *Amer. Mineral.* in press.

Morrison J. and Valley J.W. (1988) Post–granulite facies fluid infiltration in the Adirondack Mountains. Geology **16**, 513–516.

Morse S.A. (1982) A partisan review of Proterozoic anorthosites. *Amer. Mineral.* **67**, 1087–1100.

Mummery R. (1973) Coronite amphibolites from the whitestone area, Parry Sound, Ontario. M.S. thesis, McMaster Univ.

Nadeau L. (1983) Deformation of leucogabbroic rocks at Parry Sound, Ontario. M.S. thesis, Carleton Univ.

Oliver N. and Wall V.J. (1987) Metamorphic plumbing system in Proterozoic calc-silicates, Queensland, Australia. *Geology* **15**, 793–796.

Robie R.A., Bethke P.M., Toulmin M.S. and Edwards J.L. (1966) X-ray crystallographic data, densities, and molar volumes of minerals. In *Handbook of Physical Constants* (ed. S.P. Clark Jr.), Geol. Soc. Amer. Memoir **97**, 27–73.

Rubinson M. and Clayton R.N. (1969) Carbon-13 fractionation between aragonite and calcite. *Geochim. Cosmochim. Acta* **33**, 997–1002.

Serdyuchenko D.P. (1973) Some Precambrian scapolite-bearing rocks evolved from evaporites. *Lithos* **8**, 1–7.

Shaw D.M. (1960) The geochemistry of scapolite. Part I: Previous work and general mineralogy. *J. Petrol.* **1**, 218–260.

Sharma T. and Clayton R.N. (1965) Measurement of $^{18}O/^{16}O$ ratios of total oxygen of carbonates. *Geochim. Cosmochim. Acta* **29**, 1347–1353.

Sheppard S.M.F. and Schwarcz H.P. (1970) Fractionation of carbon and oxygen isotopes and magnesium between coexisting metamorphic calcite and dolomite. *Contrib. Mineral. Petrol.* **26**, 161–198.

Shieh Y.-N. and Schwarcz H.P. (1974) Oxygen isotope studies of granite and migmatite, Grenville province of Ontario, Canada. *Geochim. Cosmochim. Acta* **38**, 21–45.

Sommer M.A. and Rye D.M. (1978) Oxygen and carbon isotope internal thermometry using benthic calcite and aragonite foraminifera pairs. Short Papers of the 4th Inter. Conf., Geochron., Cosmochron., Isotope Geol., 1978, U.S. Geol. Surv. Open File Rep. **78-701**, 408–410.

Srikantappa C., Raith M. and Ackermand D. (1985) High-grade regional metamorphism of ultramafic and mafic rocks from the Archean Sargur Terrane, Karnataka, south India. *Precamb. Res.* **30**, 189–219.

Taylor H.P. (1977) Water/rock interactions and the origin of H_2O in granitic batholiths. *J. Geol. Soc. London* **133**, 509–558.

Thompson D.L. (1983) The nature of anorthosite-country rock interaction during granulite facies metamorphism. M.S. thesis, McMaster Univ.

Tuisku P. 1985. The origin of scapolite in the Central Lapland schist area, Northern Finland; preliminary results. *Geol. Surv. Finland Bull.* 331, 159–173.

Valley J.W. and O'Neil J.R. (1984) Fluid heterogeneity during granulite facies metamorphism in the Adirondacks: stable isotope evidence. *Contrib. Mineral. Petrol.* **85**, 158–173.

Valley J.W. (1986) Stable isotope geochemistry of metamorphic rocks. In *Stable Isotopes in High Temperature Geological Processes* (eds. J.W. Valley, H.P. Taylor Jr., O'Neil J.R.) Reviews in Mineralogy **16**, 445–489.

Vanko D.A. and Bishop F.C. (1982) Occurrence and origin of marialitic scapolite in the Humboldt Lopolith, N.W. Nevada. *Contrib. Mineral. Petrol.* **81**, 277–289.

von Breeman O., Davidson A., Loveridge W.D. and Sullivan R.W. (1986) U-Pb geochronology of Grenville tectonites, granulites and igneous precursors, Parry Sound, Ontario. In *The Grenville Province* (eds. J.M. Moore, A. Davidson, A.J. Baer) Geol. Assoc. Can. Spec. Pap. **31**, 191-207.

von Knorring O. and Kennedy W.Q. (1958) The mineral paragenesis and metamorphic status of garnet-hornblende-pyroxene-scapolite gneiss from Ghana (Gold Coast). *Min. Mag.* **31**, 846-859.

Wilkinson J.F.G. (1974) Garnet clinopyroxenite inclusions from diatremes in the Gloucester area, New South Wales, Australia. *Contrib. Mineral. Petrol.* **46**, 275-299.

Wilson A.F. and Baksi A.K. (1983) Widespread ^{18}O depletion in some Precambrian granulites of Australia. *Precamb. Res.* **23**, 33-56.

Wu T.-W. and Kerrich R. (1986) Combined oxygen isotope-compositional studies of some granitoids from the Grenville Province of Ontario, Canada: implications for source regions. *Can. J. Earth Sci.* **23**, 1412-1432.

CHAPTER VI

CONCLUSIONS

A systematic analysis of scapolite thermodynamic data, phase equilibria, mixing relations, and carbon isotope systematics has demonstrated the utility of scapolite in sensing fluid composition in a wide range of lithologies in high grade metamorphic settings. In addition to these aspects, which were completely lacking when the work was inititated, I believe the most important conclusions of this dissertation are the constraints placed on CO_2 activities (a_{CO_2}) in granulites and gneisses, and the scale of carbon isotope heterogeneity in the Central Gneiss Belt of the southwestern Grenville Province.

The calculation of a_{CO_2} in regional metamorphic granulites from the Grenville Province, the Furua Complex of Tanzania, the southern India granulite terrane, and the Bergen Arcs of Norway demonstrate that the a_{CO_2} is variable but generally less than 0.5. They are not consistent with a CO_2–fluid phase at the inferred peak conditions for granulite facies metamorphism for these terranes. If H_2O activities are correspondingly low, as has been inferred for most granulites, fluid absent metamorphism is likely, or a mixed CO_2–H_2O fluid is present. Calculation of a_{CO_2}, a_{H_2O}, and fugacities of C–O–H–S fluid species in the Furua Complex samples makes a strong case for fluid absent metamorphism for this complex, in which scapolite is widely developed, and for which carbonic fluid inclusions are reported. In contrast to these exhumed regional granulite settings, some deep crustal xenoliths from New South Wales, Tanzania, Lesotho, and W. Germany, yield a_{CO_2} significantly greater than 0.5, indicating a CO_2–rich fluid phase may be present. Likewise,

scapolite-bearing meta-anorthosite adjacent to marble and some scapolite calc-silicate gneisses from the Grenville Province indicate that a_{CO_2} was locally high (>0.5) and are consistent with the former presence of a CO_2-rich fluid. The scapolite-bearing meta-anorthosite may be an example of interaction of anorthosite with a CO_2-rich fluid, and small anorthosite plutons similar to the Whitestone Anorthosite should be targets for evaluation of fluid-rock interaction in other terranes. Although scapolite may be present in some granulites, its presence should not be taken as *a priori* evidence that a CO_2 fluid phase is present at the time of granulite facies metamorphism. As with the presence of biotite or hornblende and their implications for a_{H_2O}, carbonate scapolite requires a finite a_{CO_2}, but not the presence of a free fluid phase.

The second major contribution of this dissertation is the demonstration of the utility of scapolite in accurately recording $\delta^{13}C$, and the confirmation of previously observed regional carbon isotopic heterogeneity in a high grade terrane. Isotopic analysis of scapolite in meta-anorthosite indicates post-granulite metamorphic gradients in $\delta^{13}C$ and identification of mixing between two carbon isotopic reservoirs on a 100 m to km scale. Analysis of regional granulite facies gneisses yields a $10^{o}/_{oo}$ range in $\delta^{13}C$ across the Central Gneiss Belt (-1 to $-11^{o}/_{oo}$). This range precludes the large scale exchange and homogenization of carbon isotopic values that would be expected if pre-metamorphic fluids were flushed and replaced by an externally derived, CO_2-rich fluid. Although the range of values precludes identification of a distinct source of carbon in the gneisses, and determination of the timing for the introduction of carbon, the range of $\delta^{13}C$ overlaps that recorded in calc-silicates, marbles, and skarns from the same terrane. Thus, a source of carbon external to the terrane need not be invoked to account for the presence of carbon in these rocks.

Future studies should be directed at refining the thermodynamic calculations and making the isotopic measurements of this study more general. More restrictive experiments on the stability of end member meionite, evaluation of the

effects of Al–Si disorder on meionite stability, and direct experiments on activity–composition relations in carbonate–sulfate scapolites are needed for more accurate calculation of a_{CO_2} from scapolite equilibria. The major source of imprecision in the calculation of a_{CO_2} is the equilibration temperature of the silicate assemblage. As the activity model and meionite decarbonation reaction are highly temperature sensitive, these aspects should be refined as precisely as possible. More carbon (and sulfur) isotope analyses of scapolite granulites need to be made for the Grenville Province (detailed sampling of known localities and delineation of different occurrences) and from other terranes in order to further evaluate the scale of isotopic heterogeneity. These problems notwithstanding, it is anticipated that the major conclusions of this dissertation will stand.

APPENDIX 1

Sample Localities

Sample localities are taken from those plotted on maps published by the Canadian Department of Mines and Technical Surveys, Ottawa, Ontario, and on repository at the University of Michigan. Samples are designated by an upper case letter corresponding to the name of the map sheet used:

1:125,000 map sheets

A Algonquin
B Bobcaygeon
BA Bancroft
BI Byng Inlet
C Coniston
GL Golden Lake
H Huntsville
M Muskoka
MA Mattawa
NB North Bay
O Orillia
PS Parry Sound
S Sundridge
T Tomika

1:50,000 map sheets

PS Parry Sound
S Magnetawan (Magnetawan is sub-sheet of Sundridge 1:125,000)

Sample locality numbers without a year designation (e.g., 85A, 86B, 86E) were collected during the 1984 field season. Sample localities are given in terms of latitude and longitude (degrees, minutes ('), seconds (")), if plotted on the 1:125,000 series maps, or the northing-easting metric coordinate system for the 1:50,000 maps and for the Sudbury, Mattawa, and North Bay 1:125,000 maps. If a thin section was cut for the sample it is designated by a "+" in column 2, and mineral assemblages are compiled in Appendix 2. If no thin section was cut a subjective hand sample description of the sample is given. Most samples were collected from outcrops along Ontario highways, with the highway given in column 3. If the sample was collected off a main highway (e.g., along farm or logging roads), this is designated by a "-" sign followed by a brief description of where the road can be found relative to a main highway.

Locality Number	TS or lithology if TS not cut	Hwy	Latitude Northing	Longitude Easting
A1	+	60	45-30'-10"	78-00'-10"
A2	+	"	45-30'-40"	78-16'-00"
A3	+	"	45-33'-30"	78-17'-00"
A4	+	"	45-35'-00"	78-17'-00"
			East end Brewer Lake	
A5	+	"	0.5 km W of road to Opeongo L. dock and store	
A6	+	"	45-34'-10"	78-32'-20"
A7	+	"	45-32'-55"	78-39'-05"
B1	+	35	44-39'-20"	78-46'-20"
			Miners Bay road cut	
B2	+	"	44-50'-40"	78-46'-00"
B3	+	121	1 km E int Hwys 35 & 121	
B4	qz-fld gneiss	"	44-59'-50"	78-18'-45"
B5	+	"	44-59'-10"	78-17'-20"
			2.3 km N of Tory Hill	
B6	+	503	44-55'-30"	78-17'-15"
B7	+	121	44-58'-50"	78-37'-40"
B8	+	503	44-48'-40"	78-35'-40"
			"Shoe Tree" locality NE Kinmount	
B8-2	hbl meta-anorthosite	121	44-57'-00"	78-40'-00"
B9	calc-silicate	503	44-49'-00"	78-35'-00"
B10	+	"	44-50'-30"	78-33'-20"
B11	+	"	44-54'-30"	78-23'-40"
			1.5 km W. int Hwys 503 & 507	
B12	+	507	44-53'-55"	78-22'-40"
B13	bi metagabbro	-	44-53'-30"	78-21'-50"
			Side Rd to Trooper Lk.	
B14	+	503	44-56'-10"	78-18'-20"
B15	calc-silicate	648	44-59'-10"	78-13'-55"
			Int Hwys 648 & 121	
B16	amphibolite	"	44-59'-59"	78-13'-45"
B17	bi-qz-fld paragneiss	648	44-57'-40"	78-06'-40"
B18	+	"	44-57'-50"	78-07'-40"
B19	Amphibolite	"	44-58'-40"	78-06'-58"
B20	+	"	44-59'-20"	78-06'-50"
B21	calc-silicate	121	44-59'-20"	78-07'-30"
B22	di skarn	"	44-59'-20"	78-08'-00"
B23	+	"	44-59'-30"	78-08'-50"
B24	+	"	44-59'-10"	78-11'-45"
B25	+	"	44-59'-00"	78-13'-00"
B26	+	648	44-59'-00"	78-14'-15"
B27	+	"	44-58'-40"	78-14'-30"
B28	+	"	44-58'-43"	78-15'-20"
B29	+	"	44-58'-40"	78-14'-40"
B30	actin skarn	-	44-58'-00"	78-17'-35"
			Rd W. of 121, N. of McCue Lk.	
B31	+	-	44-57'-30"	78-16'-55"
B32	+	507	44-54'-05"	78-22'-50"
B33	+	"	44-53'-20"	78-22'-50"

B34	calc-silicate	"	44-53'-05"	78-23'-25"
B35	gt-bi meta-pelite, marble, metagabbro		44-52'-40"	78-23-30"
BAcrg	+	-	45-18'-00"	77-35'-50"
			Craigmont Quarry, York R.	
BA1	+	-	45-15'-30"	77-58'-55"
			S. shore Baptiste Lk., NW Bancroft	
BA2	+	127	45-15'-35"	77-58'-00"
BA3	+	"	45-14'-55"	77-56'-50"
BA4	+	523	45-20'-00"	77-56'-35"
BA5	+	"	45-29'-00"	77-56'-20"
BA6	+	-	45-24'-15"	77-35'-50"
BA7	+	62	45-25'-40"	77-39'-55"
BA8	+	"	45-26'-40"	77-39'-55"
BA9	+	"	45-27'-00"	77-40'-20"
BA10	+	"	45-27'-30"	77-40'-00"
BA11	amphibolite		45-20'-00"	77-35'-50"
BA12	syenite		45-23'-15"	77-29'-00"
BA13	qz-fld gneiss		45-23'-15"	77-29'-55"
BA14	+		45-07'-20"	77-52'-00"
BA15	+		45-27'-55"	77-23'-30"
BA16	+		45-27'-05"	77-23'-25"
BA17	+		45-26'-30"	77-22'-25"
BA18	+		45-26'-30"	77-19'-50"
BA19	+		45-19'-00"	77-23'-10"
BA20	+		45-18'-35"	77-30'-00"
BI1	granite orthogneiss		See Tucillo, M.E., M.S. thesis,	
BI2	gt orthogneiss		Univ. Michigan, for locations of BI samples	
BI3	+			
BI4	+			
BI5	grey qz-fld gneiss			
BI6	pink qz-fld gneiss			
BI7	+			
BI8	gt paragneiss			
BI9	gt paragneiss			
BI10	gt paragneiss			
BI11	gt paragneiss			
BI12	gt orthogneiss			
BI13	gt orthogneiss			
BI14	pink qz-feld gneiss			
BI15	grey paragneiss			
BI16	pink qz-feld gneiss			
BI17	pink qz-feld gneiss			
BI18	pink qz-feld gneiss			
BI19	pink qz-feld gneiss			
BI20	pink qz-feld gneiss			
BI21	pink qz-feld gneiss			
BI22	pink qz-feld gneiss			
BI23	pink qz-feld gneiss			
BI24	pink qz-feld gneiss			
BI25	+			
BI26	gt grey paragneiss			
BI27	gt grey paragneiss			

BI28	gt grey paragneiss			
BI29	gt grey paragneiss			
BI30	gt grey paragneiss			
BI32	+			
BI34	+			
BI35	+			
BI36	+			
BI37	gt granulite			
BI38	gt granulite			
BI39	+			
BI40	+			
C1	+	17	5150500	531500
GL1	metagabbro	60	45-30'-35"	77-56'-15"
GL2	gt paragneiss	"	45-31'-30"	77-53'-30"
GL3	+	"	45-31'-35"	77-53'-00"
GL4	gt bi metagabbro	"	45-32'-10"	77-52'-20"
GL5	+	"	45-32'-15"	77-51'-55"
GL6	+	"	45-32'-25"	77-51'-40"
GL7	amphibolite	"	45-32'-15"	77-51'-15"
GL8	+	"	45-30'-15"	77-45'-30"
GL9	amphibolite	"	45-30'-05"	77-43'-50"
GL10	amphibolite	"	45-30'-30"	77-33'-20"
GL11	amphibolite	"	45-30'-00"	77-33'-05"
GL12	amphibolite	"	45-30'-10"	77-31'-40"
GL13	+	62	45-47'-40"	77-11'-00"
GL14	+	"	45-47'-50"	77-10'-15"
GL15	orthogneiss	"	45-47'-50"	77-10'-05"
GL16	+	"	45-47'-05"	77-11'-00"
GL17	granitic orthogneiss	"	45-36'-55"	77-30'-45"
GL18	amphibolite	"	45-37'-15"	77-28'-40"
GL19	orthogneiss	-	45-37'-35"	77-24'-00"
			Side Rd off 60 from Deacon	
GL20	amphibolite	512	45-37'-15"	77-30'-45"
			Side Rd off 512 E. of Killaloe Sta.	
GL21	+	-	45-32'-30"	77-30'-45"
GL22	charnockitic gneiss	-	45-32'-35"	77-30'-45"
GL23	calc-silicate	512	45-31'-05"	77-30'-45"
GL24	bi metagabbro	62	45-36'-05"	77-30'-45"
GL25	+	62	45-46'-45"	77-14'-10"
GL26	+	40	45-44'-20"	77-00'-20"
GL27	+	17	45-44'-00"	77-00'-00"
			Int. 17 and 40	
GL28	+	60		
H1	+	35	45-18'-35"	78-59'-25"
H2	+	"	45-17'-50"	78-58'-35"
H3	amphibolite	"	45-16'-45"	78-53'-40"
H4	+	"	45-15'-10"	78-54'-10"
			Int. 35 and 117	
H5	+	117	45-15'-10"	78-56'-40"
H6	+	35	45-00'-45"	78-42'-10"
H7	+	118	45-06'-30"	78-35'-55"
H8	gt amphibolite	"	45-06'-00"	78-35'-40"
H9	+	121	45-02'-30"	78-29'-10"

H10	+	"	45-02'-05"	78-27'-30"
H11	+	"	45-01'-35"	78-23'-25"
H12	+	-	45-00'-40"	78-26'-05"
			Side rd. off 121 to Blue Hawk Lk.	
H13	+	121	45-02'-05"	78-27'-15"
H14	+	648	45-03'-30"	78-04'-40"
H15	+	127	45-18'-50"	78-02'-30"
H16	+	"	45-21'-25"	78-04'-20"
H17	+	"	45-23'-10"	78-05'-35"
H18	+	"	45-24'-40"	78-07'-58"
H19	+	"	45-26'-30"	78-10'-25"
H20	+	"	45-26'-50"	78-10'-35"
H21	gt paragneiss	"	45-27'-15"	78-11'-05"
H22	+	"	45-27'-35"	78-11'-25"
H23	+	648	45-00'-25"	78-13'-00"
H24	+	"	45-02'-30"	78-13'-50"
H25	sample lost	-	45-05'-40"	78-08'-25"
			Side rd. off 648 N. of Mumford	
H26	sample lost	-	45-06'-00"	78-08'-25"
H27	hbl metagabbro	60	45-29'-30"	78-02'-10"
H28	hbl metagabbro	"	45-28'-40"	78-05'-30"
H29	amphibolite	"	45-29'-50"	78-11'-05"
H30	metagabbro	"	45-29'-35"	78-12'-00"
H31	flat charn gneiss	"	45-29'-20"	78-12'-30"
H32	gt paragneiss	"	45-28'-25"	78-46'-30"
H33	flat charn gneiss	"	45-25'-30"	78-50'-15"
H34	flat charn gneiss	"	45-22'-45"	78-55'-05"
H35	flat charn gneiss	"	45-20'-35"	78-56'-25"
H36	calc-sil, amphib	35	45-17'-10"	78-56'-20"
H37	+	"	45-15'-40"	78-53'-50"
H38	calc-silicate	"	45-12'-30"	78-52'-40"
H39	charnockitic gneiss	"	45-07'-50"	78-50'-25"
H40	+	118	45-02'-10"	78-45'-50"
			New rd., not on old Haliburton sheet	
MPI	+	-	45-01'-15"	79-45'-40"
M-0	+	-	45-01'-25"	79-46'-50"
			Side rd. off 69 to Gibson Ind. Res.	
M1	+	69	45-02'-00"	79-46'-30"
M2	+	"	45-02'-35"	79-46'-45"
M3	+	-	45-03'-45"	79-48'-30"
			Side rd. W. off 69 picnic site	
M4	pink qz fld gneiss	69	45-04'-05"	79-46'-55"
M5	gt qz fld migmatite	169	45-06'-05"	79-36'-45"
M6	+	7	45-06'-30"	79-35'-35"
M7	paragneiss	"	45-07'-45"	79-39'-15"
M8	+	"	45-08'-25"	79-40'-00"
M9	+	"	45-10'-25"	79-39'-20"
M10	+	"	45-08'-55"	79-39'-50"
M11	gt migmatite	141	45-16'-10"	79-39'-15"
M12	gt migmatite	"	45-16'-25"	79-40'-15"
M13	+	"	45-16'-30"	79-40'-10"
M14	+	"	45-17'-20"	79-44'-15"
M15	+	"	45-16'-55"	79-45'-45"
M16	gt charnockite	69	45-16'-25"	79-50'-00"
M17	+	"	45-15'-30"	79-49'-35"
M18	+	"	45-17'-25"	79-50'-55"

M19	+	"	45-17'-40"	79-51'-40"
M20	+	"	45-17'-32"	79-51'-50"
M21	metagabbro	"	45-17'-35"	79-52'-00"
M22	+	"	45-17'-55"	79-52'-20"
M23	+	"	45-18'-05"	79-52'-25"
M24	mafic granulite	"	45-18'-25"	79-54'-00"
M25	mafic granulite	"	45-18'-25"	79-57'-45"
M26	mafic granulite	"	45-18'-25"	79-56'-05"
M27	mafic granulite	"	45-18'-40"	79-58'-40"
M28	mafic granulite	"	45-20'-00"	79-59'-30"
M29	gt amphibolite	518	45-20'-00"	79-59'-50"
M30	gt amphibolite	"	45-20'-00"	79-58'-20"
M31	gt amphibolite	"	45-20'-00"	79-57'-55"
M32	+	"	45-20'-20"	79-56'-20"
M33	amphibolite	"	45-20'-25"	79-55'-20"
M34	+	"	45-20'-45"	79-54'-50"
M35	charnockitic gneiss	"	45-21'-45"	79-52'-20"
M36	orthogneiss	"	45-22'-00"	79-51'-15"
M37	gt charnock gneiss	"	45-22'-15"	79-49'-30"
M38	+	-	45-23'-30"	79-47'-00"
			Rd. north from Orrville to McKellar	
M39	gt amphibolite	-	45-24'-20"	79-47'-15"
M40	amphibolite	-	45-24'-25"	79-47'-55"
M41	+	-	45-25'-40"	79-48'-30"
M42	gt migmatite	-	45-26'-50"	79-51'-15"
M43	charnockitic gneiss	-	45-27'-30"	79-51'-35"
M44	gt migmatite	-	45-28'-25"	79-51'-50"
M45	+	-	45-29'-30"	79-51'-55"
M46	gt charnock gneiss	-	45-29'-40"	79-52'-00"
M47	gt bi migmat. gneiss	124	45-28'-55"	79-56'-25"
M48	+	"	45-57'-30"	79-47'-15"
M49	bi-gt paragneiss	-	45-27'-05"	79-13'-00"
			Side rd off 592 & 11 Novar	
M49a	+	124	45-28'-00"	79-59'-25"
M50	paragneiss	11	45-23'-05"	79-01'-00"
M51	+	"	45-25'-30"	79-14'-15"
M52	gt bi paragneiss	"	45-27'-05"	79-13'-30"
M53	+	"	45-31'-50"	79-19'-10"
			On Sundridge 1:125,000 sheet	
			Outcrop S. of MOT garage S. of Emsdale	
M54	+	"	45-33'-10"	79-20'-30"
M55	gt paragneiss	60	45-20'-20"	79-11'-10"
M56	gt bi paragneiss	"	45-20'-30"	79-10'-35"
M57	+	"	45-20'-30"	79-10'-10"
M58	+	"	45-20'-40"	79-09'-30"
M59	gt paragn, calc-sil	"	45-21'-30"	79-08'-15"
M60	gt charnock gneiss	"	45-21'-50"	79-06'-45"
M61	gt charnock gneiss	"	45-21'-20"	79-04'-25"
M62	gt charnock gneiss	"	45-20'-50"	79-20'-20"
M63	gt charnock gneiss	"	45-20'-00"	79-01'-00"
M64	gt charnock gneiss	117	45-12'-30"	79-02'-05"
M65	gt charnock gneiss	"	45-11'-30"	79-04'-15"
M66	gt charnock gneiss	"	45-09'-05"	79-06'-35"
M67	gt charnock gneiss	2	45-16'-20"	79-10'-45"
M68	gt grey paragneiss	"	45-17'-40"	79-12'-00"
M69	gt charnock gneiss	11	45-20'-20"	79-13'-45"

M70	gt charnock gneiss	3	45-17'-20"	79-20'-30"
M71	+	"	45-17'-30"	79-23'-25"
M72	gt granulite	"	45-17'-15"	79-24'-20"
M73	paragneiss	"	45-16'-30"	79-25'-20"
M74	calc-sil, paragneiss	141	45-14'-40"	79-36'-10"
M75	gt bi paragneiss	"	45-13'-20"	79-30'-30"
M76	gt bi paragneiss	"	45-12'-55"	79-30'-15"
M77	pink/grey paragneiss	"	45-13'-20"	79-27'-20"
M78	gt calc-silicate	"	45-10'-50"	79-25'-00"
M79	pink fld hbl gneiss	"	45-10'-50"	79-21'-00"
M80	+	11	45-12'-55"	79-18'-30"
M81	+	"	45-12'-30"	79-18'-25"
M82	gt calc-silicate	"	45-10'-20"	79-18'-45"
M83	charnockitic gneiss	118	45-02'-35"	79-20'-30"
M84	gt charnock gneiss	"	45-03'-30"	79-24'-20"
M85	gt calc-silicate	"	45-03'-30"	79-24'-35"
M86	orthogneiss	"	45-03'-40"	79-26'-10"
M87	granitic orthogneiss	"	45-04'-00"	79-27'-50"
M88	+	"	45-04'-30"	79-28'-30"
M89	+	"	45-50'-25"	79-29'-20"
M90	charn. orthogneiss	"	45-06'-00"	79-30'-20"
M91	granitic orthogneiss	"	45-06'-25"	79-33'-30"
MA-0	+	17	5126000	656100
MA1	gt amphibolite	"	5127600	666100
MA2	gt amphibolite	"	5128200	669600
MA3	+	"	5128300	670000
MA4	+	"	5128500	671050
MA5	orthogneiss, metagab	"	5131300	678100
MA6	amphibolite	"	5130800	684900
MA7	+	"	5128400	691750
MA8	bi hbl orthogneiss	"	5127500	694390
MA9	gt amphibolite	"	5128400	699850
MA10	gt amphib, orthogn	"	5125400	706250
MA11	orthogneiss	533	5132300	676000
MA12	gt amphibolite	"	5142400	660200
MA13	amphibolite	"	5144550	657500
MA14	gt amphibolite	"	5147550	657300
MA15	+	"	5150900	655700
NB1	gt metagabbro	11	5128500	620800
NB2	gt amphibolite	17	5128750	621900
NB3	no sample			
NB4	gt amphibolite	"	5128700	622800
NB5	ep amphibolite	583	5150500	620800
NB6	hbl di mafic gneiss		5135300	628400
			Side rd. E. of Feronia	
NB7	amphibolite	17	5127100	628000
NB8	gt amphibolite	17	5126300	631500
NB9	gt amphibolite	17	5126000	632500
NB10	gt amphibolite	17	5125750	633700
NB11	gt orthogneiss	17	5125600	635700
NB12	gt orthogneiss	-	5120300	640600
			Rd W. of Bonfield along L. Nosbonsing	
NB13	gt amphibolite	-	5122500	637900
			Rd N. of L. Nosbonsing	

NB14	pink gt orthogneiss	17	5126200	632500
NB15	pink gt orthogneiss	-	5127500	633700
			Rd N. of Astorville, L. Nosbonsing	
NB16	pink gt orthogneiss	654	5115400	624250
NB17	grey gt orthogneiss	654	5116000	623500
NB18	pink orthogneiss	-	5114700	618000
			Rd. off 654 N. to Deepwater Pt.	
NB19	amphibolite	-	5115450	615600
			Rd N. of & // to 654	
NB20	pink paragneiss	654	5112500	615400
NB21	amphibolite	654	5110900	616000
NB22	gt orthogneiss	534	5105700	615400
NB23	gt amphibolite	-	5090100	619050
			Side Rd E. of Storie	
NB24	cpx gt orthogneiss	-	5106300	630450
			Side Rd. NE. of Powasson	
NB25	gt orthogneiss	11	5108100	626350
NB26	gt orthogneiss	"	5100300	628250
NB27	+	"	5121600	625300
NB28	+	"	5112800	626750
NB29	+	"	5111000	626650
NB30	+	-	5104100	631000
			Side rd. due E. of Powasson	
NB31	gt orthogneiss	-	5109050	639100
			Side rd NE. of Chiswick	
01	granitic orthogneiss	69	44-46'-10"	79-41'-20"
02	granitic orthogneiss	"	44-47'-15"	79-42'-00"
03	grey gneiss	"	44'47'-55"	79-42'-50"
04	granitic orthogneiss	"	44-48'-15"	79-44'-05"
05	pink/grey mig paragn	501	44-48'-30"	79-45'-25"
06	+	69	44-50'-25"	79-44'-20"
07	+	"	44-52'-05"	79-44'-30"
08	+	"	44-52'-30"	79-44'-50"
			Rd cut bridge over Go Home Lk	
09	+	-	44-52'-50"	79'41'-50"
			Rd E. from 69 to Severn Falls	
010	+	-	44-53'-20"	79-38'-00"
011	+	"	44-58'-20"	79-46'-20"
			side rd 0.75 km S. of Gibson R. bridge	
012	na	"	44-58'-00"	79-46'-25"
			side rd 1.5 km S. of Gibson R. bridge	
013	+	"	44-57'-10"	79-46'-40"
014	+	"	44-57'-05"	79-46'-20"
015	+	"	44-55'-00"	79-46'-20"
016	+	"	44-55'-30"	79-46'-20"
017	+	"	44-56'-15"	79-46'-20"
PS1	+	124	45-26'-45"	80-01'00"
PS2	+	"	45-26'-20"	80-01'30"
PS3	+	"	45-24'-40"	80-01'15"
PS4	gt amphibolite	69	45-20'-30"	80-00'20"
PS5	+	"	45-20'-40"	80-00'30"
			Int. 69 south & 69B	
PS6	+	-	45-19'-25"	80-01'-30"
			Rd. from Parry Sound to Parry Is.	

PS7	+	-	45-20'-30"	80-02'-20"
PS8	+	-	45-20'-30"	80-04'-00"
			Rd from mainland to Parry Is, at town of Parry Island (Ind. Res.)	
PS9	+	69	45-21'-30"	80-20'-30"
			Int 69 north & 69B, GAC/MAC trip stop 1-1	
PS10	gt migmatite	69	45-24'-00"	80-03'-45"
PS11	granitic gneiss	"	45-20'-30"	80-06'-50"
			Int. 69 & rd. to Killbear Prov. Pk.	
PS12	granitic gneiss	-	45-26'-50"	80-10'-30"
			Rd. to Killbear Prov. Pk.	
PS13	+	-	45-25'-00"	80-14'-05"
PS14	+	-	45-23'-30"	80-14'-45"
PS15	granitic gneiss	-	45-24'-50"	80-15'-00"
PS16	+		45-28'-30"	80-10'-30"
S1	+	-	45-30'-30"	79-52'-30"
			Side rd. E. of McKellar	
S2	+	124	45-33'-10"	79-55'-20"
S3	+	"	45-33'-30"	79-55'-20"
S4	+	"	45-34'-15"	79-55'-05"
S5	mafic gneiss	"	45-35'-05"	79-54'-20"
S6	mafic gneiss	"	45-35'-20"	79-54'-20"
S7	gt migmatite	"	45-37'-45"	79-52'-45"
S8	gt granite gneiss	"	45-38'-30"	79-51'-40"
S9	pink paragneiss	"	45-36'-20"	79-53'-30"
S10	gt amphib, gt paragn	"	45-48'-30"	79-55'-30"
S11	gt grey gneiss	522	45-55'-05"	79-57'-00"
S12	mylon. gt gneiss	"	45-54'-20"	79-55'-40"
			Side rd. S. from Arnstein	
S13	gt orthogneiss	522	45-58'-30"	79-37'-40"
S14	+	"	45-59'-00"	79-38'-35"
S15	+	"	45-58'-30"	79-39'-30"
S16	gt, ep amphibolite	"	45-55'-05"	79-49'-50"
S17	amphibolite	"	45-57'-00"	79-46'-00"
S18	gt amphibolite	"	45-58'-00"	79-42'-35"
S19	+	"	45-58'-10"	79-42'-10"
S20	+	"	45-58'-50"	79-39'-40"
S21	mafic gneiss	11	45-56'-45"	79-21'-55"
S22	gray orthogneiss	"	45-54'-40"	79-22'-00"
S23	+	"	45-52'-45"	79-22'-30"
S24	bi orthogneiss		45-49'-35"	79-28'-10"
			Rd from S. River to Mikiskew Prov. Pk.	
S25	gt bi orthogneiss	11	45-45'-30"	79-25'-05"
S26	+	"	45-44'-35"	79-26'-25"
S27	gt orthogneiss	"	45-44'-35"	79-26'-10"
S28	calc-sil, paragneiss	"	45-37'-45"	79-24'-50"
S29	+	"	45-36'-00"	79-22'-40"
S30	+	592	45-30'-25"	79-16'-20"
S31	+	518	45-32'-35"	79-15'-35"
			Rd. to Kearyney form 11, Emsdale	
S32	+	"	45-34'-20"	79-09'-45"
S33	gt grey paragneiss	"	45-34'-50"	79-07'-55"
S34	+	"	45-35'-00"	79-07'-45"
S35	gt bi orthogneiss	124	45-43'-15"	79-31'-45"

S36	bi orthogneiss	"	45-42'-30"	79-35'-35"
S37	gt amphibolite	"	45-39'-20"	79-49'-00"
S38	gt meta-anorth	"	45-39'-05"	79-50'-50"
			Int. Hwys 124 & 520 E. Dunchurch	
S39	gt orthogn, amphibol	520	45-39'-20"	79-50'-40"
S40	gt metagabbro	"	45-41'-00"	79-51'-15"
S41	+	"	45-41'-30"	79-51'-50"
S42	+	"	45-41'-50"	79-53'-20"
S43	gt metagabbro		45-39'-10"	79-50'-00"
SD1	gt orthogneiss	69	5094100	533450
SD2	gt paragneiss	"	5094700	533100
SD3	qz-feld gneisss	-	5093400	530000
			Rd W. of 69 Bigwood	
SD4	qz-feld gneisss	-	5093400	529000
SD5	qz-feld gneisss	-	5093400	528800
SD6	qz-feld gneisss	-	5093400	527300
SD7	qz-feld gneisss	-	5093400	526500
SD8	qz-feld gneisss	-	5093300	524800
SD9	gt amphibolite	-	5101600	531500
			Rd to Bigwood Bay, S. of 607	
SD10	grey paragneiss	64	5105000	532500
SD11	gt amphibolite	"	5105700	534700
SD12	migmatitic gneiss	"	5106000	543900
SD13	hbl orthogneiss	"	5110900	546400
SD14	amphibolite	-	5111200	546800
			Rd to Bear Lk. NW of 64	
SD15	orthogneiss	64	5109900	547900
SD16	amphibolite	535	5118500	543800
SD17	gt amphibolite	"	5126200	543700
SD18	calc-silicate	-	5134300	538100
			Rd W. of 535 St. Charles	
SD19	gt amphibolite	-	5134300	534000
SD20	bi amphibolite	17	5144600	544000
SD21	gt amphibolite	"	5146600	537000
SD22	gt metagabbro	"	5147100	535800
SD23	gt amphibolite	"	5146600	516800
SD24	gt amphibolite	537	5139200	517800
SD25	amphibolite	"	5134100	513200
SD26	amphibolite	17	5116900	517500
SD27	gt metagabb, orthogn	64	5112200	551350
SD28	gt hbl meta-anor	-	5113900	556400
			Rd. E of N. Monetville	
SD29	hb bi orthogneiss	64	5117900	553100
SD30	gt bi orthogneiss	"	5126300	561100
SD31	amphibolite	"	5128500	559000
SD32	amphibolite	"	5129000	634000
SD33	grey paragneiss	"	5136000	567300
SD34	gt amphibolite	-	5140200	570300
			Dirt Rd on farm N. of 17	
SD35	calc-silic, amphib	-	5175100	551000
SD36	grey qz fld gneiss	539	5145200	554150
SD37	meta-ultramafite	"	5148150	555250
SD38	di amphibolite	"	5148400	555300
SD39	bi gt orthogneiss	"	RR cut 1 km SE River Valley	
SD40	orthogneiss	64	between River Valley & Field	

T1	gt metabasite	64	5168600	581950
T2	hbl orthogneiss	11	5171500	594400
T3	bi metasyenite	-	5151000	617750
			Rd to Tomiko, NW of Hwy 11	
T4	+	533	5152500	655000
T5	gt amphibolite	"	5153250	645600
T6	gt amph, musc paragn	63	5151950	641650
WSA1	+	-	Same locality as S86E-25 series	

Sept. 1985 field trip with A. Davidson

A85A-1	+	60	E. boundary of Algonquin park, 2.7 km east of "East Gate".
A85A-2	+	"	8.7 km east of stop 3-5, GAC/MAC trip
A85A-3	+	"	Same locality as GAC/MAC trip, stop 3-5.
H85A-1	+	35	Stop 2-9, GAC/MAC trip: Dragon's Head
M85A-1	+	11	45-12'-55" 79-18'-30" Int 11 & 141 W. to Parry Sound
M85A-2	calc-silicate	118	45-04'-00" 79-27'-50"
M85A-3	+	"	45-06'-20" 79-35'-25" Int. 118 and Muskoka Rd. 7
M85A-4	+	M7	Same location as M8
M85A-5	+	M38	45-01'-00" 79-40'-45"
M85A-6	+	"	45-01'-25" 79-45'-40"
M85A-7	meta-ultramafite	-	45-08'-25" 79-31'-40" Rt. 25 S. of Windemere on Roseau Lk.
PS85A-0	+	69	45-18'-35" 79-58'-30"
PS85A-1	+	"	45-23'-20" 80-03'-15"
PS85A-2	+	"	45-21'-30" 80-02'-10" Hwy 69 road cut N. of Parry Sound Stop 1-1, GAC/MAC field trip
PS85A-3	+	-	45-21'-45" 80-01'-10" Mill Lake Quarry
PS85A-4	+	-	45-19'-40" 80-02'-00" Stop 1-2, GAC/MAC field trip
PS85A-5	+	-	45-18'-45" 80-02'-20" Emily St., SE. of Parry Sound
PS85A-6	+	-	45-19'-15" 80-01'-50"
PS85A-7	+	-	45-20'-20" 80-01'-00"
PS085A-8	+	-	45-21'-45" 80-01'-10"
S85A-1	+	124	45-27'-50" 80-05'-30" GAC/MAC field trip stop 2-1
S85A-2	+	"	45-34'-15" 79-55'-00"
S85A-3	+	-	45-38'-50" 79-53'-50" Farley's side Rd off 124
S85A-4	+		45-39'-40" 79-47'-40"

May 1986 GAC/MAC granulite field trip. See guidebook for locations.

A86B3-3a	+	60	Day 3, stop 3-3, Hwy 60, Algonquin Park.

A86B3-5a	+	"	Day 3, stop 3-5, Hwy 60, Algonquin Park.
H86B2-6	+	11	Day 2, stop 2-6, Hwy 11
PS86B1-1	+		Day 1, stop 1-1, Hwy 69 road cut.
PS86B1-2	+		" "
PS86B1-3	+		" "
PS86B1-4	+		" "
PS86B1-5	+		" "
PS86B1-6	+		" "
PS86B1-7	+		" "
PS86B1-8	+		" "
PS86B1-11	+		" "
PS86B2-1	+		Day 1, stop 1-2, Boat Works, Emily St.
PS86B2-2	+		" "
PS86B2-3	+		" "
PS86B2-4	+		" "

Sept. 1986 field trip with M.A. Cosca.

M86E-1	+	11	45-18'-20"	79-14'-45"
PS86E-1	gt amphibolite	17	45-14'-35"	79-48'-45"
			Muskoka 1:125,000 map	
PS86E-2	amphib, mafic gran	69	5021500	578850
			Int. 69 S. and 69B.	
PS86E-3	amph, maf & fels gne	"	5022350	577700
			Long outcrop on 69 S. of McDougal St.	
PS86E-4	+	"	5022900	577500
PS86E-5	mafic, gran gneiss		5023350	577100
PS86E-6	+	"	5023500	577750
PS86E-7	+	"	5023200	575500
			Series of samples along 69 road cut	
PS86E-8	+	-	5024550	576300
			Mill Rd. betw 69 and 124	
PS86E-9	hbl gt meta-anorth	-	5025050	577450
			Limbert Rd. off Mill Rd.	
PS86E-10	+	-	5025500	576050
			Mill Rd.	
PS86E-11	grey flat paragneiss	-	5026150	576200
			Mill Rd.	
PS86E-12	+	-	5026950	577450
			Burnside Rd. E. off int 124 & Mill Rd.	
PS86E-13	gt ep meta-anorth	-	5026450	526450
			Burnside Rd.	
PS86E-14	gt amphibolite	124	5028150	576300
PS86E-15	+	-	5033050	577200
			Long Lk. Estates Rd.	
PS86E-16	+	-		
			Long Lk. Estates Rd.	
PS86E-17	+	-	5032350	577650
			Long Lk. Estates Rd., Ferguson res.	
PS86E-18	gt cpx amphibolite	124	5033700	576950
PS86E-19	+	"	5034150	577450
PS86E-20	+	-	5075450	577700
			Rd. to Ardberg off 124	

PS863-21	+	-	5035600	577700
PS86E-22	+	-	5036300	577850
PS86E-23	+	-	5037000	577750
PS86E-24	+	-	5037800	577350
			Sample series at W. margin WSA	
PS86E-25	gt amphibolite	-	5038750	576550
PS86E-26	+	69	5023600	574950
PS86E-28	+	"	5025250	574500
PS86E-30	+	"	5026200	574100
PS86E-31	+	"	5027350	573600
PS86E-32	+	-	5018500	574450
			Rd. W. of bridge to Parry Is.	
PS86E-33	+	-	5018200	575050
			Outcrop just E. of bridge to Parry Is.	
PS86E-34	+	-	5022100	576300
			Dam, Sequin R. Cascade St.	
S86E-1	+	520	5061150	585600
S86E-2	gt orthgneiss	"	5060900	586550
S86E-3	gt amphibolite	"	5060900	586500
S86E-4	+	"	5060900	587600
S86E-5	+	-	5059100	587800
			Whitestone Lk. Rd., W. off 520	
S86E-7	+	520	5057100	590300
S86E-8	+	-	5053700	585750
			W. off 124 on Farley's side road	
S86E-9	gt orthogneiss	-	5053450	587400
			10 -17, S. arms of Whitestone Lk.	
S86E-10	+	-	5055100	585200
S86E-11	+	-	5055250	585400
S86E-12	+	-	5055250	585600
S86E-13	+	-	5055400	586250
S86E-14	+	-	5055350	586500
S86E-15	+	-	5055300	586650
S86E-16	+	-	5055300	587200
S86E-17	+	-	5055325	587300
S86E-18	+	124	5043050	583950
S86E-19	+	-	5053450	587400
			Int. 124 & Farley side rd.	
S86E-20	+	-	5055400	587875
S86E-21	+	-	5055400	588400
S86E-22	+	-	5055400	588300
S86E-23	+	-	5055750	587850
S86E-24	+	-	5056000	587800
S86E-25	+	-	5056700	587675
S86E-26	+	-	no sample	
S86E-27	+	-	5056900	587900
S86E-28	+	-	5057300	588300
S86E-29	gt metadiorite	-	5057500	588600
S86E-30	cpx metadiorite	-	5057650	588900
S86E-31	+	-	5057000	587650
S86E-32	+	-	5057050	587600
S86E-33	+	-	5057000	587500
S86E-34	+	-	5057000	587250
S86E-35	+	-	5057150	587150
S86E-36	+	-	5057100	586850

S86E-37	+	-	5057050	586750
S86E-38	+	-	5056900	586500
S86E-39	+	-	5056850	586150
S86E-40	+	-	5056000	585800
S86E-41	+	-	5056600	585550
S86E-42	+	-	5056650	585600
S86E-43	+	-	5056650	584800
S86E-44	+	-	5056600	684350
S86E-45	+	-	5056450	584100
S86E-53	+	11	See M53 locality	

APPENDIX 2

Mineral Assemblages

Abbreviations

X	Phase present
S	Secondary or retrograde
Al	Allanite
Am	Amphibole (Hornblende unless otherwise noted)
A	Actinolite
C	Cummingtonite
H	Hornblende
Ap	Apatite
Bi	Biotite
Cc	Calcite
Ch	Chlorite
Cpx	Clinopyroxene
Do	Dolomite
Ep	Epidote
Gr	Graphite
Gt	Garnet
Kf	K-feldspar
M	Microcline
P	Perthite
Ky	Kyanite
Mu	Muscovite
Ne	Nepheline
Ol	Olivine
Opx	Orthopyroxene
Ox	Oxide
M	Magnetite
I	Ilmenite
Ne	Nepheline
Pg	Plagioclase
Qz	Quartz
Ru	Rutile
Sc	Scapolite
Serp	Serpentine
Sf	Sulfide
Py	Pyrite
Po	Pyhrrotite
Si	Sillimanite
Sp	Spinel
Ti	Titanite
Wo	Wollastonite
Zc	Zircon

1:125,000 map sheets

A	Algonquin
B	Bobcaygeon
BI	Byng Inlet
C	Coniston
GL	Golden Lake
H	Huntsville
M	Muskoka
MA	Mattawa
NB	North Bay
O	Orillia
PS	Parry Sound
PSO	
S	Sundridge
T	Tomika

PS86E Parry Sound 1:50,000

S86E Magnetawan 1:50,000

Sample	Sc	Qz	Pg	Gt	Kf	Opx	Cpx	Am	Bi	Cc	Ox	Sf	Ti	Ap	Other
ARM4	X	X	X	X				X	X	S	X	X		X	
A1a			X	X		X	X	X	X		X			X	
A1b			X					X	X		X				
A2a		X	X	X	M,P	X			S					X	
A2b		X	X	X	M	X	X	X	X					X	Zc
A2c		X	X	X	M	X	X	X	X		X			X	
A2d		X	X			X		X	X						
A3a		X	X	X		X	X	X	X					X	
A3b		X	X	X	P				X						
A3c		X	X			X	X		X		X			X	Zc
A4a		X	X			X	X	X			X			X	
A4a		X	X			X	X	X							
A5a			X	X		X	X	X	X						Ol
A5b			X	X		X	X	X	X		X			X	
A6a		X	X	X			X	X	X			Py		X	Ru,Zc
A6b		X	X	X	P	X			S						
A6c		X	X	S	M,P				S		M	Py			
A7a		X	X			X	X	X			X			X	
A85A-1	X	X					X			X		Py	X		
A85A-2			X			X		X			X				
A85A-2b		X	X			X	X	X	X						
A85A-3a	X	X	X	X	M		X			X			X		Wo
A85A-3b	X	X	X	X			X			S		Py	X	X	
A85A-3c	X	X					X			X			X		
A85A-3d	X	X	X	X			X						X		Gr
A85A-3e	X	X		X			X			X			X		
A86A-3f	X	X	?	X			X			X			X		Wo
A86B3-5a	X	X	X	X			X			X			X		Wo
A86B3-3a	X		X			X	X	X	X					X	
A86B3-3b			X	X		X	X	X	X					X	
A86B3-3c	X		X			X	X	X	S	S	X			X	
B1a									X	X				X	
B1c		X	X		M			X	X				X		
B2b		X	X		M		X			X			X		
B2c		X	X		M	X				S	X		X		Zc
B3a		X	X		M		X			X				X	
B5			X		P		X		X	X					
B6a								X	X	X					
B6b		X	X		M			X	X	X					
B7a	X		X						X	S				X	
B7b	X		X						X					X	
B8b	X		?		X		X			X					
B9a		X	X				X	X					X		
B10	X	X			M		X		X	X					Gr
B11	X	X	X		M		X			X					
B12		X	X				X	X							
B14b		X	X		M,P								X	X	
B18a		X	X	X	M				X						Zc
B20			X		M		X	X					X	X	
B20a	X						X	X		X			X		
B22a	X		X				X	X	X				X		
B23b	X		X				X	X	X	S			X		
B23d		X					X			X					
B24	X						X		X	X					
B25a,b			X					X	X						
B26a	X	X	X				X	X	X	X			X		
	Sc	Qz	Pg	Gt	Kf	Opx	Cpx	Am	Bi	Cc	Ox	Sf	Ti	Ap	Other

	Sc	Qz	Pg	Gt	Kf	Opx	Cpx	Am	Bi	Cc	Ox	Sf	Ti	Ap	Other
B26b	X	X	X				X	X	X	X			X		
B27a		X	X		P					S					
B27C	X		X		M		X			X			X		
B27d	X				M		X			X			X		
B29			X		P				X	X	X				
B28a		X	X		P,M				X	X				X	Ne
B31		X	X					X					X		
B32A	X	X	X				X								
B33a		X	X			X	X	H,C	X	X					
BAcrg1															
BAcrg2	X	X	X							S	M				Zc,Mu(S)
BA1a		X	X		M		X		X	X			X	X	
BA1b		X	X		P		X		S				X		
BA2		X	X		P			S	X					X	Ep
BA3		X	X				X	X	S	S			X		
BA4			X				X	X			X		X		
BA5		X	X						X						
BA6a		X	X		M			X	X		X	X	X		
BA6b		X	X				X	X	S	S		X			Mu(S)
BA7a		X	X				X	X	X					X	Zc
BA7b		X	X					X	X		X			X	Zc
BA7c			X				X	X			X				Zc
BA7d		X	X			X	X	X			X				Zc
BA7-1		X	X					X	X	S				X	
BA7-2		X	X				X	S	S			X		X	Mu(S)
BA8		X	X					X	X			X	X		Gr?
BA9a		X	X	X		X	X	X			X			X	
BA9b		X	X	X	M				X		X	X			
BA9c		X	X	X		X	X	X			X	X			
BA10		X	X			X		X	S		X	X		X	
BA14b			X		M		X						X		Zc
BA14c	X		X				X		X	X			X		
BA15A	X		X				X		X				X		Zc
BA15b	X	X					X						X	X	
BA16		X	X		P,M		X		S			X	X		
BA17a	X	X	X				X		X	X	X	X			Zc
BA17b	X	X	X		P,M		X			X			X		Zc
BA18b			X				X		X				X		Zc
BA18c		X	X		M		X				X		X	X	Zc
BA19	X	X							X	X					Zc
BA18a		X	X		P,M		X			S			S	S	Zc
BA20b	X	X	X				X	X				X	X		Zc
BA20c		X	X		P			X	X			X	X	X	
BI3c		X	X	X	P			X	X					X	
BI4b		X	X	X				X	X			X	X	X	
BI7		X	X	X			X	X	X			X		X	Zc
BI25a			X	X				X	X						
BI31		X	X	X	X		X	X	X						
BI34a			X	X		X	X	X	X		X		X		
BI35		X	X	X			X		X		X	X	X	X	Zc
BI36a		X	X	X				X	X		X			X	
BI36c		X	X	X				X	X		X				Ru
BI49		X	X	X	M				X				X		
BI31		X	X	X	P			X	X					X	
C1a		X	X	X					X						Zc
C1b	X	X	X	X			X	X		S			X		Ep
	Sc	Qz	Pg	Gt	Kf	Opx	Cpx	Am	Bi	Cc	Ox	Sf	Ti	Ap	Other

	Sc	Qz	Pg	Gt	Kf	Opx	Cpx	Am	Bi	Cc	Ox	Sf	Ti	Ap	Other
GL3b		X	X	X	P,M		X	X						X	Zc
GL5a		X	X	X	M	X			X		X				
GL6		X	X	X		X	X	X			I,M	Py			
GL8b		X	X	X		X		X	X					X	
GL13a		X	X		P,M			X	X				X	X	
GL14b		X		X					X						
GL16a		X	X					X	X						
GL21b		X	X			R		H,C	X					X	Zc
GL25		X	X				X	X	S						
GL26a	X	X	?		?		X			X		X	X		
GL26b	X	X					X			X		X	X		
GL27a	X				X		X			X			X		
GL28b	X		X				X			X			X		Zc
GL28a-1	X		X		M		X			X			X		Ep,Zc
GL28a-2	X				M		X			X			X		Ep
GL28c		X	X		M			X	X				X	X	
GL28l									X	X					Gr
H1		?	X	X		X		X						X	
H2b		X	X	X	P,M				X					X	Zc
H2c		X	X	X					X						Zc
H2d			X	X		X	X	X	X		X			X	
H4		X	X	X	M		?		X						Ep
H5		X	X	X				X	X					X	Zc
H6		X	X	X				H,C							
H7b		X	X				X		X					X	
H7c		X	X		X							X			Gr
H9a										X					Serp
H9b		X	X				X	X					X	X	
H10b			X		M		X			X				X	
H11a		X	X		P,M		X	X	X	X				X	
H12		X	X		M					X	X				
H13	X	X	X				X		X	X			X		
H14	X	X	X		P,M			X	X						
H15a			X					H,C							
H16			X					X	X	S					
H17a		X	X					X	X						
H17c		X	X				X	H,C	X						
H18		X	X	X				X							
H19		X	X			X	X	X			X				
H20		X	X			X		X	X	S					
H20d		X	X		P,M			X	S		M				Zc
H22		X	X	X		X			X		X			X	
H23a	X		X					X	X	X			X		
H24									X	X					
H37a		X	X	X		X	X		X					X	
H40a	X	X	X	X			X	X		X			X		Ep
H40b	X			X			X	X		X			X		Ep
H40c-1	X	X					X			X			X		Ep,Zc
H40c-2	X	X	X	X	M		X	X		X			X		Ep
H40d	X	X	X	X			X			X			X		Ep
H40f	X	X		X			X			X					Ep
H85A-1		X	X	X	P			X	X				X		
H85A-1a'		X	X	X		X	X		X						
H85A-1a		X	X	X	M			X	X		X			X	
H85A-1b	X	X	X	X			X						X		
H85A-1d	X	X	X	X									X		
H85A-1e	X	X	X	X			X						X		
	Sc	Qz	Pg	Gt	Kf	Opx	Cpx	Am	Bi	Cc	Ox	Sf	Ti	Ap	Other

	Sc	Qz	Pg	Gt	Kf	Opx	Cpx	Am	Bi	Cc	Ox	Sf	Ti	Ap	Other
H85A-1(3)		X	X	X			X						X		
H85A-3		X	X	X	P,M				X						Mu
H85A-15e			X	X			X	X	X						
H86B2-6a			X	X		X	X	X	X		X			X	
MPIa							X			X					Ol,Gr
MPIb	X		X	X			X	X					X		
MPId	X		X				X	X		X		X	X		
M-O		X		X	X				X						Zc
M1		X	X	X					X						Zc
M2a		X	X	X					X						Zc
M2b		X	X	X			X	X	X				X	X	Zc
M3a			X					X	X				X		Ep(S)
M3b		X	X					X	X	X			X		
M6a			X	X			X	X	X			X		X	
M6b		X	X	X				X	X			X		X	
M8		X	X	X				X	X					X	
M9a		X	X	X			X	X	X						Zc
M10		X	X	X		X	X	X			X	X		X	
M13b		X	X	X			X	X	X		X				
M14		X	X	X				X	X		X	X			Ru
M15a			X	X				X	X		X	X	X	X	
M15b		X	X	X				X	X						Ep
M17			X					X	X						
M18a		X	X		M				X						
M18b		X	X	X				X					X		Ep
M18c	X	X	X					X	X			Po			
M18d	X	X	X					X					X		Ep
M19		X	X					X	X				X	X	Ep
M20b		X	X			X		X	X						
M22a		X	X					X	X					X	
M22b		X	X				X	X			X		X		
M22c		X	X					X	X		X	X		X	
M23		X	X			X	X	X						X	
M32d			X	X		X		X			X				
M34a		X	X				X	X	S				X		
M34b			X			X	X	X	S						
M38		X	X	X		X		X	S					S	
M41c		X	X	X	P				S						
M45a		X	X	X		X		X	S		X			X	
M45c			X	X		X	X	X			X			X	
M48		?	X	X		X		X	X					X	Zc
M49	X	X	X	X			X	X	X					X	
M51b		X	X	X				X	X		X				
M54b		X	X	X	M				X						Mu
M54b-2		X	X	X					X	S				X	Mu(S)
M57a		X	X	X					X					X	Zc,Ru,Gr
M57b			X	X		X	X	X	X					X	
M57c		X	X	X			X	X	X						Zc
M58		X	X	X		X	X	X	S		X			X	
M71b		X	X	X		X	X	X	X		X			X	
M80d		X	X	X	M			X	X					X	Zc
M81			X	X		X	X	X			X				
M88e			X	X	P,M			X	X					X	Zc
M89a		X	X	X		X			X					X	
M85A-1			X	X		X	X	X	X		X			X	
M85A-1b	X		X	X			X	X						X	Sp
	Sc	Qz	Pg	Gt	Kf	Opx	Cpx	Am	Bi	Cc	Ox	Sf	Ti	Ap	Other

	Sc	Qz	Pg	Gt	Kf	Opx	Cpx	Am	Bi	Cc	Ox	Sf	Ti	Ap	Other
M85A-3			X	X				X	X		X			X	
M85A-4			X	X				X	X		X			X	Ru
M85A-5a	X	X		X			X			X					Ep(S)
M85A-5c	X	X		X			X			X			X		
M85A-6a		X	X	X						X					Wo
M86E-1a	X		X	X			X					Py	X		
M86E-1b-1	X	X	X	X			X			X			X		Wo
M86E-1b-3	X	X		X			X			X					Wo
M86E-1c-2	X		X	X			X			X			X		Wo
M86E-1d-1	X	X		X			X			X					
M86E-1d-2	X	X	X	X			X						X		Wo
M86E-1e	X	X	X	X			X							X	
MA-O										X					Serp
MA3		X	X	X				X	X				X	X	
MA4b		X	X	X				X	X						
MA7		X	?	X	M		X	H,C	X		X			X	
MA15		X			M										Mu
MA15b		X		X	M										Mu
MAT84B-20		X	X		X					X					Gr
NB27		X	X	X					X				X		
NB28			X	X				X	X		X				
NB29			X	X			X	X	X					X	Zc
NB30		X	X	X	P		X	X	X		X			X	
06a		X	X	X	M			X	X		X	X			Zc
06b		X	X	X				X	X						
06d		X	X	X				X	X					X	Zc
07a		X		X	P,M				X						
07b		X	X	X				X	X					X	
08b	X	X		X	M		X			X			X		Zc
08c	X	X		X			X						X		
08e	X	X	X	X			X			X		X	X		Ep
08f	X	X		X	M		X						X		
09a		X	X	X				X	X						
09B		X	X	X			X	X	X			X			
010b		X	X	X	P,M				X						
011		X		X	P,M				X		X	X		X	Zc
013a		X	X	X		X	X	X	S		X			X	Zc
013b			X	X			X	X	S					X	
013c		X	X	X	X			X	X		X				
014b		X	X	X				X	X		X			X	Zc
015a		X	X	X	X			X	X		X			X	Zc
015b		X	X	X	P	X		X	X					X	
016		X	X	X				X	X						
017		X		X	M		X			X					Zc
PS1a		?	X						X			X	X	X	Ep
PS2		X	X	X				X	X			X	X	X	
PS3		X	X	X				X	X	X		X	X	X	Ru?
PS5			X	X			X	X	X			X			
PS6			X	X			X	X					X	X	
PS7a	X	X	X	X				X	X		I	Py	X	X	Zc
PS7b	X	X	X	X				X			I	X			
PS7c	X	X	X	X			X	X			X		X	X	
PS7f		X	X	X				X						X	
	Sc	Qz	Pg	Gt	Kf	Opx	Cpx	Am	Bi	Cc	Ox	Sf	Ti	Ap	Other

	Sc	Qz	Pg	Gt	Kf	Opx	Cpx	Am	Bi	Cc	Ox	Sf	Ti	Ap	Other
PS7g		X	X	X			X	X		X	I,M	Py		X	
PS8		X	X	X	P,M				X	S					Mu(S)
PS9a		X	X	X				X	X			X	X	X	
PS9b		X	X		M			X	X						Zc
PS13		X	X	X				X	X			X			
PS14a		X	X		M			X			X				Ep,Zc
PS16		X	X						X			X	X		Ep
PS85A-0a	X	X	X	X	X				X					X	
PS85A-0b		X	X					X	X						
PS85A-1a	X		X						X						Ep,Mu(S)
PS85A-2a		X	X					X	X		I		X	X	
PS85A-2c	X	?	X	X				X	X		M			X	Ep
PS85A-2e		X	X					X					X		Ep
PS85A-3d			X					X	X						Ep
PS85A-4			X			X	X	X			I			X	
PS85A-5		X	X	X				X					X		Zc
PS085A-5	X	X	X	X				X		X			X	X	Zc
PS85A-6a		X	X			X	X	S	S						
PS85A-6b		X	X	X		X	X	X	X		X				
PS85A-7	X	X	X				X	X		X		X			
PS085A-8a	X	X	X	X			X	X			I		X	X	
PS08TA-8b	X	X	X	X				X	X		X		X	X	
PS085A-8c	X	X	X	X				X	X		I,M	Py	X	X	
PS085A-23		X	X	X			X								Wo
PS085A-24	X	X	X	X			X	X	S				X	X	
PS085A-25	X	X	X	X			X	X	X		X			X	Ru
PS86B1-1	X	X	X	X				X	X	S	X		X	X	
PS86B1-2		X	X	X			X	X			X				
PS86B1-3		X	X	X				X	X				X	X	Zc
PS86B1-4		X	X	X				X			X			X	
PS86B1-5		X	X	X			X	X			X			X	
PS86B1-6		X	X	X				X	X	X	X			X	Zc
PS86B1-7		X	X	X			X	X			X			X	Zc
PS86B1-8			X	X			X	X		X	X				Zc
PS86B1-11	X	X	X	X				X	X	S			X	X	Ep
PS86B2-1	X	X	X	X				X	X	X	X		X		
PS86B2-2			X	X		X	X	H,C,A							
PS86B2-3	X	X	X	X				X	X		X		X	X	
PS86B2-4		X	X				X	X		X			X		Ep
PS86B3-1		X	X	X		X	X	S	S		X		X	X	
PS86E-4Nd		X	X	X				X	X	X	I		S		
PS86E-6a		X	X	X				X	X	X	X		X	X	
PS86E-6b		X	X	X			X	X		X			X	X	
PS86E-7e	X	X	X	X				X	X	X			X	X	Ep
PS86E-8	X	X	X	X				X	S		I		X	X	Ep,Mu(S)
PS86E-10	X	X	X	X				X	X	S	X			X	Ep,Mu(S)
PS86E-12		X	X	X				X	X	X			X	X	Ep
PS86E-15	X		X	X				X	X					X	Ep
PS86E-16a	X	X	X	X				X			I		X		Ep
PS86E-17			X	X			X	X			I		X		Ep
PS86E-19b		X	X						X						Ep
PS86E-19c		X	X					X	X	X					Ep,Chl(S)
PS86E-19d		X	X							S					Ep,Mu(S)
PS86E-20		X	X					X	X	S					Ep,Mu(S)
PS863-21			X					X	S						Ep,Mu(S)
PS86E-22			X							X					Ep
PS86E-23	X	X	X					X	X	X			X	X	Ep
PS86E-24a	X		X				X	X		X					
	Sc	Qz	Pg	Gt	Kf	Opx	Cpx	Am	Bi	Cc	Ox	Sf	Ti	Ap	Other

	Sc	Qz	Pg	Gt	Kf	Opx	Cpx	Am	Bi	Cc	Ox	Sf	Ti	Ap	Other
PS86E-24b	X		X					X							Ep
PS86E-24d	X	X	X	X				X	X	X	I		X		Ep
PS86E-24e	X	X	X	X				X	X				X	X	Ep
PS86E-24f	X	X	X	X				X	X		I		X	X	Ep
PS86E-26c		X	X	X				X	X		I,M	Py,Po		X	
PS86E-28b		X	X	X				X	X	S	X			X	Ru
PS86E-30b			X					X	X				X		Ep,Ru
PS86E-30c	X		X						X						Ep,Mu(S)
PS86E-30d		X	X	X	X				X			Py			Ky,Gr,Mu,R
PS86E-31	X	X	X	X				X	X	X	I		X	X	Ep
PS86E-32a	X	X	X	X				X	X	X					Ep
PS86E-32b	X	X	X	X				X	X	X	I		X	X	Ep
PS86E-33		X	X	X				X	X					X	Zc
PS86E-34	X	X	X	X				X	X		I		X	X	Zc
S2		X	X	X			X	X	X						
S2a							X			X	Sp				Serp,Ch
S2e		X	X	X		X	X	X		S	X				
S4c		X	X	X			X	X			X				
S11		X	X	X					X						
S14b		X	X	X					X					X	
S14c		X	X					X	X				X	X	
S15		X	X	X					X						Ky,Ru
S19a		X	X					X	X	S			X	X	Ep
S20a		X	X	X				X			I		X		
S23		X	X	X				X							
S26		X	X	X				H,C	X						
S29b			X	X				X	X		I		X	X	Zc
S30b		X	X	X		X			X				X		Zc
S31b			X	X				X	X					X	
S32		X	X	X		X	X		X		X			X	
S34		X	X	X		X	X	X	X		X			X	Zc
S42		?	X	X			X	X			X				
S59		X	X	X				X	X						
S85A-1b-1		X	X	X		X	X				M	Py			
S85A-1b-2		X	?	X	X				X						Si
S85A-1b-3		X	X	X	?				X						Si,Ru
S85A-1c		X	X	X					X						Ru
S85A-2		X	X		X										
S85A-2a-1	X	X	X	X			X					Py	X	X	
S85A-2a-2		X	X	X			X			X		Py,Cpy		X	
S85A-2d		X	X				X			S			X	X	
S85A-3a	X	X	X	X			X	X							
S85A-3b	X	X	X	X			X	X	X		I,H				
S85A-3c	X	X	X	X				X	X				X		
S85A-4			X						X						Ep
S85A-4'		X	X	X				X	X	X			X		
S85A-8a	X		X						X			Py			Ep,Mu
S85A-8b	X	X	X						X			Py	X	X	Ep,Mu(S)
S85A-8c		X	X				X	X	X						
S85A-9a	X	X	X	X			X						X		
S86E-1a		X		X			X	X		X	X		X		
S86E-4b		X	X					X		X	I		X		
S86E-5b		X	X	X			X	X		X	X			X	
S86E-7b			X	X		X	X	X	S		I	Py,Po		X	
S86E-8c-1		X		X			X			X			X		Wo
S86E-8c-2	X		X	X			X	X		X			X		
	Sc	Qz	Pg	Gt	Kf	Opx	Cpx	Am	Bi	Cc	Ox	Sf	Ti	Ap	Other

	Sc	Qz	Pg	Gt	Kf	Opx	Cpx	Am	Bi	Cc	Ox	Sf	Ti	Ap	Other
S86E-8i		X	X	X		R	X	S	S	S	M	Py,Po		X	
S86E-10	X		X	X			X	X	S		I,M			X	Ep(S)
S86E-11	X		X	X			X	X						X	
S86E-12	X	?	X	X			X	X	S		M			X	
S86E-13b	X	X	X	X			X	X	S	S	I,M		S	S	
S86E-14a-1		X	X	X			X			S	I,M			X	
S86E-14a-2	X	X	X	X			X	S	S					S	
S86E-15		X	X	X			X	X			X			X	
S86E-16e		X		X			X			X					
S86E-16g							X			X	Sp				
S86E-16f-1		X	X	X		X	X	X		S	I,M	Py		X	
S86E-16f-2		X	X	X		X	X	X		S	I	Py		X	
S86E-16f		X	X	X			X	X		S	X				
S86E-17b		X	X	X		X	X	X			X			X	
S86E-18b			X	X			X			X			X	X	
S86E-18c		X	X	X		R	X	X	S	S	S		X		
S86E-20			X	X				X	S		I,M			X	Ep
S86E-21a		X	X	X		X	X	X	S	S	I			X	Zc
S86E-22		X	X			R	X	X			X				
S86E-23							X	X	X	X			X		Do,Ol
S86E-24a								X	X	X	Sp		X		Do,Ol
S86E-24b		X	X	X		X		X	S		I,M			X	Zc
S86E-25a	X		X	X			X	X	S		X		X	X	Ep
S86E-25b	X		X				X	X			I		X	X	Ep
S86E-25c	X	?	X	X			X	X	X		I		X		
S86E-25f		X	X	X			X	X		X	X			X	
S86E-25i	X	X	X				X	X		X	X		X	X	Ep,Zc
S86E-25n	X			X			X			X					Ep
S86E-27a							X		X	X					Ol
S86E-27b	X						X	X		X					
S86E-28			X	X		X	X	X			I,M			X	
S96E-31a	X	?	X				X	X		S	I		S		Ru
S86E-31b		X	X	X				H,C,A	X	S	I			S	
S86E-31d-1							X			X	Sp				Ol
S86E-31d-2							X	X	X	X	Sp				Ol
S86E-31d-3		X	X	X		X	X	X	X	X	X	X	X	X	Layered
S86E-32		X	X	X		X	X	X	X	X	I,M			X	
S86E-33		X	X	X		X	X	X	X	X	I	Py		X	Zc
S86E-34	X	X	X	X			X	X	S		I		X	X	
S86E-35	X	X	X	X			X	X	S	S	I,M		X	X	
S86E-36b	X	X	X	X			X	X			I	Py	X	X	Ep(S),Zc
S86E-37	X	X	X	X			X	X	X	S	I		X	X	Ep(S)
S86E-38a			X	X		X		X	S	S	I			X	
S86E-38b	X		X					X	S					X	Ep
S86E-39	X	X	X	X			X	X	S	S	I,M		X	X	Ru
S86E-40	X	X	X	X			X	X	S	S	I,M			X	
S86E-41	X	X	X	X			X	X	S		I,M			X	
S86E-42	X		X				X	X	S	S	I,M	Py		X	
S86E-43	X		X				X			S	I,M	X		X	
S86E-44	X	X	X				X	X		S	I,M		X	X	
S86E-45	X		X				X	X			I,M		X		
S86E-53a	X	X	X	X			X	X			X			X	
T46		X	X					X	X		X			X	
WSA1	X	X	X							S					Mu
	Sc	Qz	Pg	Gt	Kf	Opx	Cpx	Am	Bi	Cc	Ox	Sf	Ti	Ap	Other

Samples contributed by Dr. T.C. Devaraju, Karnatak Univeristy, Dharwad, India.
Locality: Sargur Terrane, southern India, mafic granulite and calc-silicate.

	Sc	Qz	Pg	Gt	Kf	Opx	Cpx	Am	Bi	Cc	Ox	Sf	Ti	Ap	Other
TCD2		X	X				X			X	I,M		X		
TCD4	X	X	X				X						X	X	
TCD5	X	X	X	X			X						X	X	
TCD8	X	X	X				X						X	X	
TCD18c		X	X				X						X	X	
TCD25	X	X	X	X			X						X		
TCD33a	X		X	X			X	H,C,A			I,M	Py			Ep(S)
TCD33		X	X	X		X	X	X			I,M			X	
TCD34		X	X	X		X	X	H,C		S	I,M	Po			
TCD39	X	X	X	X		X	X	H,C			I,M				Po

Sample contributed by Dr. C. Srikantappa, Dept. Geology, Univ. Mysore, India
Locality: Sargur Terrane, southern India, mafic granulite.

	Sc	Qz	Pg	Gt	Kf	Opx	Cpx	Am	Bi	Cc	Ox	Sf	Ti	Ap	Other
285	X		X	X		X	X	X			I,M				

Samples contributed by Dr. A.J. Stolz, Univ. Tasmania,
Hobart, Tasmania. Locality: New South Wales, xenoliths.

	Sc	Qz	Pg	Gt	Kf	Opx	Cpx	Am	Bi	Cc	Ox	Sf	Ti	Ap	Other
32-80	X						X	X			I,M	Py			
32-90	X		X				X	X			I,M	Py			

Samples contributed by Dr. H. Austreim, Mineralogisk-Geologisk
Museum, Oslo, Norway. Locality: Bergen Arcs, meta-anorthosite.

	Sc	Qz	Pg	Gt	Kf	Opx	Cpx	Am	Bi	Cc	Ox	Sf	Ti	Ap
HA54/83	X		X	X			X		S					
HA53/80	X		X	X		X	X		S	S	X			X
HA46/85	X	X	X	X		X	X	X			X			
HA10/83	X		X	X			X	X						

Samples contributed by Dr. A. Davidson, GSC, Ottawa, Canada.
Locality: Central Gneiss Belt, southwestern Ontario.

	Sc	Qz	Pg	Gt	Kf	Opx	Cpx	Am	Bi	Cc	Ox	Sf	Ti	Ap	
80DMA5a			X	X			X						X		Al
80DMA35c	X		X	X				X			X				
80DMA55h-4	X		X	X				X					X		Ep
80DMA77-5a	X	X	X	X				X	X				X		
80DMA168c	X	X	X				X	X							
80DMA348d	X	X	X	X				X	X		X			X	
80DMA348e	X	X	X	X				X	X		X				Zc,Ep
80DMA351f	X		X				X	X							
80DMA397a	X		X	X			X		X						
80DMA473b	X		X	X		X	X	X	X		X		X		Ru
80DMA614p	X		X	X		X	X	X			X				
80DML214a	X		X	X			X	X							
80DMM47b	X		X					X	X	X			X		
82DMT114a	X		X	X			X			X			X		
82DMT114d	X	X					X			X			X		
83DMP5e	X	X	X	X											Zc,Al
85DM52b				X				X							
85DMP102a		X	X					X	X						Ep
85DMP174-1a	X	X	X	X			X	X	X		X			X	
85DMP272-2a	X	X	X	X		X	X	X							
	Sc	Qz	Pg	Gt	Kf	Opx	Cpx	Am	Bi	Cc	Ox	Sf	Ti	Ap	Other

Samples contributed by C.M. Marmont, Ontario Ministry of Mines and Northern Development. Locality: Central Gneiss Belt, meta-anorthosite.

	Sc	Qz	Pg	Gt	Kf	Opx	Cpx	Am	Bi	Cc	Ox	Sf	Ti	Ap	
CCM 0043			X	X		X	X	X							
CCM 0078			X	X		X	X				I,M			X	
CCM 0102			X	X			X	X			I,M			X	
CCM 0114	X		X	X		X	X	X			I,M			X	
CCM 0118		X	X			X	X	X			I,M				
MMJ 3011	X		X				X	X					X	X	Ep
MMJ 3021			X	X			X	X			X				
MMJ 3023	X		X					X							Ep
MMJ 3024	X	X	X	X					S		I,M		X	X	Ep
MMJ 3041	X	X	X				X				I,M				

Appendix 3

Microprobe Analyses

Electron microprobe analyses were obtained on the Cameca CAMEBAX microprobe at the University of Michigan. The microprobe was operated at an accelerating voltage of 15 kV and sample current of 10 nA for all analyses. A focused beam was used for clinopyroxene, garnet, orthopyroxene, and titanite analyses. Either a slightly defocussed beam or a rastered beam scanning a 4μ area were used for epidote, plagioclase, and scapolite analyses, in order to minimize volatilization of light elements. Well characterized natural and synthetic silicates and oxides were used as standards. Analyses were normalized to 3 (titanite), 4 (pyroxene), 5 (plagioclase), and 8 (garnet, epidote) cations. Scapolite formulae were calculated on the basis of Si + Al = 12, and Cl + CO_3 + SO_4 = 1 in the anion site. Wt % CO_2 was recalculated from this assumption. Fe was calculated as Fe_2O_3 for scapolite, plagioclase, and epidote analyses. Fe^{3+} for garnet and pyroxene was calculated form charge balance and stoichiometry. In the tabulation of garnet and pyroxene analyses, Fe was analyzed as FeO, but recalculated as FeO^1 after Fe^{3+} and Fe_2O_3 were determined. For epidote analyses all iron was calculated as Fe^{3+} and H_2O was calculated from the assumption of 1.00 molecule of OH.

Scapolite Analyses

SAMPLE	ARM4	A85A-1	A85A -3a	A85A -3a	A85A -3b	A85A -3d-1	A85A -3d-2	A86B 3-3a	A86B -3-3b-3	B11
SiO_2	47.34	47.04	46.07	46.07	46.03	43.83	46.47	45.73	45.28	56.00
Al_2O_3	26.19	26.76	27.96	27.96	28.64	28.66	27.38	25.97	25.94	22.89
Fe_2O_3	0.28	0.19	0.16	0.16	0.20	0.15	0.22	0.14	0.19	0.03
MnO	0.01	0.00	0.00	0.00	0.00	0.00	0.01	0.02	0.02	0.00
CaO	15.97	16.84	18.69	18.69	18.87	19.92	18.18	16.89	16.81	7.66
Na_2O	4.41	3.79	3.06	3.06	2.88	2.20	3.26	3.61	3.78	9.31
K_2O	0.18	0.39	0.09	0.09	0.15	0.22	0.11	0.11	0.07	0.95
Cl	0.34	0.49	0.04	0.04	0.08	0.06	0.10	0.06	0.02	2.80
SO_3	2.05	0.61	0.09	0.09	0.00	0.00	0.00	5.11	5.48	0.05
CO_2	3.22	3.85	4.73	4.73	4.77	4.66	4.68	1.77	1.59	1.56
-O=Cl	0.08	0.11	0.01	0.01	0.02	0.01	0.02	0.01	0.00	0.63
TOTAL	99.96	99.85	100.88	100.88	101.60	99.69	100.39	99.40	99.18	100.62
Si	7.263	7.183	6.995	6.995	6.922	6.776	7.081	7.188	7.163	8.098
Al	4.737	4.817	5.005	5.005	5.078	5.224	4.919	4.812	4.837	3.902
Fe	0.032	0.022	0.018	0.018	0.023	0.017	0.025	0.017	0.023	0.003
Mn	0.001	0.000	0.000	0.000	0.000	0.000	0.000	0.003	0.003	0.000
Ca	2.625	2.755	3.040	3.040	3.040	3.299	2.968	2.844	2.849	1.187
Na	1.312	1.122	0.901	0.901	0.840	0.660	0.963	1.100	1.160	2.611
K	0.035	0.076	0.017	0.017	0.029	0.016	0.021	0.022	0.014	0.175
Cl	0.088	0.127	0.010	0.010	0.020	0.016	0.026	0.016	0.005	0.686
SO_4	0.236	0.070	0.010	0.010	0.000	0.000	0.000	0.603	0.651	0.005
CO_3	0.675	0.803	0.980	0.980	0.980	0.984	0.974	0.381	0.344	0.308

SAMPLE	B26a	BA20a	C1b	DEB83C -4	GL28a-1	GL28b	H10	H13	H85A -1e(1)	H85A -1e(2)
SiO_2	46.44	53.38	46.34	45.63	51.15	52.45	53.56	56.16	46.10	45.77
Al_2O_3	27.63	23.98	27.70	27.71	24.96	24.68	23.94	22.71	27.44	27.50
Fe_2O_3	0.03	0.04	0.07	0.10	0.06	0.03	0.13	0.07	0.06	0.14
MnO	0.00	0.02	0.00	0.01	0.01	0.00	0.00	0.00	0.02	0.00
CaO	18.16	10.14	18.45	19.22	12.94	11.00	10.41	7.69	18.37	18.65
Na_2O	3.34	7.94	3.36	3.33	6.24	7.66	7.66	10.34	3.09	3.16
K_2O	0.13	0.82	0.11	0.10	0.46	0.34	0.76	0.94	0.14	0.14
Cl	0.09	2.10	0.02	0.09	1.12	1.82	1.84	2.72	0.04	0.06
SO_3	0.04	0.04	0.00	0.01	0.79	1.82	0.79	0.39	0.02	0.00
CO_2	4.69	2.35	4.79	4.66	3.09	2.61	2.27	1.47	4.73	4.60
-O=Cl	0.02	0.47	0.00	0.02	0.25	0.41	0.42	0.61	0.01	0.01
TOTAL	100.53	100.34	100.84	100.84	100.57	102.00	100.94	101.88	100.01	100.01
Si	7.053	7.845	7.039	6.993	7.618	7.718	7.859	8.126	7.052	7.024
Al	4.947	4.155	4.961	5.007	4.382	4.282	4.141	3.874	4.948	4.976
Fe	0.003	0.004	0.008	0.012	0.007	0.003	0.014	0.008	0.007	0.013
Mn	0.000	0.002	0.000	0.010	0.001	0.000	0.000	0.000	0.003	0.000
Ca	2.955	1.597	3.008	2.991	2.065	1.734	1.636	1.192	3.010	3.066
Na	0.984	2.263	0.990	0.990	1.802	2.186	2.180	2.901	0.917	0.940
K	0.025	0.154	0.021	0.012	0.087	0.064	0.142	0.174	0.027	0.027
Cl	0.023	0.523	0.005	0.023	0.283	0.454	0.458	0.667	0.010	0.036
SO_4	0.005	0.004	0.000	0.001	0.088	0.022	0.087	0.042	0.002	0.000
CO_3	0.972	0.472	0.995	0.976	0.629	0.524	0.455	0.291	0.988	0.964

SAMPLE	H85A -1d-1	H85A -1b	H85A -1(3)	Mpib	Mpid	M49	M53	M86E -1b	M86E -1C-2	08e
SiO_2	44.73	45.65	46.80	48.06	48.04	46.21	45.82	50.33	47.71	46.07
Al_2O_3	28.21	28.16	27.26	27.07	26.83	26.58	26.72	25.66	26.91	27.75
Fe_2O_3	0.06	0.14	0.25	0.04	0.10	0.22	0.14	0.04	0.02	0.13
MnO	0.00	0.02	0.02	0.00	0.00	0.00	0.00	0.00	0.00	0.00
CaO	19.65	18.91	17.54	16.19	15.73	16.84	17.12	13.63	16.15	18.28
Na_2O	2.51	2.96	3.36	4.36	4.41	3.78	3.62	5.84	4.32	3.28
K_2O	0.14	0.06	0.13	0.58	0.34	0.08	0.02	0.57	0.39	0.36
Cl	0.04	0.02	0.12	0.73	0.49	0.05	0.03	1.15	0.51	0.35
SO_3	0.10	0.00	0.05	0.02	0.01	4.17	3.96	0.07	0.04	0.03
CO_2	4.65	4.79	4.64	3.96	4.25	2.38	2.50	3.45	4.19	4.36
-O=Cl	0.01	0.00	0.03	0.16	0.11	0.01	0.01	0.26	0.12	0.08
TOTAL	100.08	100.71	100.14	100.85	100.09	100.30	99.92	100.48	100.12	100.53
Si	6.882	6.937	7.115	7.211	7.235	7.150	7.111	7.495	7.207	7.017
Al	5.118	5.063	4.885	4.789	4.765	4.850	4.889	4.505	4.793	6.983
Fe	0.007	0.014	0.029	0.000	0.011	0.028	0.016	0.004	0.002	0.015
Mn	0.000	0.003	0.003	0.000	0.000	0.000	0.000	0.000	0.000	0.000
Ca	3.239	3.162	2.857	2.603	2.538	2.792	2.846	2.175	2.614	2.988
Na	0.749	0.842	0.991	1.269	1.288	1.134	1.090	1.687	1.266	0.969
K	0.027	0.014	0.025	0.111	0.065	0.016	0.004	0.108	0.075	0.070
Cl	0.010	0.005	0.031	0.186	0.125	0.013	0.008	0.290	0.131	0.090
SO_4	0.012	0.002	0.006	0.002	0.001	0.485	0.462	0.008	0.005	0.003
CO_3	0.978	0.992	0.963	0.812	0.874	0.502	0.530	0.702	0.865	0.906

SAMPLE	PS7a	PS7b	PS7c	PS7e	PS85A -0a	PS85A -1a	PS85A -2c	PS085A -5-1	PS085A -5-12	PS85A -7
SiO_2	45.45	45.34	46.25	46.62	52.47	46.52	46.54	47.12	47.74	45.84
Al_2O_3	27.39	27.50	27.63	27.46	24.30	26.63	27.35	26.99	26.25	28.11
Fe_2O_3	0.16	0.21	0.09	0.12	0.07	0.01	0.07	0.24	0.13	0.18
MnO	0.00	0.00	0.00	0.00	0.05	0.00	0.01	0.01	0.09	0.00
CaO	17.62	17.55	18.25	18.04	11.43	16.75	18.15	16.81	15.77	18.59
Na_2O	3.39	3.42	3.21	3.38	7.00	3.91	3.30	3.87	4.50	2.94
K_2O	0.18	0.12	0.13	0.19	0.75	0.11	0.11	0.27	0.38	0.20
Cl	0.16	0.05	0.07	0.16	1.54	0.14	0.07	0.33	0.61	0.14
SO_3	0.33	0.77	0.03	0.10	0.38	2.05	0.04	0.01	0.07	0.03
CO_2	4.45	4.26	4.71	4.53	2.83	3.45	4.74	4.40	4.00	4.63
-O=Cl	0.00	0.00	0.00	0.00	0.00	0.00	0.00	0.00	0.00	0.00
TOTAL	99.13	99.22	100.37	100.63	100.83	99.57	100.38	100.15	99.54	100.66
Si	7.016	6.997	7.041	7.082	7.762	7.165	7.086	7.163	7.281	6.964
Al	4.984	5.003	4.959	4.918	4.238	4.835	4.914	4.837	4.719	5.036
Fe	0.019	0.024	0.010	0.014	0.008	0.001	0.010	0.027	0.015	0.021
Mn	0.000	0.000	0.000	0.000	0.006	0.000	0.001	0.001	0.012	0.000
Ca	2.914	2.901	2.976	2.936	1.811	2.764	2.975	2.738	2.576	3.026
Na	1.015	1.024	0.948	0.996	2.008	1.168	0.946	1.141	1.331	0.866
K	0.035	0.024	0.025	0.037	0.142	0.022	0.031	0.052	0.074	0.039
Cl	0.042	0.013	0.018	0.049	0.386	0.037	0.018	0.085	0.158	0.036
SO_4	0.019	0.089	0.003	0.011	0.042	0.237	0.005	0.001	0.008	0.003
CO_3	0.939	0.898	0.979	0.940	0.572	0.726	0.977	0.914	0.834	0.961

SAMPLE	PS085A -8b	PS85A -8b	PS085A -13	PS085A -24	PS86B 1-1	PS86B 1-10a	PS86B 1-11"	PS86B 2-1	PS86B 2-3	PS86E -7e
SiO_2	46.05	47.18	45.85	45.76	47.19	47.35	45.80	47.85	46.13	46.21
Al_2O_3	27.13	26.18	27.47	27.27	26.99	26.79	27.24	26.25	27.02	27.51
Fe_2O_3	0.13	0.04	0.13	0.10	0.03	0.21	0.07	0.19	0.22	0.08
MnO	0.00	0.03	0.00	0.02	0.05	0.00	0.02	0.00	0.02	0.02
CaO	17.76	16.81	18.54	17.79	16.77	16.11	17.82	16.91	17.53	17.69
Na_2O	3.38	3.96	3.18	3.39	3.73	3.98	3.28	3.94	3.64	3.46
K_2O	0.17	0.15	0.05	0.06	0.28	0.31	0.14	0.39	0.25	0.14
Cl	0.08	0.08	0.01	0.02	0.25	0.39	0.07	0.49	0.30	0.10
SO_3	0.82	2.43	0.08	1.33	0.03	0.12	0.18	0.00	0.48	0.10
CO_2	4.21	3.32	4.72	4.00	4.49	4.27	4.57	4.20	4.12	4.62
-O=Cl	0.02	0.02	0.00	0.00	0.06	0.09	0.02	0.11	0.07	0.02
TOTAL	99.71	100.16	100.03	99.75	99.75	99.44	99.17	100.11	99.64	99.91
Si	7.082	7.254	7.032	7.048	7.167	7.199	7.054	7.287	7.098	7.051
Al	4.918	4.746	4.968	4.952	4.833	4.801	4.946	4.713	4.902	4.949
Fe	0.015	0.005	0.015	0.012	0.003	0.022	0.008	0.021	0.025	0.009
Mn	0.000	0.000	0.000	0.003	0.006	0.000	0.003	0.000	0.003	0.003
Ca	2.926	2.769	3.046	2.936	2.729	2.624	2.940	2.759	2.890	2.892
Na	1.008	1.181	0.946	1.013	1.099	1.173	0.980	1.164	1.086	1.024
K	0.033	0.029	0.010	0.012	0.054	0.060	0.028	0.076	0.059	0.027
Cl	0.021	0.021	0.003	0.005	0.064	0.101	0.018	0.127	0.078	0.026
SO_4	0.095	0.281	0.009	0.154	0.003	0.014	0.021	0.000	0.055	0.011
CO_3	0.884	0.698	0.988	0.841	0.932	0.886	0.961	0.873	0.867	0.963

SAMPLE	PS86E -8	PS86E -10	PS86E -15	PS86E -16a	PS86E -23-1	PS86E -24b	PS86E -24d	PS86E -24f	PS86E -31	PS86E -34
SiO_2	45.67	46.87	47.20	45.57	47.18	45.83	46.71	46.31	46.87	47.41
Al_2O_3	27.39	27.34	26.82	27.38	26.56	27.44	27.21	27.16	27.09	26.42
Fe_2O_3	0.10	0.11	0.05	0.05	0.04	0.02	0.06	0.09	0.08	0.11
MnO	0.00	0.04	0.03	0.02	0.03	0.01	0.03	0.00	0.02	0.01
CaO	17.87	17.11	16.05	17.99	16.46	18.05	16.88	17.51	17.58	16.01
Na_2O	3.39	3.68	4.27	3.36	4.04	3.51	3.88	3.46	3.52	4.37
K_2O	0.09	0.16	0.24	0.10	0.20	0.12	0.14	0.12	0.11	0.10
Cl	0.06	0.25	0.37	0.06	0.39	0.03	0.31	0.08	0.14	0.55
SO_3	0.91	0.56	0.67	0.45	0.77	0.02	0.28	1.43	0.07	0.28
CO_2	4.18	4.21	3.98	4.43	3.88	4.72	4.27	3.89	4.60	3.96
-O=Cl	0.01	0.06	0.08	0.01	0.09	0.01	0.07	0.02	0.03	0.12
TOTAL	99.65	100.27	99.60	99.40	99.46	99.74	99.70	100.03	100.05	99.10
Si	7.030	7.110	7.186	7.024	7.213	7.034	7.114	7.095	7.137	7.242
Al	4.970	4.890	4.814	4.976	4.787	4.965	4.886	4.905	4.863	4.758
Fe	0.012	0.013	0.006	0.006	0.005	0.002	0.007	0.010	0.009	0.013
Mn	0.000	0.005	0.004	0.003	0.004	0.001	0.004	0.000	0.003	0.001
Ca	2.751	2.781	2.618	2.971	2.696	2.968	2.754	2.874	2.868	2.620
Na	1.012	1.083	1.261	1.004	1.198	1.045	1.146	1.028	1.039	1.295
K	0.018	0.015	0.047	0.020	0.039	0.024	0.027	0.023	0.021	0.019
Cl	0.016	0.064	0.096	0.016	0.101	0.008	0.080	0.021	0.036	0.142
SO_4	0.105	0.064	0.077	0.052	0.088	0.002	0.032	0.165	0.008	0.032
CO_3	0.879	0.872	0.828	0.932	0.811	0.990	0.888	0.814	0.956	0.826

SAMPLE	S4d	SUN84B -18	S85A -2a	S85A -2b	S85A -2d	S85A -3a(c)	S85A -3a(r)	S85A -3b	S85A -3c	S86E -8c
SiO_2	47.77	47.47	47.37	47.65	47.65	46.90	47.60	46.25	45.92	47.28
Al_2O_3	26.80	26.41	27.37	26.84	26.97	26.67	27.10	27.58	28.12	26.69
Fe_2O_3	0.04	0.32	0.06	0.02	0.09	0.33	0.14	0.12	0.08	0.13
MnO	0.00	0.10	0.00	0.00	0.00	0.00	0.00	0.04	0.00	0.02
CaO	16.26	16.38	17.53	16.16	16.40	16.60	16.66	18.36	18.23	16.36
Na_2O	4.32	4.20	3.72	4.13	3.99	3.83	4.04	3.09	3.12	4.10
K_2O	0.53	0.20	0.21	0.39	0.53	0.20	0.26	0.14	0.20	0.27
Cl	0.47	0.31	0.26	0.60	0.51	0.43	0.48	0.07	0.12	0.33
SO_3	0.13	1.40	0.01	0.02	0.01	1.52	0.46	0.05	0.01	0.17
CO_2	4.19	3.64	4.53	4.08	4.21	3.52	4.00	4.69	4.67	4.30
-O=Cl	0.11	0.07	0.06	0.14	0.12	0.10	0.11	0.02	0.03	0.07
TOTAL	100.40	100.36	101.00	99.75	100.25	99.90	100.63	100.39	100.47	99.58
Si	7.223	7.247	7.137	7.211	7.197	7.183	7.180	7.046	6.969	7.205
Al	4.777	4.753	4.863	4.789	4.803	4.817	4.820	4.954	5.031	4.795
Fe	0.005	0.037	0.007	0.002	0.010	0.038	0.016	0.014	0.009	0.015
Mn	0.000	0.000	0.000	0.000	0.000	0.000	0.000	0.000	0.000	0.003
Ca	2.634	2.679	2.830	2.620	2.654	2.724	2.692	2.996	2.964	2.671
Na	1.267	1.243	1.087	1.212	1.169	1.138	1.182	0.913	0.918	1.212
K	0.102	0.039	0.040	0.075	0.102	0.039	0.050	0.027	0.039	0.053
Cl	0.120	0.080	0.066	0.154	0.131	0.088	0.123	0.018	0.031	0.085
SO_4	0.015	0.161	0.001	0.002	0.001	0.175	0.052	0.006	0.001	0.019
CO_3	0.865	0.759	0.933	0.844	0.868	0.737	0.825	0.976	0.968	0.895

SAMPLE	S86E -10	S86E -25a	S86E -25c	S86E -25i	S86E -25n	S86E -27d	S86E -34	S86E -36b	S86E -41	S86E -45-1
SiO_2	45.70	46.17	46.10	46.82	45.77	45.23	46.30	46.40	46.07	45.35
Al_2O_3	26.91	27.56	27.48	27.09	27.64	28.21	26.90	27.22	27.74	27.41
Fe_2O_3	0.09	0.08	0.06	0.08	0.04	0.03	0.10	0.13	0.10	0.09
MnO	0.02	0.03	0.02	0.01	0.02	0.00	0.03	0.03	0.02	0.01
CaO	17.85	18.07	17.91	17.23	17.90	18.44	17.02	17.65	18.33	17.67
Na_2O	3.40	3.42	3.33	3.68	3.27	3.14	3.70	3.27	3.17	3.38
K_2O	0.10	0.12	0.21	0.22	0.30	0.08	0.19	0.12	0.10	0.08
Cl	0.02	0.05	0.15	0.14	0.35	0.21	0.16	0.11	0.01	0.02
SO_3	2.76	0.41	0.13	0.24	0.28	0.13	1.12	0.59	0.00	2.23
CO_2	3.18	4.51	4.53	4.50	4.19	4.46	3.94	4.33	4.79	3.48
-O=Cl	0.00	0.01	0.03	0.03	0.08	0.05	0.04	0.02	0.00	0.00
TOTAL	100.03	100.41	99.89	99.98	99.68	99.88	99.42	99.83	100.33	99.71
Si	7.083	7.043	7.047	7.134	7.010	6.915	7.122	7.094	7.018	7.007
Al	4.917	4.957	4.953	4.866	4.990	5.085	4.878	4.906	4.982	4.993
Fe	0.010	0.009	0.007	0.009	0.005	0.003	0.010	0.015	0.011	0.010
Mn	0.003	0.004	0.003	0.001	0.003	0.000	0.004	0.000	0.003	0.001
Ca	2.964	2.953	2.933	2.813	2.937	3.020	2.805	2.891	2.991	2.925
Na	1.022	1.012	0.987	1.087	0.971	0.931	1.104	0.970	0.937	1.013
K	0.020	0.023	0.041	0.043	0.059	0.016	0.037	0.023	0.019	0.016
Cl	0.005	0.013	0.039	0.036	0.091	0.054	0.042	0.029	0.003	0.005
SO_4	0.321	0.047	0.015	0.027	0.032	0.015	0.129	0.068	0.000	0.261
CO_3	0.673	0.940	0.946	0.936	0.877	0.931	0.829	0.903	0.997	0.734

SAMPLE	S86E -45-2	S86E -53a	80DMA 348c	80DMA 614p	85DMP -174-1a	85DMP 272-2a	CCM 0114	MMJ 3024	MMJ 3011	MMJ 3041
SiO_2	45.37	46.20	45.60	44.69	46.98	45.57	45.12	46.04	45.35	45.44
Al_2O_3	27.72	26.05	25.97	26.42	25.60	26.29	26.79	27.64	27.85	27.05
Fe_2O_3	0.14	0.12	0.23	0.09	0.11	0.25	0.19	0.10	0.12	0.14
MnO	0.07	0.00	0.00	0.00	0.00	0.00	0.03	0.05	0.01	0.05
CaO	18.11	16.82	16.36	17.33	15.56	17.19	17.68	17.89	18.73	17.50
Na_2O	3.06	3.86	3.84	3.58	4.29	3.75	3.27	3.21	2.90	3.38
K_2O	0.15	0.05	0.11	0.08	0.11	0.04	0.08	0.14	0.08	0.12
Cl	0.12	0.03	0.05	0.07	0.07	0.06	0.02	0.09	0.01	0.04
SO_3	0.00	4.14	5.03	4.44	3.94	4.55	4.12	0.17	0.34	3.43
CO_2	4.61	2.38	1.82	2.10	2.45	2.09	2.39	4.53	4.57	2.78
-O=Cl	0.03	0.01	0.01	0.02	0.02	0.01	0.00	0.02	0.00	0.01
TOTAL	99.32	99.64	99.00	98.78	99.09	99.78	99.69	99.84	99.96	99.92
Si	6.976	7.208	7.180	7.072	7.306	7.142	7.059	6.963	6.961	7.051
Al	5.024	4.792	4.821	4.928	4.694	4.858	4.941	5.037	5.039	4.949
Fe	0.016	0.014	0.027	0.011	0.012	0.030	0.021	0.012	0.014	0.016
Mn	0.009	0.000	0.000	0.000	0.000	0.000	0.004	0.007	0.001	0.007
Ca	2.983	2.811	2.760	2.938	2.592	2.694	2.963	2.963	3.080	2.909
Na	0.912	1.168	1.173	1.099	1.294	1.100	0.992	0.962	0.863	1.017
K	0.029	0.010	0.022	0.017	0.022	0.008	0.016	0.028	0.016	0.024
Cl	0.031	0.008	0.013	0.019	0.018	0.016	0.005	0.024	0.003	0.011
SO_4	0.000	0.485	0.595	0.528	0.460	0.536	0.489	0.020	0.039	0.400
CO_3	0.969	0.507	0.392	0.453	0.521	0.448	0.511	0.957	0.958	0.590

SAMPLE	MMJ 3023	WSA -1Core	WSA -1Rim	BOLT	HDG	DC6	UK-1	X27	TCD 4	TCD 5
SiO_2	46.28	50.00	50.49	46.64	46.27	47.75	44.51	45.34	43.73	43.73
Al_2O_3	27.09	25.38	25.11	27.23	27.08	26.25	27.57	27.69	29.07	28.52
Fe_2O_3	0.08	0.11	0.09	0.01	0.07	0.16	0.07	0.11	0.25	0.23
MnO	0.01	0.02	0.03	0.00	0.02	0.00	0.08	0.03	0.02	0.07
CaO	17.33	14.04	13.72	17.04	17.56	16.25	18.50	18.24	20.40	20.40
Na_2O	3.55	5.44	5.62	4.13	3.21	4.16	2.92	3.19	2.08	2.06
K_2O	0.29	0.61	0.55	0.12	0.17	0.33	0.10	0.17	0.16	0.10
Cl	0.22	0.96	1.12	0.47	0.07	0.72	0.08	0.19	0.03	0.03
SO_3	2.01	0.54	0.46	0.03	0.02	0.17	0.00	0.00	0.06	0.03
CO_2	3.40	3.39	3.24	4.20	4.68	3.81	4.60	4.52	4.69	4.67
-O=Cl	0.05	0.22	0.25	0.11	0.02	0.16	0.02	0.04	0.01	0.01
TOTAL	100.21	100.27	100.18	99.76	99.13	99.44	98.41	99.44	100.48	99.83
Si	7.100	7.507	7.565	7.107	7.101	7.281	6.936	6.977	6.728	6.784
Al	4.900	4.493	4.435	4.893	4.899	4.719	5.064	5.023	5.272	5.216
Fe	0.009	0.012	0.010	0.001	0.008	0.018	0.008	0.013	0.029	0.027
Mn	0.001	0.003	0.004	0.000	0.003	0.000	0.011	0.004	0.003	0.009
Ca	2.848	2.258	2.202	2.787	2.887	2.655	3.088	3.007	3.362	3.390
Na	1.056	1.584	1.633	1.220	0.955	1.230	0.882	0.952	0.621	0.620
K	0.057	0.117	0.105	0.023	0.033	0.064	0.020	0.033	0.031	0.020
Cl	0.057	0.244	0.284	0.121	0.018	0.186	0.021	0.050	0.008	0.008
SO_4	0.232	0.061	0.052	0.003	0.002	0.019	0.000	0.000	0.007	0.003
CO_3	0.712	0.735	0.664	0.875	0.980	0.794	0.979	0.950	0.985	0.989

SAMPLE	TCD 25	TCD 33A	TCD 39	SRI 285(C)	SRI 285(R)	HA 10/83	HA 46/85	HA 53/80	HA 54/83	STOLZ 32-90
SiO_2	43.37	46.73	45.94	46.53	46.91	46.06	48.45	47.19	45.69	44.90
Al_2O_3	29.03	26.00	26.24	25.61	25.89	26.77	25.33	25.46	26.62	27.17
Fe_2O_3	0.22	0.10	0.12	0.16	0.16	0.13	0.11	0.06	0.14	0.33
MnO	0.01	0.03	0.02	0.02	0.00	0.02	0.01	0.02	0.00	0.03
CaO	19.76	16.73	16.84	16.20	16.70	16.75	14.50	15.62	17.12	17.75
Na_2O	2.17	4.13	4.00	4.15	4.11	3.63	4.85	4.40	3.51	3.25
K_2O	0.11	0.03	0.03	0.04	0.03	0.18	0.51	0.07	0.08	0.13
Cl	0.05	0.04	0.02	0.02	0.04	0.26	0.54	0.13	0.13	0.02
SO_3	0.03	4.77	4.96	5.23	4.84	3.28	4.21	5.63	5.14	4.13
CO_2	4.66	2.04	1.94	1.78	2.01	2.61	1.79	1.45	1.72	2.40
-O=Cl	0.01	0.01	0.00	0.00	0.01	0.06	0.12	0.03	0.03	0.00
TOTAL	99.40	100.59	100.11	99.74	100.68	99.63	100.18	100.00	100.12	100.11
Si	6.707	7.247	7.171	7.278	7.270	7.121	7.424	7.335	7.114	7.004
Al	5.293	4.753	4.829	4.722	4.730	4.879	4.576	4.665	4.886	4.996
Fe	0.026	0.012	0.014	0.019	0.019	0.015	0.013	0.007	0.016	0.039
Mn	0.001	0.004	0.003	0.003	0.000	0.003	0.001	0.003	0.000	0.004
Ca	3.274	2.779	2.816	2.715	2.773	2.774	2.380	2.601	2.856	2.963
Na	0.651	1.242	1.211	1.259	1.235	1.088	1.441	1.326	1.060	0.983
K	0.022	0.006	0.006	0.008	0.006	0.036	0.100	0.014	0.016	0.026
Cl	0.013	0.011	0.005	0.005	0.011	0.068	0.140	0.034	0.034	0.005
SO_4	0.003	0.556	0.582	0.615	0.563	0.381	0.485	0.657	0.601	0.484
CO_3	0.983	0.433	0.413	0.380	0.426	0.551	0.375	0.309	0.365	0.511

Plagioclase Analyses

SAMPLE	ARM4	A85A -3a-1	A85A -3a-2	A85A -3b	A85A -3d-1	A85A -3d-2	A86B 3-3a	A86B -3-3b-3	B11	B26a
SiO_2	58.24	51.41	47.52	50.87	56.39	60.73	57.09	56.40	65.48	56.76
Al_2O_3	27.39	31.03	33.35	32.31	27.68	24.97	26.89	27.32	21.90	27.76
Fe_2O_3	0.04	0.02	0.04	0.10	0.00	0.08	0.07	0.05	0.03	0.03
CaO	8.74	14.09	17.30	14.74	10.24	6.54	9.06	8.93	2.72	9.51
Na_2O	6.79	3.56	1.85	3.17	5.97	7.95	6.34	6.20	10.14	6.16
K_2O	0.11	0.13	0.07	0.09	0.13	0.12	0.24	0.21	0.16	0.15
TOTAL	101.31	100.24	100.13	101.28	100.41	100.39	99.69	99.11	100.43	100.37
Si	2.572	2.319	2.263	2.290	2.523	2.692	2.568	2.552	2.869	2.538
Al	1.426	1.674	1.748	1.715	1.460	1.305	1.426	1.457	1.131	1.463
Fe	0.001	0.004	0.001	0.004	0.000	0.003	0.002	0.002	0.001	0.001
Ca	0.413	0.682	0.824	0.710	0.490	0.311	0.437	0.433	0.128	0.455
Na	0.581	0.314	0.159	0.276	0.518	0.683	0.553	0.544	0.862	0.534
K	0.006	0.008	0.004	0.005	0.007	0.007	0.014	0.012	0.009	0.009

SAMPLE	BA20a	C1b	DEB83C -4	GL28a-1	GL28b	H10	H13	H85A -1e(1)	H85A -1e(2)	H85A -1d-1
SiO_2	63.70	57.33	56.37	62.51	67.78	64.47	66.50	55.93	55.51	51.13
Al_2O_3	22.85	27.25	27.88	23.73	20.10	22.83	21.71	26.97	28.76	30.97
Fe_2O_3	0.00	0.07	0.00	0.09	0.02	0.09	0.04	0.04	0.10	0.07
CaO	3.72	9.11	9.78	4.80	0.36	3.42	2.42	9.17	10.62	13.91
Na_2O	9.33	6.61	6.10	8.81	11.54	9.67	10.15	6.25	5.42	3.54
K_2O	0.31	0.20	0.15	0.22	0.02	0.26	0.23	0.24	0.22	0.22
TOTAL	99.91	100.57	100.28	100.16	99.82	100.74	101.05	98.60	100.63	99.84
Si	2.816	2.551	2.522	2.764	2.966	2.822	2.899	2.542	2.485	2.329
Al	1.191	1.430	1.471	1.237	1.037	1.178	1.116	1.445	1.518	1.664
Fe	0.000	0.002	0.000	0.003	0.001	0.003	0.001	0.001	0.003	0.002
Ca	0.176	0.451	0.469	0.227	0.017	0.160	0.113	0.446	0.509	0.679
Na	0.800	0.570	0.529	0.756	0.979	0.821	0.858	0.551	0.471	0.313
K	0.017	0.011	0.009	0.012	0.001	0.015	0.013	0.014	0.013	0.013

SAMPLE	H85A -1b	H85A -1(3)	Mpib	Mpid	M49	M53	M65	M85A-6a	M86E -1b	M86E -1C-2
SiO_2	50.12	59.83	59.04	59.94	57.76	56.87	63.59	62.18	62.11	60.79
Al_2O_3	32.15	25.60	26.29	25.38	27.00	27.49	22.69	24.13	24.01	24.64
Fe_2O_3	0.12	0.05	0.01	0.02	0.16	0.12	0.10	0.03	0.01	0.01
CaO	15.01	7.14	7.81	6.87	8.68	9.24	3.60	5.62	5.27	5.84
Na_2O	2.97	7.40	7.23	7.60	6.64	6.26	9.37	8.55	8.59	8.09
K_2O	0.08	0.26	0.28	0.25	0.25	0.14	0.41	0.23	0.23	0.36
TOTAL	100.45	100.28	100.66	100.06	100.49	100.12	99.76	100.74	100.22	99.73
Si	2.277	2.662	2.617	2.634	2.574	2.548	2.814	2.742	2.748	2.708
Al	1.722	1.343	1.374	1.265	1.418	1.452	1.184	1.254	1.252	1.294
Fe	0.004	0.002	0.000	0.001	0.005	0.004	0.003	0.001	0.000	0.000
Ca	0.730	0.340	0.371	0.311	0.414	0.444	0.171	0.265	0.250	0.279
Na	0.262	0.638	0.622	0.623	0.574	0.544	0.804	0.731	0.737	0.699
K	0.005	0.015	0.016	0.014	0.014	0.008	0.023	0.006	0.013	0.020

SAMPLE	08e	015b	PS7a	PS7b	PS7c	PS7g(e) matrix	PS7g(e) porph	PS7g matrix	PS7g porph	PS85A -0a
SiO_2	55.28	61.25	55.42	56.48	57.67	58.05	53.65	63.85	61.00	61.10
Al_2O_3	28.58	24.42	27.89	27.51	26.99	26.45	29.74	22.57	24.27	24.61
Fe^{3+}	0.08	0.04	0.11	0.10	0.06	0.05	0.06	0.11	0.03	0.06
CaO	10.87	5.93	9.93	8.98	8.97	8.25	11.96	3.59	5.55	5.94
Na_2O	5.54	8.20	5.83	6.17	6.33	6.89	4.81	9.53	8.24	8.14
K_2O	0.24	0.28	0.18	0.25	0.27	0.29	0.20	0.31	0.35	0.43
TOTAL	100.59	100.12	99.36	99.49	100.29	99.98	100.32	99.96	99.44	100.28
Si	2.473	2.718	2.506	2.546	2.580	2.595	2.416	2.819	2.723	2.705
Al	1.508	1.277	1.487	1.462	1.424	1.394	1.579	1.175	1.277	1.285
Fe	0.003	0.001	0.004	0.003	0.002	0.003	0.002	0.004	0.001	0.002
Ca	0.522	0.282	0.481	0.434	0.430	0.395	0.572	0.170	0.265	0.282
Na	0.481	0.706	0.511	0.539	0.549	0.597	0.420	0.816	0.713	0.699
K	0.014	0.016	0.010	0.014	0.015	0.017	0.011	0.017	0.020	0.024

SAMPLE	PS85A -1a	PS85A -2c	PS085A -5-1	PS085A -5-12	PS85A -7	PS085A -8b	PS85A -8b	PS085A -13	PS085A -23	PS085A -24
SiO_2	52.52	54.24	59.21	59.21	51.69	56.19	52.67	58.03	58.90	54.54
Al_2O_3	29.91	29.33	26.34	26.34	31.85	27.60	30.65	26.58	25.90	28.97
Fe_2O_3	0.03	0.05	0.04	0.04	0.09	0.08	0.02	0.12	0.03	0.06
CaO	12.15	11.89	7.67	7.67	13.73	9.56	12.95	8.58	7.20	11.09
Na_2O	4.41	4.90	7.27	7.27	3.74	6.05	4.23	6.82	7.30	5.27
K_2O	0.06	0.15	0.23	0.23	0.10	0.24	0.06	0.07	0.26	0.15
TOTAL	99.08	100.56	100.76	100.76	101.20	99.72	100.58	100.20	99.59	100.08
Si	2.399	2.437	2.622	2.622	2.320	2.529	2.373	2.591	2.637	2.456
Al	1.611	1.554	1.375	1.375	1.686	1.465	1.628	1.400	1.367	1.538
Fe	0.001	0.002	0.001	0.001	0.003	0.003	0.001	0.004	0.001	0.002
Ca	0.595	0.572	0.364	0.364	0.661	0.461	0.625	0.410	0.345	0.535
Na	0.391	0.427	0.624	0.624	0.325	0.528	0.370	0.591	0.634	0.460
K	0.003	0.009	0.013	0.013	0.005	0.014	0.003	0.004	0.015	0.009

SAMPLE	PS86B 1-1	PS86B 1-6	PS86B 1-7	PS86B 1-8	PS86B 1-9b	PS86B 1-10a	PS86B 1-11"	PS86B 2-1	PS86B 2-3	PS86E -6b
SiO_2	58.49	61.79	63.95	63.8	63.50	58.18	55.22	58.57	55.21	60.12
Al_2O_3	25.95	23.72	22.19	22.39	22.62	26.20	27.65	25.93	27.77	25.31
Fe_2O_3	0.03	0.11	0.09	0.03	0.09	0.03	0.08	0.06	0.07	0.04
CaO	7.61	4.56	3.17	3.083	3.27	7.67	9.98	8.04	10.09	6.83
Na_2O	7.01	8.89	9.81	9.59	9.62	7.03	5.48	6.73	5.86	7.63
K_2O	0.26	0.26	0.21	0.29	0.20	0.23	0.09	0.26	0.18	0.24
TOTAL	99.35	99.33	99.42	99.18	99.30	99.34	98.50	99.59	99.18	100.19
Si	2.630	2.751	2.833	2.836	2.818	2.615	2.526	2.634	2.500	2.674
Al	1.376	1.245	1.159	1.173	1.184	1.388	1.491	1.375	1.483	1.327
Fe	0.001	0.004	0.003	0.001	0.003	0.001	0.003	0.002	0.002	0.001
Ca	0.367	0.217	0.150	0.147	0.155	0.369	0.489	0.387	0.450	0.325
Na	0.611	0.768	0.843	0.827	0.828	0.613	0.486	0.587	0.515	0.658
K	0.015	0.015	0.012	0.016	0.011	0.013	0.005	0.015	0.010	0.014

SAMPLE	PS86E -7e	PS86E -8	PS86E -10	PS86E -12	PS86E -15	PS86E -16a	PS86E -17	PS86E -23-1	PS86E -24b	PS86E -24d
SiO_2	56.69	55.30	54.80	53.36	54.92	53.81	54.03	54.51	56.11	56.53
Al_2O_3	27.46	27.80	28.85	29.53	28.79	28.73	28.95	29.04	27.51	27.80
Fe_2O_3	0.03	0.02	0.08	0.04	0.09	0.04	0.08	0.09	0.05	0.08
CaO	9.25	9.97	10.84	11.80	10.59	11.09	11.24	11.29	9.36	9.34
Na_2O	6.37	6.02	5.44	4.92	5.58	5.30	5.26	5.04	6.24	6.23
K_2O	0.14	0.07	0.06	0.05	0.06	0.13	0.04	0.11	0.20	0.06
TOTAL	99.94	99.18	100.07	99.70	100.03	99.10	99.60	100.08	99.47	100.04
Si	2.542	2.502	2.466	2.416	2.470	2.445	2.446	2.459	2.528	2.534
Al	1.451	1.483	1.531	1.576	1.526	1.539	1.544	1.544	1.461	1.469
Fe	0.001	0.001	0.003	0.001	0.003	0.001	0.003	0.003	0.002	0.003
Ca	0.444	0.483	0.523	0.572	0.510	0.540	0.545	0.546	0.452	0.449
Na	0.554	0.528	0.475	0.432	0.487	0.467	0.462	0.441	0.545	0.542
K	0.008	0.004	0.003	0.003	0.003	0.008	0.002	0.006	0.012	0.003

SAMPLE	PS86E -24f	PS86E -31	PS86E -34	S3b	S4d	S10b	S32	SUN84B -18	S85A -2a	S85A -2b
SiO_2	55.31	57.94	58.25	57.71	60.86	58.89	58.64	59.04	58.80	60.92
Al_2O_3	28.20	26.73	26.03	26.97	24.75	26.84	26.42	26.04	26.71	24.38
Fe_2O_3	0.07	0.04	0.05	0.07	0.02	0.06	0.12	0.08	0.04	0.01
CaO	9.93	8.71	7.88	8.49	6.04	7.93	7.81	7.62	8.13	5.91
Na_2O	5.99	6.55	7.28	6.85	7.81	7.15	7.12	7.33	6.89	8.08
K_2O	0.00	0.13	0.12	0.23	0.65	0.27	0.37	0.14	0.26	0.14
TOTAL	99.50	100.10	99.61	100.32	100.13	101.14	100.48	100.25	100.83	99.44
Si	2.495	2.594	2.608	2.571	2.705	2.599	2.605	2.625	2.608	2.723
Al	1.299	1.411	1.374	1.416	1.297	1.397	1.384	1.365	1.397	1.285
Fe	0.002	0.001	0.002	0.002	0.001	0.002	0.004	0.003	0.001	0.001
Ca	0.480	0.418	0.378	0.405	0.288	0.375	0.372	0.363	0.386	0.283
Na	0.524	0.569	0.632	0.592	0.673	0.612	0.614	0.632	0.593	0.700
K	0.000	0.007	0.007	0.013	0.037	0.015	0.021	0.008	0.015	0.008

SAMPLE	S85A -2d	S85A -3a(c)	S85A -3a(r)	S85A -3b	S85A -3c	S86E -8c	S86E -10	S86E -25a	S86E -25c	S86E -25i
SiO_2	58.10	53.71	54.22	54.04	54.09	59.66	55.33	54.92	56.48	59.31
Al_2O_3	26.76	30.19	29.63	29.01	29.34	25.24	28.28	28.58	27.48	25.60
Fe_2O_3	0.01	0.10	0.09	0.08	0.04	0.08	0.06	0.09	0.04	0.04
CaO	8.02	12.24	11.50	11.66	11.47	6.42	10.59	10.60	9.34	7.14
Na_2O	6.79	4.63	4.88	4.92	5.04	7.71	5.52	5.37	6.15	7.35
K_2O	0.40	0.08	0.10	0.23	0.18	0.24	0.23	0.18	0.28	0.28
TOTAL	100.08	100.95	100.42	99.94	100.16	99.35	100.01	99.74	99.77	99.72
Si	2.595	2.408	2.440	2.442	2.436	2.672	2.491	2.481	2.540	2.653
Al	1.409	1.595	1.572	1.546	1.558	1.333	1.501	1.522	1.457	1.350
Fe	0.000	0.003	0.003	0.003	0.001	0.003	0.002	0.003	0.001	0.001
Ca	0.384	0.588	0.555	0.565	0.553	0.308	0.511	0.513	0.450	0.342
Na	0.588	0.402	0.426	0.431	0.440	0.670	0.482	0.470	0.536	0.638
K	0.023	0.004	0.005	0.013	0.010	0.014	0.013	0.010	0.016	0.016

SAMPLE	S86E -34	S86E -36b	S86E -41	S86E -45-1	S86E -45-2	S86E -53a	80DMA 348c	80DMA 614p	85DMP -174-1a	85DMP 272-2a
SiO_2	56.04	55.35	53.47	52.69	52.69	58.14	57.38	54.74	59.79	57.26
Al_2O_3	27.73	28.41	29.51	30.32	30.32	26.30	26.33	28.15	25.25	26.81
Fe_2O_3	0.05	0.06	0.03	0.12	0.12	0.16	0.11	0.07	0.10	0.04
CaO	9.79	10.28	11.74	12.25	12.25	8.06	8.23	10.49	6.32	8.62
Na_2O	5.93	5.60	4.71	4.37	4.37	6.85	6.61	5.57	7.62	6.72
K_2O	0.28	0.25	0.18	0.18	0.18	0.19	0.42	0.19	0.36	0.12
TOTAL	99.82	99.95	99.64	99.93	99.93	99.70	99.08	99.21	99.44	99.57
Si	2.522	2.491	2.425	2.387	2.387	2.609	2.592	2.482	2.678	2.572
Al	1.471	1.508	1.578	1.619	1.619	1.391	1.402	1.505	1.333	1.420
Fe	0.002	0.002	0.001	0.004	0.004	0.005	0.004	0.002	0.003	0.001
Ca	0.471	0.496	0.570	0.595	0.595	0.387	0.398	0.510	0.303	0.415
Na	0.516	0.489	0.414	0.384	0.384	0.596	0.579	0.490	0.662	0.585
K	0.016	0.014	0.010	0.010	0.010	0.011	0.024	0.011	0.021	0.007

SAMPLE	CCM 0114	MMJ 3024	MMJ 3011	MMJ 3011	MMJ 3023	DC6	TCD 4	TCD 5	TCD 25	TCD 33A
SiO_2	52.30	53.64	53.99	52.70	52.54	56.09	45.37	45.15	44.53	59.12
Al_2O_3	30.53	29.80	29.22	30.28	30.27	27.55	35.26	34.92	35.85	26.02
Fe_2O_3	0.08	0.06	0.11	0.09	0.07	0.10	0.22	0.17	0.17	0.06
CaO	12.80	11.88	11.53	12.72	12.61	9.84	18.67	19.00	18.65	7.76
Na_2O	4.09	4.66	4.92	4.12	4.25	5.80	0.89	0.81	0.82	7.33
K_2O	0.20	0.16	0.24	0.42	0.18	0.11	0.02	0.03	0.03	0.03
TOTAL	100.00	100.20	100.01	100.33	99.92	99.49	100.43	100.08	100.05	100.32
Si	2.372	2.421	2.438	2.382	2.382	2.535	2.084	2.089	2.051	2.630
Al	1.632	1.585	1.555	1.613	1.618	1.468	1.909	1.905	1.947	1.364
Fe	0.003	0.002	0.004	0.003	0.002	0.005	0.008	0.006	0.006	0.002
Ca	0.622	0.574	0.558	0.616	0.613	0.476	0.919	0.942	0.920	0.370
Na	0.360	0.408	0.431	0.361	0.374	0.508	0.079	0.055	0.073	0.632
K	0.012	0.009	0.014	0.024	0.010	0.006	0.001	0.002	0.002	0.002

SAMPLE	TCD 39	SRI 285C	SRI 285(R)	HA 10/83	HA 46/85	HA 53/80	HA 54/83	STOLZ 32-90
SiO_2	58.34	58.73	59.00	55.48	59.83	60.95	55.53	55.42
Al_2O_3	26.36	26.16	25.73	28.36	25.35	24.89	28.32	28.06
Fe_2O_3	0.06	0.06	0.11	0.04	0.08	0.05	0.03	0.13
CaO	7.95	7.80	7.54	10.26	6.67	6.41	10.45	10.19
Na_2O	7.18	7.05	7.18	5.51	7.49	7.76	5.46	5.57
K_2O	0.04	0.17	0.16	0.19	0.43	0.34	0.48	0.41
TOTAL	99.93	99.97	99.72	99.84	99.85	100.40	100.27	99.78
Si	2.605	2.625	2.643	2.502	2.671	2.704	2.493	2.500
Al	1.388	1.378	1.359	1.508	1.334	1.302	1.499	1.492
Fe	0.002	0.002	0.004	0.001	0.003	0.002	0.001	0.004
Ca	0.380	0.374	0.362	0.496	0.319	0.305	0.503	0.492
Na	0.622	0.611	0.624	0.482	0.648	0.668	0.475	0.487
K	0.002	0.010	0.009	0.011	0.029	0.019	0.028	0.024

Garnet Analyses

SAMPLE	ARM4	A85A -3a	A85A -3b	A85A -3d	A85A -3f	A86B 3-3b-3	C1b	DEB83C -4	H85A -1b	H85A -1d-1
SiO_2	38.87	37.99	38.21	39.78	39.17	39.31	38.63	38.14	38.24	39.17
TiO_2	0.08	0.00	0.07	0.27	0.29	0.00	0.08	0.01	0.14	0.26
Al_2O_3	21.30	20.98	20.75	20.87	29.87	21.41	20.81	21.14	15.58	19.21
Cr_2O_3	0.05	0.02	0.00	0.05	0.00	0.05	0.00	0.06	0.09	0.05
Fe_2O_3	0.72	0.59	0.82	1.15	0.64	0.98	0.00	0.44	8.45	4.02
FeO	23.67	26.01	24.80	3.96	3.94	24.46	20.10	23.84	18.97	5.64
MnO	2.05	1.62	1.36	0.10	0.11	2.57	1.55	1.77	1.24	0.28
MgO	4.85	1.07	1.46	0.22	0.24	7.94	1.49	1.52	0.07	0.02
CaO	9.98	12.47	12.98	34.65	22.72	4.65	16.66	13.50	24.44	34.91
FeO^1	23.03	25.48	24.07	2.93	3.36	23.58	20.10	23.45	11.38	2.03
Total	100.93	100.22	99.72	100.02	96.40	100.49	99.32	100.03	99.63	99.95
Si	3.003	3.014	3.035	3.017	3.017	3.022	3.046	3.012	3.059	3.000
Ti	0.005	0.000	0.004	0.015	0.017	0.000	0.005	0.001	0.008	0.015
Al	1.940	1.963	1.943	1.866	1.895	1.940	1.935	1.968	1.469	1.735
Cr	0.003	0.002	0.000	0.003	0.000	0.003	0.000	0.004	0.006	0.003
Fe^{3+}	0.047	0.035	0.049	0.066	0.037	0.057	0.000	0.026	0.509	0.232
Fe^{2+}	1.484	1.692	1.600	0.186	0.217	1.517	1.326	1.550	0.762	0.130
Mn	0.134	0.109	0.091	0.006	0.007	0.167	0.103	0.118	0.084	0.018
Mg	0.559	0.127	0.173	0.025	0.028	0.910	0.175	0.179	0.008	0.002
Ca	0.826	1.060	1.104	2.815	2.782	0.383	1.410	1.142	2.095	2.865

SAMPLE	H85A -1e(1)	H85A -1e(2)	M49	M65	M85A -6a	M86E -1b	M86E -1c-2	O8d	O15b	PS7a
SiO_2	38.57	38.95	38.87	38.66	39.4	39.47	39.61	39.06	38.45	37.89
TiO_2	0.30	0.26	0.07	0.05	0.74	0.36	0.32	0.29	0.03	0.02
Al_2O_3	15.14	18.73	19.56	21.53	20.66	20.59	21.08	20.28	20.96	20.57
Cr_2O_3	0.00	0.05	0.00	0.01	0.03	0.06	0.02	0.00	0.00	0.01
Fe_2O_3	9.06	4.23	2.97	0.27	1.97	1.83	1.31	2.79	0.81	1.08
FeO	15.73	11.34	20.89	26.12	2.40	2.55	2.51	5.85	27.41	25.56
MnO	0.82	0.78	4.34	0.88	0.07	0.06	0.17	0.44	3.36	1.97
MgO	0.02	0.03	1.35	5.81	0.12	0.19	0.06	0.02	2.81	2.03
CaO	27.96	29.19	15.36	6.82	36.57	35.89	35.56	33.61	7.74	11.33
FeO^1	7.58	7.54	18.22	25.88	0.63	0.90	1.33	3.35	26.68	24.59
Total	99.45	99.76	100.74	99.91	100.19	99.35	99.46	99.84	100.84	99.49
Si	3.071	3.033	3.060	3.012	2.976	3.007	3.010	2.988	3.032	3.019
Ti	0.018	0.015	0.004	0.003	0.042	0.021	0.018	0.017	0.002	0.001
Al	1.421	1.719	1.816	1.978	1.839	1.849	1.888	1.830	1.948	1.932
Cr	0.000	0.003	0.000	0.001	0.003	0.004	0.001	0.000	0.000	0.001
Fe^{3+}	0.543	0.248	0.176	0.016	0.112	0.105	0.075	0.160	0.048	0.065
Fe^{2+}	0.505	0.491	1.201	1.688	0.040	0.058	0.085	0.214	1.761	1.640
Mn	0.055	0.051	0.289	0.058	0.004	0.004	0.004	0.029	0.224	0.133
Mg	0.002	0.003	0.158	0.675	0.014	0.022	0.014	0.002	0.330	0.241
Ca	2.385	2.435	1.246	0.569	2.959	2.929	2.895	2.760	0.654	0.967

SAMPLE	PS7b	PC7c -9	PS7c -15	PS7g(e) w/sc	PS7g(e) w/cpx	PS7g	PS85A -2c	PS085A -5	PS085A -8b	PS085A -13 w/Sc,Pg
SiO_2	38.10	38.50	39.06	38.38	37.95	37.52	38.27	38.13	38.04	38.79
TiO_2	0.09	0.05	0.00	0.02	0.04	0.03	0.00	0.00	0.03	0.07
Al_2O_3	20.47	21.43	21.31	21.02	20.82	20.44	20.93	20.91	20.68	20.87
Cr_2O_3	0.00	0.00	0.00	0.01	0.09	0.00	0.00	0.00	0.00	0.01
Fe_2O_3	0.22	0.39	0.00	1.22	1.12	0.79	0.88	1.25	1.08	1.40
FeO	24.99	23.47	24.50	24.90	23.62	30.46	23.80	26.01	26.02	23.85
MnO	0.51	0.79	0.76	1.27	1.8	1.23	3.81	1.65	0.80	0.82
MgO	2.53	2.49	2.99	2.52	2.31	1.22	1.62	3.14	2.49	3.27
CaO	12.33	13.74	12.31	12.61	13.11	8.78	11.98	10.47	11.53	13.15
FeO^1	24.79	23.11	24.50	23.80	22.61	27.22	23.02	24.89	25.04	22.59
Total	99.04	100.50	100.93	100.85	99.85	97.23	100.51	100.44	99.69	100.97
Si	3.029	3.003	3.034	3.021	2.995	3.020	3.021	2.995	3.014	3.011
Ti	0.005	0.003	0.000	0.001	0.002	0.002	0.000	0.000	0.002	0.004
Al	1.918	1.971	1.952	1.926	1.937	1.940	1.948	1.936	1.932	1.910
Cr	0.000	0.000	0.000	0.001	0.002	0.000	0.000	0.000	0.000	0.001
Fe^{3+}	0.013	0.023	0.000	0.071	0.067	0.012	0.052	0.074	0.065	0.082
Fe^{2+}	1.650	1.509	1.593	1.548	1.494	1.928	1.521	1.636	1.661	1.468
Mn	0.034	0.052	0.050	0.090	0.12	0.084	0.255	0.110	0.054	0.054
Mg	0.300	0.290	0.346	0.292	0.272	0.146	0.191	0.368	0.294	0.378
Ca	1.050	1.148	1.024	1.050	1.108	0.757	1.013	0.881	0.979	1.093

SAMPLE	PS085A -13 porph	PS085A -13 resorb	PS085A -23	PS085A -24	PS86B 1-1	PS86B 1-6	PS86B 1-7	PS86B 1-8	PS86B 1-9b core	PS86B 1-9b rim
SiO_2	38.96	38.56	38.87	38.78	38.06	37.76	37.15	37.85	37.70	37.76
TiO_2	0.08	0.11	0.38	0.04	0.03	0.02	0.04	0.02	0.03	0.06
Al_2O_3	20.91	20.79	19.20	21.20	20.83	20.39	20.61	20.48	20.36	20.39
Cr_2O_3	0.02	0.05	0.01	0.01	0.02	0.03	0.02	0.01	0.01	0.05
Fe_2O_3	1.50	1.52	3.95	1.13	0.60	1.25	0.82	1.07	1.14	1.21
FeO	24.11	24.22	6.64	25.15	25.78	29.51	31.90	31.56	30.37	28.16
MnO	0.60	1.05	0.35	0.80	1.29	1.52	1.51	1.46	2.52	3.22
MgO	3.72	3.97	0.12	5.46	1.56	1.20	1.15	1.08	0.92	0.72
CaO	12.82	11.86	33.69	9.14	11.73	9.73	7.56	8.03	8.44	10.07
FeO^1	22.76	22.85	3.09	24.13	25.24	28.39	31.17	30.60	29.34	27.07
Total	101.37	100.76	99.66	100.69	99.36	100.29	100.03	100.60	100.46	100.55
Si	3.007	2.996	2.992	2.998	3.037	3.017	2.993	3.017	3.027	3.031
Ti	0.005	0.006	0.022	0.002	0.002	0.001	0.002	0.001	0.002	0.001
Al	1.902	1.904	1.742	1.932	1.959	1.921	1.458	1.933	1.926	1.922
Cr	0.001	0.003	0.001	0.000	0.001	0.002	0.001	0.001	0.001	0.003
Fe^{3+}	0.087	0.089	0.229	0.066	0.036	0.075	0.049	0.064	0.069	0.073
Fe^{2+}	1.471	1.486	0.199	1.562	1.686	1.899	2.102	2.042	1.972	1.819
Mn	0.039	0.069	0.023	0.052	0.087	0.103	0.103	0.099	0.171	0.218
Mg	0.428	0.460	0.014	0.630	0.186	0.143	0.135	0.129	0.110	0.086
Ca	1.060	0.987	2.778	0.757	1.003	0.833	0.653	0.689	0.726	0.863

SAMPLE	PS86B 1-10a core	PS86B 1-10a rim	PS86B 1-11"	PS86B 2-1	PS86B 2-3 core	PS86B 2-3 rim	PS86E -6B core	PS86E -6B rim	PS86E -7e	PS86E -8
SiO_2	38.25	38.32	38.00	38.15	38.66	38.51	38.20	38.26	37.94	38.12
TiO_2	0.06	0.04	0.04	0.04	0.04	0.08	0.07	0.06	0.04	0.04
Al_2O_3	20.50	20.87	20.57	20.52	20.72	20.94	20.48	20.48	20.11	20.44
Cr_2O_3	0.02	0.01	0.02	0.00	0.02	0.00	0.10	0.02	0.00	0.02
Fe_2O_3	1.33	1.00	1.12	1.27	1.34	0.85	1.55	1.50	1.66	1.57
FeO	25.77	26.06	27.72	26.27	25.50	25.75	25.27	25.55	25.95	24.43
MnO	1.15	0.65	1.72	0.80	1.19	0.91	1.09	0.88	1.48	3.13
MgO	2.40	2.75	1.96	2.03	2.82	2.78	3.23	2.78	1.45	1.79
CaO	11.66	11.40	10.00	11.81	11.47	11.29	11.49	11.75	12.33	12.44
FeO^1	24.57	25.16	26.71	0.01	24.30	24.95	23.88	24.20	24.45	23.02
Total	99.94	100.20	100.14	74.63	100.56	100.31	100.09	99.93	99.46	100.57
Si	3.027	3.015	3.021	3.030	3.033	3.026	3.004	3.019	3.034	3.009
Ti	0.004	0.002	0.002	0.002	0.002	0.005	0.004	0.004	0.002	0.002
Al	1.912	1.936	1.928	1.921	1.916	1.940	1.899	1.905	1.896	1.902
Cr	0.001	0.001	0.001	0.000	0.001	0.000	0.006	0.001	0.000	0.001
Fe^{3+}	0.079	0.059	0.067	0.076	0.079	0.050	0.092	0.089	0.100	0.093
Fe^{2+}	1.628	1.657	1.778	1.671	1.596	1.641	1.572	1.599	1.637	1.521
Mn	0.077	0.043	0.116	0.054	0.074	0.061	0.073	0.059	0.100	0.209
Mg	0.283	0.323	0.232	0.240	0.330	0.326	0.379	0.327	0.173	0.211
Ca	0.989	0.961	0.852	1.005	0.964	0.950	0.968	0.993	1.056	1.052

SAMPLE	PS86E -12	PS86E -15	PS86E -16a	PS86E -17 w/ep,pg	PS86E -24f	PS86E -31	PS86E -34 core	PS86E -34 rim	S3b	S4c
SiO_2	38.34	38.58	38.44	38.31	38.65	38.22	38.79	38.91	38.45	38.56
TiO_2	0.05	0.06	0.04	0.06	0.05	0.06	0.03	0.03	0.03	0.04
Al_2O_3	20.39	20.67	20.81	20.58	20.94	20.62	20.78	20.85	20.96	20.83
Cr_2O_3	0.00	0.02	0.00	0.01	0.03	0.00	0.01	0.00	0.00	0.00
Fe_2O_3	1.72	1.51	1.08	1.30	1.07	1.07	1.41	1.38	0.81	1.29
FeO	24.54	26.04	26.95	24.66	25.96	25.56	26.50	26.83	27.41	28.25
MnO	2.66	1.23	1.04	1.15	1.21	1.56	1.19	0.98	3.36	1.34
MgO	2.05	3.12	2.62	1.85	2.63	1.20	3.35	3.24	2.81	4.30
CaO	12.39	11.07	10.39	13.42	11.50	12.84	10.08	10.19	7.74	7.45
FeO^1	22.99	24.68	25.98	23.49	25.00	24.59	25.23	25.59	26.68	27.09
Total	100.59	100.94	100.40	100.17	101.08	100.16	100.87	101.17	100.84	100.90
Si	3.020	3.015	3.030	3.023	3.020	3.032	3.032	3.035	3.015	3.015
Ti	0.003	0.004	0.002	0.004	0.003	0.004	1.915	0.002	0.003	0.002
Al	1.894	1.904	1.934	1.915	1.929	1.928	0.001	1.917	1.936	1.920
Cr	0.000	0.001	0.000	0.001	0.002	0.000	0.083	0.000	0.004	0.000
Fe^{3+}	0.102	0.089	0.064	0.077	0.063	0.064	0.000	0.081	0.023	0.076
Fe^{2+}	1.576	1.614	1.714	1.552	1.635	1.633	1.651	1.671	1.765	1.773
Mn	0.177	0.081	0.069	0.077	0.080	0.105	0.079	0.065	0.069	0.089
Mg	0.241	0.364	0.308	0.218	0.306	0.142	0.391	0.377	0.614	0.501
Ca	1.046	0.927	0.877	1.135	0.963	1.091	0.844	0.851	0.570	0.624

SAMPLE	S4d	S10b	S28c	S32	SUN84B -18 core	SUN84B -18 rim	S85A -2a	S85A -2b	S85A -2d	S85A -3a core
SiO_2	39.27	38.84	38.68	39.07	37.86	38.45	39.13	39.77	39.43	39.24
TiO_2	0.34	0.20	0.06	0.02	0.00	0.13	0.11	0.04	0.07	0.05
Al_2O_3	20.38	20.83	21.18	21.64	20.88	21.24	20.07	20.16	20.26	22.11
Cr_2O_3	0.02	0.00	0.01	0.00	0.00	0.00	0.04	0.02	0.01	0.02
Fe_2O_3	2.10	0.50	0.87	0.23	0.71	0.41	3.88	3.12	3.33	1.30
FeO	4.00	27.58	23.3	26.72	23.44	22.83	5.61	4.68	6.00	22.49
MnO	0.24	1.48	0.78	1.15	4.79	1.88	0.24	0.21	0.30	0.83
MgO	0.12	4.95	5.57	5.46	3.69	4.76	0.10	0.07	0.13	8.97
CaO	34.76	7.14	10.01	7.65	8.38	10.08	34.62	34.51	34.09	6.86
FeO^1	2.11	27.13	22.52	26.01	22.80	22.46	2.12	1.88	3.00	21.32
Total	99.34	101.07	99.68	101.23	99.11	99.41	100.31	99.78	100.62	100.70
Si	3.005	3.019	3.007	3.010	3.010	3.010	2.980	3.037	2.993	2.972
Ti	0.020	0.012	0.004	0.001	0.000	0.008	0.006	0.002	0.004	0.003
Al	1.839	1.909	1.941	1.965	1.957	1.960	1.802	1.815	1.815	1.975
Cr	0.001	0.000	0.001	0.000	0.000	0.000	0.002	0.002	0.001	0.001
Fe^{3+}	0.121	0.029	0.051	0.013	0.043	0.024	0.223	0.179	0.190	0.074
Fe^{2+}	0.135	1.765	1.465	1.677	1.517	1.472	0.135	0.120	0.191	1.352
Mn	0.016	0.097	0.051	0.075	0.322	0.125	0.015	0.014	0.019	0.053
Mg	0.014	0.574	0.646	0.627	0.437	0.556	0.011	0.008	0.015	1.013
Ca	2.850	0.595	0.834	0.631	0.714	0.845	2.825	2.823	2.772	0.557

SAMPLE	S85A -3a rim	S85A -3b	S85A -3c core	S85A -3c rim	S86E -8c	S86E -8i core	S86E -8i rim	S86E -10	S86E -25a	S86E -25c core
SiO_2	39.58	38.86	38.92	39.16	38.23	38.81	38.98	38.33	38.67	38.50
TiO_2	0.10	0.02	0.05	0.05	0.10	0.04	0.06	0.11	0.05	0.07
Al_2O_3	22.15	21.09	21.18	21.47	19.46	20.82	20.88	20.60	20.86	21.02
Cr_2O_3	0.02	0.00	0.00	0.00	0.03	0.00	0.02	0.01	0.00	0.00
Fe_2O_3	0.23	1.22	1.33	1.47	2.87	1.30	1.27	1.18	1.33	1.12
FeO	22.38	25.49	25.78	24.43	20.89	29.34	30.03	24.69	24.32	24.26
MnO	0.55	0.61	0.68	0.55	0.76	0.87	0.96	1.48	1.34	1.31
MgO	8.23	5.13	6.37	5.77	0.86	3.98	3.72	3.10	3.76	4.19
CaO	7.80	9.33	7.75	10.07	19.05	7.11	7.04	11.34	11.26	10.95
FeO^1	22.17	24.40	24.59	23.10	18.31	28.17	28.89	23.63	23.12	22.40
Total	100.83	100.66	100.87	101.64	99.67	101.10	101.82	99.78	100.39	99.56
Si	2.998	3.011	2.997	2.989	3.025	3.036	3.037	3.024	3.018	2.998
Ti	0.006	0.001	0.003	0.003	0.006	0.002	0.004	0.007	0.003	0.004
Al	1.978	1.927	1.923	1.932	1.816	1.920	1.918	1.916	1.919	1.930
Cr	0.001	0.000	0.000	0.000	0.002	0.000	0.001	0.001	0.000	0.000
Fe^{3+}	0.013	0.071	0.077	0.085	0.171	0.076	0.074	0.070	0.078	0.066
Fe^{2+}	1.406	1.582	1.585	1.476	1.213	1.845	1.884	1.560	1.511	1.516
Mn	0.035	0.040	0.044	0.036	0.051	0.058	0.063	0.099	0.089	0.086
Mg	0.930	0.593	0.732	0.657	0.101	0.464	0.432	0.365	0.438	0.487
Ca	0.633	0.775	0.639	0.823	1.615	0.596	0.588	0.958	0.941	0.914

SAMPLE	S86E -25c rim	S86E -33	S86E -34 core	S86E -34 rim	S86E -36b	S86E -40	S86E -41 core	S86E -41 rim	S86E -53a core	S86E -53a rim
SiO_2	38.78	37.46	38.74	38.31	38.35	38.84	38.58	38.60	39.17	38.93
TiO_2	0.03	0.07	0.08	0.08	0.08	0.04	0.06	0.03	0.06	0.02
Al_2O_3	21.05	20.67	20.81	21.02	20.71	20.61	21.06	20.86	21.66	21.77
Cr_2O_3	0.00	0.00	0.04	0.06	0.02	0.00	0.02	0.02	0.00	0.00
Fe_2O_3	1.10	0.95	0.05	0.90	1.33	1.76	1.43	1.41	0.83	0.98
FeO	23.39	32.29	25.90	24.79	26.44	25.33	26.18	25.92	22.18	23.73
MnO	1.45	1.00	0.89	0.69	1.09	0.94	0.63	0.71	0.47	0.99
MgO	3.42	1.76	4.80	4.37	3.48	6.51	6.63	5.90	6.78	6.04
CaO	12.34	7.16	8.61	10.45	10.30	7.33	6.84	7.95	10.05	9.31
FeO^1	22.40	31.44	25.86	23.98	25.24	23.75	24.89	24.66	21.43	22.85
Total	100.57	100.51	99.88	99.86	100.60	99.78	100.14	100.14	100.45	100.89
Si	3.020	2.994	3.023	2.998	3.004	3.025	2.992	3.003	2.996	2.986
Ti	0.002	0.004	0.005	0.005	0.005	0.002	0.003	0.010	0.003	0.001
Al	1.932	1.947	1.920	1.939	1.912	1.892	1.925	0.157	1.953	1.969
Cr	0.000	0.000	0.002	0.004	0.001	0.000	0.001	0.000	0.000	0.000
Fe^{3+}	0.064	0.057	0.068	0.053	0.079	0.103	0.083	0.063	0.048	0.057
Fe^{2+}	1.460	2.103	1.629	1.571	1.655	1.548	1.616	0.211	1.372	1.467
Mn	0.096	0.068	0.059	0.046	0.072	0.062	0.041	0.001	0.030	0.064
Mg	0.397	0.210	0.560	0.510	0.406	0.756	0.767	0.682	0.773	0.691
Ca	1.029	0.613	0.722	0.876	0.864	0.612	0.568	0.913	0.824	0.765

SAMPLE	85DMP 174-1a -1	85DMP 174-1a -2	80DMA -614P corona	80DMA -614P porph.	85DMP -272-2a	80DMA -348c core	80DMA -348c rim	SRI 285	TCD 5	TCD 25
SiO_2	38.92	39.06	38.87	38.98	39.59	38.54	38.49	39.16	37.98	37.89
TiO_2	0.02	0.02	0.03	0.04	0.01	0.04	0.01	0.30	0.57	0.20
Al_2O_3	21.31	21.21	21.19	21.20	21.70	21.45	21.09	21.53	13.55	13.47
Cr_2O_3	0.01	0.01	0.03	0.12	0.08	0.00	0.01	0.06	0.12	0.06
Fe_2O_3	0.89	1.26	0.82	0.75	0.71	0.51	0.80	0.74	11.21	11.84
FeO	25.16	23.90	24.38	22.72	22.32	23.62	25.09	24.33	14.45	14.67
MnO	1.11	1.08	2.46	3.60	1.03	0.95	1.17	0.77	0.35	0.36
MgO	6.41	5.52	5.76	6.33	7.98	4.89	4.82	8.52	0.08	0.02
CaO	7.17	10.02	7.20	6.66	7.58	10.35	8.78	5.79	32.05	31.71
FeO^1	24.35	22.77	23.65	22.04	21.66	23.16	24.37	23.66	4.37	4.03
Total	100.19	100.95	100.01	99.72	100.34	99.89	99.54	100.53	100.28	99.58
Si	3.013	3.005	3.028	3.034	3.022	2.999	3.020	2.990	2.999	3.015
Ti	0.001	0.001	0.002	0.002	0.001	0.002	0.001	0.017	0.034	0.012
Al	1.945	1.924	1.946	1.945	1.952	1.968	1.951	1.938	1.261	1.263
Cr	0.001	0.001	0.002	0.007	0.005	0.000	0.001	0.004	0.007	0.004
Fe^{3+}	0.052	0.073	0.048	0.044	0.041	0.030	0.047	0.043	0.666	0.709
Fe^{2+}	1.556	1.466	1.542	1.436	1.385	1.508	1.601	1.512	0.289	0.268
Mn	0.073	0.070	0.162	0.237	0.067	0.063	0.078	0.050	0.023	0.024
Mg	0.740	0.633	0.669	0.735	0.908	0.567	0.564	0.970	0.009	0.002
Ca	0.595	0.826	0.601	0.555	0.620	0.863	0.738	0.474	2.711	2.703

SAMPLE	TCD 33a	TCD -39	HA 10/83	HA 46/85	HA 53/80	HA 54/83
SiO_2	39.30	39.57	41.35	40.13	40.15	40.42
TiO_2	0.02	0.05	0.07	0.12	0.19	0.16
Al_2O_3	21.82	22.03	22.74	21.43	21.64	22.42
Cr_2O_3	0.04	0.07	0.02	0.00	0.01	0.02
Fe_2O_3	1.03	1.10	0.80	1.33	1.12	0.97
FeO	24.19	23.37	13.65	21.15	21.11	17.43
MnO	0.70	0.66	0.18	0.66	0.47	0.28
MgO	8.36	8.90	16.16	10.70	11.20	13.00
CaO	6.33	6.26	5.78	5.64	5.57	6.52
FeO^1	23.26	22.78	12.93	19.95	20.11	16.56
Total	100.86	101.42	100.03	99.96	100.46	100.35
Si	2.990	2.934	3.004	3.035	3.014	2.988
Ti	0.001	0.003	0.004	0.007	0.011	0.009
Al	1.957	1.959	1.948	1.911	1.915	1.954
Cr	0.002	0.004	0.001	0.000	0.001	0.001
Fe^{3+}	0.059	0.062	0.044	0.076	0.063	0.054
Fe^{2+}	1.481	1.438	0.786	1.263	1.263	1.024
Mn	0.045	0.042	0.011	0.042	0.030	0.018
Mg	0.948	1.001	1.751	1.207	1.254	1.433
Ca	0.516	0.506	0.450	0.457	0.448	0.516

Clinopyroxene Analyses

SAMPLE	A85A -3a	A85A -3b	H85A -1b	H85A -1e(2)	M3.14d	M49	M65	M86E -1b	M86E -1c-2	O8e
SiO_2	49.85	49.60	48.43	48.15	50.37	49.10	50.62	53.15	53.09	50.96
TiO_2	0.17	0.24	0.23	0.29	0.07	0.43	0.41	0.04	0.00	0.03
Al_2O_3	1.56	1.74	2.10	2.18	1.01	3.95	3.13	1.14	0.99	1.26
Cr_2O_3	0.01	0.04	0.02	0.00	0.02	0.03	0.03	0.00	0.01	0.09
Fe_2O_3	0.27	3.23	1.22	1.08	1.53	2.74	3.64	0.00	0.00	2.61
FeO	17.67	18.72	24.13	23.72	15.92	15.29	10.76	8.02	9.82	14.18
MnO	0.17	0.27	0.51	0.75	0.33	0.55	0.15	0.06	11.43	0.28
MgO	7.24	7.18	2.59	2.94	8.02	7.66	12.14	12.54	0.08	9.08
CaO	22.81	22.62	21.37	21.14	23.04	22.12	21.92	24.43	24.13	24.34
Na_2O	1.16	0.35	0.55	0.63	0.34	0.81	0.76	0.35	0.31	0.34
FeO^1	17.43	15.81	23.03	22.75	14.54	12.78	7.49	8.02	9.82	11.78
Total	100.67	101.08	100.05	99.91	99.27	100.17	100.29	99.73	99.86	100.77
Si	1.955	1.919	1.946	1.947	1.965	1.887	1.895	1.990	2.002	1.948
Ti	0.005	0.007	0.007	0.009	0.002	0.012	0.012	0.001	0.000	0.001
Al	0.072	0.079	0.099	0.104	0.046	0.179	0.138	0.050	0.440	0.051
Cr	0.000	0.001	0.001	0.000	0.001	0.001	0.001	0.000	0.000	0.001
Fe^{3+}	0.008	0.094	0.037	0.033	0.045	0.081	0.103	0.000	0.000	0.075
Fe^{2+}	0.572	0.512	0.775	0.770	0.475	0.411	0.235	0.251	0.310	0.377
Mn	0.006	0.009	0.017	0.026	0.011	0.018	0.005	0.002	0.003	0.007
Mg	0.423	0.414	0.155	0.147	0.467	0.439	0.678	0.700	0.643	0.517
Ca	0.958	0.938	0.920	0.916	0.963	0.911	0.879	0.980	0.975	0.995
Na	0.088	0.026	0.043	0.049	0.026	0.060	0.055	0.025	0.023	0.027

SAMPLE	O15b	PS7c	PS7g(e)	PS7g	PS085A -13 porph	PS085A -13 neo	PS86B1 -7	PS86E -6b core	PS86E -6b rim	PS86E -17
SiO_2	50.77	50.96	50.33	49.78	49.65	51.57	49.42	49.87	50.70	50.51
TiO_2	0.15	0.14	0.14	0.10	0.45	0.13	0.01	0.40	0.36	0.26
Al_2O_3	1.58	2.27	2.40	1.32	3.53	1.71	1.18	3.82	3.30	3.03
Cr_2O_3	0.02	0.00	0.01	0.00	0.03	0.05	0.01	0.03	0.04	0.05
Fe_2O_3	4.55	4.67	2.74	3.95	4.28	3.16	2.67	1.32	1.77	1.72
FeO	14.56	11.76	11.41	20.48	12.34	10.81	20.25	12.05	11.62	13.07
MnO	0.58	0.11	0.20	0.21	0.22	0.20	0.23	0.06	0.10	0.14
MgO	10.76	11.36	10.76	6.02	10.81	11.38	5.90	10.29	10.66	9.67
CaO	21.56	23.90	22.56	21.45	22.82	23.90	20.65	21.69	22.18	22.35
Na_2O	0.64	0.54	0.66	0.96	0.74	0.58	0.87	0.63	0.73	0.72
FeO^1	10.47	7.56	8.95	16.93	8.49	7.97	17.85	10.86	10.03	11.52
Total	101.08	101.51	98.75	100.72	101.02	100.65	98.79	98.97	99.87	99.97
Si	1.919	1.900	1.927	1.942	1.875	1.934	1.965	1.906	1.917	1.917
Ti	0.004	0.004	0.004	0.003	0.013	0.004	0.000	0.012	0.010	0.016
Al	0.07	0.100	0.108	0.061	0.157	0.076	0.055	0.172	0.147	0.136
Cr	0.001	0.000	0.000	0.000	0.001	0.001	0.000	0.001	0.001	0.002
Fe^{3+}	0.129	0.131	0.079	0.116	0.122	0.089	0.080	0.038	0.050	0.049
Fe^{2+}	0.331	0.236	0.287	0.553	0.268	0.250	0.594	0.348	0.317	0.366
Mn	0.019	0.003	0.006	0.007	0.007	0.006	0.008	0.002	0.003	0.004
Mg	0.607	0.632	0.614	0.350	0.580	0.637	0.350	0.587	0.601	0.547
Ca	0.873	0.955	0.925	0.896	0.923	0.960	0.880	0.888	0.893	0.909
Na	0.047	0.039	0.049	0.073	0.054	0.042	0.067	0.047	0.054	0.053

SAMPLE	S3b	S4c	S10b	S28c	S32	S42	S85A -3a	S85A -3b	S86E -8c	S86E -8i core
SiO_2	50.37	50.51	50.92	49.59	51.55	50.80	51.44	50.77	49.56	52.08
TiO_2	0.42	0.22	0.29	0.44	0.18	0.24	0.26	0.26	0.13	0.23
Al_2O_3	3.72	2.47	2.84	4.86	2.28	2.61	3.51	3.76	1.95	2.41
Cr_2O_3	0.03	0.02	0.00	0.10	0.07	0.03	0.01	0.01	0.04	0.02
Fe_2O_3	4.48	5.61	4.06	4.43	2.98	4.24	0.85	4.79	2.97	3.81
FeO	11.87	13.56	12.15	9.86	11.78	10.89	7.53	8.48	18.97	13.39
MnO	0.15	0.29	0.39	0.13	0.17	0.22	0.08	0.07	0.15	0.13
MgO	11.24	11.40	11.27	11.89	12.87	11.77	13.12	12.93	6.03	10.35
CaO	21.15	20.39	21.73	21.95	20.84	22.57	21.98	23.26	21.52	20.76
Na_2O	1.18	1.15	0.93	0.94	0.62	0.81	0.71	0.83	0.99	1.58
FeO[1]	7.84	8.51	8.50	5.88	9.10	7.07	6.77	4.18	16.30	9.96
Total	100.58	100.57	100.93	100.21	100.66	100.36	98.73	100.86	99.64	101.33
Si	1.885	1.901	1.906	1.851	1.924	1.905	1.929	1.874	1.944	1.944
Ti	0.012	0.006	0.008	0.012	0.005	0.007	0.007	0.007	0.004	0.006
Al	0.164	0.110	0.125	0.214	0.100	0.115	0.155	0.164	0.090	0.106
Cr	0.001	0.001	0.000	0.003	0.002	0.001	0.000	0.000	0.001	0.001
Fe^{3+}	0.126	0.159	0.114	0.124	0.084	0.120	0.024	0.133	0.088	0.107
Fe^{2+}	0.246	0.268	0.266	0.184	0.284	0.222	0.212	0.129	0.535	0.311
Mn	0.005	0.009	0.012	0.004	0.005	0.007	0.003	0.002	0.005	0.004
Mg	0.627	0.640	0.629	0.662	0.716	0.658	0.734	0.712	0.353	0.576
Ca	0.848	0.822	0.871	0.878	0.833	0.907	0.883	0.920	0.904	0.830
Na	0.086	0.084	0.068	0.068	0.045	0.059	0.051	0.059	0.075	0.114

SAMPLE	S86E -8i rim	S86E -23	S86E 25a	S86E -25c	S86E -33	S86E -34 core	S86E -34 rim	S86E -36b	S86E -40	S86E -41 core
SiO_2	52.82	54.01	49.51	50.53	50.28	50.73	49.97	49.02	49.78	49.98
TiO_2	0.11	0.32	0.61	0.41	0.15	0.34	0.28	0.41	0.42	0.43
Al_2O_3	1.96	1.49	5.29	4.19	1.77	3.73	3.60	4.40	4.07	4.04
Cr_2O_3	0.02	0.00	0.03	0.02	0.05	0.00	0.00	0.02	0.02	0.00
Fe_2O_3	2.31	0.13	1.76	2.82	2.35	1.33	2.23	3.39	2.35	2.85
FeO	10.92	1.78	11.65	10.30	18.92	10.50	10.65	13.09	9.29	9.83
MnO	0.07	0.00	0.17	0.11	0.20	0.09	0.04	0.08	0.07	0.07
MgO	11.70	16.99	10.13	11.11	6.85	11.04	11.03	9.51	11.97	11.88
CaO	21.97	25.18	21.14	22.54	19.83	22.17	22.31	21.57	22.08	21.79
Na_2O	1.15	0.14	0.94	0.91	1.21	0.75	0.66	0.92	0.65	0.80
FeO[1]	8.84	1.67	10.07	7.77	16.81	9.30	8.65	10.04	7.18	7.26
Total	100.95	99.93	99.65	100.41	99.50	99.48	98.77	99.36	98.59	99.10
Si	1.963	1.963	1.874	1.889	1.965	1.916	1.904	1.874	1.887	1.887
Ti	0.003	0.009	0.017	0.012	0.004	0.010	0.008	0.012	0.012	0.012
Al	0.086	0.064	0.236	0.185	0.082	0.166	0.162	0.198	0.182	0.180
Cr	0.001	0.000	0.001	0.001	0.002	0.000	0.000	0.001	0.001	0.000
Fe^{3+}	0.065	0.003	0.050	0.079	0.069	0.038	0.064	0.098	0.067	0.081
Fe^{2+}	0.275	0.051	0.319	0.243	0.550	0.294	0.276	0.321	0.228	0.230
Mn	0.002	0.000	0.005	0.003	0.007	0.003	0.001	0.003	0.002	0.002
Mg	0.648	0.921	0.572	0.619	0.394	0.622	0.627	0.542	0.677	0.669
Ca	0.875	0.980	0.857	0.903	0.830	0.897	0.910	0.883	0.897	0.881
Na	0.083	0.010	0.069	0.066	0.092	0.055	0.049	0.068	0.048	0.059

SAMPLE	S86E -41 rim	S86E -53a	80DMA -614p core	80DMA -614p rim	85DMP -174-1a core	85DMP -174-1a rim	85DMP -272-2a	TCD 33a	TCD 39	SRI 285
SiO_2	50.70	51.53	50.90	51.36	50.51	51.91	50.52	51.45	51.73	49.93
TiO_2	0.35	0.33	0.33	0.33	0.37	0.20	0.46	0.35	0.30	0.45
Al_2O_3	3.55	3.41	3.75	3.68	4.29	2.96	4.79	3.60	3.73	4.66
Cr_2O_3	0.00	0.00	0.04	0.05	0.01	0.03	0.06	0.04	0.03	0.01
Fe_2O_3	2.22	1.13	1.51	2.12	2.93	2.69	2.96	2.66	3.33	3.39
FeO	8.71	8.16	9.45	8.40	10.52	8.91	8.33	8.63	7.91	8.45
MnO	0.04	0.10	0.48	0.20	0.19	0.15	0.13	0.08	0.08	0.13
MgO	12.16	12.80	11.89	12.74	11.28	12.66	12.51	12.96	13.31	12.27
CaO	22.65	22.28	21.45	22.06	21.23	22.16	21.66	21.35	22.12	21.61
Na_2O	0.75	0.71	0.84	0.87	1.15	1.00	1.07	1.04	1.09	1.08
FeO^1	6.72	7.15	8.09	6.49	7.89	6.49	5.67	6.23	4.91	5.40
Total	99.14	99.44	99.28	99.90	99.85	100.25	99.83	99.76	100.63	98.93
Si	1.907	1.926	1.916	1.911	1.895	1.928	1.878	1.913	1.903	1.875
Ti	0.010	0.009	0.009	0.009	0.010	0.006	0.013	0.010	0.008	0.013
Al	0.157	0.150	0.166	0.162	0.190	0.130	0.21	0.158	0.162	0.206
Cr	0.000	0.000	0.001	0.001	0.000	0.001	0.002	0.001	0.001	0.000
Fe^{3+}	0.063	0.032	0.093	0.059	0.083	0.075	0.083	0.075	0.092	0.096
Fe^{2+}	0.211	0.224	0.255	0.202	0.248	0.202	0.176	0.194	0.151	0.170
Mn	0.001	0.003	0.015	0.006	0.006	0.005	0.004	0.003	0.002	0.004
Mg	0.682	0.713	0.668	0.707	0.631	0.701	0.694	0.719	0.730	0.687
Ca	0.013	0.892	0.865	0.879	0.853	0.882	0.863	0.850	0.872	0.870
Na	0.055	0.051	0.061	0.063	0.084	0.072	0.077	0.079	0.078	0.074

SAMPLE	HA 10/83	HA 46/85	HA 54/83
SiO_2	50.63	49.69	49.15
TiO_2	0.50	0.73	1.10
Al_2O_3	6.88	6.77	7.31
Cr_2O_3	0.01	0.04	0.00
Fe_2O_3	2.16	5.29	1.20
FeO	4.83	9.20	6.55
MnO	0.03	0.16	0.02
MgO	13.43	10.97	12.09
CaO	22.69	20.29	21.62
Na_2O	1.09	1.86	1.08
FeO^1	2.89	4.45	5.47
Total	100.31	100.25	99.04
Si	1.847	1.826	1.831
Ti	0.014	0.020	0.031
Al	0.296	0.293	0.321
Cr	0.000	0.001	0.000
Fe^{3+}	0.059	0.146	0.034
Fe^{2+}	0.088	0.137	0.171
Mn	0.001	0.005	0.001
Mg	0.731	0.601	0.672
Ca	0.887	0.838	0.863
Na	0.077	0.133	0.078

Orthopyroxene Analyses

SAMPLE	A86B -3-3b-3	M65	015b	S3b	S10b	S32	S86E -33	80DMA -614p	85DMP -272-2a	TCD -39
SiO_2	51.98	51.40	50.25	51.54	51.49	51.37	49.00	51.95	53.04	53.27
TiO_2	0.08	0.05	0.08	0.04	0.07	0.07	0.08	0.03	0.03	0.00
Al_2O_3	2.51	1.02	0.59	1.23	1.36	1.54	0.51	2.04	2.00	2.05
Cr_2O_3	0.03	0.01	0.01	0.01	0.00	0.04	0.00	0.02	0.04	0.55
Fe_2O_3	1.16	1.64	1.91	1.43	1.03	1.84	0.37	2.12	0.10	2.23
FeO	22.13	28.15	33.93	28.08	27.33	26.67	40.05	23.80	21.39	21.07
MnO	0.79	0.35	1.32	0.28	0.56	0.32	0.42	1.44	0.30	0.16
MgO	22.34	18.94	14.46	18.94	19.07	19.95	9.62	20.23	23.19	24.02
CaO	0.34	0.46	0.51	0.58	0.49	0.43	0.93	0.61	0.33	0.35
Na_2O	0.01	0.02	0.03	0.01	0.00	0.01	0.03	0.03	0.01	0.02
FeO^1	21.09	26.67	32.22	26.79	26.41	24.97	39.72	21.89	21.30	19.07
Total	100.33	100.56	101.38	100.85	100.48	100.54	100.68	100.36	100.34	101.72
Si	1.927	1.953	1.957	1.951	1.953	1.937	1.981	1.926	1.954	1.918
Ti	0.002	0.001	0.002	0.001	0.002	0.002	0.002	0.001	0.001	0.000
Al	0.110	0.046	0.027	0.055	0.061	0.068	0.024	0.089	0.087	0.089
Cr	0.001	0.000	0.000	0.000	0.000	0.001	0.000	0.001	0.001	0.016
Fe^{3+}	0.032	0.047	0.056	0.041	0.029	0.054	0.011	0.059	0.003	0.061
Fe^{2+}	0.654	0.848	1.050	0.849	0.838	0.788	1.344	0.679	0.657	0.584
Mn	0.025	0.011	0.044	0.009	0.018	0.010	0.014	0.045	0.009	0.005
Mg	1.235	1.073	0.840	1.069	1.079	1.122	0.580	1.174	1.274	1.312
Ca	0.014	0.019	0.021	0.024	0.020	0.017	0.040	0.029	0.013	0.014
Na	0.001	0.001	0.002	0.001	0.000	0.001	0.002	0.002	0.001	0.001

SAMPLE	SRI 285	HA 46/85
SiO_2	51.77	52.21
TiO_2	0.07	0.11
Al_2O_3	2.75	3.61
Cr_2O_3	0.02	0.01
Fe_2O_3	0.85	1.15
FeO	22.95	20.42
MnO	0.37	0.27
MgO	21.6	23.54
CaO	0.53	0.54
Na_2O	0.04	0.04
FeO^1	22.19	19.38
Total	100.19	100.86
Si	1.927	1.905
Ti	0.002	0.003
Al	0.121	0.155
Cr	0.001	0.000
Fe^{3+}	0.024	0.032
Fe^{2+}	0.691	0.592
Mn	0.012	0.008
Mg	1.199	1.281
Ca	0.021	0.021
Na	0,003	0.003

Epidote Analyses

SAMPLE	C1b core	C1b rim	DEB83C -4	PS85A -1a	PS85A -2c	PS86B 1-11"	PS86E -7e	PS86E -8	PS86E -10	PS86E -12
SiO_2	39.41	39.27	39.26	38.22	38.71	37.87	37.82	37.95	38.13	38.04
TiO_2	na	na	na	0.16	na	0.14	0.15	0.20	0.12	0.17
Al_2O_3	28.69	28.89	27.71	27.37	26.21	25.93	25.90	25.83	25.78	1.63
Fe_2O_3	7.40	6.75	8.10	8.50	9.93	10.17	10.22	10.30	10.85	10.21
MnO	na	na	0.19	0.09	0.02	0.10	0.06	0.08	0.13	0.06
CaO	23.82	24.29	24.03	23.68	23.74	23.35	23.43	23.40	23.40	23.50
H_2O	1.95	1.96	1.95	1.92	1.92	1.90	1.90	1.90	1.91	1.91
Total	101.27	101.16	101.20	99.94	100.53	99.46	99.48	99.66	100.32	100.05
Si	3.021	3.007	3.020	2.982	3.020	2.991	2.986	2.993	2.990	2.986
Ti	-	-		0.009	-	0.006	0.009	0.012	0.007	0.01
Al	2.593	2.608	2.514	2.517	2.410	2.414	2.411	2.401	2.383	2.421
Fe^{3+}	0.427	0.389	0.469	0.499	0.583	0.605	0.608	0.612	0.641	0.603
Mn	-	-	0.012	0.006	0.001	0.007	0.004	0.005	0.009	0.004
Ca	1.960	1.996	1.981	1.979	1.984	1.975	1.982	1.977	1.966	1.976

SAMPLE	PS86E -15	PS86E -16a matrix	PS86E -16a porph	PS86E -17	PS86E -23-1	PS86E -24b	PS86E -24d	PS86E -24f	PS86E -31	S86E -25a
SiO_2	37.97	37.93	38.10	37.99	38.92	37.96	38.14	37.87	38.95	38.53
TiO_2	0.12	0.13	0.05	0.09	na	0.07	0.16	0.19	na	0.15
Al_2O_3	26.21	25.42	26.31	25.78	27.63	27.62	26.26	26.37	25.73	27.22
Fe_2O_3	9.83	10.86	9.39	10.74	7.48	8.52	9.95	9.89	10.96	8.57
MnO	0.17	0.03	0.09	0.04	0.06	0.10	0.11	0.03	0.11	0.04
CaO	23.11	23.41	23.34	25.36	23.51	23.74	23.10	23.47	23.27	23.25
H_2O	1.90	1.90	1.90	1.91	1.92	1.92	1.90	1.90	1.92	1.91
Total	99.31	99.68	99.18	100.11	99.48	99.93	99.62	99.72	100.94	99.67
Si	2.999	2.995	3.007	2.983	3.042	2.962	3.003	2.979	3.038	3.016
Ti	0.007	0.008	0.003	0.005	-	0.004	0.009	0.011	-	0.009
Al	2.441	2.366	2.448	2.387	2.546	2.540	2.437	2.445	2.366	2.512
Fe^{3+}	0.585	0.646	0.558	0.635	0.440	0.500	0.590	0.586	0.643	0.507
Mn	0.011	0.002	0.006	0.003	0.006	0.007	0.007	0.002	0.007	0.003
Ca	1.956	1.980	1.973	1.982	1.968	1.984	1.948	1.977	1.944	1.950

SAMPLE	S86E -25n
SiO_2	38.97
TiO_2	0.11
Al_2O_3	31.44
Fe_2O_3	2.96
MnO	0.00
CaO	24.48
H_2O	1.96
Total	99.92
Si	2.981
Ti	0.006
Al	2.836
Fe^{3+}	0.171
Mn	0.000
Ca	2.006

Titanite Analyses

SAMPLE	PS7c	PS085A -8b	PS86B 1-10a
SiO_2	30.34	30.28	30.01
TiO_2	37.09	36.57	36.75
Al_2O_3	1.55	1.53	1.55
Fe_2O_3	0.39	0.56	0.52
MnO	0.02	0.00	0.03
MgO	0.00	0.00	0.00
CaO	28.61	28.91	28.47
Na_2O	0.02	0.01	0.02
K_2O	0.01	0.01	0.01
Cl	0.01	0.01	0.00
F	0.72	0.57	0.68
P_2O_5	0.07	0.10	0.00
Total	98.83	98.55	98.04
Si	0.999	0.997	0.995
Ti	0.919	0.906	0.916
Al	0.060	0.059	0.061
Fe^{3+}	0.010	0.014	0.014
Mn	0.001	0.000	0.001
Mg	0.000	0.000	0.000
Ca	1.009	1.020	1.011
Na	0.001	0.001	0.001
K	0.000	0.000	0.000
Cl	0.001	0.001	0.000
F	0.075	0.059	0.071
P	0.002	0.003	0.000

Appendix 4

Activity Models for Chapter II

Pyroxene

The ideal activity models for clinopyroxene used in this study are summarized in the text, equations 17 and 18 for hedenbergite and diopside, respectively. the model used for orthopyroxene is that of Wood and Banno (1973) in which the activity of ferrosilite is taken as:

$$a^{Opx}_{Fe_2Si_2O_6} = [X^{M1}_{Fe^{2+}}][X^{M2}_{Fe^{2+}}].$$

Pyroxene analyses are normalized to 4 cations and Fe^{3+} is calculated from charge balance and stoichiometry. After subtracting the atomic amounts of Ca, Na, and Mn from the M2 site, and subtracting Al^{vi}, Ti, Cr, and Fe^{3+} from the M1 site, Fe^{2+} is partitioned into each remaining site in the same ratio as $Fe^{2+}/(Fe^{2+} + Mg)$ in the mineral.

The equilibrium constant for the FS barometer includes a term for $a^{Opx}_{Fe_2Si_2O_6}$ that is raised to the 3rd power. Because the two site model involves the square of X_{Fe}, the activity of ferrosilite calculated above is taken to the 3rd power in calculating the equilibrium constant for Reaction 3, although the thermodynamic data for ferrosilite are based on a 2 cation formula (6 moles of Fs for Reaction 3). When calculating the activity of $FeSiO_3$ simply as mole fraction of Fe^{2+}, the exponent for Fs in Reaction 3 is raised to the 6th power.

Plagioclase

The activity of anorthite in plagioclase was calculated according to the model of Newton et al. (1980), also given in Newton and Haselton (1981), Newton and Perkins (1982), and Newton (1983). Plagioclase analyses were normalized to 5 cations, and X^{Pg}_{An} = Ca/(Ca + Na). The activity of anorthite is calculated from the following relations:

$$RT\ln\gamma^{Pg}_{An} = (X^{Pg}_{Ab})^2[2050 + 9392 \cdot X^{Pg}_{An}]$$

$$a^{Pg}_{CaAl_2Si_2O_8} = \gamma^{Pg}_{An}\,[X^{Pg}_{An} \cdot (1 + X^{Pg}_{An})^2]/4$$

Garnet

Grossular, pyrope, and almandine activities were calculated using the quaternary garnet mixing model of Ganguly and Saxena (1984), with the Ca–Fe mixing parameters for the grossular–almandine join calculated by Anovitz and Essene (1987a). The Ca–Mg, Ca–Mn, Fe–Mg, Fe–Mn, and Mg–Mn mixing parameters are the same as in Ganguly and Saxena (1984). Use of these parameters yields the

following analytical expressions for the activity coefficient of grossular, pyrope, and almandine:

$$RT\ln\gamma^{Gt}_{Ca} = (X^{Gt}_{Mg})^2\cdot(4047 - 1.5T - 6094X^{Gt}_{Ca}) + (X^{Gt}_{Fe^{2+}})^2\cdot(150 - 1.5T + 7866X^{Gt}_{Ca}) + X^{Gt}_{Mg}X^{Gt}_{Fe^{2+}}\cdot[3290 - 3.0T + 886X^{Gt}_{Ca} + 2300(X^{Gt}_{Mg} - X^{Gt}_{Fe^{2+}}) + 4640(1 - 2X^{Gt}_{Ca})] + X^{Gt}_{Fe^{2+}}\cdot X^{Gt}_{Mn}[2117 - 1.5T + 3933X^{Gt}_{Ca} - 1967(1 - 2X^{Gt}_{Ca})] + X^{Gt}_{Mg}X^{Gt}_{Mn}[2524 - 1.5T - 3047X^{Gt}_{Ca} + 1524(1 - 2X^{Gt}_{Ca})] + 2300\cdot[X^{Gt}_{Mg}X^{Gt}_{Fe^{2+}}\cdot X^{Gt}_{Mn}]$$

$$RT\ln\gamma^{Gt}_{Mg} = (X^{Gt}_{Ca})^2\cdot(1000 - 1.5T + 6094X^{Gt}_{Mg}) + (X^{Gt}_{Fe^{2+}})^2\cdot(2500 - 4600X^{Gt}_{Mg} + 3000\cdot(X^{Gt}_{Mn})^2 + X^{Gt}_{Ca}X^{Gt}_{Fe^{2+}}\cdot[1757 + 747X^{Gt}_{Mg} - 3933(X^{Gt}_{Ca} - X^{Gt}_{Fe^{2+}}) + 4640(1 - 2X^{Gt}_{Mg})] + X^{Gt}_{Fe^{2+}}\cdot X^{Gt}_{Mn}[4350 - 2300X^{Gt}_{Mg} + 1150(1 - 2X^{Gt}_{Mg})] + X^{Gt}_{Ca}X^{Gt}_{Mn}[5524 + 3047X^{Gt}_{Mg} - 1524(1 - 2X^{Gt}_{Mg})] + 3933\cdot[X^{Gt}_{Ca}X^{Gt}_{Fe^{2+}}\cdot X^{Gt}_{Mn}]$$

$$RT\ln\gamma^{Gt}_{Fe^{2+}} = (X^{Gt}_{Mg})^2\cdot(200 + 4600X^{Gt}_{Fe^{2+}}) + (X^{Gt}_{Ca})^2(4083 - 1.5T - 7866X^{Gt}_{Fe^{2+}}) + X^{Gt}_{Mg}X^{Gt}_{Ca}[943 - 1633X^{Gt}_{Fe^{2+}} - 3047(X^{Gt}_{Mg} - X^{Gt}_{Ca}) - 4640(1 - 2X^{Gt}_{Fe^{2+}})] + X^{Gt}_{Ca}X^{Gt}_{Mn}[2117 - 1.5T - 3933X^{Gt}_{Fe^{2+}} + 1917(1 - 2X^{Gt}_{Fe^{2+}})] + X^{Gt}_{Mg}X^{Gt}_{Mn}[-1650 + 2300X^{Gt}_{Fe^{2+}} - 1150(1 - 2X^{Gt}_{Fe^{2+}})] + 3048\cdot[X^{Gt}_{Mg}X^{Gt}_{Ca}X^{Gt}_{Mn}]$$

Because there are three equivalent 8-coordinated sites in garnet, the activity of $Ca_3Al_2Si_3O_{12}$, $Mg_3Al_2Si_3O_{12}$, and $Fe_3Al_2Si_3O_{12}$ are calculated as

$$a^{Gt}_{Ca_3Al_2Si_3O_{12}} = (X^{Gt}_{Ca}\gamma^{Gt}_{Ca})^3,$$

$$a^{Gt}_{Mg_3Al_2Si_3O_{12}} = (X^{Gt}_{Mg}\gamma^{Gt}_{Mg})^3, \text{ and}$$

$$a^{Gt}_{Fe_3Al_2Si_3O_{12}} = (X^{Gt}_{Fe^{2+}}\cdot\gamma^{Gt}_{Fe^{2+}})^3.$$

APPENDIX 5

Mineral formulae, abbreviations, and symbols.

Albite (Ab):	$NaAlSi_3O_8$
Almandine (Alm):	$Fe_3Al_2Si_3O_{12}$
Andradite (And):	$Ca_3Fe_2Si_3O_{12}$
Anhydrite (Anhy):	$CaSO_4$
Anorthite (An):	$CaAl_2Si_2O_8$
Calcite (Cc):	$CaCO_3$
Ca–Tschermakite (CaTs):	$CaAl_2SiO_6$
Clinozoisite (CZo):	$Ca_2Al_3Si_3O_{11}OH$
Corundum (Cor):	Al_2O_3
Diopside (Di):	$CaMgSi_2O_6$
Enstatite (En):	$MgSiO_3$
Fayalite (Fa):	Fe_2SiO_4
Ferrosilite (Fs):	$FeSiO_3$
Gehlenite (Ge):	$Ca_2Al_2SiO_7$
Grossular (Gr):	$Ca_3Al_2Si_3O_{12}$
Hematite (Hm):	Fe_2O_3
Kyanite (Ky):	Al_2SiO_5
Magnetite (Mt):	Fe_3O_4
Meionite (Me):	$Ca_4Al_6Si_6O_{24}CO_3$
Mg–Tschermakite (MgTs):	$Mg_{0.5}AlSi_{0.5}O_3$
Pistacite (Ps):	$Ca_2Fe^{3+}_3Si_3O_{11}OH$
Pyrope (Py):	$Mg_3Al_2Si_3O_{12}$
Quartz (Qz):	SiO_2
Sillimanite (Sill):	Al_2SiO_5
Sulfate Meionite ($MeSO_4$):	$Ca_4Al_6Si_6O_{24}SO_4$
Titanite	$CaTiSiO_5$
Wollastonite (Wo):	$CaSiO_3$
Zoisite (Zo):	$Ca_2Al_3Si_3O_{11}OH$

Cc: calcite
Cpx: clinopyroxene
Ep: epidote
Gt: garnet
Hbl: hornblende
Kfs: potassium feldspar
Opx: orthopyroxene
Pg: plagioclase
Sc: scapolite

S^{o}_{0}: zero-point, configurational entropy, J mol^{-1} K^{-1}.
S^{o}_{298} : molar entropy at 1 bar, 298 K, J mol^{-1} K^{-1}.
S^{P}_{T}: molar entropy at P and T, J mol^{-1} K^{-1}.
V^{o}_{298} : molar volume at 1 bar, 298 K, cm^3
V^{P}_{T}: molar volume at P and T, cm^3
ΔS: entropy change of reaction or solid phases
ΔV: volume change of reaction or solid phases
ΔG^{o}_{298} : molar Gibbs free energy at 1 bar, 298 K, kJ mol^{-1}.
a^{i}_{j}: activity of component i in phase j
X^{i}_{j}: mole fraction of component i in phase j
γ^{i}_{j}: activity coefficient of component i in phase j
X^{Sc}_{Mg}: Ca/(Ca+Na+K), or EqAn (100[Al-3]/3), where stated.